3-2021

Optimal Defense of High Value Airborne Assets

Isaac E. Weintraub

Optimal Defense of High Value Airborne Assets

DISSERTATION

Isaac E. Weintraub, Civilian, Department of Defense

AFIT-ENG-DS-21-M-091

DEPARTMENT OF THE AIR FORCE
AIR UNIVERSITY

AIR FORCE INSTITUTE OF TECHNOLOGY

Wright-Patterson Air Force Base, Ohio

AFIT-ENG-DS-21-M-091

OPTIMAL DEFENSE OF HIGH VALUE AIRBORNE ASSETS

DISSERTATION

Presented to the Faculty

Graduate School of Engineering and Management

Air Force Institute of Technology

Air University

Air Education and Training Command

in Partial Fulfillment of the Requirements for the

Degree of Doctor of Philosophy in Electrical Engineering

Isaac E. Weintraub, BSME, MSEE

Civilian, Department of Defense

March 2021

AFIT-ENG-DS-21-M-091

OPTIMAL DEFENSE OF HIGH VALUE AIRBORNE ASSETS

DISSERTATION

Isaac E. Weintraub, BSME, MSEE
Civilian, Department of Defense

Committee Membership:

Meir Pachter, Ph.D.
Chair

Richard Cobb, Ph.D.
Member

Lt. Col. Michael Zollars, Ph.D.
Member

Eloy Garcia, Ph.D.
Member

Abstract

Optimal control theory and differential game theory is applied to the study of the defense of high value airborne assets, particularly in the case of a single threat such as an adversarial aircraft or missile. Rather than utilizing onboard defenses of the high value airborne asset, defense is proposed using a teamed unmanned combat air vehicle.

The common scenario throughout this dissertation involves the defense of a high value airborne asset (evader) teamed with an unmanned combat vehicle (defender) against a single threat (pursuer). The unmanned combat air vehicle (defender), provides defense in one of two ways: kinetic or directed energy. When defense is kinetic in nature, the defender launches a missile which strives to reach the threat before the threat reaches the high value airborne asset – damage to the pursuer is dealt through capture. When defense is provided through directed energy, the defender strives to keep the incoming threat inside his weapon engagement zone for as long as possible – damage to the pursuer is dealt over time.

Leveraging differential game theory and optimal control theory, a series of scenarios are proposed and solved which illustrate different optimal strategies for the successful defense of a high value airborne asset against the incoming threat. In the event that defense is kinetic in nature, the defender-evader team strives to be as far (in range) from the captured pursuer at final time while the pursuer strives to minimize said range. When defense is provided by means of directed energy, the pursuer strives to capture the evader in minimum time while the defender strives to maximally expose the pursuer prior to the evader's capture.

In addition to considering the optimal strategies for the successful defense of a high

value airborne asset against an incoming threat, an investigation of various numerical methods is conducted. The investigation compares and contrasts four different direct methods. The comparisons between the different numerical methods are used to suggest a single method that may be applicable for future hardware implementation.

In memory of my mother, Miriam Leeper-Kende. "Everything happens for a purpose," she once told me; "The reason why will become clear later." She was able to see me start my degree and unable to see me finish it. For your inspiration and passion, I dedicate this work to you.

Acknowledgements

I would like to express my very great appreciation to Dr. Meir Pachter for his valuable and constructive suggestions during the planning and development of this research work. His willingness to give his time so generously has been very much appreciated. From the beginning, Dr. Pachter has guided me in my research. He has always had an attentive ear, and his assistance has been invaluable.

I would also like to thank my committee: Dr. William Baker, Dr. Richard Cobb, Dr. Eloy Garcia, and Lt. Col. Michael Zollars, Ph.D. Thank you for your guidance and instruction throughout this endeavor. Dr. Baker and Dr. Cobb, thank you for the tools that you have prepared me with; this work would not have been possible without the valuable lessons you provided over this endeavor. Dr. Garcia, thank you for your attentive ear and advice in the area of differential games, our many discussions have shaped this work into what it is today. Lt. Col. Zollars, thank you for guiding me to the finish line.

I would like to thank the faculty and staff of the Department of Computer and Electrical Engineering for assisting me with the process and procedures required for obtaining my degree. Dr. Julie Jackson and Ms. Alicia Sprinkle, thank you for always having an attentive ear, assisting me with processing each memo, and helping me comply with the student handbook.

I would like to acknowledge the support of Mr. Howard Emsley at the Air Force Research Laboratories. Thank you for supporting me in this opportunity. Your supervision in the subject matter has aided me in keeping this research relevant to the needs of the United States Air Force.

I would like to acknowledge the support from my family. To my father, thank you for believing in me and encouraging me to complete this dissertation. To my late mother, her commitment to my dreams is echoed in the many hand-written pages

which made this work possible. I would very much like to thank my wife; you have supported and encouraged me in my commitment to higher education. Your profound belief in my work and abilities allowed me to persevere and stay committed to my dreams; thank you so much!

To my friends and colleagues at Air Force Research Laboratory, I would like to thank you for your encouragement and support. I can faithfully say that this work is a reflection of our meetings and discussions. Please consider this work to be partly your own; your contributions and advice have spanned the entirety of this work.

Isaac E. Weintraub

Table of Contents

Page

Page

List of Figures

List of Tables

List of Abbreviations

Abbreviation		Page
HVAA	High Value Airborne Asset	1
DCA	Defensive Counter Air	1
RPA	Remotely Piloted Aircraft	1
ISR	Intelligence, Surveillance, and Reconnaissance	2
IADS	Integrated Air Defense System	2
C2	Command and Control	2
PN	Proportional Navigation	6
OCP	Optimal Control Problem	6
2-D	two-dimensional	6
DG	Differential Game	6
3-D	three-dimensional	6
WEZ	Weapon Engagement Zone	6
BVR	Beyond Visual Range	7
PMP	Pontryagin's Minimum Principle	9
UGSs	Unattended Ground Sensors	21
DED	Directed Energy Defense	32
NLP	Nonlinear Program	38
TPBVP	Two Point Boundary Value Problem	45
SSM	Single Shooting Method	46
MSM	Multiple Shootings Method	46
ECM	Even Collocation Method	46
PSM	Pseudospectral Method	46

Abbreviation		Page
ODE	Ordinary Differential Equation	46
SQP	Sequential Quadratic Programming	47
KKT	Karush-Kuhn-Tucker	47
LGR	Legandre-Gauss-Radau	55
ATDDG	Active Target Defense Differential Game	70
ZET	Zero Exposure Time	146
AFRL	Air Force Research Laboratory	244
AFIT	Air Force Institute of Technology	244

OPTIMAL DEFENSE OF HIGH VALUE AIRBORNE ASSETS

I. Introduction

"What we call the beginning is often the end.
And to make an end is to make a beginning.
The end is where we start from."
— T. S. Eliot, Little Gidding

1.1 Motivation

The defense of a High Value Airborne Asset (HVAA) in theater is one of the many priorities considered in offensive and defensive aerial operations [1]. Typical means of providing defense to HVAAs include fighter escort and passive mission planning around offensive systems. In the event that missiles are engaged on the HVAA, various options are considered including, but not limited to: Defensive Counter Air (DCA), evasive maneuvers, chaff, flares, decoys, and electronic countermeasures [2]. As adversary air and missile threats continue to grow in quantity and capability [1], the need for effective airborne defensive strategies and solutions also grows.

Identified as an area with potential advantages for meeting the challenges of a newly forming adversarial environment, autonomous systems provide a considerable opportunity to enhance future Air Force operations [3]. Described as "game-changing" [4], autonomous systems are of interest to the Air Force toward ensuring air superiority. In a recent report, unmanned systems were determined to be a "preferred alternative for dangerous missions" [5]. Currently, Remotely Piloted Aircraft (RPA) are employed to assist a broad range of Air Force missions [6]. Programs such

as Loyal Wingman have been proposed to assist missions such as Intelligence, Surveillance, and Reconnaissance (ISR), air interdiction, counter Integrated Air Defense System (IADS), offensive counter air, Command and Control (C2), and weapons hosting [7]. Rather than viewing autonomy as an intrinsic property of an unmanned vehicle in isolation, the design and operation of autonomous systems needs to be considered in terms of human-system collaboration [8]. The consideration of manned-unmanned teams is a way to address autonomous systems in future engagements, and in this case, for HVAA defense.

1.2 Problem Statement

This work focuses on the defense of a HVAA from an inbound threat such as a missile or adversarial aircraft. Defense is provided using an autonomous platform which contains either missiles or directed energy weapons. The problem statement which motivates this work is the following: *How may a HVAA be defended against an incoming threat when it is teamed with a defender?*

1.3 Research Questions, Tasks, and Scope

In this work, the HVAA is defined as the "evader," the attacking threat or adversary is referred to as the "pursuer," and a friendly asset is referred to as the "defender." The defender and the evader make up a team which conflicts with the objective of the pursuer. Specifically, the pursuer's goal is to capture the evader while the cooperative team made up of the defender and evader aim to protect the evader from the pursuer. Two means of providing DCA are considered herein: kinetic defense and directed energy defense.

Research Questions.

Hypothesis: *The successful defense of a High Value Airborne Asset may be solved utilizing differential game theory as well as optimal control theory.* From the hypothesis, the following are a list of research questions which arise:

1. How may meaningful mathematical models be generated for HVAA defense scenarios? The models used in this work, accompanied with a discussion of their various assumptions and limitations, are presented in Section 3.2.

2. How may HVAA defense scenarios be posed and solved as either optimal control problems or differential games? A series of HVAA defense scenarios are considered as either optimal control problems or differential games in Chapter IV and Chapter V. When solving a scenario where only one agent aims to optimize its behavior, optimal control theory is leveraged. However, when two agents, at odds with one another, strive to perform optimally, a differential game is considered. Both optimal control theory and differential games are discussed, in brief, in Section 3.3.

3. How may HVAA defense differential games be transformed into optimal control problems which may be solved either analytically or numerically? In Chapter III, Apollonius Circle and how it relates to solving two-agent pursuit-evasion scenarios is described. The use of Apollonius Circle for transforming a differential game into an optimal control problem is demonstrated in Sections 4.1 and 4.2. In Section 4.1, the solution to the differential game is found analytically. In Section 4.2, the solution to the differential game is found numerically.

4. In the event that a HVAA can't maneuver, what are the optimal strategies of both the defender and the pursuer in the three-agent problem? In Sections 4.1 and 4.2, the saddle-point strategies of the defender and pursuer for the kinetic

defense of a non-maneuvering HVAA are presented. In Section 5.2, the optimal defender strategy for the directed energy defense of a non-maneuvering HVAA is presented.

5. How should the HVAA aid in its own defense if it is able to maneuver? The defense of a HVAA which is able to maneuver is considered in Sections 4.3 and 4.4. Using a 2-D kinematic model as described in Section 3.2, the turn rates of the HVAA are bounded and the HVAA is allowed to maneuver. Using direct methods of optimal control theory, the optimal strategy for a maneuverable HVAA is found when both the pursuer and defender are assumed to be missiles guided by proportional navigation.

6. What unique aspects occur when the defender is a missile or directed energy weapon, and what are the critical parameters for the defender to be successful? Various kinetic and directed energy defense scenarios are considered in Chapter IV and Chapter V. In each of the scenarios, a discussion of the optimal agent strategies is presented along with examples. For each scenario, the parameters which influence the optimal strategies are described.

7. What numeric methods are suitable for aerospace hardware systems which require fixed time steps and minimal computational effort? Considering four direct methods of optimal control, the kinetic defense of a maneuvering HVAA is posed and solved in Section 4.4. Assuming a fixed mesh of time, a comparative study is conducted between different direct methods of solving optimal control problems. For each of the four methods the following is emphasized: the computational time, the number of algorithmic iterations, the number of cost-functional evaluations, the ultimate functional evaluation, and the feasibility of the solution.

Research Tasks.

The following research tasks aim to address the research questions posed above.

1. Develop meaningful mathematical models to pose and solve HVAA defense scenarios.

2. Describe HVAA Defense as either a differential game or an optimal control problem; pose and solve them using either analytic or numeric methods.

3. Using geometric methods, describe how HVAA defense differential games may be transformed into optimal control problems, which can be solved either analytically or numerically.

4. Pose and solve 2-D and 3-D HVAA defense differential games where the defender is either a kinetic weapon or directed energy weapon. Consider both the kinetic and directed energy defense of a non-maneuvering evader. Determine optimal strategies taken by the defender to protect the evader.

5. Investigate the optimal maneuvers made by a slower moving HVAA if engaged by a faster, more maneuverable, pursuer in the event that a defender with similar capabilities as the pursuer is in the local airspace. Consider agents to be restricted to a plane.

6. Formulate both kinetic and directed energy defense scenarios and identify critical parameters of interest which influence the outcome of HVAA defense scenarios.

7. Investigate efficient direct methods for computing optimal solutions which could potentially be implemented on hardware.

A scenario matrix which describes the various engagements considered in the scope of this research is shown in Table 1. Scenarios 1-3 consider kinetic defense,

while Scenarios 4-6 consider directed energy defense. In Scenario 1, the pursuer and defender implement the Proportional Navigation (PN) guidance law while the evader's strategy is solved as an Optimal Control Problem (OCP) in the two-dimensional (2-D) Cartesian plane. In Scenario 2 and 3, a Differential Game (DG) is considered between the pursuer and the defender. In this DG the evader has constant bearing and the defender strives to intercept the pursuer before the pursuer can intercept the evader. In Scenario 3, the engagement from Scenario 2 is extended to three-dimensional (3-D) Cartesian space. In Scenario 4 and 5, an OCP is considered where the defender makes use of a directed energy weapon and aims at maximizing the time that the pursuer is inside the Weapon Engagement Zone (WEZ). In Scenario 4, special attention is given to the pursuer and the defender. The optimal defender strategy for keeping the pursuer in its WEZ for the maximum amount of time is found when the pursuer is constant speed and non-maneuvering. In Scenario 5, the results of Scenario 4 are extended to include the evader. In this scenario, the evader is assumed to be non-maneuvering, the pursuer aims to capture the evader in minimum time, and the defender aims to keep the pursuer in its WEZ for the maximum amount of time. In Scenario 6, the results of Scenario 4 are extended from the 2-D Cartesian plane to 3-D Cartesian space.

Table 1. Research Scenario Matrix

Scenario	Pursuer	Evader	Defender	2-D/3-D	Defense
1	PN	OCP	PN	2-D	Kinetic
2	DG	Const.	DG	2-D	Kinetic
3	DG	Const.	DG	3-D	Kinetic
4	Const.	N/A	OCP	2-D	Directed Energy
5	OCP	Const.	OCP	2-D	Directed Energy
6	Const.	N/A	OCP	3-D	Directed Energy

Research Scope and Assumptions.

The scenario which is considered in this research is that of the defense of a single HVAA teamed with a cooperative defender against a single threat. This generalized engagement involves a total number of three agents. At the onset of the scenario, aircraft are considered to be in motion at their respective altitude and velocity.

The consideration of an effective HVAA defense requires development of meaningful models. A common assumption for long range scenarios where agents are considered Beyond Visual Range (BVR) is to consider the engagement in 2-D rather than 3-D. By reducing the solution space to 2-D the assumption is made that the relative altitude difference between agents is small compared to their range. This assumption is commonly made to reduce the computational complexity of the added third-dimension and allow for planar geometry to be utilized. Additionally, one may model agents using simple motion. This model allows agents to turn instantaneously and is a common assumption in differential games [9]. Simple motion is often used when turn radii of agents is small relative to the spacing between agents. Simple motion models are more common in literature because analytic expressions for optimal strategies are less common under turn rate constraint. In general, the use of turn rate constraints requires solutions to be obtained numerically rather than analytically. In this work, Chapter III describes the mathematical methods and models used to pose and solve the HVAA defense scenarios of interest.

Differential game theory distinguishes between games of kind and games of degree [9]. A game of kind is one where the objective is to find the domain of strategies or initial conditions where a specific player wins or loses the game. A couple of examples of this are: *Was the evader captured by the pursuer, or was the evader able to escape?* and *Where should a player begin in order to guarantee that he wins or loses?* Games of kind are concerned with the outcome of an engagement, whereas games of degree

are concerned with how well an objective has been achieved. Some examples of a game of degree include: *Assuming one of the players wins the game, how fast can that player win?* or *Assuming that a player loses the game, how can that player minimize their loss?* The scope of this work is restricted to solving games of degree. Identifying the space of initial conditions of all agents which ensure successful defense is considered as future work.

Obtaining insight into the defense of a HVAA using mathematical models requires the abstraction of physical systems into tractable models. This abstraction of physical systems commonly involves assumptions of those physical systems. Common assumptions include factors such as modeling fidelity, sensor measurement models, communication integrity between agents, and governing guidance strategies. Considerable effort is required to develop numerical models which address each of these factors. Because the focus of this work is to gather intelligent conclusions about the actions taken by the pursuer, evader, and defender, the development of accurate high-fidelity systems is outside the scope of this work. Rather, simplified 2-D and 3-D models are used to analyze the optimal strategies of multi-agent problems. It is assumed that optimal solutions are representative of their high-fidelity counterparts.

In order to simplify the models, it is assumed that all sensors produce perfect measurements, hence sensor noise is neglected. While this is not realistic, because real systems make measurements which involve uncertainty, it is not the goal of this work to model or accurately represent measurement or process uncertainty in this work. Further, the idea of limited communication between agents is also not addressed; messages between agents are assumed to arrive frequently and reliably. Scenarios involving restricted communication, although interesting, fall outside the scope of work.

It is the focus of this work to consider differential games, where the strategies

of agents are not predetermined. However, in some cases, the guidance strategies of players may be assumed to solve problems using optimal control theory. The single agent optimal control problem may be used to gather insight into the optimal behavior of a single agent and is, in general, more tractable than solving differential games.

Considering a kinematic level of modeling, the mass of individual agents is not considered, only their orientation and position in space are considered. The states and equations of motion for all agents are described in each control problem, whether 2-D or 3-D.

For the directed energy scenarios, circular and spherical regions are used. This model assumes that the directed energy weapons are assumed to be effective in all directions, independent of vehicle orientation. The spherical and circular models also assume that the directed energy weapons are effective inside a specified range and ineffective, otherwise.

1.4 Research Methodology

There exist multiple approaches for solving optimal control problems. These approaches are typically classified as either direct or indirect methods. The indirect method aims at solving optimal control problems by finding the states and co-states which in-turn define the optimal control. The general approach for posing and solving indirect optimal control problems involves utilizing the Hamiltonian, forming co-state equations, and leveraging Pontryagin's Minimum Principle (PMP) for scenarios involving constraints [10, 11, 12]. The direct method solves optimal control problems by utilizing nonlinear programs to iteratively search for the optimal control and state trajectories directly [13, 14, 15, 16, 17, 18].

In order to solve differential games, the utilization of analytic methods described in [9] provide a means of posing and solving differential games. While there exist meth-

ods of posing and solving optimal control problems directly using nonlinear programs, less common are methods of computing differential games directly. Differential games strive at locating a saddle-point strategy corresponding to optimal performance from multiple players. Using the methods described by Isaacs [9] and direct transcription methods [18, 19], various HVAA defense scenarios are posed and solved in this work.

1.5 Expected Contributions

The expected contributions for this research effort are as follows:

1. Solutions to HVAA defense optimal control problems and differential games
2. Optimal strategies for providing successful defense of a HVAA using either a kinetic or directed energy weapon
3. A comparative study of direct methods for finding optimal strategies for HVAA defense focusing on methods suitable for hardware implementation
4. Provide tools for mission analysis concerning HVAA defense, remote sensing, and pursuit-evasion

Combined, these contributions provide the necessary analytical foundation for the autonomous defender whose mission is the defense of the HVAA.

1.6 Document Outline

This dissertation contains six chapters. In Chapter I, the motivation of solving optimal HVAA defense problems is provided including the research questions, tasks, scope, and methodology. Chapter II provides a literature review for multi-agent differential games highlighting relevant work to HVAA defense. Also in Chapter II is a section which describes the research gaps and how this work addresses the gaps in

literature. Chapter III describes the methodology and techniques used for the proposed research, followed by the solution approach for each research task. Chapter IV presents the optimal strategy for defending a HVAA when doing so with a kinetic weapon.Chapter V presents the optimal strategy for defending a HVAA when doing so with a directed energy weapon. Finally, in Chapter VI, a summary of remarks, the contributions made, and identified future work are provided.

II. Literature Review

> The only thing greater than the power of the mind is the courage of the heart
>
> — John Forbes Nash Jr.

2.1 Introduction

This chapter includes an in-depth literature review of multi-agent pursuit-evasion as it relates to optimal HVAA defense. First, this section begins with outlining seminal work in the area of differential games highlighting important contributions and potential applications. Following this, a taxonomy of pursuit-evasion differential games is discussed: one-on-one (1v1), N-pursuers-1-evader (Nv1), 1-pursuer-M-evaders (1vM), N-pursuers-M-evaders (NvM), the active target defense differential games (ATDDG) with at least three players, and ISR in an optimal sense as it relates to directed energy defense. A more descriptive difference between differential game theory and optimal control theory is presented in Chapter III.

2.2 Seminal Work

The development of differential games started with the works of Isaacs [20, 21, 22, 23, 24, 9]. In these publications, Isaacs outlined the idea of posing problems governed by differential equations in a dynamic game-theoretic framework; he called this paradigm "Differential Games". In his seminal treatise [9], Isaacs employed the principles of game theory, calculus of variations, and control theory, albeit unknown to him, to solve problems involving a dynamic conflict between multiple agents/players [9]. Isaacs used the method of differential dynamic programming and introduced critical mathematical constructs such as dispersal, universal, and equivocal surfaces

used to describe the optimal flow field in games and derive optimal saddle point strategies.

It is important to recognize some of the founders of static/dynamic games and optimal control including RAND scientists such as Richard E. Bellman, Leonard D. Berkovitz, David H. Blackwell, Melvin Dresher, Wendell H. Flemming, and John F. Nash. Early contributions on dynamic games in the former Soviet Union were published by N. Krasovskii, A. Melikyan, L. S. Pontryagin, and A. I. Subbotin [25]. Furthermore, the first conference dedicated exclusively to dynamic games: "First International Conference on the Theory and Applications of Differential Games" in Amherst, MA, September 29-October 1, 1969, was organized by Ho and Leitmann. Isaacs, Berkovitz, Bernhardt, Blaquiere, Breakwell, Case, Friedman, Merz, Pontryagin, and Shubik were among the invited speakers at the conference. Although Pontraygin was not able to attend the meeting, these mathematicians and scientists planted the seeds of the theory of optimal control and differential games.

Of the large number of mathematicians and scientists that were involved in the development of differential games, Rufus Isaacs, Richard Bellman, John Breakwell, and Lev Pontryagin can be seen as principal contributors to the development of the theory of differential games; Isaacs being the father of differential games. His seminal work and his book, with motivating examples, highlight the possible use of differential games [20, 9]. Bellman, known for the method of dynamic programming, provided a tool whereby state feedback optimal strategies could be directly obtained as opposed to methods based on necessary conditions as in the calculus of variations [26, 27]. Pontryagin, a Soviet mathematician, is recognized as developing his Maximum Principle, more commonly referred to as, "Pontryagin's Minimum Principle" (PMP). The use of PMP was developed to assist with satisfying the necessary conditions for optimal control in the presence of hard constraints on control. Using methods derived

by these four mathematicians, differential games were formulated and solved in many works to be described throughout this survey.

2.3 Pursuit-Evasion

At the center of differential games lies the fundamental conflict of two parties known as "Pursuit-Evasion". Pursuit-evasion involves at least two agents or groups, labeled pursuers and evaders. The goal of a pursuer is to capture evading agents, while the converse is the goal of an evader, to avoid being captured by a pursuer. This is a zero-sum game where the cost/payoff is the time-to-capture. Basic questions arise, *What path should an evader or pursuer take to achieve their goal of avoiding or ensuring capture; and, under optimal play, by either pursuer or evader, is capture at all possible?* In this chapter, this conflict is briefly discussed and the current literature available describing strategies, methods, and applications as they relate to optimal HVAA defense is presented. For a more complete review of differential games, great historical documentation and literature surveys of Isaacs' work is documented in [25, 28].

The idea of pursuit-evasion differential games is not limited to physical entities chasing after one another; Isaacs defined kinematic equations that described the surfaces upon which states were constrained. Using these differential equations, one can propose problems in a multitude of research areas including but not limited to economics, sports, robotics, and air-combat. This survey focuses on differential games involving pursuit-evasion. It is important to note that the applications of these mathematical tools are not limited to simple toy problems, rather they serve as a syllogism for more complex scenarios that may not be suitable for the public domain.

2.4 One Pursuer, One Evader Differential Games (1v1)

The premise of a differential game starts with the conflict between two players who share a common performance functional; the goal of the pursuer and evader are counter to one another, where one tries to maximize the performance functional/payoff and the other tries to minimize the cost or payoff. These are minimax problems, that is, zero-sum-games, since an optimal solution is one in which one player's strategy strives to minimize the performance functional while the other aims to maximize the same performance functional. Constraints on the player's come in the form of dynamics. These constraints can be linear or nonlinear. The classical problem of pursuit-evasion can be seen in an early work by Ho, Bryson, and Baron [29]. In their work, a two-player differential game was formulated in a Linear-Quadratic form to capture the basic pursuit-evasion conflict. Later, in the NASA technical report of [30], differential models were employed in order to gauge the differences in performance between a manually piloted vehicle and an optimally controlled one as provided in the earlier work [29]. The experiment showed that the use of differential games indeed provided useful information to pilots, but a cautionary statement at the end of the technical report stated that, "...differential game problems will, in general, be more complicated theoretically than their optimal control counterparts." The NASA report concluded that the idea of solving differential games was thought to be useful as information provided to a pilot, but not yet accepted to be a means of automatic control, a popular research topic today.

In a dissertation by Satimov [31], the application of differential games was envisioned for use in various fields such as economics and military operations. Satimov also stated that in the case of a single-player, differential games amount to optimal control problems, and that different modifications of Isaacs' method give the necessary and sufficient conditions for optimality. The relationship between optimal control

and differential games is through the use of variational techniques [9, 12]. If all but one of the player's control laws are given, the differential game reverts to a one-sided optimal control problem.

Homicidal Chauffeur Differential Game.

In his seminal text, Isaacs proposed the famous "Homicidal Chauffeur" toy problem [9]. In this game, a hypothetical slow but highly maneuverable holonomic pedestrian is pitted against a driver of a motor vehicle that is faster but less maneuverable (a.k.a. a Dubins Car). In this somewhat macabre scenario, the driver attempts to run over the pedestrian. The question to be solved is: Under what circumstances, and with what strategy, can the driver of the car guarantee that he can always catch the pedestrian or conversely, the pedestrian guarantee that he can indefinitely elude the car. And, if the pedestrian's demise is guaranteed, what is the chauffeur's optimal strategy that will minimize the time-to-capture of the pedestrian, and what is the latter's strategy to maximize his time? Surveys have documented the history and notable work related to the "Homicidal Chauffeur Differential Game" [32, 25, 33, 34], going into detail and expanding about the various aspects of this problem. Figure 1 shows the geometry of the Homicidal Chauffeur game where the pursuer, P, has a minimum turn radius specified by R and the evader, E, can maneuver freely. Figure 1 also includes a plot of the performance functional which is the solution of the differential game. Constant-value lines are shown on the x-y plane.

A definitive work on the Homicidal Chauffeur differential game is Merz's Ph.D. thesis [35]. Merz investigated the Homicidal Chauffeur differential game in great detail describing two new singular lines known as: "switch envelope" and "focal line." These new lines further expand on Isaacs' "barrier", "universal", and "equivocal" singular lines. His work gives great detail and insight into the problem. Breakwell

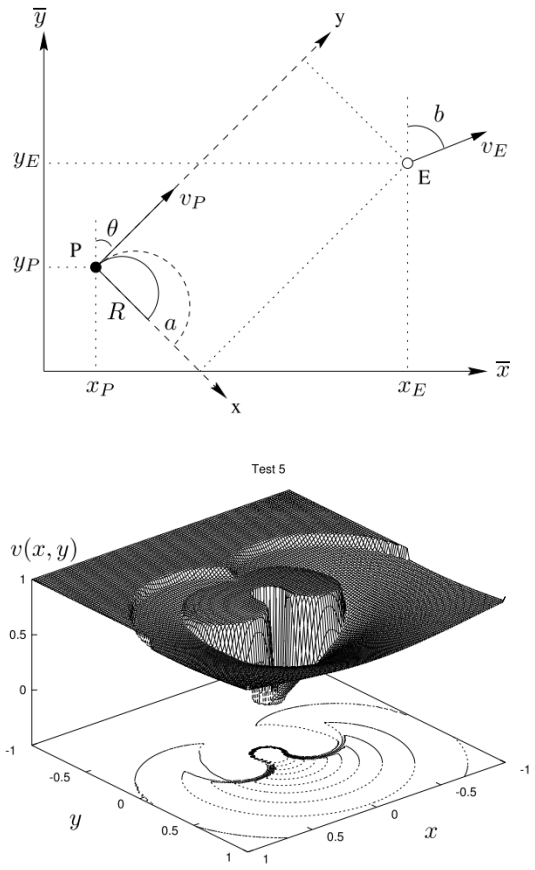

Figure 1. A coordinate frame and performance functional describing the Homicidal Chauffeur problem [34]. The Pursuer, P, had minimum turn radius specified by R.

and Merz helped motivate the complete solution of the Homicidal Chauffeur game at a conference in 1969 [36]. Marchal also studied the Homicidal Chauffeur game in great detail describing how using Pontryagin's Minimum Principle could assist the interpretation of complex solutions [32].

The Differential Game of Two Cars.

A variation of the Homicidal Chauffeur differential game is the differential game of two cars, where two players, each controlling a car with minimum turning radius, are engaged in a pursuit-evasion game. In early work, Meier investigated the game of two cars, where both players had the same minimum turn radius, the pursuer was

slower than the evader, and capture was defined by coming inside the range, l, of the evader [37]. Another analysis of the game of two cars was performed by Getz and Pachter [38, 39]. In their papers, regions of capture, escape, and barrier surfaces between those regions were presented. Figure 2 describes the geometry of the game of two cars. Radius R_1 and R_2 describe the minimum turning radii of each player, u_1 and u_2 describe the curves associated with a max rate turn, and w_1 and w_2 describe each player's velocity.

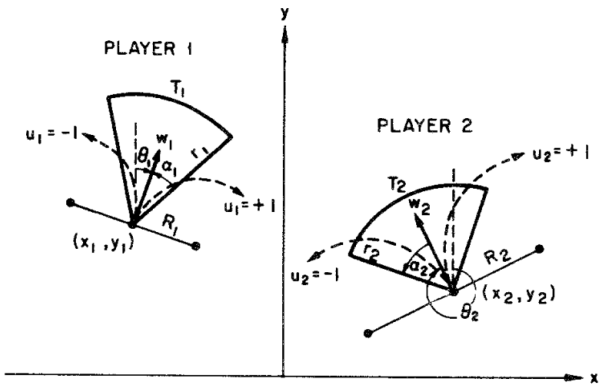

Figure 2. The coordinate frames and turning radii used to describe the game of two cars [38] is shown. The minimum turning radii of each player is labeled R_1 and R_2, the curves associated with a max rate turn are labeled u_1 and u_2, and the players velocities are labeled w_1 and w_2. © 1981 Springer Nature

In [38] both agents have sector based regions of capture, typical of an aerial dogfight; but, in [39], the regions of capture were different, describing a heterogeneous model of on-board weapon systems. Similarly, in [40], Greenfield looked into the game of two cars, endowing the pursuer with a surveillance capability of range, l. The objective, to escape the surveillance region in minimum time. In an earlier work, Lewin investigated a similar differential game called the "Surveillance-Evasion Differential Game" [41]. In the game, the evader strives to escape as soon as possible from the pursuer's detection circle, while the pursuer's desire is the opposite. Rather than consider point capture, Greenfeld and Lewin were interested in surveillance range.

A complete analysis performed by Bera, Makkapati, and Kothari goes into detail of both games of kind and degree with studies on differing agents' speeds, capture radius, and maneuverability constraints [42]. In their work, they develop the three-dimensional plots of the state space, highlighting the barrier and switching surfaces for the different scenarios.

Pursuit-Evasion in Constrained Environments.

In an effort to consider differential games in a more realistic way, the introduction of boundaries and constraints on states allows for finite spaces and regions to be included in the game formulation. By imposing limitations on physical states, the pursuit-evasion differential game can be restricted to a bounded area or obstacles may be applied. In a paper by Fisac and Sastry [43], a two-player differential pursuit-evasion game is proposed where an obstacle is added to delay the pursuer's capture or avoid it entirely. Similarly, Oyler, Kabamba, and Girard considered pursuit-evasion games in the presence of obstacles that inhibit the motion of the players [44]. In their work, the use of polygons, line-segments, and asymmetric obstacles (an obstacle that affects one player differently than another) are developed. Fuchs and Khargonekar motivated the use of escort regions through manipulation of the performance functional [45]. Kalyanam, Casbeer, Sundaram, and Pachter constrained their pursuer and evader to road networks [46]. In another work, a one-sided constraint is imposed where the pursuer is not restricted to a road network, while the evader is [47].

Pursuit-Evasion with Insufficient Information.

In cases where one or more agents do not have complete information about the state of the game, these are problems called differential games of "Insufficient Information." In his seminal work, Isaacs stated that the ability to pose problems

which restricted information to the individual players "...appears to be the most vital area for future research" [9]. Roxin and Tsokos, introduced stochastics as a means of modeling partial information that one agent might have relative to another [48]. Chernousko and Melikyan described a differential game where incomplete information is provided to one of the agents [49]. This idea was proposed in order to account for information delay or gaps of information during game play. Yavin proposed an incomplete information pursuit-evasion differential game by restricting the pursuer's information on bearing and allowed the evader to have perfect information in the engagement [50]. Giovannangeli, Heymann and Rivlin tackled the problem of pursuit while avoiding convex obstacles by using Apollonius Circles to provide paths in which the pursuer's visibility of the evader is guaranteed throughout the engagement [51]. In [52], Hexner considered the problem where a parameter is unavailable to only one player at the beginning of the game, and the other has only a probability density function that describes the parameter. Pachter and Yavin investigated the effects of noise on the Homicidal Chauffeur problem by introducing stochasics to the pursuit-evasion differential game dynamics [53]. Battistini and Shima also employed a stochastic variable to overcome the limitations imposed by bearing-only measurements made by a pursuer [54]. Using a Kalman filter a performance functional is used which maximizes observability of the evader. Their Monte-Carlo simulations show that the maximum observability functional outperforms a minimum range objective cost functional in the successful pursuit of an evader under uncertainty.

Basimanebotlhe and Xue also employed stochastics to study the optimal control in a differential game with nonlinear stochastic equations where two players are subjected to noisy measurements [55]. Lin, Qu, and Simaan presented an N-pursuer-1-evader differential game where the evader can observe all the pursuers but the pursuers have limited observations of each other and the evader [56]. Kalyanam, Cas-

beer, Sundaram, and Pachter investigated a pursuit-evasion game where a pursuer engaged an evader through using Unattended Ground Sensors (UGSs) that detect the evader's passage in a road network; when the pursuer arrives at an instrumented node, the UGSs inform the pursuer if and when the evader visited the node [47, 57, 46].

Pursuit Evasion in Aerial Engagements.

Applications of pursuit-evasion differential games relating to tactical air-to-air applications have been investigated. Shinar and Gutman developed a closed-form solution to a 3-Dimensional missile-aircraft pursuit-evasion game [58]. Shinar also investigated a realistic pursuit-evasion engagement involving a missile engaged on an aircraft and air-to-air scenarios using variational methods [59]. Shinar concluded that, although the work was done in the plane, the move to 3-D should not present much difficulty. Hillberg and Chalmers investigated a pursuit-evasion game between two realistic aircraft in a dogfight. They took into account constraints such as structural limits and aerodynamic stall, and used the air-vehicle's separation distance as a metric for optimization. Considering naval applications, Pachter and Milch framed their two-player engagement as a Homicidal Chauffeur differential game where the dynamics of the ships are taken into account [60]. Greenwood developed a realistic differential game in 3-dimensions by modeling fighter aircraft [61]. Greenwood used the dynamics of two fighter aircraft in space and even considered firing envelopes as part of his analysis. Ehtamo and Raivio considered a numerical approach to solving a pursuit-evasion differential game involving a missile-aircraft encounter [62]. Imado and Kuroda proposed a differential game involving a pursuit-evasion engagement involving a missile and an aircraft. In the game formulation, the miss-distance was used as a payoff/cost functional [63]. Shinar, Glizer, and Turetsky, investigated a pursuit-evasion game where the dynamics of the pursuer can be changed during the

pursuit a finite number of times [64]. In [65], the evader has the ability to change its dynamics during the engagement a finite number of times. Merz investigated the problem of pursuit or evasion selection if both agents were endowed with capture sets and the prior assignment had not been implemented [66]. Related to dog-fights and aerial combat, Merz's concern was with role assignment in pursuit-evasion differential games and of course the outcome. In more recent work, Garcia, et al. have investigated target area defense differential games described in more detail in Section 2.8.

Other 1V1 Works.

The Homicidal Chauffeur problem is an example of a pursuit-evasion game with turn constraints imposed on the pursuer. Games where both players have simple motion kinematics (holonomic) are also of interest. One such scenario involves the interception of one ship by another. Given two ships of constant speed the question becomes: *What heading should the pursuer take to close in on his target fastest.* The solution can be found using basic geometry [67]. Figure 3 shows the application of Apollonius Circles to a three-body engagement [68].

Another example of posing the pursuit-evasion problems using simple motion kinematics in a differential game is in a work by Leitmann [69]. In his paper, a simple differential game between a pursuer and evader was proposed, and variational techniques were applied to determine outcomes of the game where terminal miss distance was used as the payoff/cost functional.

In [70], Calise and Yu use simple motion kinematics as well as expanded control energy to formulate a game involving the pursuit-evasion of two aircraft at medium to long range. Using a reduced-order model based on control energy, Calise and Yu are able to find trajectories similar to minimum time intercept using only four states to model the encounter.

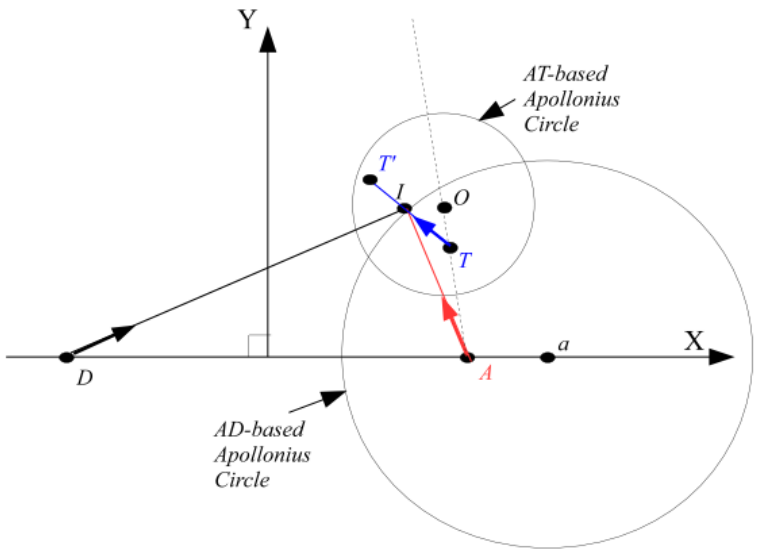

Figure 3. The use of an Apollonius Circle to pursuit-evasion differential games described in [68]. In this example, the attacker, A, defender, D, and target T have constant velocity motion with fixed headings. © 2015 IEEE

The "Lion and the Man" differential game discussed by Quincampoix is a pursuit-evasion differential game where the lion pursues a man [71]. The lion and the man are free to change their velocity direction instantaneously but are limited to the intensity with which they do so. Since the lion is faster than the man, the regions of escape and capture are of interest and were numerically determined.

2.5 N Pursuers, 1 Evader (Nv1)

The two-pursuer-1-evader problem had been well documented [72, 73, 74, 75, 76, 77, 78]. Hagedorn and Breakwell investigated two pursuers engaging one evader which was required to pass between the two pursuers [72]. Pashkov, Terekhov, and Levchenkov considered the game of degree by employing as a payoff/cost functional: the distance between the object being pursued and the pursuer closest to it, when a fixed-time engagement terminates [73, 74]. Others such as Ganebny, Kumkov, Le Menec, Patsko studied the three-player game in detail by briefly discussing the

surfaces of the differential game when pursuers were both stronger, both weaker, and one stronger-one-weaker than the evader [75]. In their paper, Garcia, Fuchs, and Milutinovic study the case where faster pursuers cooperate to capture a slower evader in minimum time [77]. The evader, knowing that it is being pursued by two cooperative pursuers, tries to maximize the capture time, while the pursuers aim to minimize capture time. A solution of this differential game is determined based on the geometric properties of the game. Unlike previous work, Kalyanam, Darbha, Khargonekar, Pachter, and Chandler set up a problem of two pursuers and one evader in a restricted environment (grid road network); moreover, the pursuers do not have direct knowledge of the location of the evader [76]. The two pursuers, instead are notified, when they reach a node if the evader had passed through that node or not. Hayoun and Shima restrict the pursuer's controls to be bounded and their intercept times equal [78]. Using two "strong" pursuers, closed-form optimal controls are derived, and it is shown that the addition of a second pursuer introduces a new singular zone to the game space in which the pursuers can guarantee equal misses, regardless of the evader's actions.

In the more general case, where there are N-pursuers and 1-evader, challenges with task allocation and strategy become more apparent. To aid the task allocation between the N-pursuers, Huang and Bakolas employ the Voronoi diagram construct. It is often used when capture of an evader within a bounded domain is considered [79, 80]. In their work, Borowko and Rzymowski present sufficient conditions for the existence of an evasion strategy where simple motion kinematics for the players is considered [81]. Chodun investigated a more general of N-pursuers engaged against one evader in his work [82]. Huang et al. employed a decentralized control scheme based on the Voronoi partition of the game domain, where the pursuers jointly shrink/minimize the area of the evader's Voronoi cell [79]. Figure 4 is a visualization of the

individual pursuer cells from [80].

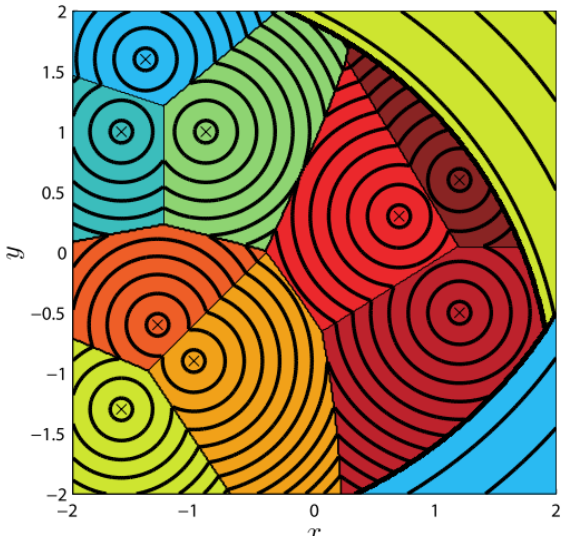

Figure 4. A Voronoi Diagram [80] describing the task allocation in an N-pursuer-1-evader problem. Each color describes a cell from which a pursuer would capture an evader if starting in that cell. © 2010 IEEE

Ibragimov, Salimi, and Amini investigated the N-pursuer-1-evader problem in their work by focusing on guaranteed escape of the evader [83]. Alias, Noorsuria, Ramli, Ibragimov, and Narzullaev imposed controls constraints on the players and allow for the speed of the players to vary up to a maximum speed of 1 [84]. In their paper, they focus on the game of degree by briefly discussing the estimation of the time to capture. Kothari, Manathara, and Postlethwaite considered identical non-holonomic players [85]. In their work, they find that "solving such a problem is computationally intractable," and instead propose a computationally efficient algorithm to obtain approximate solutions. Next, Awheda and Schwartz and separately Al-Talabi developed solutions to the multi-pursuer single-superior-evader pursuit-evasion differential game using fuzzy logic methods [86, 87]. In Aweheda [86], the formation control mechanism guaranteed that the pursuers were distributed around the superior evader in order to avoid collision between pursuers and guaranteed that the capture regions of each pair of adjacent pursuers were such that the capture of the fast evader was guar-

anteed. VonMoll et al. also have considered multiple pursuers engaged on a single evader [88, 89, 90]. By utilizing the Apollonius Circles, they exploit the benefits of cooperation amongst the pursuers in order to reduce the capture time of the evader.

2.6 1 Pursuer, M Evaders (1vM)

The single pursuer against M-evaders differential game is a game where a pursuer tries to capture M-evaders in finite time. One challenge is to select the order in which the pursuer accomplishes his task in minimum time. In, these problems the pursuer is faster, more maneuverable, or has other advantages over the evaders.

The case which involves two evaders and one pursuer has received much attention [91, 92, 93, 94, 95]. Fuchs, Khargonekar, and Evers investigated the case where a single pursuer engages two evaders [91]. The goal of their work was to investigate a differential game where the pursuer tries to capture either of the evaders, minimizing its cost, and the evaders strive to escape the pursuer for as long as possible, increasing the payoff/functional of the pursuer. Fuchs and Khargonekar also investigated the manipulation of payoff/cost functionals to achieve attacker retreat through defender cooperation [92]. With one pursuer and two evaders they show that under certain conditions, the defenders should cooperate with the attacker so that retreat becomes the most attractive option; thereby, fulfilling the defensive goal of protecting the high-value target. Scott and Leonard investigated a scenario where two evaders employ coordinated strategies to evade a single pursuer, but also to keep them close to each other [93]. In [94], Breakwell and Hagedorn investigated the capture of two evaders in succession by one pursuer in minimum time. Pachter and Yavin proposed a differential game of pursuit-evasion with one pursuer and two evaders, the motion of the players being affected by noise [95]. In their work, a stochastic game of degree is considered, where the pursuer strives to maximize the probability of his winning the game, i.e.,

of capturing at least one of the evaders. A 3-Dimensional pursuit-evasion differential game consisting of a pursuer engaged against a team consisting of two evaders was proposed by Abramyants, Maslov, and Yakhno [96]. The team of evaders consisted of a true evader and false decoy evaders; the evaders coordinate their actions to ensure the true evader escapes without capture.

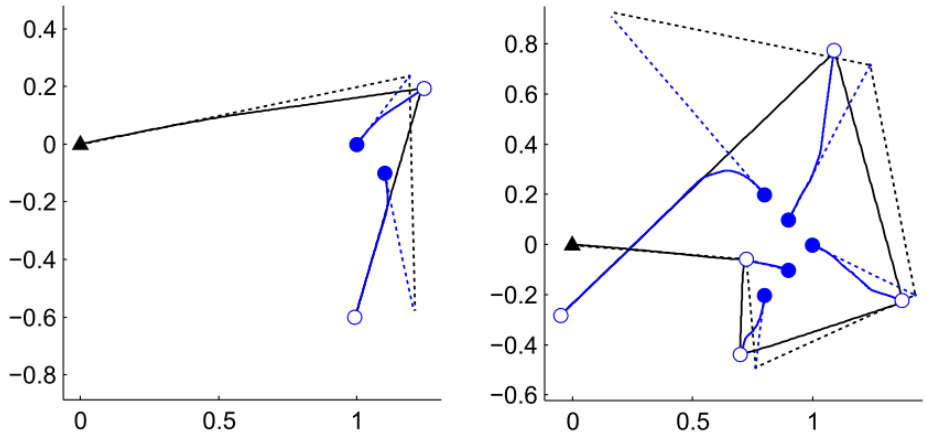

(a) 2-evader case (b) 5-evader case

Figure 5. Example of 1-pursuer-2-evader engagement and 1-pursuer-5-evader engagement found in [97]. Since the pursuer is much more capable than the evaders, capture of all agents is guaranteed. © 2013 IEEE

In a more general case of one pursuer engaged against many evaders, the pursuer aims at capturing all evaders, while the evaders coordinate their escape. Liu and Zhou investigated a game involving a single-pursuer-multiple-evader pursuit-evasion game where a superior pursuer attempts to minimize the total capture time of all the evaders [97]. In Figure 5 the capture of M-evaders in succession is shown [97]. Scott and Leonard motivated a model of pursuit, herding, and evasion for three agents [93]. In their work, a single pursuer, e.g. a bear, chooses a target point along the line connecting two evaders, and the two evaders, e.g. a mother caribou and her calf, each choosing a strategy that trades-off evasion and herding. In [84] the study of capture time for many pursuers against one or more evaders is investigated. Wang

and Peng formulate and solve a pursuit-evasion game in which a single faster player chases several homogeneous evaders [98]. In their work, they apply a task allocation method to simulate the optimal engagements for "fixed sequence capture" and "free sequence capture" of the pursuer.

2.7 N Pursuers, M Evaders (NvM)

The most general case of N-pursuers and M-evaders allows for more complex engagements to be analyzed. Katz et al. investigated a zero-sum differential game formulation for the control of military air operations using the method of characteristics [99]. Although their examples were shown for 1-pursuer 1-evader, their work has extensions to N-pursuer M-evader problems. Rusnak proposed a dynamic game called "The Lady and the Body-Guards versus the Bandits" [100]. The Bandits team's objective is to capture the Lady while the Lady and her Body-Guards objective is to prevent it. The Body-Guards are trying to intercept the Bandits prior to their arrival to the proximity of the Lady. In [100], the formulation and solution of the game is presented. As described in Section 2.8, this problem is a similar problem, but with more players involved. A creative approach to handling the task allocation of many agents was proposed by Bakolas and Tsiotras by employing the Voronoi diagram construct [80]. Using the Voronoi diagram, such that a pursuer residing inside a given set of partitions can intercept a moving target faster than any other pursuer outside the set. Another means of task allocation was proposed in [101] where Awheda and Schwartz proposed a fuzzy logic based decentralized control scheme using the Apollonius Circles construct.

2.8 Active Target Defense Differential Games (ATDDG)

Target Defense Differential Games (TDDG) are recently introduced pursuit-evasion differential games with three agents. A target (T) is pursued by an agent called the Attacker (A). A third player, the defender (D) pursues A in order to defend T. T and D cooperate while playing against A. The outcome of the three-player game is simple: If D captures A before A captures T, then the target is successfully defended; however, if A captures T before D can capture A, then the defense is unsuccessful and A is the winner. When the target is able to maneuver in the three-player game and this scenario is known as the Active Target Defense Differential Game (ATDDG). Figure 6 describes the geometry used to describe ATDDGs [102, 103].

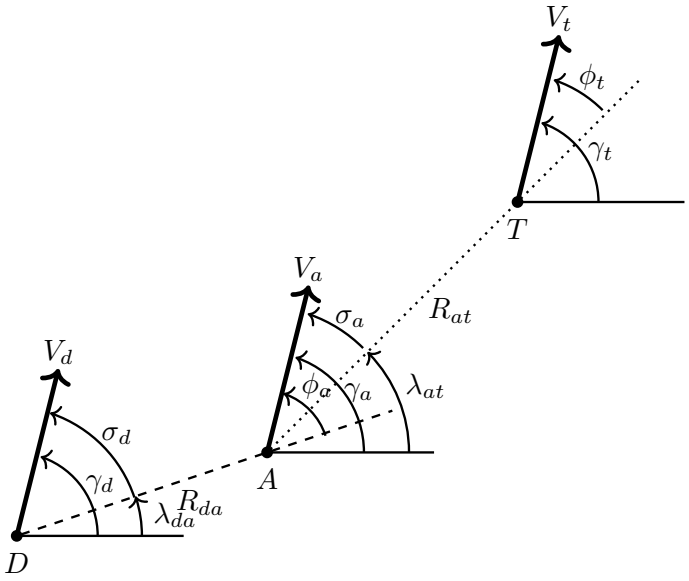

Figure 6. Defender-Attacker-Target Geometry describing the Active Target Defense Differential Games where the defender pursues the attacker who pursues the actively maneuvering target [102, 103].

There exist a number of popular performance metrics that are used when posing the ATDDG. In games of kind, the interest lies with the outcome of the defense: does the target succeed in evading the attacker or is it captured? In games of degree, when the target escapes, the range from the attacker to the target at the instant when the

attacker is intercepted by the defender is used. When the target is captured by the attacker, the distance between the defender and the attacker at the instant of capture of the target by the attacker is used. These range metrics are popular because they help to quantify the outcome of the engagement and are readily computed. Other metrics, such as time to capture, are also of interest.

The two-players one target game of [104] is an early version of target defense. In the paper, a two-player differential game is played wherein one of the players wants the state of the system to reach a target, while the other player wants the state of the system to avoid this target. Introduced by Boyell, the defense of a ship from an incoming torpedo using a counter-weapon was described [105, 106]. Yamasaki and Balakrishnan proposed the defense of an active target by launching a defensive missile [107, 108]. In their work, they proposed a closed-loop feedback control law to defend a target aircraft. Using simple motion kinematics, Pachter, Garcia, and Casbeer consider a zero-sum three-agent pursuit-evasion differential game [67]. The two-agent team consisted of the target and defender.

Rubinsky and Gutman presented an analysis of the end-game ATDDG scenario based on the attacker-target miss distance for a non-cooperative target-defender. The authors develop linearization-based attacker maneuvers in order to evade the defender and continue pursuing the target using the LQ paradigm [109, 110]. Rusnack, Weiss, and Hexner had also analyzed the ATDDG. In their work, the limiting values of the three participants optimal strategies are studied as the quadratic weight on the defending missiles acceleration command were reduced to zero [111]. They show that in the limit, the intercepting missiles and the target's optimal strategies are identical in form to that obtained in the game without the defending missile. Ratnoo and Shima's work includes a game theoretic analysis of the ATDDG problem using conventional guidance laws for both attacker and defender [112, 113]. The cooperative strategies

proposed by [114] allowed for a maneuverability disadvantage of the defender with respect to the attacker and the results show that the optimal target maneuver is either constant or arbitrary depending upon the missile-defender zero-effort-miss distance state variable. Shafermen and Shima implemented a Multiple Model Adaptive Estimator (MMAE) to identify the guidance law and parameters of incoming missiles and optimize defender strategies to minimize the control effort [115]. Earl and D'Andrea present a scenario where multiple agents defend a common target from a group of pursuers [116]. Earl and D'Andrea commented that the task assignment of defending agents was "...most difficult to solve when the capabilities of the adversaries are comparable." Sun, Chen, Qi, and Lin investigated the three-agent game using zero-effort-miss (ZEM) [117].

The team involving Casbeer, Fuchs, Garcia, Pachter, Pham, Von-Moll, and Weintraub have investigated the ATDDG in great detail [67, 68, 118, 119, 120, 102, 103, 121, 122, 123]. Pachter, Garcia, and Casbeer analyzed the ATDDG using simple motion kinematics [67, 68]. In their work, they consider a three-player differential game which involves the defender engaged in the pursuit of the attacker, and the attacker engaged in the pursuit of the target, which is trying to evade the attacker. To find the optimal strategy for the defender to intercept the attacker, the geometric concept of the Apollonius Circle is used. In their analysis, they are able to look at the critical target/attacker speed ratio to ensure the target's survival. Figure 3 shows how these circles are used in the simple motion kinematics case [68].

Garcia, Casbeer, Pham, and Pachter continued their investigation for optimal maneuvers when the defender and attacker use Pure Pursuit and Proportional Navigation [118]. In [119, 120] Casbeer, Garcia, and Pachter considered the use of two defenders to better engage the attacker. Garcia, Casbeer, Fuchs, and Pachter investigated when the defender had a non-zero capture radius, and its effect on the simple

motion kinematics example in [122]. While in previous work, information between all players was shared, Weintraub, Garcia, Casbeer, and Pachter investigated the optimal evasion of the Target assuming the defender's and attacker's control laws were proportional navigation [102, 121]. Information was restricted to the attacker and defender, and heading rate constraints were imposed on the target. Later, in [103], an Extended Kalman Filter was used to investigate the same engagement with sensor models.

2.9 Directed Energy Defense

The Directed Energy Defense (DED) scenario considers the defense mechanism to be energy-based rather than kinematic. This differs from the ATDDG which aimed at solving the kinematic interception of an attacking agent in order to defend a target vehicle. The DED scenario considers three agents: the target, attacker, and defender. The goal of the defender is to keep the attacker inside its Weapon Engagement Zone (WEZ) of the defender for as long as possible before it reaches the target. If the attacker is in the WEZ for some predetermined amount of time, the attacker may be considered neutralized.

Similar to the DED scenario is the ISR mission of maximum observation. In the maximum observation problem, an ISR platform solves for the strategy which keeps a target within a connection range for the maximum amount of time. By utilizing the mathematical models for maximum contact time in an ISR problem, the maximum time exposure of a directed energy weapon can be posed and solved. Although energy-based defense is a means of removing enemy threats, few publications are available which address DED as a multi-agent control problem, motivating the inclusion of an ISR mission review.

ISR missions have been of great interest to the aerospace community [124, 125,

126, 127]. One goal of an ISR platform is the observation of a target, whether it be moving or stationary. The mathematics of maximum-time surveillance to DED assumes that the target in the surveillance problem is an attacking threat in the DED problem. The threat in the DED problem is mobile, and the goal is to keep the threat inside an envelope of a defender's WEZ for as long as possible. For an ISR mission persistent surveillance corresponds to observing the target for as long as possible; in the DED scenario, this amounts to keeping the target inside the WEZ for as long as possible.

The task of observation of slower ground targets by an aerial platform were considered in [128, 129, 130]. In [128], a quad-rotor utilizing a downward-pointing camera tracks a ground vehicle restricted to a road network. In [129], an ISR platform equipped with a gimbaled camera was considered, thus allowing the ISR platform to observe a ground target at various aspect angles. Similarly, Skydio, a startup company aimed at personal unmanned air platforms, has considered a quad-rotor aircraft for persistent surveillance of a mobile ground target [130]. The quad-rotor platform performs persistent surveillance and obstacle avoidance in order to record a designated mobile target.

Some examples of works that consider multiple ISR platforms that act in coordination, tasked with identifying a single mobile target are [131, 132]. In [131], sensor coverage effectiveness for a single mobile target and a group of mobile sensors was investigated. In their work, the authors showed the connection between the numbers of searchers, the amount of searcher motion, and how that trade-off was dependent on the amount of motion for the searcher relative to the target. In [132], the coverage of a mobile sensor network resulting from continuous movement of sensors was studied. In their work, the authors took a game theoretic approach and obtained the optimal mobility strategy for sensors and intruders.

Investigation of differential games concerning the surveillance of an evading agent were considered in [133, 134, 41, 135, 136, 137]. In these differential games a pursuer with a detection region was pitted against an evader whose goal was to escape as soon as possible. The differential game studied by Dobbie and Taylor considered a fast pursuer with turn restrictions and circular surveillance region against a slower maneuverable evader capable of instantaneous changes in heading [133, 134]. Different to Taylor's work, Lewin imposed a turning rate constraint on the pursuer and allowed the pursuer's speed to vary from full stop to a bounded maximum [41, 135]. Another differential game investigated by Fuchs involved a fast pursuer with a specific radar cross section pitted against a slower and less maneuverable evader [136]. In the game, the pursuer strives to accumulate enough information about the target to achieve a defined probability of identification while the evader tries to evade the pursuer to remain undetected.

In similar work, a numerical approach to solving the maximal information sharing between UAVs was presented in a work by Garnett and Flenner [138]. In their work, a model for maximal information sharing between UAVs was posed and solved utilizing optimal control. They assumed the ISR platform was faster than the targets being tracked and a polar function was utilized to model sensor effectiveness. Because of model complexity, they required the use of a nonlinear program solver to numerically find the optimal control that maximized the sensing problem.

While the previous works have described optimal means of conducting ISR missions when the ISR platform is faster than the target (evader), less common is the consideration of conducting ISR on targets that are faster. In an early work by Breakwell, a pursuit-evasion game was posed wherein a slower pursuer was employed against a faster evader [139]. Breakwell, also considered a nonzero capture radius for the slower pursuer. The approach taken by Breakwell solved for the acquisition of a

faster evader by a slower pursuer, but the DED scenario requires keeping the evader within the surveillance range, akin to a WEZ, of the pursuer for as long as possible in addition to acquiring it as soon as possible. To successfully protect the evader, the defender must neutralize the threatening attacker before it reaches the evader.

2.10 Research Gaps

This work addresses the defense of an evader from an attacking pursuer by teaming the evader with a defender. Two defense mechanisms are considered: Kinetic capture of the pursuer by the defender and maximal exposure of the pursuer by the defender's directed energy weapon.

Formulating differential games around aircraft were considered in Isaacs' seminal text [9]. To achieve the objectives of this work, meaningful mathematical models must be developed. Using kinematic models, aircraft are modeled in both 2-D and 3-D Cartesian space. Simple motion is often used when the turn radii of agents is small relative to the spacing between agents. In this scenario (small turn circle relative to vehicle range) it has been shown in [140] that optimal strategies assuming simple models provide a very similar performance when implemented in turning rate constrained vehicles. Simple motion models are more common in literature because analytic expressions for optimal strategies are less common under turn rate constraint. In general, the use of turn rate constraints requires solutions to be obtained numerically rather than analytically. In this work, Chapter III describes the mathematical methods and models used to pose and solve the HVAA defense scenarios of interest.

In their work, Garcia, Casbeer, and Pachter investigated an evader engaged by a faster pursuer using pure pursuit and defended by a similarly capable defender also using pure pursuit [121]. In their analysis, the evader's motion was not restricted to a maximum turn rate. Moreover, simple motion was considered in order to obtain

analytic and numeric solutions in [67, 68, 118, 119, 120]. To address this gap, one aim of this work is to include turn rate constraints for the evader in planar engagements.

A bulk of the research performed on the active target defense scenario assumes that the evader is free to travel in any direction to aid in its defense [67, 118, 141, 68, 142]. One aim of this work is to investigate HVAA defense with a non-maneuvering evader.

Previous work on the ATDDG considered defense to be through kinematic capture of the pursuer by the defender restricted to a plane, similar to long-range missile defense scenarios [105, 106, 67, 68, 118, 119, 120, 121, 122, 142, 143, 144, 111]. An investigation of optimal defense strategies for the active target defense scenario in 3-D Cartesian space is not found in literature. To address this gap, one aim of this work is to consider kinematic defense in 2-D and 3-D Cartesian space.

Many works have considered pursuit strategies for achieving maximum observability of an evader [41, 133, 134, 135, 136, 139]. By leveraging the work in this area, differential game theory, and optimal control theory, one aim of this work is to solve the active target defense scenario when the defender is endowed with a directed energy weapon.

Various indirect methods have been used for investigating the active target defense scenario in [105, 106, 67, 68, 142, 143, 144, 111]. A study of various direct optimal control methods to the active target defense scenario is not found in literature. To address this gap, one aim of this work is to compare various direct methods to the active target defense scenario emphasizing hardware implementation. The means of directly computing the optimal control for a specified system has been a popular research topic for the scientific community. In his survey paper, Betts [145] describes in great detail various methods of computing optimal control directly. Betts, goes into detail, describing various advantages and disadvantages of direct and indirect methods. Rao described four different direct methods in his survey including more

modern approaches of solving optimal control problems [19]. In Section 4.4, each of the direct methods described in Rao's survey are considered. The four direct methods include: Single Shooting Method [146, 11], Multiple Shootings Method [13, 14], Collocation Method [18], and Pseudospectral Method [147, 148, 149, 150].

2.11 Concluding Remarks

In summary, the research in pursuit-evasion differential games has been significant since the inception of Isaacs' work. By posing tactical scenarios, which involve multiple players as differential games, the optimal strategies for all players in the game may be achieved. This literature review has outlined a significant body of work in the area of multi-agent pursuit-evasion and has highlighted specific work in the active target defense scenario and work related to the directed energy defense scenario. Even though numerous works have investigated these tactical problems, these three-agent problems still remain open.

III. Methodology

> Nothing takes place in the world whose meaning is not that of some maximum or minimum.
>
> — Leonhard Euler

This chapter presents the methodology used to evaluate the problems presented in Chapter I. First, the various models used to mathematically describe aircraft are presented. Next, the methods of solving optimal control problems and differential games are described. After that, the Apollonius Circle is presented, emphasizing how the geometry may be leveraged to solve pursuit-evasion engagements. Then, a proposal of how geometric methods may be leveraged to transform the defense differential game into an optimal control problem. Next, the generalized kinetic defense and directed energy defense objectives are presented. Finally, a solution approach for solving each of the research questions is presented.

3.1 Overview

Investigating the optimal strategies for the successful defense of a HVAA, one must utilize mathematical models for the aircraft involved. The abstraction of real aircraft systems into a set of governing differential equations will be referred to as the *model*. Utilizing these models, several scenarios are posed which correspond to the kinetic and directed energy defense of a HVAA. This work aims to leverage geometric tools, such as the Apollonius Circle, to either solve or aid in the optimal solutions to the various engagements. When analytic solutions are intractable, the use of a Nonlinear Program (NLP) may be used to directly compute optimal strategies or control. The objective of this research is to develop optimal strategies for the aerial defense of a HVAA which are either kinetic or directed energy in nature.

3.2 Models

In this work, mathematical models are used to represent aircraft in space. In the case where aircraft are far from one another and are at relatively similar altitudes, a 2-D model with simple motion may be sufficient. While a high-fidelity model which considers every nuance of an aircraft in flight would be accurate and realistic, tractable closed-form solutions to optimal control problems which use high-fidelity models are unlikely. By considering kinematic models, the following benefits are seen:

1. The number of required states is dramatically reduced.
2. Visualization of the state space becomes easier.
3. Closed form solutions may become tractable.
4. Solutions to the optimal control problems may be computed very quickly.
5. Computed optimal solutions serve as great initial seeds to more complex optimal control problems which may be otherwise intractable analytically.

Vehicle Motion in Two-Dimensions.

When the range between aircraft and missiles are relatively large compared to their respective altitudes, the use of a 2-D model may be sufficient when analyzing aircraft guidance strategies. As previously mentioned, one advantage of posing pursuit-evasion scenarios in 2-D is that the number of states used to model the engagement is reduced. As a result of the reduced state space, the likelihood of finding optimal strategies in closed-form increases rather than those involving many states; and, numerical simulations operate faster when analytic solutions are intractable. When considering a planar aircraft model, the equations of motion for the individual

aircraft/missiles are of the form:

$$\begin{aligned} \dot{x}_i(t) &= v_i \cos \psi_i(t) \\ \dot{y}_i(t) &= v_i \sin \psi_i(t) \\ \dot{\psi}_i(t) &= u(t). \end{aligned} \tag{3.1}$$

Define for each agent i, the North (y_i), East (x_i), speed (v_i), and heading angle (ψ_i). In eq. (3.1), the heading rate is utilized for controlling the aircraft location in the 2-D Cartesian plane.

Since Isaacs, the term *simple motion* has been used to describe a vehicle whose control input is its heading, not its heading rate. When the range between aircraft are relatively large compared to their respective altitudes and the turning radius is small compared to the range between vehicles, a simple motion 2-D model may be sufficient when analyzing aircraft guidance strategies. When considering a simple motion model in 2-D, the equations of motion for the individual aircraft/missiles are of the form:

$$\begin{aligned} \dot{x}_i(t) &= v_i \cos \psi_i(t) \\ \dot{y}_i(t) &= v_i \sin \psi_i(t) \\ \psi_i(t) &= u(t). \end{aligned} \tag{3.2}$$

This model differs from eq. (3.1), as the heading is utilized for controlling the aircraft's motion in the 2-D Cartesian plane. By controlling the heading directly, instantaneous turns are considered. The dynamics described in eq. (3.2) are less realistic than those in eq. (3.1); however, analytic solutions to pursuit-evasion scenarios are more tractable as a result of commanding the heading directly.

Vehicle Motion in Three-Dimensions.

When agents are far in range and differ greatly in altitude, the aircraft may be modeled in 3-D using a turn rate and heading rate limited model. This model is an extension of the 2-D vehicle motion in eq. (3.1) and is as follows:

$$\begin{aligned}
\dot{x}_i &= v_i \cos\gamma_i(t) \cos\psi_i(t) \\
\dot{y}_i &= v_i \cos\gamma_i(t) \cos\psi_i(t) \\
\dot{z}_i &= v_i \sin\gamma_i(t) \\
\dot{\psi}_i &= u_1(t) \\
\dot{\gamma}_i &= u_2(t).
\end{aligned} \tag{3.3}$$

Define for each agent i, the North (y_i), East (x_i), altitude (z_i), speed (v_i), heading angle (ψ_i), and flight path angle (γ_i). The heading rate and flight path angle rate are used for controlling the aircraft position in the Cartesian space. These equations of motion are purely kinematic in nature and therefore neglect mass, inertia, and any form of acceleration. In the event where turn and climb-rates constraints are imposed, the control magnitude may be bounded to model the physical limitations of aircraft.

If vehicles are very far from one another and differ greatly in altitude a simple motion model in 3-D implies that a vehicle climbs/dives and turns relatively quickly compared to the distance it traverses in Cartesian space. This model is a simplification

of the 3-D vehicle dynamics in eq. (3.3) and is as follows:

$$\begin{aligned}
\dot{x}_i &= v_i \cos\gamma_i(t) \cos\psi_i(t) \\
\dot{y}_i &= v_i \cos\gamma_i(t) \cos\psi_i(t) \\
\dot{z}_i &= v_i \sin\gamma_i(t) \\
\psi_i &= u_1(t) \\
\gamma_i &= u_2(t).
\end{aligned} \tag{3.4}$$

Different from eq. (3.3), the 3-D simple motion model in eq. (3.4) allows for the heading and flight path angle to be instantaneously changed. While vehicles require time to change their flight path angle or heading rate, this model suggests that the time it takes for maneuvers to be made is small compared to the overall distance traversed. Further, it assumes that the vehicle is capable of making such maneuvers, no matter how aggressive.

3.3 Solution Methodology

One may use optimal control theory as well as differential game theory to understand optimal defense tactics. In this section, the general optimal control problem and differential game problem are described. Two popular approaches to solving optimization problems include the indirect and direct methods; both are presented in brief.

In optimal control theory, the metric by which the performance is measured and subsequently leveraged to find an optimal control is called the *objective cost*. In differential game theory the performance measure is called the *value function* of the game. When HVAA defense is posed as an optimal control problem or differential game the corresponding term is used to describe the performance measure.

Optimal Control.

In optimal control theory, the goal is to find the controls which cause a system to satisfy a set of constraints while at the same time minimize some performance criterion [146]. One aim of this work is to determine the trajectory of a defending asset whose aim is to eliminate a threat farthest from the HVAA. Using optimal control theory, in a general sense, the goal is to find the control input $\mathbf{u}^*(t)$ in the set of admissible controls $\mathbb{U}$, that causes the system dynamics, $\dot{\mathbf{x}} = \mathbf{f}(\mathbf{x}(t), \mathbf{u}(t), t)$ given some initial condition at t_0 to follow an optimal trajectory, $\mathbf{x}^*(t)$, in the set of admissible trajectories $\mathbb{X}$, that minimizes the objective cost, J, and satisfies the boundary and path constraints.

Define the objective cost as follows:

$$J = \Phi(\mathbf{x}(t_f), \mathbf{u}(t_f), t_f) + \int_{t_0}^{t_f} g(\mathbf{x}(t), \mathbf{u}(t), t)\ \mathrm{d}t. \tag{3.5}$$

The objective cost is a functional – it is a mapping of the state space trajectories, $\mathbf{x}(t)$; control input signals, $\mathbf{u}(t)$; and time, t to a scalar value, J. The objective cost is constructed of a terminal penalty, $\Phi(\cdot)$ and running cost, $g(\cdot)$. This form of the objective cost is called the *Bolza problem* [146]. When the integrand $g(\cdot) = 0$, the objective cost depends solely upon the terminal penalty, $\Phi(\cdot)$; in this case, the objective cost is called the *Mayer problem*. When the terminal penalty $\Phi(\cdot) = 0$, the objective cost depends solely upon the running cost, $g(\cdot)$; in this case, the objective cost is called the *Lagrange problem*.

In scenarios where only one agent's strategy is optimized, the goal is to find that agent's optimal control, $\mathbf{u}(t)$, which minimizes the objective cost, J. When finding the control which minimizes, J, one must ensure that the dynamics are upheld. The

dynamics, also referred to as the equations of motion, are as follows:

$$\dot{\mathbf{x}} = \mathbf{f}(\mathbf{x}(t), \mathbf{u}(t), t), \ t \in [t_0, t_f]. \tag{3.6}$$

Moreover, the boundary conditions on states, control, or time, are described as follows:

$$\mathbf{h}(\mathbf{x}(t_0), \mathbf{u}(t_0), t_0, \mathbf{x}(t_f), \mathbf{u}(t_f), t_f) = \mathbf{0}, \ t \in [t_0, t_f]. \tag{3.7}$$

Finally, through an inequality constraint, the path constraints are described as follows:

$$\mathbf{c}(\mathbf{x}(t), \mathbf{u}(t), t) \leq \mathbf{0}, \ t \in [t_0, t_f]. \tag{3.8}$$

Optimal Control - Indirect Method.

Indirect methods of optimal control [10] utilize the calculus of variations [12] and Pontryagin's Minimum Principle [151] to develop the necessary optimality conditions which relate the optimal states, $\mathbf{x}^*(t)$, and control, $\mathbf{u}^*(t)$, to the optimal costates, $\mathbf{p}^*(t)$; the superscript, $*$, represents optimality. To compute the costates, the calculus of variations describes the Hamiltonian as the inner product of the costates and the state dynamics summed with the integrand of the objective cost (running cost),

$$\mathscr{H}(\mathbf{x}(t), \mathbf{u}(t), \mathbf{p}(t), t) = g(\mathbf{x}(t), \mathbf{u}(t), t) + \mathbf{p}^T(t) \left[\boldsymbol{f}(\mathbf{x}(t), \mathbf{u}(t), t)\right]. \tag{3.9}$$

If the control, $\mathbf{u}(t)$, is unbounded, taking the following partials derivatives of the Hamiltonian provides the necessary conditions for optimality:

$$\dot{\mathbf{x}}^*(t) = \frac{\partial \mathscr{H}}{\partial \mathbf{p}}(\mathbf{x}^*(t), \mathbf{u}^*(t), \mathbf{p}^*(t), t) \tag{3.10}$$

$$\dot{\mathbf{p}}^*(t) = -\frac{\partial \mathscr{H}}{\partial \mathbf{x}}(\mathbf{x}^*(t), \mathbf{u}^*(t), \mathbf{p}^*(t), t) \tag{3.11}$$

$$\mathbf{0} = \frac{\partial \mathscr{H}}{\partial \mathbf{u}}(\mathbf{x}^*(t), \mathbf{u}^*(t), \mathbf{p}^*(t), t). \tag{3.12}$$

Equations (3.10) to (3.12) are used only when the control is unbounded. If there are limits on the control, the use of Pontryagin's Minimum Principle (PMP) is required,

$$\mathscr{H}(\mathbf{x}^*(t), \mathbf{u}^*(t), \mathbf{p}^*(t), t) \leq \mathscr{H}(\mathbf{x}^*(t), \mathbf{u}(t), \mathbf{p}^*(t), t). \tag{3.13}$$

Simply stated in eq. (3.13), for all admissible controls, u, the Hamiltonian is a minimum under optimal control. Boundary conditions are also developed depending upon where the states or time is fixed or free. Utilizing the transversality conditions,

$$\begin{aligned} &\left[\frac{\partial \Phi}{\partial \mathbf{x}}(\mathbf{x}^*(t_f), t_f) - \mathbf{p}^*(t_f)\right]^T \delta \mathbf{x}_f \ + \\ &\left[\mathscr{H}(\mathbf{x}^*(t_f), \mathbf{u}^*(t_f), \mathbf{p}^*(t_f), t_f) + \frac{\partial \Phi}{\partial t}(\mathbf{x}^*(t_f), t_f)\right] \delta t_f = 0, \end{aligned} \tag{3.14}$$

the Two Point Boundary Value Problem (TPBVP) is formed.

While the indirect approach provides the optimal states, costates, and control for a given objective, analytic solutions quickly become intractable when nonlinear equations of motion, and/or the number of states grows. The challenge of interpreting the costates, and computing the necessary conditions can present difficulties with solving optimal control problems indirectly.

Optimal Control - Direct Method.

Rather than solving the optimal control using the calculus of variations, direct methods serve as a means of finding optimal state and control trajectories using a numerical search algorithm [17]. Four popular direct methods for solving optimal control problems include the Single Shooting Method (SSM), Multiple Shootings Method (MSM), Even Collocation Method (ECM), and Pseudospectral Method (PSM). These methods have various similarities and differences which are of interest to this work. A brief description of each method along with the various advantages and disadvantages between each of the four methods is presented.

Single Shooting Method (SSM).

SSM, outlined in Figure 7, is a numerical technique for finding the optimal control to a dynamic system which achieves a given objective subject to boundary conditions and path constraints. The procedure begins with some initial state, $\mathbf{x}_0$, and a guess for the control for the entire time series, $\{u_k | k = 1, \ldots, N\}$. Using the guess for the control and the initial state, an NLP solver, such as Matlab's `FMINCON()`, computes the optimal control through iterative search. The NLP performs the search for the optimal control by first *shooting* the dynamics forward through time using an Ordinary Differential Equation (ODE) solver such as the Runge-Kutta Method [152]. Next, the NLP computes the objective cost using the propagated state trajectories. After the cost is computed, the NLP evaluates if a local minimum has been found. If the cost is a minimum, by some convergence criteria, the guess is considered the optimal control. However, if the objective cost is not considered a minimum, then an update to the guess for the control is made, and the process starts again. One such method for updating the guess is the method of finite differences. As is the case in `FMINCON()`, the searching gradient is computed using finite differences.

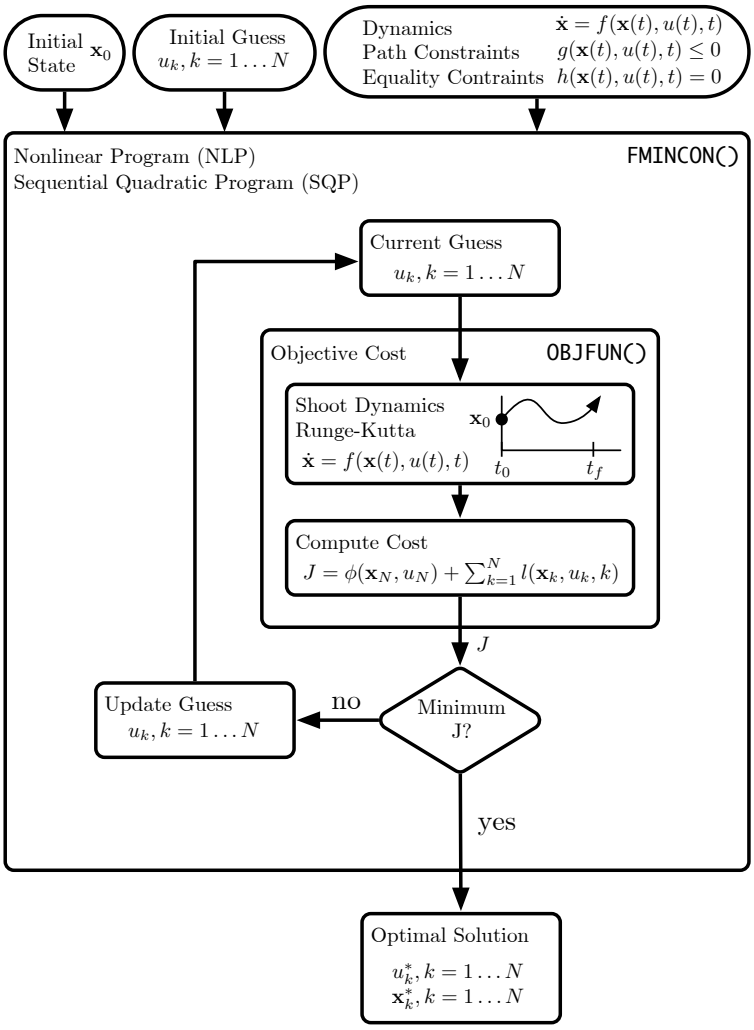

Figure 7. Shooting Method Flow Diagram

There exist multiple numerical techniques to update the guess for the control, one popular technique is the method of Sequential Quadratic Programming (SQP) [16]. The SQP algorithm, in short, is a gradient-based technique for finding the optimal control which minimizes the objective cost subject to equality and inequality constraints. It strives to satisfy the first-order necessary conditions for optimality, called Karush-Kuhn-Tucker (KKT) conditions, by updating guesses until the objective cost is at a minimum and all constraints are satisfied to some tolerance. To determine how to update the guess for the control, the algorithm perturbs the control throughout

its trajectory. By observing the change in the objective cost, as a function of the perturbations, updates are chosen to improve the guess for optimal control. In the event the KKT conditions are satisfied, the optimal guess for the control sequence, $\{u_k^*|k = 1, \ldots, N\}$, and optimal states, $\{\mathbf{x}_k^*|k = 1, \ldots, N\}$, is produced.

The requirements to begin the shooting method is a guess for the control sequence u_k. Assuming that time is discretized evenly from t_0 to t_f into N points, the initial guess is described as

$$u_k,\ k = 1 \ldots N. \tag{3.15}$$

The overall size to compute the optimal control using the shooting method is quite large. Assuming that time is evenly discretized into N points, the dynamics would need to be propagated every time the objective cost is computed (N-times). Further, let R be the number of iterations required to obtain an optimal control. Since perturbations are made at every time step, the number of times the dynamics are forward propagated would be approximately $R(N + 1)$. (The 1 represents the evaluation of the current guess, while the N represents the evaluation for each perturbation made of the guess.)

Since the dynamics are guaranteed by the accuracy of the ODE solver, the feasibility of the solution is ideal. Although the computational time associated with using an ODE solver may be large, it ensures that the dynamics are upheld. In the ATDS the initial state ($\mathbf{x}_0$) is provided, the final state is free, and no equality constraints are applied.

Multiple Shooting Method (MSM).

MSM differs from single shooting in that it aims at reducing the computational time by parallelizing the shooting operation. Breaking the shooting operation into smaller segments, MSM makes use of multiple processors to shoot each segment in

parallel. In exchange for parallelizing the shooting operations, discontinuities occur in-between each connecting interval. A series of equality constraints, one at each transition from one interval to the next are formed as *continuity constraints*. Figure 8 describes the process of searching for the optimal control and optimal state trajectories using MSM.

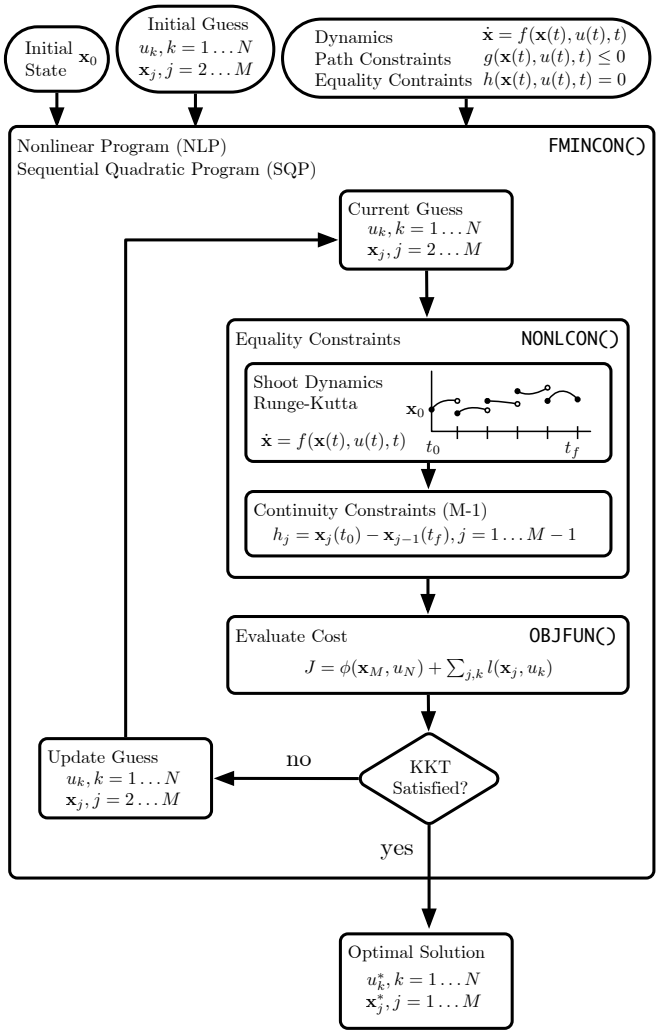

Figure 8. Multiple Shooting Method Flow Diagram

The procedure begins with a guess for the control for the entire time series, $\{u_k | k = 1, \dots, N\}$, and a value for the states at the beginning of each segment. Assuming there are M segments, n states, and the initial state is known to be $\mathbf{x}_0$, the size of

the initial guess for the states at each segment is $n(M-1)$. In total, the size of the guess is $N + n(M-1)$ when the initial states are known.

Using the SQP algorithm, the optimal states and control are iteratively searched for until the KKT conditions are satisfied. If the step size of the guess is below some threshold, the change in the objective cost is also below some threshold, and if the feasibility (defined as the equality constraints from the continuity conditions) is within some tolerance, then the NLP returns the optimal control as well as the values of the states at the beginning of each of the segments.

Although the overall size of MSM is less than the shooting method, it still requires the use of an ODE solver such as the Runge-Kutta Method. Since the shootings are conducted in parallel, the size of the algorithm is reduced. If the number of computational threads is equal to the number of segments, the effective computational time for shooting the dynamics is reduced by a factor of M. However, the introduction of the continuity constraints requires the addition of $n(M-1)$ unknowns to be solved in addition to the control.

Even Collocation Method (ECM).

ECM takes advantage of computational efficiency by transcribing a dynamic optimization problem, which requires numerical methods for solving differential equations, into a static optimization problem. The method begins with considering the dynamics and control at evenly spaced points in time from t_0 to t_f. Consider N points, the guess for the states and control are as follows:

$$\mathbf{x}_k,\ k = 1, \ldots, N \tag{3.16}$$

$$u_k,\ k = 1, \ldots, N. \tag{3.17}$$

Using the guess for the state and control trajectories, ECM imposes the dynamics as a set of equality constraints rather than using an ODE solver such as the Runge-Kutta Method. The equality constraints are formed by a simple subtraction,

$$\dot{\mathbf{x}} - \mathbf{f}(\mathbf{x}(t), u(t), t) = 0 \quad t \in [t_0, t_f]. \tag{3.18}$$

Assuming that there are n states, the number of equality constraints formed from imposing the dynamics are nN given by the first-order Euler approximation:

$$\mathbf{h}_k(\mathbf{x}_k, u_k, k) = \mathbf{x}_{k+1} - \mathbf{x}_k - \mathbf{f}(\mathbf{x}_k, u_k, k)\Delta t \quad k = 1, 2, ..., N. \tag{3.19}$$

Using the definition of the equality constraints in eq. (3.19) to satisfy the dynamics of the problem, an ODE solver is no longer required to propagate the dynamics. Rather, the dynamics are satisfied through an equality constraint which the NLP considers *feasibility criteria*. The flow diagram which describes ECM can be seen in Figure 9. The procedure begins by providing a guess for the state and control trajectories. As described, the dynamics are transcribed into an equality constraint, and a `FOR()` loop is used to compute each equality constraint at every time step. Additionally, the objective cost is computed as a function of the states and control. Since the collocation points are evenly spaced, any terms inside the integral of the objective cost are approximated using a quadrature method such as trapezoidal or rectangular integration. Using the SQP search described earlier, the objective cost and equality constraints are minimized through iterative search until the KKT conditions are satisfied. Upon completion, the solution provides the optimal control and corresponding state trajectories at each collocation point.

In this analysis, there are N evenly spaced collocation points. However, a finer or coarser mesh can be implemented to increase or reduce the number of collocation

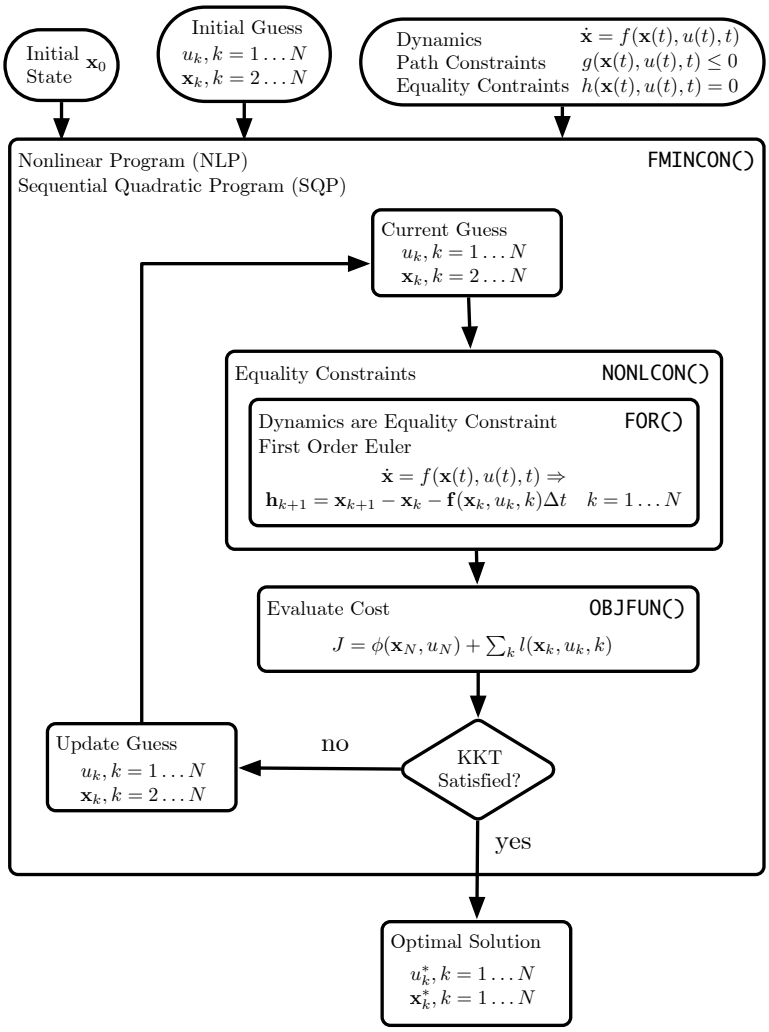

Figure 9. Even Collocation Direct Method Flow Diagram

points. By reducing the number of points, the number of function evaluations may be reduced. By increasing the number of points, the accuracy of the quadrature is increased at the cost of computational effort. Using the First-Euler approximation of the dynamics as an equality constraint it is important to consider if the meshing becomes too coarse; if this is the case then the small time step assumption made earlier may no longer hold. Methods of changing the spacing between nodes are described as adaptive meshing techniques. The general concept of adaptive meshing is to decrease the spacing between nodes where more accurate computations of the

states are required and allow the spacing of other areas to be larger to reduce the total number of points. For this comparative study, the use of adaptive meshing is not considered. Since the ODE solvers employed in the shooting method are fixed time-step solvers, fixed meshing is used for the collocated methods to make a *fair* comparison.

The overall size of ECM is much smaller than SSM and MSM. By allowing the dynamics to be accurate to a prescribed threshold, the use of ODE solvers is eliminated. In the example, the derivative is computed using a first-order Euler's Method which isn't the most accurate, but for small time steps is sufficient. Furthermore, using a low-order quadrature method such as rectangular integration, the objective cost is computed. Since there are no uses of ODE solvers, the size of ECM is to find the optimal solution to the state and control trajectories, a size of $N(n+1)$. Assuming there are R iterations, the number of function evaluations will be around the order of $RN(n+1)$.

Pseudospectral Method (PSM).

PSM refers to a series of techniques which are employed to solve optimal control problems by taking advantage of efficient computational methods. Figure 10 describes the process of conducting a search for the optimal control and optimal state trajectories using PSM. PSM enforces dynamics at a set of collocation points (just as before) by means of equality constraints and the objective cost is computed through Gaussian quadrature. The state, x, can be approximated using Lagrange interpolating polynomials,

$$\hat{x}(t) \approx \sum_{i=1}^{n+1} x_i L_i(t). \tag{3.20}$$

In eq. (3.20), $\hat{x}$ is the polynomial approximation of the state, x, and the Lagrange polynomial basis is efficiently computed as

$$L_i(t) = \prod_{\substack{j=1 \\ j \neq i}}^{n+1} \frac{t - t_j}{t_i - t_j} \quad i = 1, ..., n+1. \tag{3.21}$$

By using Lagrange interpolating polynomials, there is zero error of the interpolating polynomial at each collocation point,

$$x_i = \hat{x}(t_i), \tag{3.22}$$

and since the interpolated function is a polynomial, any number of derivatives are guaranteed to exist. In-between the collocation points, the error can be found by the subtraction,

$$x(t) - \hat{x}(t) = \frac{x^{(n+1)}(\xi(t))}{(n+1)!} \prod_{i=0}^{n} (t - t_i). \tag{3.23}$$

The point ξ is the value of t where the $(n+1)^{\text{st}}$ derivative of the state x is equal to zero. It would be ideal if ξ were a constant; but, most likely ξ will depend upon t. However, the error can be bounded by choosing ξ to bound that derivative. Upon the first investigation, the error can be reduced by adding more points, but the Runge Phenomenon, where high-order derivatives cause the error to increase near the endpoints can be problematic. To overcome this phenomenon, the collocation points are spaced by the roots of an N^{th}-order Legendre polynomial on the interval $[-1, 1)$. This not only reduces the Runge Phenomenon but also leads to exponential convergence in quadrature. Using an affine transformation, the time series, $[t_0, t_f]$, must be mapped to the $[-1, 1]$ domain where the collocation points are determined by the roots of the Legendre Polynomial. The mapping to the affine transformation

is as follows:

$$\tau = \frac{2t - (t_f - t_0)}{t_f - t_0}. \tag{3.24}$$

Derivatives may also be computed by means of a matrix multiplication which is more efficient than first-order Euler approximations, and faster since operations can be computed by means of matrix multiplication rather than for-loops. Using standard techniques, a differentiation matrix eq. (3.25) may be computed [153]. Using the differentiation matrix, equality constraints eq. (3.26) are used to ensure the dynamics are upheld, namely,

$$\dot{\mathbf{x}} \approx \mathbf{D}\mathbf{x}, \tag{3.25}$$

$$\mathbf{h}(\mathbf{x}, u) = \mathbf{D}\mathbf{x} - \frac{\Delta t}{2}\mathbf{f}(\mathbf{x}, u) = \mathbf{0}. \tag{3.26}$$

Quadrature weights, w_k, are associated with the collocation scheme and approximate the integration of the running cost, as follows:

$$\int_{t_0}^{t_f} g(\mathbf{x}, u, t)\mathrm{d}t \approx \frac{t_f - t_0}{2} \sum_{k=1}^{N} w_k g(\mathbf{x}(\tau_k), u(\tau_k), \tau_k). \tag{3.27}$$

Similar to ECM, constraints (inequality or equality) may be enforced at any collocation point; equality constraints are used to enforce boundary conditions and inequality constraints are used to implement path constraints.

The use of adaptive meshing for PSM aids in computational efficiency. By increasing the polynomial order for the number of points in a mesh, it is feasible to map the entire time sequence to one mesh of points and one polynomial. However, with higher order polynomials, Runge phenomenon, can be a source of error. This Runge phenomenon is reduced by selecting the collocation points defined by Legandre-Gauss-Radau (LGR) spaced collocation points [148, 154]. To reduce the error from this phenomenon, HP-adaptive meshing [155] turns the mesh into a series

of segments which are of no higher order than a prescribed maximum number. This means that mesh refinement occurs where necessary, and in the event nonlinearities in the dynamics require more precise computation of the states, the mesh is able to adapt.

As far as computational size, PSM tends to be the most efficient means of computing the optimal control and state trajectories [18, 19, 145]. Leveraging sparse matrices and using matrix multiplications, the computational size is on the order of N for enforcing the dynamics and the order of N for computing objective cost. Exponential convergence is also seen as a result of using PSM. Since adaptive meshing is employed, the number of collocation points are reduced, and the size of the problem is less than the even collocation problem. Further, the use of Gaussian quadrature methods ensures that integrations are exact for the approximated polynomial. Also, the integral can be computed by a weighted summation of the polynomial evaluated at the collocation points. The number of function evaluations, assuming with N points, n states, and R iterations, will be of the order of $RN(n+1)$. The size of PSM is equal to that of ECM, but the efficient methods which are employed by PSM produce a more accurate approximation of the objective cost and more accurate implementation of the dynamics.

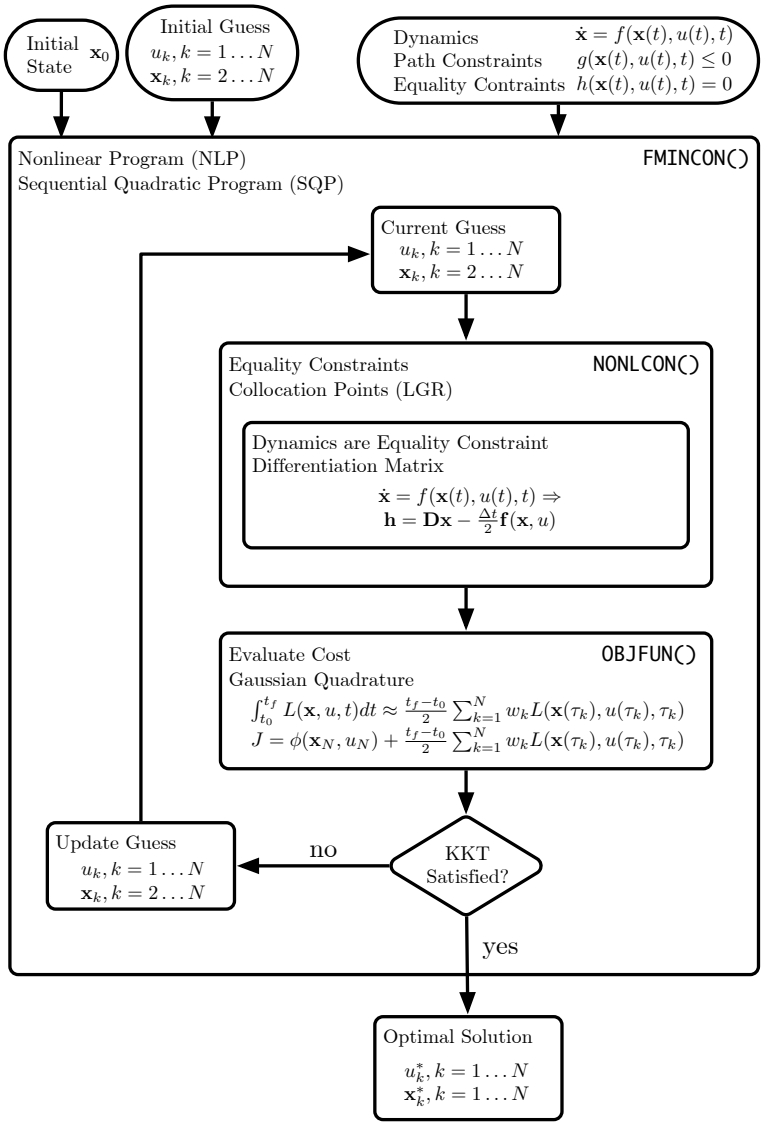

Figure 10. Pseudospectral Methods Flow Diagram

Comparison.

Each of the four methods described has various advantages and disadvantages; Table 2 summarizes the various properties of the four methods. To begin with, SSM is simple to construct, and initial guesses only require the control sequence. However, SSM inefficiently computes the cost by shooting the dynamics for each evaluation. Moreover, shooting methods are very sensitive to the initial guess due to the gradient search methods employed by the SQP. Rather than adjusting the state trajectories, SSM only modifies the control with each successive guess for the optimal control.

Similar to ECM, MSM imposes dynamics as a series of inequality constraints; but, rather than using a first-order Euler approximation to the dynamics, an ODE solver is used to forward propagate the dynamics. Also, the introduction of states to the guess reduces sensitivity to the initial guess and allows for state and control to be provided at the end of the iterative search.

As compared to SSM and MSM, the accuracy of the solution that ECM produces is poorer. While SSM and MSM provide accurate integration using ODE solvers, ECM uses a first-order Euler approximation. Furthermore, the use of rectangular integration by ECM produces a coarse approximation of analytic integration. While ECM aims at outperforming the speed of solution provided by SSM and MSM, it does so at the cost of accuracy. However, by setting the dynamics as a constraint rather than imposing the dynamics through shooting, ECM is less sensitive to initial guess than SSM and MSM.

PSM is for all intents and purposes, an accurate and efficient version of ECM. Since it uses LGR collocation points and computes integration using Gaussian quadrature, integration is exact for the approximating polynomial and is found by a simple weighted sum. PSM also makes use of a differentiation matrix to enforce the dynamics through equality constraints. This is much more efficient than ECM's for-loop.

The main disadvantage of PSM is the complexity and level of understanding required to implement the algorithm. It should be noted that tools do exist which may aid the novice control-theorist with setting up an optimization method using PSM discussed in [19, 18, 156].

Table 2. Method Property Comparison

Metric	SSM	MSM	ECM	PSM
Easy to formulate	•		•	
Guess includes control	•	•	•	•
Guess includes state		•	•	•
Solves for control traj.	•	•	•	•
Solves for state traj.	•	•	•	•
Sensitive to init. guess	•	•		
Employs ODE solvers	•	•		
Eq. constr. satisfy dynamics		•	•	•
Low convergence times		•	•	•

Table 3 presents a summary of the size of the guess and equality constraints to set up each of the four methods. While at first glance, the shooting method appears to be the smallest size, it is the most computationally inefficient means of searching for the optimal control. Due to the number of ODE solver calls, shooting takes much more time to compute than the other three direct methods. Multiple shooting aimed at reducing the computational time by shooting segments in parallel but introduced continuity constraints. Although the computational size of the problem is reduced by parallelizing the ODE solver calls, the method requires special hardware and software to perform this operation. ECM removed the requirement to shoot the dynamics; instead, the dynamics were implemented through a series of equality constraints. Since ECM does not require shooting the dynamics, a fine grid of points is required for the first-order Euler approximation for the dynamics to be sufficient. Additionally, ECM is much less sensitive to initial guesses due to gradient-based search techniques. Finally, PSM aims at reducing the error of rectangular integration and low-order dynamics by using Gaussian quadrature and spacing the points accordingly. In spacing

the LGR points, the number of collocation points is reduced to achieve the same accuracy as the other direct methods, and as a result, solutions to the optimal control problem are found much faster. Table 9 shows a comparison of the size required to run each of the four direct methods.

Table 3. Method Size

Method	Initial Guess	No. Ukn.	Eq. Const.	NLP Output
SSM	`u[k], k = 1..N`	N	0	$u_k^*,\ k = 1 \dots N$
MSM	`u[k], k = 1..N`	$N + n(M-1)$	$n(M-1)$	$u_k^*,\ k = 1 \dots N$
	`x[j], j = 2..M`			$\mathbf{x}_j^*,\ j = 2 \dots M$
ECM	`u[k], k = 1..N`	$N + n(N-1)$	$n(N-1)$	$u_k^*,\ k = 1 \dots N$
	`x[k], k = 2..N`			$\mathbf{x}_k^*,\ k = 2 \dots N$
PSM	`u[k], k = 1..N`	$N + n(N-1)$	$n(N-1)$	$u_k^*,\ k = 1 \dots N$
	`x[k], k = 2..N`			$\mathbf{x}_k^*,\ k = 2 \dots N$

Differential Games.

In pursuit-evasion, two or more agents select a control which aims at either minimizing or maximizing a common performance metric called the *value function* [9]. More specifically, the value function arises after the successful minimization/maximization of the objective cost/payoff function by the players. Here and in other instances below, it may be more accurate to say min-max the objective cost. In general, the pursuer aims at minimizing the value function, while the evader aims at maximizing it. What makes the game differential, is that the dynamics of each of the agents is defined by a set of governing equations of motion,

$$\dot{\mathbf{x}} = \mathbf{f}(\mathbf{x}(t), \mathbf{u}(t), \mathbf{v}(t), t). \tag{3.28}$$

The dynamics of a game, eq. (3.28), differs from that of the optimal control problem, eq. (3.6), in the fact that two controls, $\mathbf{u}$ and $\mathbf{v}$, are explicit. This is to emphasize that

the dynamics are influenced by both players. For the formulation, at a given time $t \in [t_0, t_f]$, the pursuer's admissible control is $\mathbf{u}(t) \in \mathbb{U}$ and the evader's admissible control is $\mathbf{v}(t) \in \mathbb{V}$. Similar to the boundary condition described in optimal control theory, eq. (3.7), a terminal constraint can be imposed as follows:

$$\mathbf{h}(\mathbf{x}(t_f), \mathbf{u}(t_f), \mathbf{v}(t_f), t_f) = \mathbf{0},\ t \in [t_0, t_f]. \tag{3.29}$$

Further, the value function of the differential game is

$$J = \Phi(\mathbf{x}(t_f), \mathbf{u}(t_f), \mathbf{v}(t), t_f) + \int_{t_0}^{t_f} g(\mathbf{x}(t), \mathbf{u}(t), \mathbf{v}(t), t)\ \mathrm{d}t. \tag{3.30}$$

It is the goal of the differential game to find the admissible optimal strategies $\mathbf{u}^*(t) \in \mathbb{U}$ and $\mathbf{v}^*(t) \in \mathbb{V}$ for all $t \in [t_0, t_f]$ such that the value function is a minimax:

$$J(\mathbf{u}^*(t), \mathbf{v}(t)) \leq J(\mathbf{u}^*(t), \mathbf{v}^*(t)) \leq J(\mathbf{u}(t), \mathbf{v}^*(t)). \tag{3.31}$$

The search for the optimal control for the pursuer and evader such that the value function as a minimax is conducted. The necessary conditions for the minimax problem relates to the Hamiltonian in eq. (3.9) just as before,

$$\mathscr{H}(\mathbf{x}(t), \mathbf{u}(t), \mathbf{v}(t), \mathbf{p}(t), t) = g(\mathbf{x}(t), \mathbf{u}(t), \mathbf{v}(t), t) + \mathbf{p}^T(t) \left[\boldsymbol{f}(\mathbf{x}(t), \mathbf{u}(t), \mathbf{v}(t), t)\right]. \tag{3.32}$$

Utilizing the Hamiltonian, eq. (3.32), which is explicit in each player's control, the necessary conditions for optimality is as follows [157]:

$$\dot{\mathbf{x}}^*(t) = \frac{\partial \mathscr{H}}{\partial \mathbf{p}}(\mathbf{x}^*(t), \mathbf{u}^*(t), \mathbf{v}^*(t), \mathbf{p}^*(t), t) \tag{3.33}$$

$$\dot{\mathbf{p}}^*(t) = -\frac{\partial \mathscr{H}}{\partial \mathbf{x}}(\mathbf{x}^*(t), \mathbf{u}^*(t), \mathbf{v}^*(t), \mathbf{p}^*(t), t) \tag{3.34}$$

$$\mathbf{0} = \frac{\partial \mathscr{H}}{\partial \mathbf{u}}(\mathbf{x}^*(t), \mathbf{u}^*(t), \mathbf{v}^*(t), \mathbf{p}^*(t), t) \tag{3.35}$$

$$\mathbf{0} = \frac{\partial \mathscr{H}}{\partial \mathbf{v}}(\mathbf{x}^*(t), \mathbf{u}^*(t), \mathbf{v}^*(t), \mathbf{p}^*(t), t) \tag{3.36}$$

or

$$. \tag{3.37}$$

The optimal control for the pursuer and the evader are those that drive the Hamiltonian to a saddle point where the pursuer minimizes the Hamiltonian and the evader maximizes it [9]. This optimal solution is commonly referred to as a saddle point strategy. The saddle point strategy explicitly states that the performance of an agent's opponent only improves when that agent performs any control which is not optimal.

While the necessary conditions for optimality serve as a means of determining the optimal state trajectories and strategies of both players, it is common to have difficulties solving the system of equations described in eqs. (3.33) to (3.37). Consequently, numerical approaches for finding the optimal state and control trajectories are pursued. Uncommon to differential games are solutions found directly using numerical techniques. Although numeric techniques exist for locating saddle points [158, 16], the topology of the Hamiltonian and objective cost in the state space is critical for locating the saddle points. Only by locating the saddle point of the Hamiltonian does one locate the optimal strategies of the differential game. One alternative to locating saddle points directly is obtained by transforming the problem of minimax into that of only minimization (transforming a differential game into an optimal control

problem). Once the differential game can be reduced to that of an optimal control problem, an analytic solution may become tractable, or direct methods may be used to solve them.

Geometric Methods for Solving Differential Games.

One popular method of transforming a differential game into an optimal control problem is by utilizing geometric tools such as Apollonius Circle [159, 68, 122, 44, 9, 67, 120, 160, 101]. When considering simple motion, Apollonius Circle solves for the optimal headings which result in a min-time interception of the slower evader by a faster pursuer. Apollonius Circle describes the locus of points for all possible interceptions depending upon the heading of the slower evader. Because the optimal trajectory of the faster pursuer is a direct mapping through the Apollonius Circle, from the heading of the slower evader, the optimization of two variables (pursuer and evader headings) into an optimization of only one (evader heading) can be conducted using the geometry of Apollonius. The Apollonius Circle for a fast pursuer and slow evader can be seen below in Figure 11.

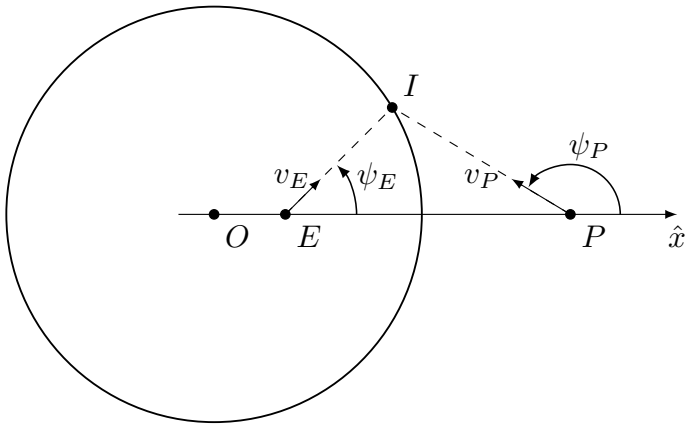

Figure 11. The min-time interception of an evader (E) by a faster pursuer(P) illustrated by the Apollonius Circle interception geometry.

In order to construct an Apollonius Circle, define the speed ratio, $\mu = v_E/v_P$.

Then, the offset of the Origin, O, from the evader, E is the following:

$$\overline{OE} = \frac{\mu^2 \overline{EP}}{1 - \mu^2} \tag{3.38}$$

Moreover, the radius of the Apollonius Circle is:

$$R = \overline{OI} = \frac{\mu \overline{EP}}{1 - \mu^2} \tag{3.39}$$

Called *Foci*, the initial conditions of the evader, E, and the pursuer, P, along with their relative velocities, μ, can fully define the Apollonius Circle as described in eqs. (3.38) and (3.39).

3.4 HVAA Defense Scenarios

This section contains a description of both kinetic and energy-based defense of a HVAA against an incoming threat. In Table 1, six different engagements are described which are considered in this work. The research scenarios detailed in this section outline how the kinetic and directed energy defense scenarios may be posed as either optimal control problems or differential games. Special attention is given to defining the engagements and how to pose and solve these problems as differential games or optimal control problems.

Notation.

Throughout this work, the states and control are vector valued functions explicit in time and denoted $\mathbf{x}(t)$ and $\mathbf{u}(t)$ respectively. For the sake of compactness, the real-valued n-dimensional state and m-dimensional control at a single instant of time are denoted as $\mathbf{x} \in \mathbb{R}^n$ and $\mathbf{u} \in \mathbb{R}^m$, respectively. The same notation is used for a single state; for example, x_i represents the x-location for an agent i for a single

instant of time.

Kinetic Defense of a Maneuvering HVAA in 2-D.

The kinetic defense of a maneuvering HVAA in 2-D is outlined in Scenario 1 of Table 1. In this scenario, the pursuer and defender are assumed to be guided by the proportional navigation guidance law, and the evader maneuvers to escape its capture by the pursuer while assisting the defender in capturing the pursuer.

The dynamics of the evader follow the 2-D vehicle motion model as described in eq. (3.1). The complete state of the optimization problem at an instant in time in the 2-D Cartesian plane is defined as $\mathbf{x}^T = [x_D, y_D, \psi_D, x_P, y_P, \psi_P, x_E, y_E, \psi_E] \in \mathbb{R}^9$. The pursuer's heading rate and the defender's heading rate is selected to be proportional to the line of sight rate to the evader and the pursuer, respectively. The evader's control is it's heading rate, $\mathbf{u}_E = \{\dot{\psi}_E\}$. The nonlinear equations of motion in the 2-D Cartesian plane, $\dot{\mathbf{x}} = \mathbf{f}(\mathbf{x}, \mathbf{u}_E)$, are defined by a system of nonlinear differential equations,

$$\begin{aligned} \dot{x}_P &= v_P \cos\psi_P, \quad \dot{x}_E = v_E \cos\psi_E, \quad \dot{x}_D = v_D \cos\psi_D \\ \dot{y}_P &= v_P \sin\psi_P, \quad \dot{y}_E = v_E \sin\psi_E, \quad \dot{y}_D = v_D \sin\psi_D \\ \dot{\psi}_P &= N_P \dot{\lambda}_{PE}, \qquad \dot{\psi}_E = u(t), \qquad\quad \dot{\psi}_D = N_D \dot{\lambda}_{DP}, \end{aligned} \tag{3.40}$$

where the proportional navigation constants for the pursuer and defender are N_P and N_D respectively. Additionally, the line of sight angles from the pursuer to the evader is λ_{PE} and the line of sight angle from the defender to the pursuer is λ_{DP}. Moreover, the control of the evader is bounded and therefore the admissible control of the evader is bounded by a turning rate constraint $\omega_{\max}$, namely,

$$u(t) \in [-\omega_{\max}, \omega_{\max}] \; \forall \; t \in [t_0, t_f]. \tag{3.41}$$

The initial state of the engagement scenario is defined as

$$\mathbf{x}^T(t_0) = \mathbf{x}_0^T = [x_{D_0}, y_{D_0}, \psi_{D_0}, x_{P_0}, y_{P_0}, \psi_{P_0}, x_{E_0}, y_{E_0}, \psi_{E_0}]. \tag{3.42}$$

It is also assumed that the engagement scenarios being solved belong to the escape set, $\mathbf{x} \in \mathscr{R}_e \subset \mathbb{R}^9$. The escape set is defined as the state trajectories wherein the defender captures the pursuer and the evader escapes capture by the pursuer; this occurs at the terminal time, t_f, and is defined as follows:

$$\mathscr{R}_e = \{\mathbf{x} | (x_P - x_D)^2 + (y_P - y_D)^2 = 0, (x_P - x_E)^2 + (y_P - y_E)^2 > 0, t = t_f\}. \tag{3.43}$$

The objective is for the evader to maneuver so as to minimize the defender-pursuer range as well as maximize the pursuer-evader range at final time: the instant in time when the defender captures the pursuer. The pursuer-evader range and the defender-pursuer range are denoted by R_{PE} and R_{DP}, respectively. Formulating the objective in terms of closure rates,

$$\begin{aligned} \min_u J &= \int_{t_0}^{t_f} \left(-\dot{R}_{PE} + \dot{R}_{DP} \right) dt \\ &= R_{PE}(t_0) - R_{PE}(t_f) + R_{DP}(t_f) - R_{DP}(t_0) \end{aligned} \tag{3.44}$$

Because the initial conditions are independent of the input, u, a cost function is desired which equivalently minimizes $R_{DP}(t_f)$ and maximizes $R_{PE}(t_f)$, namely,

$$\min_u J = -R_{PE}(t_f) + R_{DP}(t_f). \tag{3.45}$$

Kinetic Defense of a Non-Maneuvering HVAA in 2-D.

The kinetic defense of a non-maneuvering HVAA in 2-D is outlined in Scenario 2 of Table 1. In this scenario, a pursuer and defender play a differential game. In the game, the pursuer strives to minimize his distance from the evader at the instant in time that the pursuer is captured by the defender while the defender aims to maximize the very same distance.

The dynamics of each agent follows the simple motion model in 2-D from eq. (3.2). The complete state of the game at an instant in time is defined by $\mathbf{x}^T = [x_E, y_E, x_P, y_P, x_D, y_D] \in \mathbb{R}^6$. The pursuer's control variable is its instantaneous heading angle, $\mathbf{u}_P = \{\psi_P\}$. The defender's control variable is also its instantaneous heading angle, $\mathbf{u}_D = \{\psi_D\}$. The nonlinear dynamics of the game, $\dot{\mathbf{x}} = \mathbf{f}(\mathbf{x}, \mathbf{u}_P, \mathbf{u}_D)$, are defined by a system of nonlinear ordinary differential equations,

$$\begin{aligned} \dot{x}_P &= v_P \cos\psi_P, \quad \dot{x}_E = v_E \cos\psi_E, \quad \dot{x}_D = v_D \cos\psi_D \\ \dot{y}_P &= v_P \sin\psi_P, \quad \dot{y}_E = v_E \sin\psi_E, \quad \dot{y}_D = v_D \sin\psi_D. \end{aligned} \tag{3.46}$$

The admissible controls of the pursuer and the defender, are given by $\psi_P \in [-\pi, \pi] \ \forall \ t \in [t_0, t_f]$ and $\psi_D \in [-\pi, \pi] \ \forall \ t \in [t_0, t_f]$, respectively. It is assumed that the evader is non-maneuverable, and therefore the evader's heading, ψ_E, is constant. The evader's heading is also assumed to be known by both the defender (D) and pursuer (P).

The initial state of the game is defined as

$$\mathbf{x}^T(t_0) = \mathbf{x}_0^T = [x_{P_0}, y_{P_0}, x_{E_0}, y_{E_0}, x_{D_0}, y_{D_0}]. \tag{3.47}$$

In this scenario, point capture is considered. This means that the $P-D$ separation has to become zero at some time t_f for the defender to intercept the pursuer. It is

also assumed that the state of the system belongs to the escape set, denoted by $\mathbf{x} \in \mathscr{R}_e \subset \mathbb{R}^6$ and defined in eq. (3.43). In other words, given the speed ratios, the evader heading, and initial conditions ($\mathbf{x}_0$), there exists a strategy for D to intercept P before the latter captures E. The game of capture, that is, the game when the state belongs to the complement of $\mathscr{R}_e$ is not addressed in this dissertation.

The termination set, $\mathscr{C}$, which represents interception of the pursuer by the defender (and the evader escapes) is defined as

$$\mathscr{C} = \left\{ \mathbf{x} \mid \sqrt{(x_P - x_D)^2 + (y_P - y_D)^2} = 0, t = t_f \right\}. \tag{3.48}$$

The terminal time, t_f, is defined as the first time instant when the state of the system satisfies eq. (3.48), at which time the terminal state is

$$\mathbf{x}^T(t_f) = \mathbf{x}_f^T = [x_{P_f}, y_{P_f}, x_{E_f}, y_{E_f}, x_{D_f}, y_{D_f}]. \tag{3.49}$$

The objective cost is the separation distance between the pursuer and the evader at the instant in time that the defender captures the pursuer, t_f, and is described as follows:

$$J(\mathbf{u}_P(t), \mathbf{u}_D(t); \mathbf{x}_0) = \Phi(\mathbf{x}_f) = \sqrt{(x_{P_f} - x_{E_f})^2 + (y_{P_f} - y_{E_f})^2}. \tag{3.50}$$

The value function is subject to eqs. (3.46) to (3.48) and depends only on the terminal state and is therefore of the Mayer form. Its value is given by

$$V(\mathbf{x}_0) = \min_{\mathbf{u}_P(\cdot)} \max_{\mathbf{u}_D(\cdot)} J(\mathbf{u}_P(\cdot), \mathbf{u}_D(\cdot); \mathbf{x}_0). \tag{3.51}$$

Kinetic Defense of a Non-Maneuvering HVAA in 3-D.

The kinetic defense of a non-maneuvering HVAA in 3-D is outlined in Scenario 3 of Table 1. In this scenario, a pursuer and defender play the same differential game as described by Scenario 2, except that the agents move in 3-D Cartesian space rather than the 2-D Cartesian plane.

The dynamics of each agent follows the simple motion model in 3-D from eq. (3.4). The complete state of the game is defined by $\mathbf{x}^T = [x_P, y_P, z_P, x_E, y_E, z_E, x_D, y_D, z_D] \in \mathbb{R}^9$. The pursuer's control is is composed of its instantaneous heading angle and flight path angle, $\mathbf{u}_P = \{\psi_P, \gamma_P\}$. The defender's control is also its instantaneous heading and flight path angle, $\mathbf{u}_D = \{\psi_D, \gamma_D\}$. The nonlinear dynamics of the game, $\dot{\mathbf{x}} = \mathbf{f}(\mathbf{x}, \mathbf{u}_P, \mathbf{u}_D)$, are defined by a system of nonlinear ordinary differential equations,

$$\begin{aligned}
\dot{x}_P &= v_P \cos\gamma_P \cos\psi_P, \quad & \dot{x}_E &= v_E \cos\gamma_E \cos\psi_E, \quad & \dot{x}_D &= v_D \cos\gamma_D \cos\psi_D \\
\dot{y}_P &= v_P \cos\gamma_P \sin\psi_P, \quad & \dot{y}_E &= v_E \cos\gamma_E \sin\psi_E, \quad & \dot{y}_D &= v_D \cos\gamma_D \sin\psi_D \\
\dot{z}_P &= v_P \sin\gamma_P, & \dot{z}_E &= v_E \sin\gamma_E, & \dot{z}_D &= v_D \sin\gamma_D.
\end{aligned} \tag{3.52}$$

The admissible controls of the pursuer and the defender for each instance of time are given by $\psi_P, \psi_D \in [-\pi, \pi]$ and $\gamma_P, \gamma_D \in [-\pi, \pi]$, for all time, $t \in [t_0, t_f]$. It is assumed that the evader is non-maneuverable, and therefore the evader's heading, ψ_E, and flight path angle, γ_E, remain constant. The evader's heading is also assumed to be known by both the defender (D) and pursuer (P).

The initial state of the game is defined as:

$$\mathbf{x}^T(t_0) = \mathbf{x}_0^T = [x_{P_0}, y_{P_0}, z_{P_0}, x_{E_0}, y_{E_0}, z_{E_0}, x_{D_0}, y_{D_0}, z_{D_0}]. \tag{3.53}$$

Just as in the 2-D case, point-capture is considered; this means that the $P - D$ range goes to zero in order for the defender to intercept the pursuer. It is also assumed

that the state of the system belongs to the escape set, denoted by $\mathbf{x} \in \mathscr{R}_e \subset \mathbb{R}^9$. The termination set, $\mathscr{C}$, which represents the interception of the pursuer by the defender (and the evader escapes the pursuer) is defined as

$$\mathscr{C} = \left\{ \mathbf{x} \,\middle|\, (x_P - x_D)^2 + (y_P - y_D)^2 + (z_P - z_D)^2 = 0, t = t_f \right\}. \tag{3.54}$$

The terminal time, t_f is the instant in time where the state reaches the terminal, $\mathscr{C}$, specified in eq. (3.54). The terminal state is

$$\mathbf{x}^T(t_f) = \mathbf{x}_f^T = [x_{P_f}, y_{P_f}, z_{P_f}, x_{E_f}, y_{E_f}, z_{E_f}, x_{D_f}, y_{D_f}, z_{D_f}]. \tag{3.55}$$

The objective cost is

$$J(\mathbf{u}_P, \mathbf{u}_D, \mathbf{x}_0) = \Phi(\mathbf{x}_f) = (x_{P_f} - x_{E_f})^2 + (y_{P_f} - y_{E_f})^2 + (z_{P_f} - z_{E_f})^2. \tag{3.56}$$

The objective cost depends only upon the terminal state of the Active Target Defense Differential Game (ATDDG); its value function is

$$V(\mathbf{x}_0) = \min_{\mathbf{u}_P(\cdot)} \max_{\mathbf{u}_D(\cdot)} J(\mathbf{u}_P, \mathbf{u}_D, \mathbf{x}_0). \tag{3.57}$$

Maximum Exposure of a Non-Maneuvering Pursuer in 2-D.

The directed energy defense of a non-maneuvering HVAA in 2-D is outlined in Scenario 4 of Table 1. In the scenario, the defender aims to maximally expose the pursuer which, in-turn, strives to capture the evader in minimum time. Consider first, the optimal control problem for the defender to maximally expose a faster, non-maneuvering pursuer, $v_P > v_D$. The constant velocities of the defender (D) and the pursuer (P) are defined as v_D and v_P respectively. The complete state of the

two-agent scenario is $\mathbf{x}^T = [x_D, y_D, x_P, y_P] \in \mathbb{R}^4$, where (x_D, y_D) and (x_P, y_P) are the positions of D and P respectively, for any time $t \in [t_0, t_f]$. The defender's control variable is the instantaneous heading angle $\mathbf{u}_D = \{\psi_D\}$. The equations of motion for the two-agent scenario follow the simple motion model in eq. (3.2) and are as follows:

$$\begin{aligned} \dot{x}_D &= v_D \cos\psi_D, \quad & \dot{x}_P &= v_P \cos\psi_P, \\ \dot{y}_D &= v_D \sin\psi_D, \quad & \dot{y}_P &= v_P \sin\psi_P. \end{aligned} \tag{3.58}$$

The course of the non-maneuvering pursuer, ψ_P, is assumed to be constant and known by the defender. The control of the defender is its heading: $\psi_D \in [0, 2\pi)$. At the onset, the pursuer is considered to be a distance R_D (the WEZ range) from the defender; at time zero (t_0), the initial state $\mathbf{x}(t_0) \equiv \mathbf{x}_0 \in \mathscr{I}$, where

$$\mathscr{I} = \{\mathbf{x} | (x_P - x_D)^2 + (y_P - y_D)^2 - R_D^2 = 0, t = t_0\}. \tag{3.59}$$

Also, the defender is at an aspect angle θ_P from the pursuer, pictorially shown in Figure 12. The complementary angle to the aspect angle is the line-of-sight angle, λ_{PD}, also shown in Figure 12. This circular WEZ model assumes that exposure is independent of the defender's heading and is range-limited. The WEZ is assumed to have a fixed radius, R_D. In this section, the time-optimal strategy of the defender is found which maximizes the time the fast pursuer is exposed.

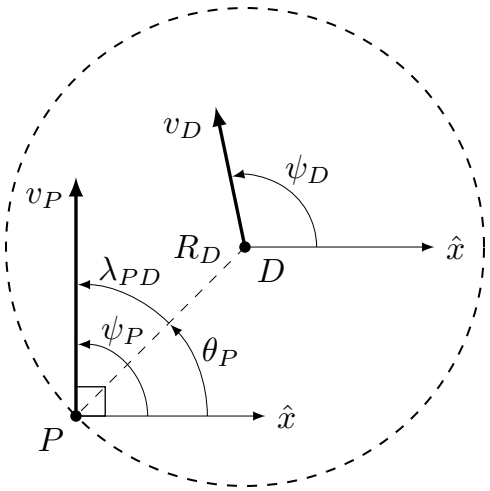

Figure 12. The initial engagement geometry consists of a defender with a circular WEZ in contact with a faster non-maneuvering pursuer.

Since the pursuer is faster than the defender, escape from the circular WEZ is guaranteed. Moreover, the termination set which represents the escape of the pursuer from the WEZ is defined as follows:

$$\mathscr{C} = \{\mathbf{x} | (x_D - x_P)^2 + (y_D - y_P)^2 - R_D^2 > 0, t = t_f\}. \tag{3.60}$$

Exposure of the pursuer by the defender is made so long as the range between the pursuer and defender is less than or equal to the WEZ radius, R_D. The terminal time, t_f, is defined as the instant in time where the state satisfies eq. (3.60); at which time, the terminal state is: $\mathbf{x}^T(t_f) = [x_{D_f}, y_{D_f}, x_{P_f}, y_{P_f}]$. Since the objective is to maximize the time by which the pursuer remains within the circular WEZ, the max-time objective cost is

$$\min_{\psi_D} \; J = \int_{t_0}^{t_f} -1 \; \mathrm{d}t \,. \tag{3.61}$$

The optimal exposure time is $t_f^* = \min J$ subject to the termination set in eq. (3.60). The goal is to find the optimal defender's heading time history which minimizes the objective cost in eq. (3.61), namely, $\psi_D^*(t) = \mathrm{argmin}_{\psi_D} J$.

Directed Energy Defense of a Non-Maneuvering HVAA in 2-D.

The directed energy defense of a non-maneuvering HVAA is described in Scenario 5 of Table 1. In this HVAA defense scenario, the pursuer aims to capture the evader in minimum time while the defender aims to maximally continuously expose the pursuer. The HVAA (evader) is non-maneuvering and as a result, the optimal strategies for the defender and the pursuer are of interest.

They dynamics of each of the three agents: pursuer, evader, and defender, follow the 2-D simple motion model as described in eq. (3.2). The pursuer, defender, and defender have constant velocity v_P, v_E, and v_D respectively. The complete state of the engagement is $\mathbf{x}^T = [x_P, y_P, x_E, y_E, x_D, y_D] \in \mathbb{R}^6$, where (x_P, y_P), (x_E, y_E), and (x_D, y_D) are the positions of P, E, and D respectively. Also define ψ_P, ψ_E, and ψ_D as the instantaneous headings of P, E, and D respectively. Consequently, the equations of motion for the three-agent scenario are:

$$\begin{aligned} \dot{x}_P &= v_P \cos\psi_P, \quad \dot{x}_E = v_E \cos\psi_E, \quad \dot{x}_D = v_D \cos\psi_D, \\ \dot{y}_P &= v_P \sin\psi_P, \quad \dot{y}_E = v_E \sin\psi_E, \quad \dot{y}_D = v_D \sin\psi_D. \end{aligned} \tag{3.62}$$

The non-maneuvering evader is on a fixed course and its position and heading are known by the pursuer. The pursuer, knowing the state of the evader, wishes to select a heading which intercepts E in minimum time. Capture is achieved when P and E are coincident (i.e., point-capture). During this pursuit, the defender has a circular WEZ with radius R_D, and it desires to keep the pursuer inside its WEZ for the maximum possible continuous time; that is, that P remains inside the WEZ without interruption.

The initial conditions for the scenario are that P and E are located in arbitrary locations in the 2-D Cartesian plane; while D is located a distance R_D from P. At

time zero (t_0), the initial state $\mathbf{x}(t_0) \equiv \mathbf{x}_0 \in \mathscr{I}$, where

$$\mathscr{I} = \{\mathbf{x} | (x_P - x_D)^2 + (y_P - y_D)^2 - R_D^2 = 0, t = t_0\}. \tag{3.63}$$

The termination set which represents the point-capture of the evader by the pursuer is defined as

$$\mathscr{C}_A = \{\mathbf{x} | (x_P - x_E)^2 + (y_P - y_E)^2 = 0, t = t_{go}\}. \tag{3.64}$$

The instant in time where the state satisfies eq. (3.64) is defined as t_{go}; also called the *time-to-go*. The termination set which represents the escape of the pursuer from the defender (the P-D range is larger than the WEZ range) is

$$\mathscr{C}_B = \{\mathbf{x} | (x_P - x_D)^2 + (y_P - y_D)^2 - R_D^2 > 0, t = t_{\text{exp}}\}. \tag{3.65}$$

The instant in time where the state satisfies eq. (3.65) is defined as t_{exp}; also called the *exposure time*. Because of the initial conditions as defined by eq. (3.63), the exposure time is the amount of time that passes until the pursuer escapes the defender's WEZ. The termination set of the entire scenario is $\mathscr{C}_A$, that is, the pursuer captures the evader regardless if the pursuer has escaped the WEZ of the defender prior to capturing the evader or if the pursuer has captured the evader before escaping the defender's WEZ. One objective of this section is to analyze the optimal strategy of the defender when t_{exp} is either less than, greater than, or equal to t_{go}. Also provided are the conditions when $t_{\text{exp}} = 0$, that is, that the defender can not expose the pursuer at all no matter the strategy of the defender.

The objective of the pursuer is to capture the evader in minimum time – to make

t_{go} a minimum. The objective cost of the pursuer is

$$J_A(\mathbf{x}_0; \psi_P(\cdot)) = \int_{t_0}^{t_{\text{go}}} 1 \, \mathrm{d}t = t_{\text{go}}. \tag{3.66}$$

The optimal time-to-go is $t^*_{\text{go}} = \min J_A$ subject to the termination set in eq. (3.64) – the pursuer and evader are collocated at final time. The goal for the pursuer is to find the optimal heading which minimizes the objective cost in eq. (3.66), namely,

$$\psi^*_P(t) = \underset{\psi_P}{\operatorname{argmin}} \; J_A. \tag{3.67}$$

The objective of the defender is to keep the pursuer inside the WEZ for as long as possible. Since the pursuer is faster than the defender, the pursuer's escape is guaranteed for a finite WEZ range, R_D. The objective cost of the defender is the same as eq. (3.61) in Section 5.1 and is as follows:

$$J_B\left(\mathbf{x}_0; \psi_D(\cdot)\right) = \int_{t_0}^{t_f} -1 \, \mathrm{d}t = -t_f. \tag{3.68}$$

The final time, $t_f = \min(t_{\text{exp}}, t_{\text{go}})$. This optimization problem ends when the states of the scenario reaches $\mathscr{C} = \mathscr{C}_A \cup \mathscr{C}_B$. The optimal exposure time is $t^*_{\text{exp}} = \min J_B$ subject to the termination set in eq. (3.65) – the pursuer is no longer contained inside the WEZ of the defender. The goal is to find the optimal defender's heading which minimizes the objective cost in eq. (3.68), namely,

$$\psi^*_D(t) = \underset{\psi_D}{\operatorname{argmin}} \; J_B. \tag{3.69}$$

Maximum Exposure of a Non-Maneuvering Pursuer in 3-D.

The directed energy defense of a non-maneuvering HVAA in 3-D is outlined in Scenario 6 of Table 1. In this scenario, a defender aims to maximally expose a non-maneuvering pursuer in the 3-D Cartesian space. This scenario is a direct extension of Scenario 4 to the 3-D Cartesian space. Define the constant speed of the defender (D) and the pursuer (P), as v_D and v_P respectively. The state space is composed of the position of the defender and the pursuer whose locations in 3-D Cartesian space are $(x_D, y_D, z_D)^T$ and $(x_P, y_P, z_P)^T$ respectively. The complete state of the exposure scenario, $\mathbf{x}$, is defined as follows:

$$\mathbf{x}^T = [x_D, y_D, z_D, x_P, y_P, z_P] \in \mathbb{R}^6. \tag{3.70}$$

The defender's control is composed of the instantaneous heading angle, ψ_D, and flight path angle, γ_D. The control vector, $\mathbf{u}$, is defined as follows:

$$\mathbf{u}^T = [\psi_D, \gamma_D] \in \mathbb{R}^2. \tag{3.71}$$

In the model, it is assumed that the position and course of the pursuer is constant and known by the defender. The dynamics for the pursuer and defender are

$$\begin{aligned} \dot{x}_P &= v_P \cos\gamma_P \cos\psi_P, \quad & \dot{x}_D &= v_D \cos\gamma_D \cos\psi_D \\ \dot{y}_P &= v_P \cos\gamma_P \sin\psi_P, \quad & \dot{y}_D &= v_D \cos\gamma_D \sin\psi_D \\ \dot{z}_P &= v_P \sin\gamma_P, & \dot{z}_D &= v_D \sin\gamma_D. \end{aligned} \tag{3.72}$$

As described in eq. (3.72), the course of the pursuer is defined by the pursuer's heading, ψ_P, and flight path angle, γ_P. The control of the defender is the heading, $\psi_D \in [0, 2\pi)\ \forall\ t \in [t_0, t_f]$, and flight path angle, $\gamma_D \in [-\pi, \pi]\ \forall\ t \in [t_0, t_f]$. At the

onset, the pursuer is a distance R_D from the defender, $\overline{DP} = R_D | t = t_0$. Aat initial time ($t_0$), the initial state $\mathbf{x}(t_0) \equiv \mathbf{x}_0 \in \mathscr{I}$, where

$$\mathscr{I} = \{\mathbf{x} | (x_P - x_D)^2 + (y_P - y_D)^2 + (z_P - z_D)^2 - R_D^2 = 0, t = t_0\}. \tag{3.73}$$

Also, the defender is located at an azimuth, ϕ, and angle relative to the z-axis, θ, with respect to the pursuer's position at the instant in time the scenario begins. The coordinates, angles, and initial conditions are shown in Figure 13. This spherical model assumes that exposure is guaranteed so long as the pursuer is within a fixed range of the defender.

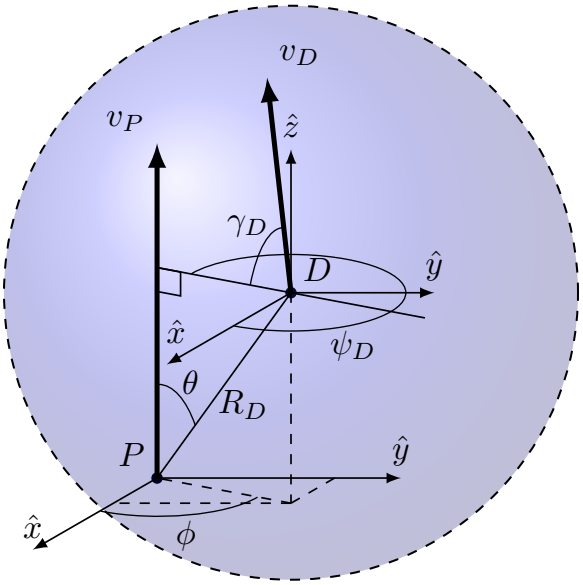

Figure 13. The initial geometry of the directed engery defense scenario occurs when the defender, with spherical WEZ, makes contact with the faster pursuer.

Since the pursuer is faster than the defender, escape from the spherical WEZ is guaranteed. Moreover, the termination set which represents the escape of the pursuer from the defender's WEZ is defined as follows:

$$\mathscr{C} = \{\mathbf{x} | (x_D - x_P)^2 + (y_D - y_P)^2 + (z_D - z_P)^2 - R_D^2 > 0 = t_f\}. \tag{3.74}$$

The terminal time, t_f, is defined as the instant in time where the state and time satisfies eq. (3.74); at which time, the terminal state is:

$$\mathbf{x}^T(t_f) = [x_{D_f}, y_{D_f}, z_{D_f}, x_{P_f}, y_{P_f}, z_{P_f}].$$

Since the objective is to maximize the time by which the pursuer remains within the circular WEZ, the max-time objective cost is as follows:

$$J = \int_0^{t_f} -1 \, \mathrm{d}t = -t_f. \tag{3.75}$$

The optimal exposure time is $t_f^* = -\min J$ subject to the termination set in eq. (3.74). The goal is to find the optimal defender's heading and flight path angle time histories which minimize the objective cost in eq. (3.75), namely, $\mathbf{u}^* = \mathrm{argmin}_{\mathbf{u}} J$.

3.5 Summary

In order to investigate the optimal strategies for the defense of a HVAA, the equations of motion in 2-D and 3-D have been described to represent aircraft engaged in pursuit, evasion, and defense. These simple motion models can be used to evaluate aircraft motion through navigational commands. Using these models, both optimal control problems and differential games can be formulated. A brief overview of the indirect method and direct method of computing optimal control was presented followed by a brief overview of differential games. Using these methods, this work aims at proposing and solving various aerial engagements to investigate optimal defensive strategies that protect a HVAA from a single threat. After the discussion on differential games and optimal control, Apollonius Circle was presented as a method for solving a pursuit-evasion differential game. Next, the generic HVAA defense differential games were described. In the kinetic defense differential game, the defender

aims at capturing the pursuer before it can capture the evader. In the directed energy defense differential game, the defender aims at exposing the pursuer for as long as possible before the pursuer captures the evader. Finally, the solution approach for solving each research task is presented in brief. The results of this work begin with Chapter IV where the kinetic defense is investigated. Also, in Chapter IV, four different direct optimal control methods are compared and contrasted for solving the optimal strategies for the kinetic defense of a HVAA against an incoming threat when the evader can maneuver. Next, in Chapter V directed energy defense is provided by maximizing the time that a pursuer is within a specified range of the defender. These chapters address the desired research tasks for this dissertation.

IV. Kinetic Defense of a HVAA

> Reflections should be bestowed until the instances relevant to practice are delineated. With a judicial amount of reason and trial and error, an answer should be attainable
>
> — Rufus Isaacs, Rand Report RM-1391-PR

An engagement scenario involving the kinetic defense of a HVAA is investigated in this chapter. In this defense scenario, an attacking missile or adversary (pursuer) aims to capture the HVAA (evader) which is teamed with a cooperative missile (defender). A successful kinetic defense occurs when the defender captures the pursuer before the pursuer captures the evader. In this work, only scenarios where the defender provides a successful defense of the evader are considered. This chapter is divided into four parts: kinetic defense of a non-maneuvering HVAA in 2-D, kinetic defense of a non-maneuvering HVAA in 3-D, kinetic defense of a maneuvering HVAA in 2-D, and a direct methods comparison for HVAA defense.

4.1 Kinetic Defense of a Non-Maneuvering HVAA in 2-D

An engagement scenario involving the defense of a non-maneuverable HVAA in the 2-D Cartesian plane is investigated in this section. In this scenario, an incoming threat (pursuer) pursues the non-maneuverable HVAA (evader) which is teamed with a cooperative missile (defender). Because the evader is non-maneuvering, the pursuer and defender play a simple game: The pursuer aims at minimizing the terminal distance with respect to the evader while the defender aims to maximize the same terminal distance. Termination of the game is defined as the time when the defender intercepts the pursuer, i.e. the pursuer and defender are collocated at final time. The saddle point state feedback strategies for the pursuer and defender are presented

in this section and the optimal saddle point strategies are compared to a heuristic approach found in literature [161]. An example shows that better performance is obtained by implementing the saddle point strategies derived herein compared to the heuristic approach.

In the defense differential game of a non-maneuvering HVAA, the speeds of the pursuer (P), evader (E), and defender (D) are constant and denoted by v_P, v_E, and v_D, respectively. The agents are modeled having simple 2-D motion as commonly found in games of Isaacs [9].

Differential Game.

Described in Section 3.4, a differential game is developed between the pursuer and the defender concerning the defense of a non-maneuvering HVAA. From the problem definition, the motion of the three agents are defined as a set of ordinary differential equations as shown in eq. (3.46). Also, the objective cost is defined in eq. (3.50) and the value function of the differential game is defined in eq. (3.51). Define the speed ratio problem parameter $\mu = v_E/v_P$. In general, the pursuer is faster than the evader, so $0 < \mu < 1$. Also, define the speed ratio $\alpha = v_D/v_P$. When the defender is faster than the pursuer, $\alpha > 1$. The speed ratios μ and α and the evader's constant heading ψ_E are the problem parameters. Using the aforementioned equations of motion in eq. (3.46) as well as the speed ratios α and μ, the dynamics may be non-dimensionalized with respect to time and are as follows:

$$\begin{aligned} \dot{x}_P &= \cos\psi_P, \quad \dot{x}_E = \mu\cos\psi_E, \quad \dot{x}_D = \alpha\cos\psi_D, \\ \dot{y}_P &= \sin\psi_P, \quad \dot{y}_E = \mu\sin\psi_E, \quad \dot{y}_D = \alpha\sin\psi_D. \end{aligned} \tag{4.1}$$

Note, that making such a transformation to non-dimensional variables reduces the number of parameters used in derivation and generalizes solutions through speed

ratios rather than requiring the use of speeds explicitly. This is an approach that is leveraged throughout this dissertation. It amounts to having one of the agent's (in this case the pursuer) have speed of unity.

There exists one costate for each state, therefore the the costate vector is $\mathbf{p}^T = [p_{x_P}, p_{y_P}, p_{x_E}, p_{y_E}, p_{x_D}, p_{y_D}] \in \mathbb{R}^6$, and the Hamiltonian of the differential game, in this case, is the inner product of the nonlinear dynamics from eq. (3.46) and the costates, $\mathbf{p}$. The Hamiltonian is

$$\begin{aligned} \mathscr{H} = & p_{x_P} \cos\psi_P + p_{y_P} \sin\psi_P + \alpha p_{x_D} \cos\psi_D \\ & + \alpha p_{y_D} \sin\psi_D + \mu p_{x_E} \cos\psi_E + \mu p_{y_E} \sin\psi_E. \end{aligned} \tag{4.2}$$

where the speeds have been normalized using the pursuer's speed, v_P, as a reference.

Theorem 1. *Consider the defense differential game of non-maneuverable aircraft described by eqs.* (3.46) *to* (3.51)*. The headings of the pursuer and the defender are constant under optimal play and their trajectories are straight lines.*

Proof. By differentiating the Hamiltonian in eq. (4.2) with respect to ψ_P and setting the derivative equal to 0, the optimal heading, ψ_P^* is

$$\frac{\partial \mathscr{H}}{\partial \psi_P} = -p_{x_P} \sin\psi_P + p_{y_P} \cos\psi_P = 0. \tag{4.3}$$

Using the trigonometric identity $\cos^2\psi_P + \sin^2\psi_P = 1$, eq. (4.3) can be written as follows:

$$\cos^2\psi_P = \frac{p_{x_P}^2}{p_{x_P}^2 + p_{y_P}^2}, \qquad \sin^2\psi_P = \frac{p_{y_P}^2}{p_{x_P}^2 + p_{y_P}^2}. \tag{4.4}$$

The second partial derivative $\frac{\partial^2 \mathscr{H}}{\partial \psi_P^2}$ is computed in order to determine wether the positive or the negative roots of eq. (4.4) are indeed the optimal pursuer headings.

Doing so, the following is obtained:

$$\frac{\partial^2 \mathscr{H}}{\partial \psi_P^2} = -p_{x_P} \cos\psi_P - p_{y_P} \sin\psi_P. \tag{4.5}$$

Substituting the obtained heading

$$\cos\psi_P^* = -\frac{p_{x_P}}{\sqrt{p_{x_P}^2 + p_{y_P}^2}}, \quad \sin\psi_P^* = -\frac{p_{y_P}}{\sqrt{p_{x_P}^2 + p_{y_P}^2}}. \tag{4.6}$$

into eq. (4.5), the second partial, $\frac{\partial^2 \mathscr{H}}{\partial \psi_P^2} > 0$. Therefore, the optimal heading in eq. (4.6) minimizes $\mathscr{H}$ and, therefore, it minimizes the terminal distance between P and E. Similarly, by computing $\frac{\partial \mathscr{H}}{\partial \psi_D} = 0$ the defender's optimal heading which maximizes the terminal distance between P and E is obtained and is as follows:

$$\cos\psi_D^* = \frac{p_{x_D}}{\sqrt{p_{x_D}^2 + p_{y_D}^2}}, \ \sin\psi_D^* = \frac{p_{y_D}}{\sqrt{p_{x_D}^2 + p_{y_D}^2}}. \tag{4.7}$$

Additionally, the costate dynamics are obtained by evaluating $-\partial \mathscr{H}/\partial \mathbf{x}$ and therefore $\dot{p}_{x_P} = \dot{p}_{y_P} = \dot{p}_{x_D} = \dot{p}_{y_D} = \dot{p}_{x_E} = \dot{p}_{y_E} = 0$; hence, all costates are constant and therefore ψ_P^* and ψ_D^* are constant. Consequently, the optimal trajectories are straight lines. ■

Given from Theorem 1, the optimal trajectories are straight lines. In such an instance, the Apollonius Circle is a relevant tool to determine the optimal headings of the agents P and D [9]. In general, a circle can be defined as the locus of points, I, with a constant ratio of distances to two given points which are called foci. In this scenario, the foci are P and D, i.e. $\beta = \frac{\overline{PI}}{\overline{DI}}$ is constant. When the circle is defined using the constant ratio of distances just described, it is commonly referred to as an Apollonius Circle and it represents an important tool to analyze pursuit-evasion problems. Consider agents P and D traveling in straight lines and at constant speeds

v_P and v_D, respectively. The constant parameter $\beta = \frac{v_P}{v_D} = \frac{1}{\alpha}$ is the speed ratio parameter. In this scenario, D strives to intercept P. D intercepts P at a point $I = (x_I, y_I)$ on the Apollonius Circle and at that point, the distance traveled by P is equal to β multiplied by the distance traveled by D. Hence, an Apollonius Circle can be constructed based on the distance between P and D and also based on the speed ratio parameter β. The center of the circle is denoted by O where the points P, D, and O are collinear as illustrated in Figure 14.

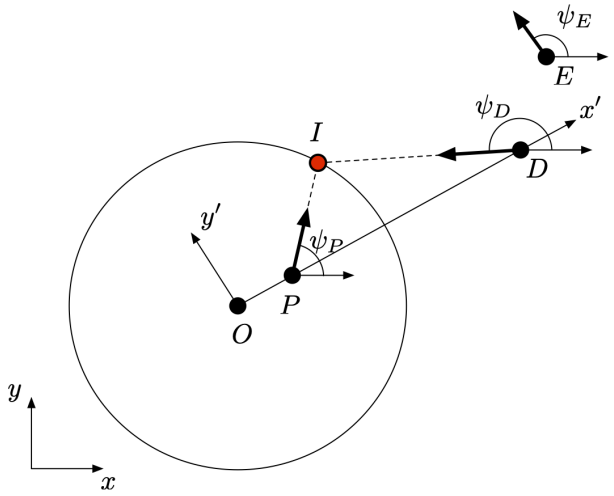

Figure 14. The Apollonius Circle (P,D) with the interception point (in red) located in the global frame.

Without loss of generality, consider the relative coordinate frame illustrated in Figure 15; where the points P and D denote the positions of the pursuer and the defender, respectively. The x'-axis of this frame goes from P to D which results in $y_P = y_D = 0$. The origin of the coordinate frame is the center of the $\overline{PD}$-Apollonius Circle. This circle is characterized as follows:

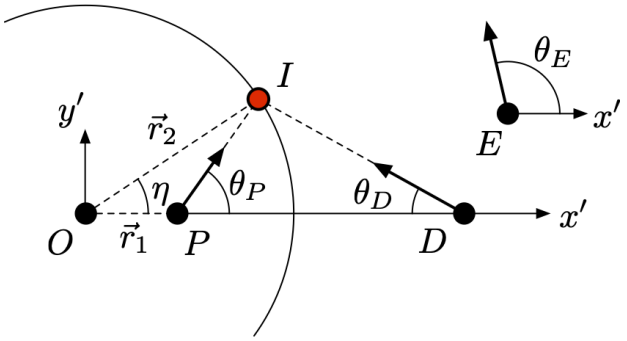

Figure 15. The Apollonius Circlex (P,D) with the interception point (in red) located in the local frame aligned with P and D.

Let $\lambda_{PD} = \tan^{-1}\left(\frac{y_D - y_P}{x_D - x_P}\right)$ be the line-of-sight (LOS) angle from P to D. The headings of the players in the relative frame are given by $\theta_P = \psi_P - \lambda_{PD}$ and $\theta_D = \pi + \lambda_{PD} - \psi_D$. The constant heading of the evader is $\theta_E = \psi_E - \lambda_{PD}$. Further, let r_1 denote the distance between P, the pursuer position, and O, the center of the Apollonius Circle. The distance r_1 is given by

$$r_1 = \frac{\beta^2 d}{1 - \beta^2}, \tag{4.8}$$

where $d = \sqrt{(x_P - x_D)^2 + (y_P - y_D)^2}$ is the distance between agents P and D. Also, let r_2 be the radius of the Apollonius Circle. Then, r_2 is given by

$$r_2 = \frac{\beta d}{1 - \beta^2}. \tag{4.9}$$

The pursuer strives to minimize the terminal distance between itself and the evader which is traveling both at constant speed, v_E, and at constant heading, ψ_E. The points E and E' represent the initial and terminal positions of the evader, respectively. The point I is the final position of the pursuer and also the final position of the defender since point capture is considered.

Using the Apollonius Circle between P and D, the optimization of two variables

can be transformed into an optimization problem of only one. The pursuer aims at a point on the Apollonius Circle, where it will be intercepted by the defender, which minimizes the terminal $\overline{PE}$ distance. The optimal interception point is calculated as follows.

Theorem 2. *Assume that* $\mathbf{x} \in R_e$*, then, the optimal interception point in the relative coordinate frame is given by* $I^* = (r_2 \cos\eta^*, r_2 \sin\eta^*)$ *where* η^* *is such that* $\nu^* = e^{i\eta^*} = \cos\eta^* + i\sin\eta^*$ *and* ν^* *is the solution of the polynomial equation*

$$\left(\tfrac{3r_1r_2}{2p}\right)^2 \nu^8 + b_7\nu^7 + b_6\nu^6 + b_5\nu^5 + b_4\nu^4 + b_3\nu^3 + b_2\nu^2 + b_1\nu + \left(\tfrac{3}{2}r_1r_2p\right)^2 = 0 \quad (4.10)$$

which minimizes the function:

$$\begin{aligned} J(\nu) =& r_2^2 + r_7^2 + \mu^2(r_1^2 + r_2^2) \\ & - r_2(\mu^2 r_1 + r_7 m^{-1})\nu - r_2(\mu^2 r_1 + r_7 m)\nu^{-1} \\ & + \mu[r_7 Q - r_2(p^{-1}\nu + p\nu^{-1})]r_3(\nu), \end{aligned} \quad (4.11)$$

where

$$r_3(\nu) = \sqrt{r_1^2 + r_2^2 - r_1 r_2(\nu + \nu^{-1})} \quad (4.12)$$

and $\nu = e^{i\eta}$. *The polynomial coefficients are*

$$
\begin{aligned}
b_7 &= r_1 r_2[(\mu r_1 + \tfrac{r_7}{\mu m})^2 - \tfrac{3}{p}(\tfrac{r_1 r_7 Q}{2} + \tfrac{r_1^2 + r_2^2}{p})] \\
b_6 &= (\tfrac{r_1 r_7 Q}{2} + \tfrac{r_1^2 + r_2^2}{p})^2 - \tfrac{3}{2} r_1^2 r_2^2 (1 - \tfrac{1}{p^2}) \\
&\quad -(r_1^2 + r_2^2)(\mu r_1 + \tfrac{r_7}{\mu m})^2 \\
b_5 &= r_1 r_2[(r_1^2 + r_2^2)(4 - \tfrac{1}{p^2}) + r_1 r_7 Q(\tfrac{1}{p} + \tfrac{1}{2}p) - \mu^2 r_1^2 \\
&\quad -2 r_1 r_7 m + \tfrac{r_7^2}{\mu^2}(\tfrac{1}{m^2} - 2)] \\
b_4 &= \tfrac{r_1^2 r_2^2}{4}(p^2 + \tfrac{1}{p^2} - 20) \\
&\quad +2(r_1^2 + r_2^2)(\mu^2 r_1^2 + r_1 r_7 (m + \tfrac{1}{m}) + \tfrac{r_7^2}{\mu^2}) \\
&\quad -2(\tfrac{r_1 r_7 Q}{2} + \tfrac{r_1^2 + r_2^2}{p})(\tfrac{r_1 r_7 Q}{2} + p(r_1^2 + r_2^2)) \\
b_3 &= r_1 r_2[(r_1^2 + r_2^2)(4 - p^2) + r_1 r_7 Q(p + \tfrac{1}{2p}) - \mu^2 r_1^2 \\
&\quad -\tfrac{2}{m} r_1 r_7 + \tfrac{r_7^2}{\mu^2}(m^2 - 2)] \\
b_2 &= (\tfrac{r_1 r_7 Q}{2} + p(r_1^2 + r_2^2))^2 + \tfrac{3}{2} r_1^2 r_2^2 (p^2 - 1) \\
&\quad -(r_1^2 + r_2^2)(\mu r_1 + \tfrac{r_7 m}{\mu})^2 \\
b_1 &= r_1 r_2[(\mu r_1 + \tfrac{r_7 m}{\mu})^2 - 3p(\tfrac{r_1 r_7 Q}{2} + p(r_1^2 + r_2^2))]
\end{aligned}
\tag{4.13}
$$

where the parameters $p = e^{i\theta_5}$, $m = e^{i\theta_7}$, *and* $Q = pm^{-1} + p^{-1}m$.

Proof. Considering the geometry in Figure 15, one may be able to derive a kinematic linkage which represents the engagement scenario. The Apollonius Circle can be represented by a crank slider mechanism as seen in Figure 16. This geometry can be described as a linkage of fixed length $r_2 = \overline{OA'}$ that rotates about the origin O. As this linkage rotates about the origin, the linkage length $r_3 = \overline{AA'}$ can vary; however, the linkage is anchored and free to rotate about point P which is co-linear with the x'-axis, i.e. $\overline{OA}$ lies on the x'-axis. In this initial problem statement, the lengths r_1 and r_2 are fixed. r_3 is free to change in length and to rotate about P. One can visualize this motion quite easily, and the following kinematic synthesis shows the relation between the rational angle η, the length of the slider, r_3, and its angle with

the x'-axis, θ_P.

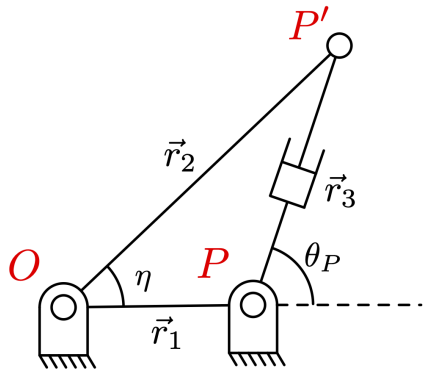

Figure 16. Apollonius Circle as Linkage Geometry

The first step in solving the relation between the free variable of the linkage is to start with the closure equation,

$$\vec{r}_2 = \vec{r}_1 + \vec{r}_3. \tag{4.14}$$

By expanding eq. (4.14) to include the Cartesian unit vectors: $\hat{i}$ and $\hat{j}$, the following is obtained:

$$|\vec{r}_2|\cos(\eta)\hat{i} + |\vec{r}_2|\sin(\eta)\hat{j} = |\vec{r}_1|\hat{i} + |\vec{r}_3|\cos(\theta_P)\hat{i} + |\vec{r}_3|\sin(\theta_P)\hat{j}. \tag{4.15}$$

Using the following shorthand notation,

$$\begin{aligned} |\vec{r}_i| &= r_i \;\forall\; i = \{1, 2, \cdots, n\}, \\ \cos(\eta) &= c_\eta, \quad \sin(\eta) = s_\eta, \\ \cos(\theta_P) &= c_{\theta_P}, \quad \sin(\theta_P) = s_{\theta_P}, \\ \cos(\theta_E) &= c_{\theta_E}, \quad \sin(\theta_E) = s_{\theta_E}, \end{aligned} \tag{4.16}$$

the linkage synthesis carried out becomes more compact. The expanded closure equa-

tion in eq. (4.15) can be re-written as follows:

$$r_2 c_\eta \hat{i} + r_2 s_\eta \hat{j} = r_1 \hat{i} + r_3 c_{\theta_P} \hat{i} + r_3 s_{\theta_P} \hat{j}. \tag{4.17}$$

Breaking eq. (4.17) into the x and y components and by isolating the slider, r_3, to the left hand side, squaring both sides, then summing both equations, the unknown angle θ_P can be eliminated from the equation. The slider length as a function of η is as follows:

$$r_3^2 = r_2^2 + r_1^2 - 2 r_1 r_2 c_\eta. \tag{4.18}$$

Now that the slider lengths are in terms of known variables, the relation of the angles θ_P and η as a function of eq. (4.17): $s_{\theta_P} = r_2 s_\eta / r_3$ can be obtained.

Next, consider the entire kinematic rejoin geometry as seen in Figure 17. The

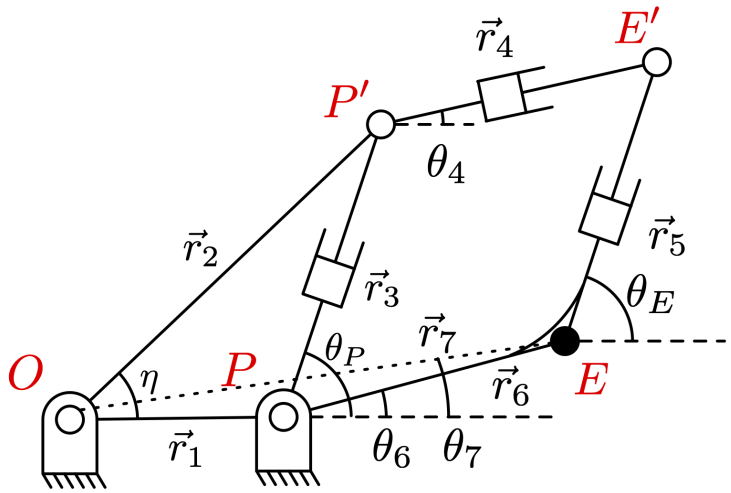

Figure 17. The geometry which represents the kinetic defense of a non-maneuvering evader in 2-D can be represented as a multi-linkage system composed of fixed linkages, sliders, and pin-joints as shown.

previous analysis is repeated beginning with the loop closure equation:

$$\vec{r}_2 + \vec{r}_4 = \vec{r}_7 + \vec{r}_5. \tag{4.19}$$

Expanding eq. (4.19) into x and y Cartesian unit vectors and separating them into component equations, the following is obtained:

$$r_2 c_\eta + r_4 c_4 = r_7 c_7 + r_5 c_{\theta_E}, \tag{4.20}$$

$$r_2 s_\eta + r_4 s_4 = r_7 s_7 + r_5 s_{\theta_E}. \tag{4.21}$$

The objective is to obtain the angle η which minimizes the distance r_4. This is accomplished by first eliminating the unknown angle θ_4 from the component equations. Much like before, r_4 is isolated on the left hand side of the equals sign, and therefore

$$r_4 c_4 = r_7 c_7 + r_5 c_{\theta_E} - r_2 c_\eta, \tag{4.22}$$

$$r_4 s_4 = r_7 s_7 + r_5 s_{\theta_E} - r_2 s_\eta. \tag{4.23}$$

Squaring both sides and summing the two resulting equations,

$$\begin{aligned} r_4^2 =& r_7^2 + r_5^2 + r_2^2 - 2r_2 r_5 (c_\eta c_{\theta_E} + s_\eta s_{\theta_E}) \\ & - 2r_2 r_7 (c_\eta c_7 + s_\eta s_7) + 2r_5 r_7 (c_{\theta_E} c_7 + s_{\theta_E} s_7). \end{aligned} \tag{4.24}$$

Next, substitute the relationship between the linkage lengths r_5 and r_3. For this problem, recall r_5 and r_3 have a linear relationship by a positive definite constant μ, such that $r_5 = \mu r_3$. Using this relation in eq. (4.24) yields

$$\begin{aligned} r_4^2 =& r_2^2 + \mu^2 r_3^2 + r_7^2 - 2\mu r_2 r_3 (c_\eta c_{\theta_E} + s_\eta s_{\theta_E}) \\ & - 2r_2 r_7 (c_\eta c_7 + s_\eta s_7) + 2\mu r_3 r_7 (c_{\theta_E} c_7 + s_{\theta_E} s_7). \end{aligned} \tag{4.25}$$

Since it is the goal to minimize the linkage length r_4 one recognizes that the minimization of r_4 is the same as a minimization of r_4^2. To perform the minimization, the

cost/payoff can be written as follows:

$$\begin{aligned} J &= r_2^2 + r_7^2 + \mu^2 r_3^2 - 2\mu r_2 \cos(\eta - \theta_5) r_3 \\ &\quad - 2 r_2 r_7 \cos(\eta - \theta_7) + 2\mu r_7 \cos(\theta_5 - \theta_7) r_3, \end{aligned} \tag{4.26}$$

where $r_2, r_7, \theta_5, \theta_7$ are constant and only r_3 is a function of the angle η. Taking the square root of eq. (4.18),

$$r_3 = \sqrt{r_1^2 + r_2^2 - 2 r_1 r_2 \cos\eta}. \tag{4.27}$$

From eq. (4.27) and the identity $\cos\eta = \frac{1}{2}(e^{i\eta} + e^{-i\eta})$, r_3 can be written in terms of $\nu = e^{i\eta} = \cos\eta + i\sin\eta$ as it is shown in eq. (4.12). Further, eq. (4.26) can be written as a function of ν in the following form:

$$\begin{aligned} J =& r_2^2 + r_7^2 + \mu^2 (r_1^2 + r_2^2) \\ &- r_2(\mu^2 r_1 + r_7 m^{-1})\nu - r_2(\mu^2 r_1 + r_7 m)\nu^{-1} \\ &+ \mu[r_7 Q - r_2(p^{-1}\nu + p\nu^{-1})]\sqrt{r_1^2 + r_2^2 - r_1 r_2(\nu + \nu^{-1})}. \end{aligned} \tag{4.28}$$

Taking the partial derivative of J from Equation (4.28) with respect to ν yields:

$$\begin{aligned} \tfrac{dJ}{d\nu} &= -r_2(\mu^2 r_1 + r_7 m^{-1}) + r_2(\mu^2 r_1 + r_7 m)\nu^{-2} \\ &\quad + \mu[r_7 Q - r_2(p^{-1}\nu + p\nu^{-1})]\tfrac{r_1 r_2(\nu^{-2} - 1)}{2\sqrt{r_1^2 + r_2^2 - r_1 r_2(\nu + \nu^{-1})}} \\ &\quad + \mu r_2 \sqrt{r_1^2 + r_2^2 - r_1 r_2(\nu + \nu^{-1})}(-p^{-1} + p\nu^{-2}). \end{aligned} \tag{4.29}$$

Setting eq. (4.29) equal to zero and multiplying by r_3,

$$\begin{aligned}
&[(\mu^2 r_1 + r_7 m)\nu^{-2} - (\mu^2 r_1 + r_7 m^{-1})] \\
&\quad \times \sqrt{r_1^2 + r_2^2 - r_1 r_2(\nu + \nu^{-1})} \\
&+\tfrac{\mu}{2} r_1(\nu^{-2} - 1)[r_7 Q - r_2(p^{-1}\nu + p\nu^{-1})] \\
&+\mu(p\nu^{-2} - p^{-1})[r_1^2 + r_2^2 - r_1 r_2(\nu + \nu^{-1})] = 0.
\end{aligned} \tag{4.30}$$

Dividing eq. (4.30) by μ, moving the terms containing r_3 to the right hand side, and multiplying both sides by ν^3, the negative exponents of ν are eliminated and the following is obtained:

$$\begin{aligned}
&\tfrac{r_1}{2}(1 - \nu^2)[r_7 Q\nu - r_2(p^{-1}\nu^2 + p)] \\
&+(p - p^{-1}\nu^2)[(r_1^2 + r_2^2)\nu - r_1 r_2(\nu^2 + 1)] = \\
&-\tfrac{\mu^2 r_1 + r_7 m - (\mu^2 r_1 + r_7 m^{-1})\nu^2}{\mu} \sqrt{(r_1^2 + r_2^2)\nu^2 - r_1 r_2(\nu^3 + \nu)}.
\end{aligned} \tag{4.31}$$

Taking the square of both sides of eq. (4.31) the common terms are arranged to obtain eq. (4.10). ■

Remark. The solution provided in Theorem 2 only requires the rooting of a polynomial and determining the optimal solution, $\nu^* = \cos\eta^* + i\sin\eta^*$, by computing the associated cost of each root. The angle η^*, is uniquely determined from $\eta^* = \cos^{-1} Re(\nu^*)$ and $\eta^* = \sin^{-1} Im(\nu^*)$, where $Re(\nu^*)$ and $Im(\nu^*)$ represent the real and the imaginary part of ν^*. This solution, although not explicit, can be easily implemented in state feedback form which is useful to provide robustness against unknown guidance laws by the pursuer or different interception strategies by the defender. In other words, given the state feedback solution, either of the players will see their performance level increased if their opponent does not follow the optimal strategy obtained in Theorem 2.

The optimal intersection point as defined by Theorem 2 provides the optimal

headings for the defender and the pursuer as follows:

$$\psi_D^* = \tan^{-1}\left(\frac{r_2 \sin\eta^* - y_D}{r_2 \cos\eta^* - x_D}\right) + \lambda_{PD}, \tag{4.32}$$

$$\psi_P^* = \tan^{-1}\left(\frac{r_2 \sin\eta^* - y_P}{r_2 \cos\eta^* - x_P}\right) + \lambda_{PD}, \tag{4.33}$$

where r_2 is defined in eq. (4.9), (x_D, y_D) and (x_P, y_P) are the locations of the pursuer and defender in the cartesian fixed frame, respectively, λ_{PD} is the LOS angle form the pursuer to the defender, and η^* is defined by Theorem 2.

Particular Case.

In the case where P and D have the same speed, $\beta = \frac{v_P}{v_D} = 1$, the optimal interception point can be obtained by rooting a quartic equation. Consider in this case, the relative frame is shown in Figure 18 where the reachable regions of P and D are separated by the orthogonal bisector of the segment $\overline{PD}$ instead of the Apollonius Circle previously described. Therefore, the optimal interception point, in this case, has coordinates $I^* = (0, y^*)$ where y^* is obtained as follows.

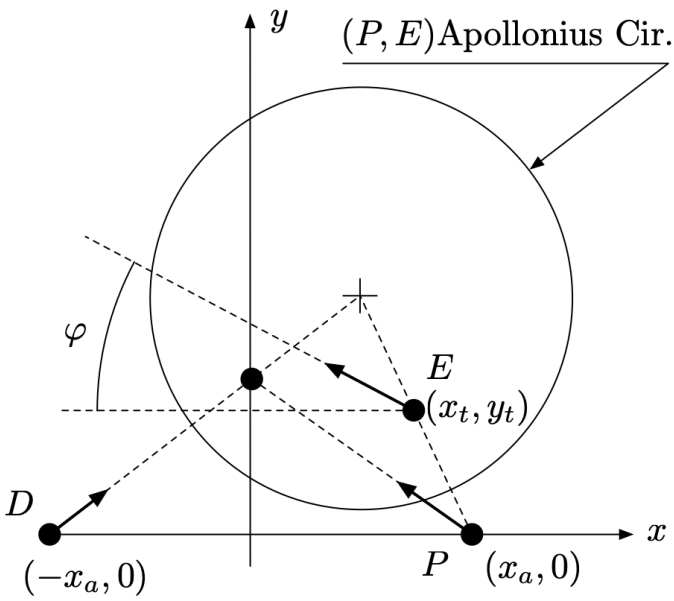

Figure 18. Apollonius Circle for the particular case: $\beta = 1$

Corollary 1. *Consider the case* $\beta = 1$ *and assume that* $\boldsymbol{x} \in R_e$*, then, the optimal interception point in the relative coordinate frame is given by* $I^* = (0, y^*)$ *where* y^* *the solution of the polynomial equation*

$$\begin{aligned} &(1+\mu^2)^2 y^4 - 2(1+\mu^2) y_E y^3 \\ &+[y_E^2 + (1+\mu^2)x_D^2 - \mu^2(y_E \sin\varphi - x_E \cos\varphi)^2] y^2 \\ &-2x_D^2[(1+\mu^2\cos^2\varphi) y_E - \mu^2 x_E \sin\varphi\cos\varphi] y \\ &+x_D^2(y_E^2 - x_D^2 \sin^2\varphi) = 0 \end{aligned} \tag{4.34}$$

which minimizes the function

$$J(y) = (x_E - \mu\sqrt{x_D^2 + y^2}\cos\varphi)^2 + (y_E - y + \mu\sqrt{x_D^2 + y^2}\sin\varphi)^2. \tag{4.35}$$

Examples.

In order to highlight the optimal strategies for the defender and pursuer, consider the same example as in [161], Section III.B. The initial positions are $D_0 = (0, 0)$,

$P_0 = (0, 10)$, $E_0 = (5, 5)$. The speeds of the missiles are $v_D = 2$, $v_P = 1$. Also, the same evader's speed as in [161], $v_E = 1$, is used. The evader fixed heading is $\psi_E = 60\,\text{deg}$.

Example 1: Optimal Defender and Optimal Pursuer.

Figure 19 shows the optimal trajectories of the encounter, where each one of the players, P and D, implement the saddle point strategies which were previously obtained. The value of the game is $V(\mathbf{x}; \psi_P^*, \psi_D^*) = 1.9864$.

Note that the optimal strategies are continuously updated. This means that at every time instant, the current positions are used to update the state of the system and compute the optimal interception point which is used to obtain the headings of P and D. The solution of the defense differential game of non-maneuverable aircraft possess the invariance property, that is, the interception point and the headings of the players are constant under optimal play. The interception point in the fixed frame remains the same when both players apply the optimal strategy derived in this section. The previous statement does not hold if at least one of the players does not follow its prescribed optimal strategy. An illustrative comparison with respect to the heuristic approach in [161] is shown in the next two examples. It is also shown that the player which implements the heuristic approach loses performance with respect to the objective of the game.

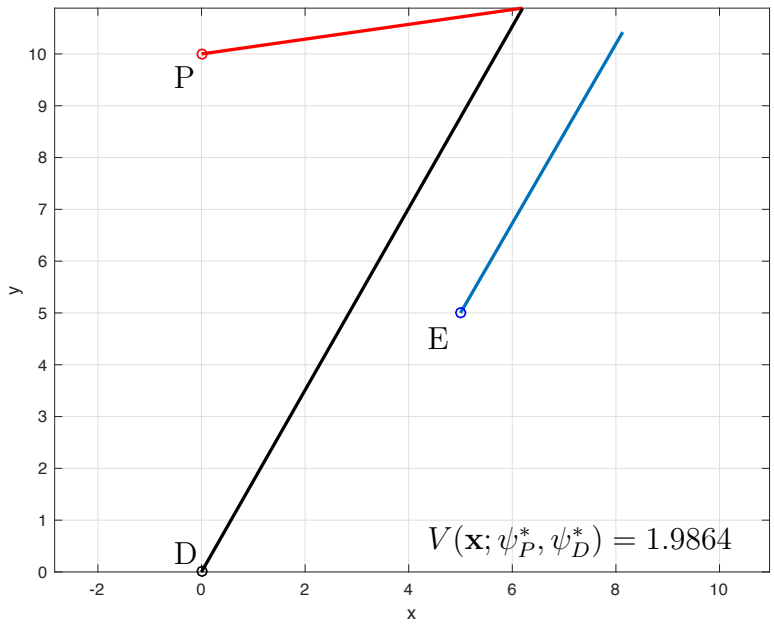

Figure 19. The trajectories of the pursuer (red), evader (blue), and defender (black) in the fixed frame, where the pursuer and defender implement optimal strategies as dictated by the differential game

Example 2: Optimal Defender and Heuristic Pursuer.

Now consider the case where the pursuer does not follow its optimal strategy derived in this section. Instead, it follows the heuristic approach in [161]. The defender implements the optimal strategy obtained in this section. The trajectories of the engagement under this selection of headings are shown in Figure 20. The defender is not only able to intercept the pursuer but it does at a distance further apart from the evader. The terminal $\overline{PE}$ separation is $V(\mathbf{x};\psi_P,\psi_D^*) = 2.6613$, that is, the pursuer is doing poorly by following a heuristic approach compared to the optimal saddle point strategy in Example 1.

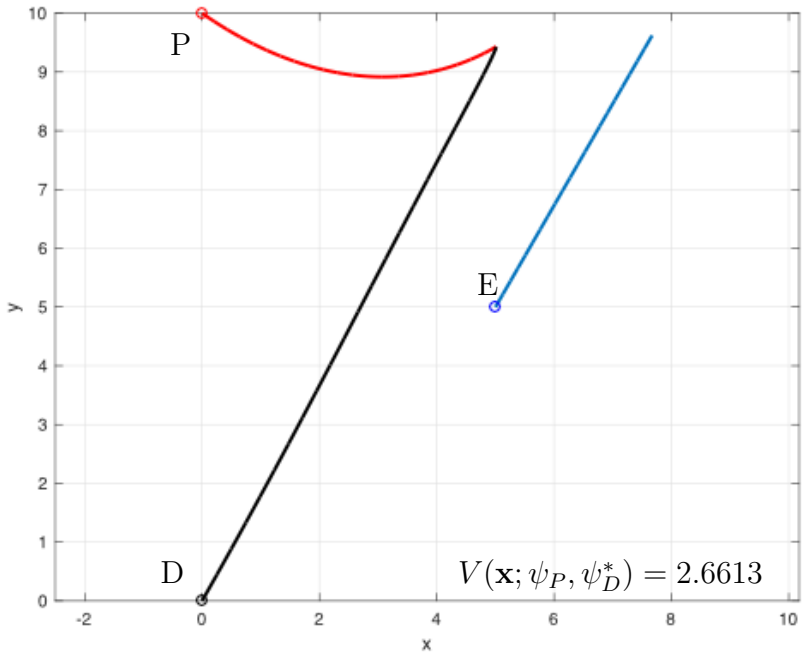

Figure 20. The trajectories of the pursuer (red), evader (blue), and defender (black) in the fixed frame, where the pursuer implements the heuristic strategy and defender implements the optimal strategy from the differential game

Example 3: Heuristic Defender and Optimal Pursuer.

Finally, consider the opposite case, that is, the pursuer follows the optimal strategy derived in this section while the defender implements the heuristic approach in [161]. The resulting trajectories are shown in Figure 21. The terminal $\overline{PE}$ separation is $V(\mathbf{x};\psi_P^*,\psi_D) = 1.9795$. In this case, the terminal distance is less than the value obtained from the saddle point solution in Example 1, and the defender's performance is deteriorated by following the heuristic approach. From this simulated analysis, $V(\mathbf{x};\psi_P^*,\psi_D) \leq V(\mathbf{x};\psi_P^*,\psi_D^*) \leq V(\mathbf{x};\psi_P,\psi_D^*)$, that is, the saddle point property holds.

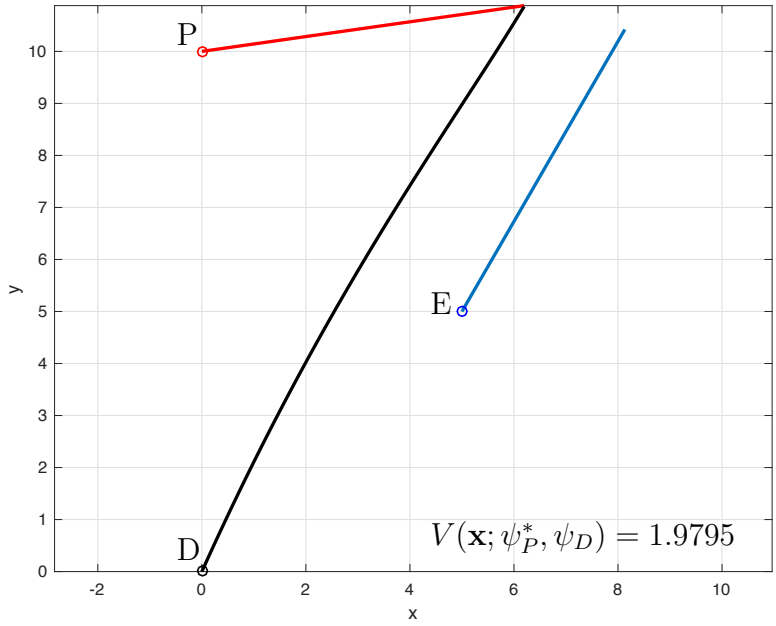

Figure 21. The trajectories of the pursuer (red), evader (blue), and defender (black) in the fixed frame, where the pursuer implements the optimal strategy from the differential game and defender implements the heuristic strategy

4.2 Kinetic Defense of a Non-Maneuvering HVAA in 3-D

In this section, the kinetic defense of a non-maneuverable HVAA in 3-D is considered. The pursuer engages the evader while the defender, which aims at intercepting the pursuer in order to protect the evader, is considered. Posing a scenario of a non-maneuvering evader, a differential game develops between two players: pursuer and defender. Preventing the evader from maneuvering, a differential game is posed where it is the goal of the defender to capture the pursuer as far from the evader as possible. A non-maneuvering evader would be representative of aircraft which are very slow to maneuver or are set on a fixed course and heading which is dictated by its mission or objective.

One common issue with posing differential games in 3-D when compared to those in 2-D is the tractability of analytic solutions. The added spatial dimension begs the use of spherical coordinates as well as additional controls. In the 2-D problem,

one control for each agent is considered (agent headings). However, in 3-D, each agent has two controls, one for heading and one for flight path angle. In total, the dynamics become more nonlinear, more controls are required to pose and solve 3-D differential games, and as a result, analytic solutions are often challenging and potentially intractable.

Differential Game.

Described in Section 3.4, a differential game is developed between the pursuer and the defender concerning the defense of a non-maneuvering HVAA. From the problem definition, the motion of the three agents is defined as a set of ordinary differential equations as shown in eq. (3.52). Also, the objective cost is defined in eq. (3.56) and the value function of the differential game is defined in eq. (3.57). Moreover, the terminal time is not fixed and is determined by the interception of the pursuer by the defender.

Define the speed ratio problem parameter $\mu = v_E/v_P$. In general, the pursuer is faster than the evader, so $0 < \mu < 1$. Also, define the speed ratio $\beta = v_P/v_D$. It is assumed that the pursuer is slower than the defender; thus, the velocities of the engagement are $v_D > v_P > v_E$. Using the aforementioned equations of motion in eq. (3.52) as well as the speed ratios β and μ, the dynamics may be non-dimensionalized with respect to the defender's speed and are as follows:

$$\begin{aligned}
&\dot{x}_P = \beta \cos\gamma_P \cos\psi_P, \quad \dot{x}_E = \mu\beta \cos\gamma_E \cos\psi_E, \quad \dot{x}_D = \cos\gamma_D \cos\psi_D \\
&\dot{y}_P = \beta \cos\gamma_P \sin\psi_P, \quad \dot{y}_E = \mu\beta \cos\gamma_E \sin\psi_E, \quad \dot{y}_D = \cos\gamma_D \sin\psi_D \\
&\dot{z}_P = \beta \sin\gamma_P, \qquad\quad \dot{z}_E = \mu\beta \sin\gamma_E, \qquad\quad \dot{z}_D = \sin\gamma_D.
\end{aligned} \tag{4.36}$$

The optimization is conducted subject to the dynamics in eq. (4.36) and trajectories with terminal state in eq. (3.55), where $\mathbf{u}_P$ and $\mathbf{u}_D$ are the players' state feedback

strategies. Define the costates as

$$\mathbf{p}^T = [p_{x_P}, p_{y_P}, p_{z_P}, p_{x_E}, p_{y_E}, p_{z_E}, p_{x_D}, p_{y_D}, p_{z_D}] \in \mathbb{R}^9. \tag{4.37}$$

In this case, where the objective cost is Mayer; the Hamiltonian of the differential game is simply the inner product of the dynamics with the costates,

$$\mathscr{H} = \langle \mathbf{p}^T, \mathbf{f}(\mathbf{x}, \mathbf{u}_P, \mathbf{u}_D) \rangle. \tag{4.38}$$

Using the speed ratios μ and β, the velocities of the agents are normalized with respect to the defender to obtain the Hamiltonian,

$$\begin{aligned} \mathscr{H} = {} & p_{x_P}\beta \cos\gamma_P \cos\psi_P + p_{y_P}\gamma \cos\gamma_P \sin\psi_P \\ & + p_{z_P}\gamma \sin\gamma_P + p_{x_E}\mu\beta \cos\gamma_E \cos\psi_E \\ & + p_{y_E}\mu\beta \cos\gamma_E \sin\psi_E + p_{z_E}\mu\beta \sin\gamma_E \\ & + p_{x_D} \cos\gamma_D \cos\psi_D + p_{y_D} \cos\gamma_D \sin\psi_D \\ & + p_{z_D} \sin\gamma_D. \end{aligned} \tag{4.39}$$

Theorem 3. *Consider the defense of a non-maneuverable agent differential game in 3-D as described by eqs.* (3.52) *to* (3.57)*. The chosen heading and flight path angles of the pursuer and defender under optimal play are constant and their optimal trajectories are straight lines. This is an extension of Theorem 1 from the 2-D Cartesian plane to the 3-D Cartesian space.*

Proof. The costate dynamics from the Hamiltonian in eq. (4.39) are obtained using the necessary conditions for optimality from eqs. (3.33) to (3.36) which are repeated

here more compactly as:

$$\dot{\mathbf{x}} = \frac{\partial \mathscr{H}}{\partial \mathbf{p}}, \quad \dot{\mathbf{p}} = -\frac{\partial \mathscr{H}}{\partial \mathbf{x}}, \quad \mathbf{0} = \frac{\partial \mathscr{H}}{\partial \mathbf{u}_P}, \quad \mathbf{0} = \frac{\partial \mathscr{H}}{\partial \mathbf{u}_D}. \tag{4.40}$$

Taking the Hamiltonian with respect to the states, the optimal costates are found to be constant because

$$\dot{\mathbf{p}} = \mathbf{0}. \tag{4.41}$$

Taking the partial of the Hamiltonian with respect to agent controls the following equations are obtained:

$$p_{z_P} \cos\gamma_P - p_{x_P} \cos\psi_P \sin\gamma_P - p_{y_P} \sin\psi_P \sin\gamma_P = 0, \tag{4.42}$$

$$p_{y_P} \cos\psi_P \cos\gamma_P - p_{x_P} \cos\gamma_P \sin\psi_P = 0, \tag{4.43}$$

$$p_{z_D} \cos\gamma_D - p_{x_D} \cos\psi_D \sin\gamma_D - p_{y_D} \sin\psi_D \sin\gamma_D = 0, \tag{4.44}$$

$$p_{y_D} \cos\psi_D \cos\gamma_D - p_{x_D} \cos\gamma_D \sin\psi_D = 0. \tag{4.45}$$

From the necessary optimality conditions described in eqs. (4.42) to (4.45), the optimal headings are found to depend solely upon the costates. Through algebraic manipulation, the optimal states as a function of the costates are

$$\psi_D = \cos^{-1}\left(\frac{p_{x_D}}{\sqrt{p_{x_D}^2 + p_{y_D}^2}}\right), \tag{4.46}$$

$$\gamma_D = \cos^{-1}\left(\frac{\sqrt{p_{x_D}^2 + p_{y_D}^2}}{\sqrt{p_{x_D}^2 + p_{y_D}^2 + p_{z_D}^2}}\right), \tag{4.47}$$

$$\psi_P = \cos^{-1}\left(\frac{p_{x_P}}{\sqrt{p_{x_P}^2 + p_{y_P}^2}}\right), \tag{4.48}$$

$$\gamma_P = \cos^{-1}\left(\frac{\sqrt{p_{x_P}^2 + p_{y_P}^2}}{\sqrt{p_{x_P}^2 + p_{y_P}^2 + p_{z_P}^2}}\right) \tag{4.49}$$

The costates are constant as described by eq. (4.41), and from eqs. (4.46) to (4.49)

the optimal control is solely dependent upon the costates. Therefore, the optimal headings of the pursuer and defender are constant and their optimal trajectories are straight lines. ■

From Theorem 3, the optimal trajectories are straight lines. Using the Cartesian coordinate frame to describe the 3-D pursuit-evasion differential game, the optimal strategies for the three-agent scenario are investigated. The governing equations are simplified by setting the origin of the Cartesian space as shown in Figure 22. By locating each agent on an orthogonal plane and orienting the y-axis parallel to the evader, some state variables may be eliminated and the analysis simplified.

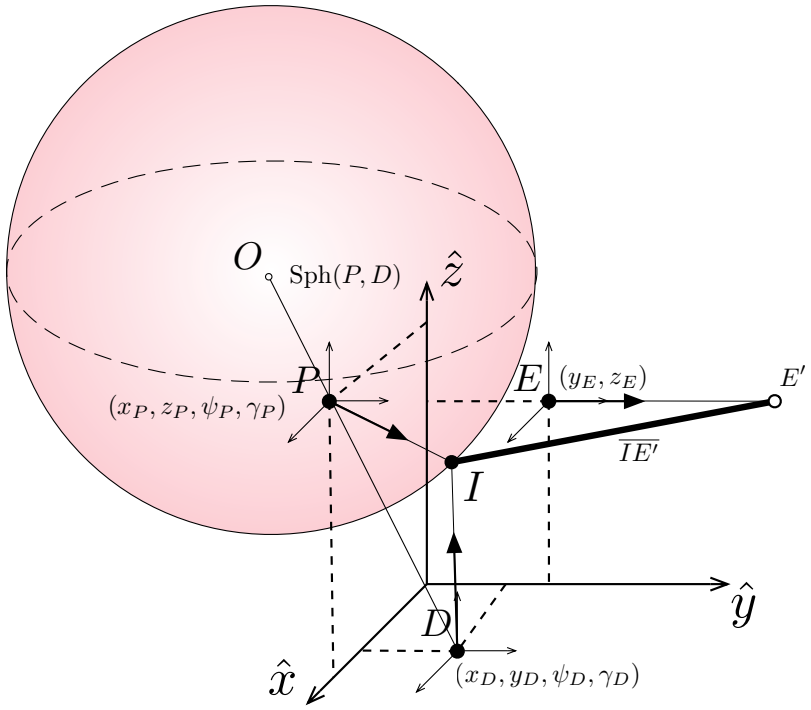

Figure 22. Interception of pursuer by defender at terminal time as characterized by a sphere constructed using the geometry of Apollonius

Using this coordinate frame, the state space is reduced by three variables, and the intersection sphere of the defender, D, and pursuer, P is described. The two-norm

distance between the pursuer and the defender is as follows:

$$d = \sqrt{(x_P - x_D)^2 + y_D^2 + z_P^2} \tag{4.50}$$

By setting the origin of the space as described in Figure 22, the variables $x_E = y_P = z_D = 0$. To fully define the intersection sphere, the sphere's origin and radius are first specified. From the geometry of Apollonius, the origin is located collinear with the points: P, and D, the position of the pursuer and defender. Define the ray passing through P and D as $\hat{x}'$, then the origin's location can be easily obtained. Designate the unit vector for the ray $\overrightarrow{PD}$ as

$$\hat{x}' = \frac{1}{d}\left((x_D - x_P)\hat{i} + (y_D)\hat{j} + (-z_P)\hat{k}\right). \tag{4.51}$$

The origin, O is collinear with $\hat{x}'$ and it lies in the opposite direction at a distance,

$$\overline{OP} = \frac{\beta^2 d}{1 - \beta^2}. \tag{4.52}$$

Simply reversing the unit vector, $\hat{x}'$ and multiplying by the magnitude of $\overline{OP}$, the location of the origin is found to to be

$$O = -\overline{OP}\hat{x}' + P. \tag{4.53}$$

More explicitly, the origin of the sphere is located at the point O defined as

$$O = \frac{1}{1 - \beta^2}\begin{bmatrix} x_P - x_D\beta^2 \\ -y_D\beta^2 \\ z_P \end{bmatrix}. \tag{4.54}$$

The radius,

$$r = \frac{\beta d}{1 - \beta^2}, \tag{4.55}$$

of the sphere is defined to be that of the radius of the Apollonius Circle whose P and D foci are at a distance, d, and the speed ratio is β.

Agent Headings.

By Theorem 3, the optimal headings of the players are constant. To obtain the optimal strategies of the pursuer and the defender the intersection point, I, determines the appropriate agents' headings and flight path angles. This is because the sphere is the locus of all possible interceptions of the pursuer by the defender. The intersection point, I, as defined by the spherical coordinates, (r, γ_O, ψ_O), radius, elevation angle, and azimuth relative to the sphere's origin is

$$\begin{aligned} x_I &= r \cos\gamma_O \cos\psi_O + x_O, \\ y_I &= r \cos\gamma_O \sin\psi_O + y_O, \\ z_I &= r \sin\gamma_O + z_O. \end{aligned} \tag{4.56}$$

From eq. (4.56), the pursuer's and defender's control which steers toward the intersection point is solved.

Pursuer Heading.

The pursuer strategy is specified by the heading, ψ_P, and flight path angle, γ_P, which leads the pursuer to reach a given intersection point on the intersection sphere. The pursuer strategy is

$$\mathbf{u}_P = \{(\gamma_P, \psi_P) | \gamma_P \in [-\pi, \pi], \psi_P \in [0, \pi]\}. \tag{4.57}$$

The intersection point, I, using Cartesian coordinates, as a function of the pursuer's heading and flight path angle is

$$\begin{aligned} x_I &= \overline{PI}\cos\gamma_P\cos\psi_P + x_P, \\ y_I &= \overline{PI}\cos\gamma_P\sin\psi_P, \\ z_I &= \overline{PI}\sin\gamma_P + z_P. \end{aligned} \tag{4.58}$$

The distance $\overline{PI}$ is

$$\overline{PI} = \sqrt{(x_P - x_I)^2 + y_I^2 + (z_P - z_I)^2}. \tag{4.59}$$

Therefore the pursuer's strategy $\mathbf{u}_P$ is obtained as a function of pursuer coordinates and intersection point coordinates: x_P, z_P, x_I, y_I, z_I. Explicitly, the pursuer's flight path angle and the heading are

$$\gamma_P = \sin^{-1}\left((z_I - z_P)\big/\overline{PI}\right), \tag{4.60}$$

$$\psi_P = \sin^{-1}\left(\frac{y_I}{\sqrt{\overline{PI}^2 - (z_I - z_P)^2}}\right). \tag{4.61}$$

Defender Heading.

Knowing the intersection point, I, one also obtains the corresponding strategy $\mathbf{u}_D$ of the defender. The intersection point of the pursuer by the defender in spherical coordinates is

$$\mathbf{u}_D = \{(\gamma_D, \psi_D) | \gamma_D \in [-\pi, \pi], \psi_D \in [0, \pi]\} \tag{4.62}$$

The intersection point, I, can be described in Cartesian coordinate frame as

$$\begin{aligned} x_I &= \overline{DI}\cos\gamma_P\cos\psi_P + x_D, \\ y_I &= \overline{DI}\cos\gamma_P\sin\psi_P + y_D, \\ z_I &= \overline{DI}\sin\gamma_P. \end{aligned} \tag{4.63}$$

The distance, $\overline{DI}$, is

$$\overline{DI} = \sqrt{(x_D - x_I)^2 + (y_D - y_I)^2 + z_I^2}. \tag{4.64}$$

Therefore the defender's strategy, $\mathbf{u}_D$ as a function of the defender coordinates and intersection point coordinates, x_D, y_D, x_I, y_I, z_I are

$$\gamma_D = \sin^{-1}\left(z_I/\overline{DI}\right), \tag{4.65}$$

$$\psi_D = \sin^{-1}\left(\frac{y_I - y_D}{\sqrt{\overline{DI}^2 - z_I^2}}\right). \tag{4.66}$$

Optimal Intersection Point.

The agent headings as defined in eqs. (4.60), (4.61), (4.65) and (4.66) are functions of a chosen intersection point, I, located on the intersection sphere. An optimization is performed to minimize the desired objective cost in eq. (3.56) by adjusting the intersection point location as follows:

$$(\gamma_O^*, \psi_O^*) = \underset{\gamma_O,\, \psi_O}{\operatorname{argmin}}\, \Phi(\mathbf{x}_f) \tag{4.67}$$

where the final time is computed as follows:

$$t_f = \frac{\overline{PI}}{v_P} = \frac{|\overline{EE'}|}{v_E} = \frac{|\overline{DI}|}{v_D}. \tag{4.68}$$

The location of the evader at the time of interception, t_f is found utilizing the speed ratio μ as

$$|\overline{EE'}| = \frac{v_E}{v_P}|\overline{PI}| = \mu|\overline{PI}|. \tag{4.69}$$

A gradient-based method can be to obtain the optimal solution and is utilized to find the optimal strategies for the pursuer and defender.

Examples.

Consider an example engagement where the agent positions are: $P_0 = (5, 0, 10)$, $E_0 = (0, 10, 5)$, $D_0 = (10, 5, 0)$, outlined in Table 4: Simulation Initial Conditions. Also, consider the agent velocities to be: $v_P = 0.9$, $v_E = 0.8$, and $v_D = 1.0$, while the evader has fixed heading and climb angle: $\psi_E = \pi/2$ and $\gamma_E = 0$.

Table 4. Simulation Initial Conditions

Agent	X-location, DU	Y-Location, DU	Z-Location, DU
Pursuer	5.00	0.00	10.0
Evader	0.00	10.0	5.00
Defender	10.0	5.00	0.00

Example 1: Optimal Defender and Optimal Pursuer.

Figure 23 shows the optimal trajectories for the scenario where each of the players, P and D, implement the saddle point strategies outlined from the solution to the differential game. The value of the game is $V(\mathbf{u}_P^*, \mathbf{u}_D^*, \mathbf{x}_0) = 9.9764$; summarized in Table 5: Simulation Results.

Note that the optimal saddle point strategies are computed at every time step and implemented for both the defender and pursuer. Utilizing the positions of all agents, the differential game is solved wherein the positions of all agents are used to obtain the appropriate instantaneous headings of the pursuer and defender. The solution of the defense of the non-maneuverable agent possesses the invariance property, where the interception point and headings of all players are constant under the saddle point solution to the differential game. If, however, any of the agents maneuver in a way not prescribed by the optimal strategies of the differential game, then the optimal headings computed will not be constant. The remaining examples in the paper implement heuristic Pure Pursuit strategies for the defender and pursuer showing that

the performance of the agents only degrades with variation from the saddle point strategies.

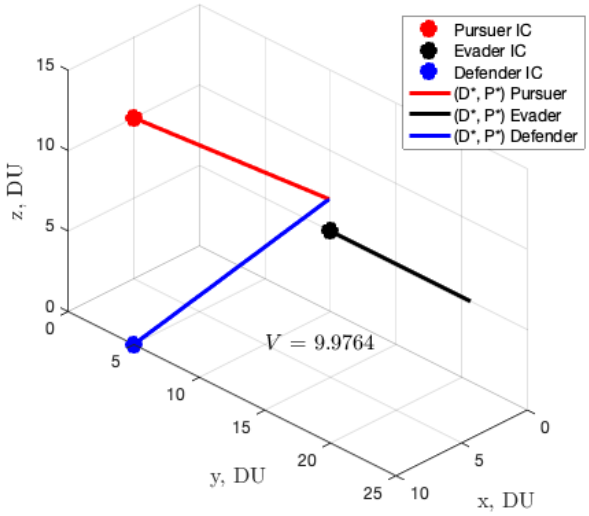

Figure 23. The kinetic defense of a non-manuvering HVAA is simulated assuming the pursuer and defender implement the optimal saddle point strategies.

Example 2: Optimal Defender and Heuristic Pursuer.

Consider the case where the pursuer does not follow the optimal saddle point strategy outlined in this work; rather, it implements the Pure Pursuit strategy, where it's heading and climb angle are chosen to point toward the evader at each time step. The equations utilized for computing the control for the suboptimal pursuer are

$$\gamma_P = \tan^{-1}\left(\frac{z_E - z_P}{\sqrt{(x_E - x_P)^2 + (y_E - y_P)^2}}\right), \tag{4.70}$$

$$\psi_P = \tan^{-1}\left(\frac{y_E - y_P}{x_E - x_P}\right). \tag{4.71}$$

The pursuer implements the Pure Pursuit guidance strategy defined by eqs. (4.70) and (4.71) and the defender implements the optimal solution to the differential game as defined by eqs. (4.65) and (4.66). The resulting simulation can be seen in Figure 24.

As a result of the sub-optimal strategy performed by the pursuer, the defender is able to capture the pursuer sooner and as a result the terminal distance is larger: $V(\mathbf{u}_P, \mathbf{u}_D^*, \mathbf{x}_0) = 10.1936$. Table 5 compares the performance of the suboptimal pursuer strategy against that of an optimal one.

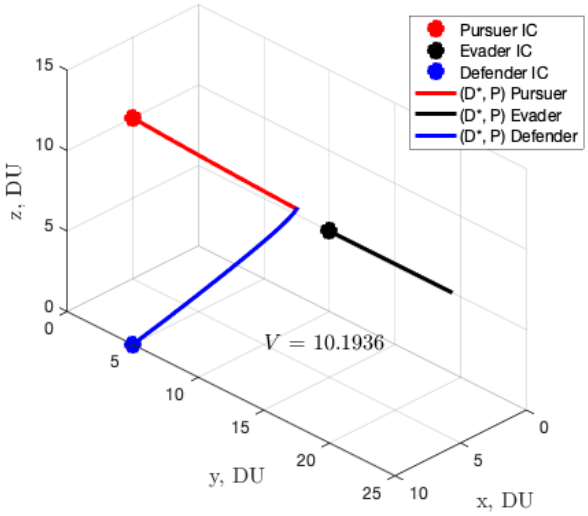

Figure 24. The kinetic defense of a non-manuvering HVAA is simulated assuming the defender implements the optimal strategy and the pursuer implements the Pure Pursuit strategy.

Example 3: Heuristic Defender and Optimal Pursuer.

Finally, consider the opposite case, wherein the pursuer follows the optimal strategy derived in this section while the defender implements the sub-optimal Pure Pursuit strategy. The Pure Pursuit headings are obtained by pointing the defender toward the pursuer, as seen in the following equations

$$\gamma_D = \tan^{-1}\left(\frac{z_P - z_D}{\sqrt{(x_P - x_D)^2 + (y_P - y_D)^2}}\right), \tag{4.72}$$

$$\psi_D = \tan^{-1}\left(\frac{y_P - y_D}{x_P - x_D}\right). \tag{4.73}$$

The pursuer, implements the optimal strategy from eqs. (4.60) and (4.61); the

resulting trajectories are shown in Figure 25. The terminal separation at final time is, as a result of the suboptimal defender strategy is less than when the saddle point strategy is implemented. The value function, describing this terminal separation is: $V(\mathbf{u}_P^*, \mathbf{u}_D, \mathbf{x}_0) = 9.2166$, showing that deviation from the solution to the differential game results in poorer performance for the defender.

Highlighted in Table 5, a comparison of the three simulations is shown, demonstrating the characteristic of the solution to a differential game. First, both the pursuer and the defender implement the optimal saddle point strategies and observe the terminal pursuer-evader range is 9.9764. When the defender implements the Pure Pursuit strategy and the pursuer implements the optimal saddle point strategy, the value function is lower and the pursuer gets closer to the evader at final time. The resulting range is 9.2166. When the pursuer implements the Pure Pursuit strategy and the defender implements the optimal saddle point strategy, the terminal range between the pursuer and evader is 10.1936. Upon implementing the heuristic suboptimal policy of the Pure Pursuit strategy, performance is reduced for that agent. This demonstrates that deviating from the optimal saddle point strategy only reduces performance for that agent, a characteristic of differential games [9].

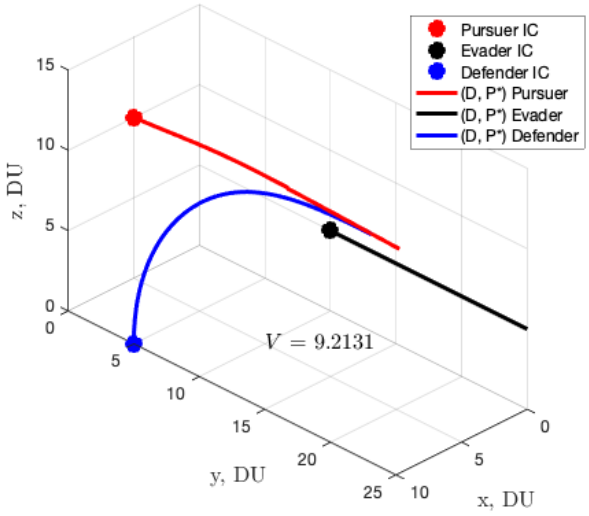

Figure 25. The kinetic defense of a non-manuvering HVAA is simulated assuming the defender implements the Pure Pursuit strategy and the pursuer implements the optimal strategy.

Table 5. Simulation Results

Defender Strategy	Pursuer Strategy	Value Function
Optimal	Optimal	`9.9764`
Pure Pursuit	Optimal	`9.2166`
Optimal	Pure Pursuit	`10.1936`

Search Performance.

Utilizing the Matlab function `FMINUNC()`, the optimal headings are computed directly. A plot of the entire space is presented in Figure 26.

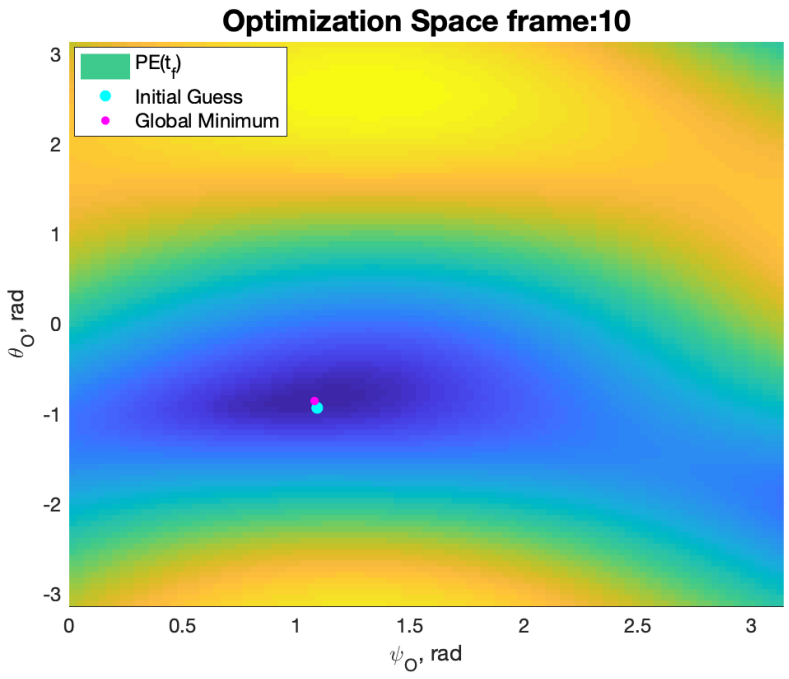

Figure 26. The objective cost evaluated over the domain of possible interception points on the interception sphere at the tenth frame

In Figure 26 one observes that the space in the example is locally convex. By seeding the optimization search with a guess for the optimal heading angles, one can converge fairly quickly with fewer functional evaluations than brute-force searching the entire domain for the minimum. Using the Matlab function, `FMINUNC()`, a gradient-based search for the optimal headings as described in eq. (4.67) is implemented. The Quasi-Newton gradient-based search algorithm is used to perform a search for the optimal interception point described by ψ_O^* and γ_O^*. The initial guess for the optimal headings is selected as the angles, ψ_O and γ_O, which describe the vector from the origin of the interception sphere to the initial location of the evader. This initial guess is relatively close to the converged global minimum, and optimal solutions are computed generally within 20-30 functional evaluations. If the initial guess were to start very far away from the optimal solution, then a gradient-based solver would not converge on the global solution. As illustrated in Figure 26, ini-

tial guesses are not far from the global minimum, and in-general, convergence to the global minimum is achieved.

Using Matlab, the gradient-based search is conducted. The initial guess for the optimal ψ_O and γ_O is shown in light-blue in Figure 26. Upon finding the optimal interception point, the headings of the pursuer and defender are then implemented using eqs. (4.60), (4.61), (4.65) and (4.66). Conducting the gradient-based search outperforms that of a brute force search. Rather than computing the terminal cost for every point on the sphere, described by the color gradient in Figure 26, the use of gradient-based techniques require fewer functional evaluations and is more efficient than the brute force evaluation of all azimuths and elevations of the objective cost.

4.3 Kinetic Defense of a Maneuvering HVAA in 2-D

In this section, a scenario consisting of a defending missile, a pursuer missile, and evading HVAA which cooperates with the defender is considered. Using optimal control theory the optimal HVAA strategy which maximizes the distance of the pursuer when captured by the defender is posed and solved. Proportional Navigation guidance laws are selected for the pursuer and defender; while constraints are held on the evader to prevent instantaneous changes in velocity. A numerical approach is presented along as an example.

Optimal Control Problem.

Described in Section 3.4, an optimal control problem is formed wherein the evader aims to outmaneuver its pursuer while a teamed defender uses proportional navigation to intercept the pursuer. It is assumed that the pursuer is faster than the evader, so that $v_P > v_E$. Also, the defender is assumed to be the same speed as the pursuer, $v_D = v_P$, meaning that the defender can not capture the pursuer vehicle unless the

evader maneuvers in such a way as to aid in the closure between the defender and pursuer.

The complete geometry of the HVAA defense scenario is shown in Figure 27; this is the very same geometry as described in the active target defense scenario, presented in Figure 6. The only change is that the attacker and target from Figure 6 are called the pursuer and evader, respectively.

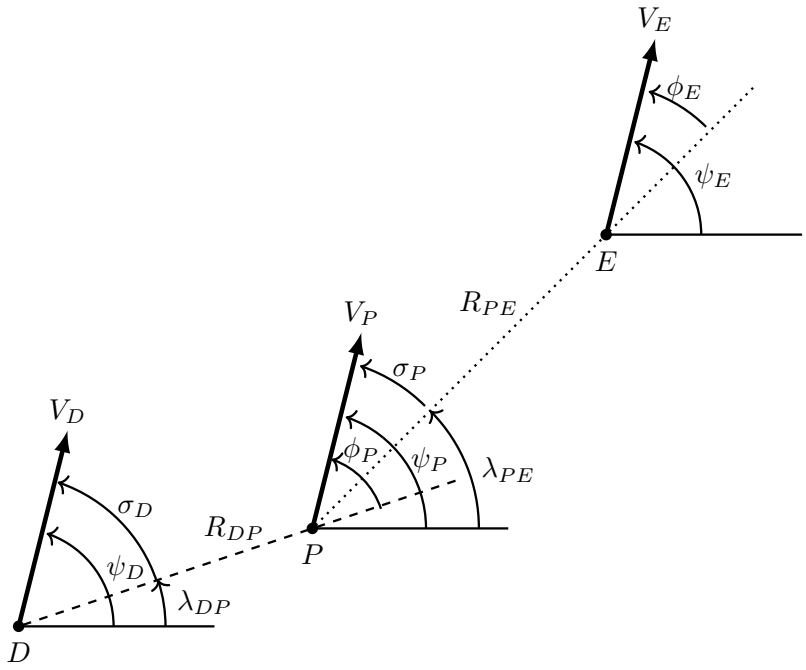

Figure 27. The active target defense scenario considers a defender (D) which aims at capturing a pursuer (P) who in-turn aims at capturing an evader (E).

Although the optimal control problem may be tractable using these equations of motion, it is possible to reduce the order of the dynamics. To formulate the problem in this reduced form, the dynamics from eq. (3.40) are transformed into polar form. By calculating and solving the optimal control problem in relative polar coordinates, calculation time is reduced since the number of nonlinear dynamic equations of motion is reduced. Once an optimal solution is found in the relative polar space, the optimal control may be translated into Cartesian space for visualization and evaluation. The

polar representation can be formed by taking the velocities along the line-of-sights and analyzing their closure based upon the line-of-sight angles. The equations of motion from eq. (3.40) are reduced using the nomenclature as illustrated in Figure 27. The line-of-sight angles derived from the locations of the defender, pursuer, and evader in the 2-D Cartesian fixed frame are

$$\lambda_{DP} = \tan^{-1}\left(\frac{y_P - y_D}{x_P - x_D}\right), \quad \lambda_{PE} = \tan^{-1}\left(\frac{y_E - y_P}{x_E - x_P}\right). \tag{4.74}$$

The angle between the velocity of an agent and its line-of-sight to its target, σ, can be found by subtracting the line-of-sight to the next target from the known heading as follows:

$$\sigma_P = \psi_P - \lambda_{PE}, \quad \sigma_D = \psi_D - \lambda_{DP}. \tag{4.75}$$

Moreover, the angle between an agent's velocity and the pursuer's line-of-sight can be calculated by subtracting the line-of-sight from the pursuer from the agent's heading as follows:

$$\phi_P = \psi_P - \lambda_{DP}, \quad \phi_E = \psi_E - \lambda_{PE}. \tag{4.76}$$

The defender-pursuer range and pursuer-evader range are obtained using the euclidean distance and are as follows:

$$R_{DP} = \sqrt{(y_P - y_D)^2 + (x_P - x_D)^2}, \; R_{PE} = \sqrt{(y_E - y_P)^2 + (x_E - x_P)^2}. \tag{4.77}$$

The line-of-sight rates between agents are as follows:

$$\dot{\lambda}_{DP} = \frac{v_P \sin\phi_P - v_D \sin\sigma_D}{R_{DP}}, \quad \dot{\lambda}_{PE} = \frac{v_E \sin\phi_E - v_P \sin\sigma_P}{R_{PE}}. \tag{4.78}$$

The angular heading rates for the defender and pursuer are as follows:

$$\dot{\psi}_D = N_D \dot{\lambda}_{DP}, \quad \dot{\psi}_P = N_P \dot{\lambda}_{PE}, \tag{4.79}$$

where N_D and N_P are the proportional navigation constants. Using the geometry as illustrated in Figure 27, the range rates between the defernder and the pursuer as well as the pursuer and the evader are as follows:

$$\dot{R}_{DP} = -v_D \cos\sigma_D + v_P \cos\phi_P, \quad \dot{R}_{PE} = -v_P \cos\sigma_P + v_E \cos\phi_E. \tag{4.80}$$

Continuing the transformation of the dynamics from Cartesian to relative polar space: the headings with respect to the line-of-sight σ_P and σ_D can be found by differentiating eqs. (4.75) and (4.76) with respect to time. To complete the polar form of the dynamic equations the angular rates of each of the agents in the engagement are also needed. The rate of change between the pursuer's heading and its line-of-sight to the evader may be found to be the difference between the heading rate of the pursuer and the line-of-sight rate between the pursuer and evader, namely:

$$\dot{\sigma}_P = \dot{\psi}_P - \dot{\lambda}_{PE} = (N_P - 1)\dot{\lambda}_{PE} = \frac{(N_P - 1)(v_E \sin\phi_E - v_P \sin\sigma_P)}{R_{PE}}. \tag{4.81}$$

Similarly, the rate of change between the defender's heading and its line-of-sight to the pursuer may be found to be the difference between the heading rate of the defender and the line-of-sight rate between the defender and pursuer:

$$\dot{\sigma}_D = \dot{\psi}_D - \dot{\lambda}_{DP} = (N_D - 1)\dot{\lambda}_{DP} = \frac{(N_D - 1)(v_P \sin\phi_P - v_D \sin\sigma_D)}{R_{DP}}. \tag{4.82}$$

Next, by differentiating eq. (4.76), the angular rate of change the pursuer's heading

and defender's line-of-sight is found to be:

$$\begin{aligned}\dot{\phi}_P &= \dot{\psi}_P - \dot{\lambda}_{DP} \\ &= N_P\dot{\lambda}_{PE} - \dot{\lambda}_{DP} \\ &= \frac{N_P(v_E \sin\phi_E - v_P \sin\sigma_P)}{R_{PE}} - \frac{v_P \sin(\phi_P) - v_D \sin(\sigma_D)}{R_{DP}}.\end{aligned} \tag{4.83}$$

Similarly for the target, the angular rate of change of the target's heading to the pursuer's line-of-sight is calculated. Recall that the input, u, is the rate of the target's heading. This will appear in the target's angular rate of change relative to the line-of-sight rate:

$$\dot{\phi}_E = \dot{\psi}_E - \dot{\lambda}_{PE} = u - \frac{v_E \sin(\phi_E) - v_P \sin(\sigma_P)}{R_{PE}}. \tag{4.84}$$

The final reduced-order form in relative polar space is:

$$\begin{bmatrix} \dot{R}_{DP} \\ \dot{R}_{PE} \\ \dot{\sigma}_D \\ \dot{\sigma}_P \\ \dot{\phi}_P \\ \dot{\phi}_E \end{bmatrix} = \begin{bmatrix} v_P \cos\phi_P - v_D \cos\sigma_D \\ v_E \cos\phi_E - v_P \cos\sigma_P \\ (N_D - 1)\dot{\lambda}_{DP} \\ (N_P - 1)\dot{\lambda}_{PE} \\ N_P\dot{\lambda}_{PE} - \dot{\lambda}_{DP} \\ u - \dot{\lambda}_{PE} \end{bmatrix}. \tag{4.85}$$

In this problem, the Hamiltonian is,

$$\begin{aligned}\mathscr{H} &= (v_P\cos\phi_P - v_D\cos\sigma_D)p_{R_{DP}} \\ &+ (v_E\cos\phi_E - v_P\cos\sigma_P)p_{R_{PE}} \\ &+ \left(\frac{(N_D-1)\,(v_P\sin\phi_P - v_D\sin\sigma_D)}{R_{DP}}\right)p_{\sigma_D} \\ &+ \left(\frac{(N_P-1)\,(v_E\sin\phi_E - v_P\sin\sigma_P)}{R_{PE}}\right)p_{\sigma_P} \\ &+ \left(\frac{N_P\,(v_E\sin\phi_E - v_P\sin\sigma_P)}{R_{PE}} - \frac{v_P\sin\phi_P - v_D\sin\sigma_D}{R_{DP}}\right)p_{\psi_P} \\ &+ \left(u - \frac{v_E\sin\phi_E - v_P\sin\sigma_P}{R_{PE}}\right)p_{\psi_E}.\end{aligned} \tag{4.86}$$

Further, the costate dynamics are given by:

$$\begin{aligned} \dot{p}_{R_{DP}} &= -\frac{\partial\mathscr{H}}{\partial R_{DP}}, & \dot{p}_{R_{PE}} &= -\frac{\partial\mathscr{H}}{\partial R_{PE}}, & \dot{p}_{\sigma_D} &= -\frac{\partial\mathscr{H}}{\partial\sigma_D}, \\ \dot{p}_{\sigma_P} &= -\frac{\partial\mathscr{H}}{\partial\sigma_P}, & \dot{p}_{\phi_P} &= -\frac{\partial\mathscr{H}}{\partial\phi_P}, & \dot{p}_{\phi_E} &= -\frac{\partial\mathscr{H}}{\partial\phi_E}. \end{aligned} \tag{4.87}$$

Evaluating from the Hamiltonian, the costate dynamics are:

$$\dot{\mathbf{p}} = \mathbf{M}\mathbf{p}. \tag{4.88}$$

where the time varying matrix, $\mathbf{M}$, is defined as

$$\mathbf{M} = \begin{bmatrix} 0 & 0 & (N_D-1)\xi_1 & 0 & -\xi_1 & 0 \\ 0 & 0 & 0 & (N_P-1)\xi_2 & N_P\xi_2 & -\xi_2 \\ -v_D\sin\sigma_D & 0 & (N_D-1)\xi_3 & 0 & -\xi_3 & 0 \\ 0 & -v_P\sin\sigma_P & 0 & (N_P-1)\xi_4 & N_P\xi_4 & -\xi_4 \\ v_P\sin\phi_P & 0 & -(N_D-1)\xi_5 & 0 & \xi_5 & 0 \\ 0 & v_E\sin\phi_E & 0 & -(N_P-1)\xi_6 & -N_P\xi_6 & \xi_6 \end{bmatrix}. \tag{4.89}$$

The time-varying coefficients inside the matrix, $\mathbf{M}$ are defined as a function of state variables and known constants as follows:

$$\begin{aligned}
&\xi_1 = \frac{v_P \sin\phi_P - v_D \sin\sigma_D}{R_{DP}^2} = \frac{\dot{\lambda}_{DP}}{R_{DP}}, \quad \xi_2 = \frac{v_E \sin\phi_E - v_P \sin\sigma_P}{R_{PE}^2} = \frac{\dot{\lambda}_{PE}}{R_{PE}}, \\
&\xi_3 = \frac{v_D \cos\sigma_D}{R_{DP}}, \quad \xi_4 = \frac{v_P \cos\sigma_P}{R_{PE}}, \quad \xi_5 = \frac{v_P \cos\phi_P}{R_{DP}}, \quad \xi_6 = \frac{v_D \cos\phi_E}{R_{PE}}.
\end{aligned} \tag{4.90}$$

Now that the state dynamics and the costates have been defined as a function of time, the next step is to determine necessary conditions for optimal input by means of Pontryagin's Minimum Principle since the heading rate is bounded as follows:

$$|u(t)| \leq \omega_{P_{max}} \; \forall \; t \in [t_0, t_f]. \tag{4.91}$$

Using eq. (4.91) and the Hamiltonian defined in eq. (4.86) the optimal control must satisfy Pontryagin's Minimum Principle [146]:

$$\mathscr{H}(\mathbf{x}^*(t), \mathbf{u}^*(t), \mathbf{p}^*(t), t) \leq \mathscr{H}(\mathbf{x}^*(t), \mathbf{u}(t), \mathbf{p}^*(t), t). \tag{4.92}$$

The states ($\mathbf{x}$) and costates ($\mathbf{p}$) are

$$\begin{aligned}
\mathbf{x}^T &= [R_{DP},\ R_{PE},\ \sigma_D,\ \sigma_P,\ \phi_P,\ \phi_E], \\
\mathbf{p}^T &= [p_{R_{DP}},\ p_{R_{PE}},\ p_{\sigma_D},\ p_{\sigma_P},\ p_{\phi_P},\ p_{\phi_E}].
\end{aligned} \tag{4.93}$$

Calculated, the admissible $u(t)$ for all $t \in [t_0, t_f]$ is

$$u^*(t) = \begin{cases} -\omega_{P_{max}}, & \text{for } p^*_{\phi_E}(t) > 0 \\ \omega_{P_{max}}, & \text{for } p^*_{\phi_E}(t) < 0. \end{cases} \tag{4.94}$$

In the case when $p^*_{\phi_E}(t) = 0$, switching occurs on the input and no information about the optimal input $u^*(t)$ can be provided. This would result in a singular problem.

According to the objective, the scenario of interest has free final time and a fixed constraint of $R_{DP}(t_f) = \varepsilon_{\text{miss}}$. Considering the boundary conditions, the boundary conditions of the states and costates are given as:

$$\begin{bmatrix} R_{DP}(t_0) \\ R_{PE}(t_0) \\ \sigma_D(t_0) \\ \sigma_P(t_0) \\ \phi_P(t_0) \\ \phi_E(t_0) \end{bmatrix} = \begin{bmatrix} R_{da_0} \\ R_{at_0} \\ \sigma_{D_0} \\ \sigma_{P_0} \\ \phi_{P_0} \\ \phi_{E_0} \end{bmatrix}, \begin{bmatrix} R_{DP}(t_f) \\ R_{PE}(t_f) \\ \sigma_D(t_f) \\ \sigma_P(t_f) \\ \phi_P(t_f) \\ \phi_E(t_f) \end{bmatrix} = \begin{bmatrix} \varepsilon_{\text{miss}} \\ \text{free} \\ \text{free} \\ \text{free} \\ \text{free} \\ \text{free} \end{bmatrix}, \begin{bmatrix} p_{R_{DP}}(t_f) \\ p_{R_{PE}}(t_f) \\ p_{\sigma_D}(t_f) \\ p_{\sigma_P}(t_f) \\ p_{\phi_P}(t_f) \\ p_{\phi_E}(t_f) \end{bmatrix} = \begin{bmatrix} \text{free} \\ \text{free} \\ 0 \\ 0 \\ 0 \\ 0 \end{bmatrix} \tag{4.95}$$

The $2n + 1$ (where n is the state dimension) relationship given by

$$\mathscr{H}(\mathbf{x}^*(t_f), \mathbf{u}^*(t_f), \mathbf{p}^*(t_f), t_f) = 0. \tag{4.96}$$

Solving the necessary conditions eqs. (4.85), (4.88) and (4.94), provides the general solution to the optimal control problem. Applying the boundary conditions given by eqs. (4.95) and (4.96) provides the solution to the 2-point boundary value problem, and consequently the optimal control problem.

Example.

The general engagement scenario has many degrees of freedom including initial conditions of the pursuer, evader, and defender. It can be easily observed that by varying the location, heading, and speed of each agent involved in the scenario that target capture or escape could occur. A general engagement is proposed which will provide an interesting case, like in Figure 28, and a numerical solution to the optimal control problem can be found.

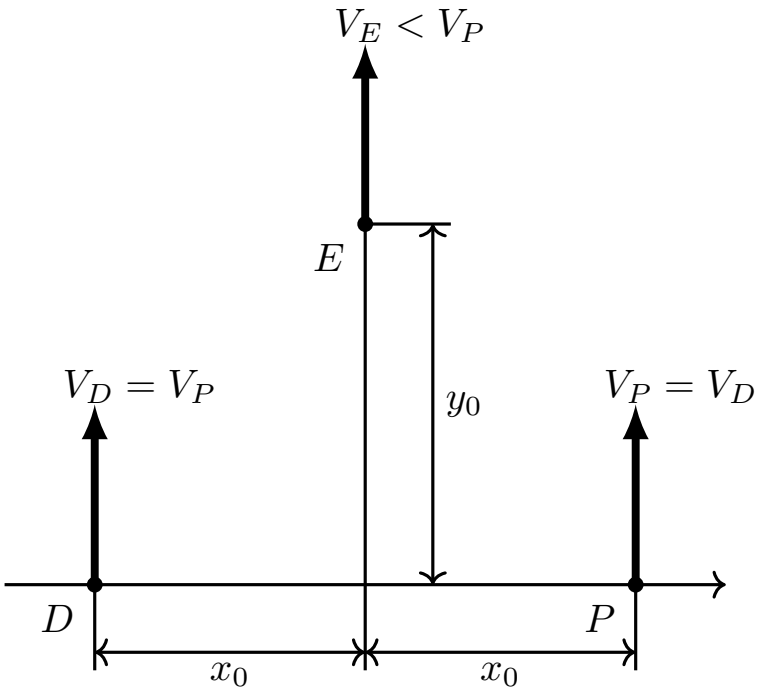

Figure 28. The initial three-agent geometry involves a defender and pursuer which are equidistant to the evader which is located in front of both agents.

Due to the complexity and nonlinearity of the dynamic optimization problem discussed earlier, a numerical tool such as Matlab can be used to solve the two point boundary value (TPBV) problem generated by the dynamic equations of motion from eq. (4.85), the costate equations from eq. (4.88), the boundary conditions from eqs. (4.95) and (4.96), and subject to constraint in eq. (4.91). There are many issues with starting with poor initial conditions, and sensitivity to the initial conditions can play a major role in finding a candidate solution to the TPVB problem. Using Matlab, one approach is to discretize the equations of motion and costates, and turn the dynamic optimization problem into a static optimization problem. The discretized form of the dynamics is advantageous since time vectors and state vectors are generated at even intervals and computational power is controllable through the number of intervals during the simulation. To discretize the dynamic equations of

motion, one can use an Euler method in eq. (4.97) as follows:

$$\mathbf{x}[k+1] = \mathbf{x}[k] + \mathbf{f}(\mathbf{x}[k], u[k], k)\Delta t. \tag{4.97}$$

Once discretized, the cost function becomes eq. (4.98).

$$J(u) = \sum_{k=1}^{N} (v_P \cos\psi_P[k] - v_D \cos\sigma_D[k] - v_E \cos\psi_E[k] + v_P \cos\sigma_P[k]). \tag{4.98}$$

In addition, the dynamic equations of motion written as constraint equations are in eq. (4.99), as follows:

$$\begin{aligned}
h_{R_{DP}}[k+1] &= R_{DP}[k+1] - R_{DP}[k] - (v_P \cos\phi_P[k] - v_D \cos\sigma_D[k])\Delta t \\
h_{R_{PE}}[k+1] &= R_{PE}[k+1] - R_{PE}[k] - (v_E \cos\phi_E[k] - v_P \cos\sigma_P[k])\Delta t \\
h_{\sigma_D}[k+1] &= \sigma_D[k+1] - \sigma_D[k] - ((N_D - 1)\dot{\lambda}_{DP})\Delta t \\
h_{\sigma_P}[k+1] &= \sigma_P[k+1] - \sigma_P[k] - ((N_P - 1)\dot{\lambda}_{PE}[k])\Delta t \\
h_{\phi_P}[k+1] &= \phi_P[k+1] - \phi_P[k] - (N_P\dot{\lambda}_{PE}[k] - \dot{\lambda}_{DP})\Delta t \\
h_{\phi_E}[k+1] &= \phi_E[k+1] - \phi_E[k] - (u[k] - \dot{\lambda}_{PE}[k])\Delta t \\
\dot{\lambda}_{DP}[k] &= \frac{v_P \sin\psi_P[k] - v_D \sin\sigma_D[k]}{R_{DP}[k]} \\
\dot{\lambda}_{PE}[k] &= \frac{v_E \sin\psi_E[k] - v_P \sin\sigma_P[k]}{R_{PE}[k]}.
\end{aligned} \tag{4.99}$$

Using these equations, the entire time history of the scenario is fed to a nonlinear program solver, such as an SQP solver, to iteratively-solve for the optimal control. Using the equations of motion as constraints at every time step, the solution that is found by perturbing the control input is ensured to be a valid scenario.

By looking at the sign of the costate equation, $u[k]$ is known to either be a minimum or maximum. For example, if $p_{\phi_E}[k] < 0$ then $u[k] = \omega_{P_{max}}$, and if $p_{\phi_E}[k] > 0$

then $u[k] = -\omega_{P_{max}}$; but, if $p_{\phi_E}[k] = 0$ then $|u[k]| < \omega_{P_{max}}$. Although no information about the optimal control may be gained from a zero costate; also $u^*[k]$ is bounded by the maximum angular rate $\omega_{P_{max}}$.

Using the initial conditions an example solution to the optimal control problem is presented. The boundary conditions to this example are shown in eq. (4.100). The constants are defined in eq. (4.101).

$$\begin{bmatrix} R_{DP} \\ R_{PE} \\ \sigma_D \\ \sigma_P \\ \phi_P \\ \phi_E \end{bmatrix}_{t_0} = \begin{bmatrix} 10.0000 \\ 11.1803 \\ 1.5708 \\ -0.6435 \\ 1.5708 \\ -0.6435 \end{bmatrix}, \begin{bmatrix} R_{DP} \\ R_{PE} \\ \sigma_D \\ \sigma_P \\ \phi_P \\ \phi_E \end{bmatrix}_{t_f} = \begin{bmatrix} 0.01 \\ \text{free} \\ \text{free} \\ \text{free} \\ \text{free} \\ \text{free} \end{bmatrix}, \begin{bmatrix} p_{R_{DP}} \\ p_{R_{PE}} \\ p_{\sigma_D} \\ p_{\sigma_P} \\ p_{\phi_P} \\ p_{\phi_E} \end{bmatrix}_{t_f} = \begin{bmatrix} \text{free} \\ \text{free} \\ 0 \\ 0 \\ 0 \\ 0 \end{bmatrix} \tag{4.100}$$

$$N_P = N_D = 3\ , \quad v_P = v_D = 1\ , \quad v_E = 0.5 < v_P\ , \quad \omega_{P_{max}} = 0.2 \tag{4.101}$$

The optimal control input $u[k]$ is solved using constants and boundary conditions.

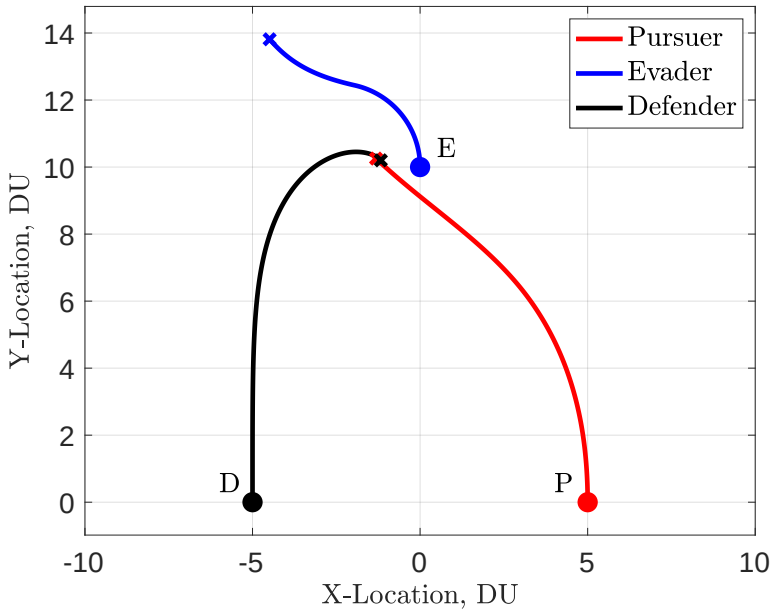

Figure 29. Scenario 1: Optimal Engagement

From Figure 29 it is observed that the evader turns toward the path of the defender, away from the pursuer in an attempt to maximize the distance from the pursuer while providing strategic assistance to the defender. From the plotted solution, the evader executes a max turn rate, staying away from the pursuer as much as possible. This was predicted by eq. (4.94), where the evader is modeled to be turn rate limited.

In Figure 30 the line-of-sight distances and optimal control are observed during the engagement. From Figure 30a it may be observed that the evader is unable to outrun the pursuer since the curve representing the pursuer-evader range, R_{PE}, is monotonically decreasing. However, the evader is able to maneuver in such a way, as to aid in the closure of the defender to the pursuer as described by the curved closure of the defender-pursuer range, R_{DP}. Effectively every engagement, no matter the initial conditions, may be described as a race of one of these curves to zero; if R_{DP} goes to zero first, the evader escapes the pursuer; however, if R_{PE} goes to zero

before R_{DP} can, then the evader is captured.

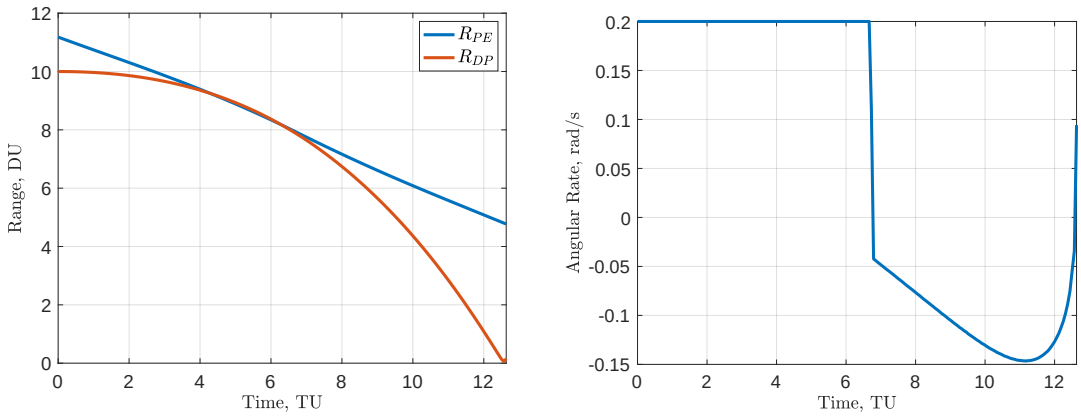

(a) Distances Between Agents

(b) Heading Rate of Evader

Figure 30. Line-of-sight and Optimal Control During Engagement Scenario

The heading rate of the evader as seen in Figure 30b shows that the maximum turn rate was executed for the first half of the engagement and then was not limited in the final half of the scenario. This curve describes that the costate $p_{\phi_E} = 0$ for the second half of the scenario, while $p_{\phi_E} < 0$ for the first half.

4.4 Direct Method Comparisons for HVAA Defense

In this section, each of the four direct methods described in section 3.3 are compared for the sake of computing the optimal control of the kinetic defense of a maneuvering HVAA in 2-D as presented in section 4.3. The HVAA defense scenario in 2-D is illustrated in Figure 27. In the engagement scenario, it is assumed that the velocities of the defender, pursuer, and evader (v_D, v_P, and v_E) are constant. Using the 2-D Cartesian fixed-frame, the dynamics of the three agents are described in eq. (3.40). The input to the system being is heading rate of the evader aircraft, $u(t) = \dot{\psi}_E(t)$.

As described in section 4.3, it is assumed that the pursuer is faster than the evader, so that $v_P > v_E$. Similarly, the defender is assumed to be the same speed as

the pursuer, $v_D = v_P$.

Direct Optimization Problem Definition.

The objective is to find the optimal control: $u^*(t)$ which produces a minimum,

$$\min_u J = -R_{PE}(t_f) + R_{DP}(t_f),$$

subject to the dynamics,

$$\begin{bmatrix} \dot{R}_{DP} \\ \dot{R}_{PE} \\ \dot{\sigma}_D \\ \dot{\sigma}_P \\ \dot{\phi}_P \\ \dot{\phi}_E \end{bmatrix} = \begin{bmatrix} v_P \cos\phi_P - v_D \cos\sigma_D \\ v_E \cos\phi_E - v_P \cos\sigma_P \\ (N_D - 1)\dot{\lambda}_{DP} \\ (N_P - 1)\dot{\lambda}_{PE} \\ N_P\dot{\lambda}_{PE} - \dot{\lambda}_{DP} \\ u - \dot{\lambda}_{PE} \end{bmatrix},$$

with

$$\dot{\lambda}_{DP} = \frac{v_P \sin\phi_P - v_D \sin\sigma_D}{R_{DP}},$$
$$\dot{\lambda}_{PE} = \frac{v_E \sin\phi_E - v_P \sin\sigma_P}{R_{PE}}.$$

The constraints on the input are:

$$|u(t)| \leq \omega_{max} \; \forall \; t \in [t_0, t_f].$$

The boundary conditions on the states are:

$$\begin{bmatrix} R_{DP}(t_0) \\ R_{PE}(t_0) \\ \sigma_D(t_0) \\ \sigma_P(t_0) \\ \phi_P(t_0) \\ \phi_E(t_0) \end{bmatrix} = \begin{bmatrix} R_{DP_0} \\ R_{PE_0} \\ \sigma_{D_0} \\ \sigma_{P_0} \\ \phi_{P_0} \\ \phi_{E_0} \end{bmatrix} \quad \& \quad \begin{bmatrix} R_{DP}(t_f) \\ R_{PE}(t_f) \\ \sigma_D(t_f) \\ \sigma_P(t_f) \\ \phi_P(t_f) \\ \phi_E(t_f) \end{bmatrix} = \begin{bmatrix} \text{free} \\ \text{free} \\ \text{free} \\ \text{free} \\ \text{free} \\ \text{free} \end{bmatrix}.$$

The final time, t_f, is judiciously chosen prior to capture.

Numerical Considerations.

For all four methods, each uses the SQP search implemented within Matlab using the function `FMINCON()`. Furthermore, the initial conditions and final time are the same for each simulation. To ensure that the same problem is being posed for each direct method, the parameters outlined in Table 6 provide a summary of the constants within the equations of motion. These values are implemented for each direct method.

Table 6. Simulation Parameters

Parameter	**Variable**	**Value**
Pursuer speed, DU/TU	v_P	`1.00`
Defender speed, DU/TU	v_D	`1.00`
Evader speed, DU/TU	v_E	`0.50`
Pursuer PN gain	N_P	`3.00`
Defender PN gain	N_D	`3.00`
Final time, TU	t_f	`11.0`
Max turn rate, rad/TU	ω_{max}	`0.20`
Number of points	N	`50.0`

The initial agent locations and headings are identical for all four simulations. Figure 28 describes the initial agent locations and headings used for each simulation. Numerically, the values in Cartesian space are summarized in Table 7. Converting the Cartesian frame to the relative polar coordinate frame the initial agent locations are as defined in Table 8.

Table 7. Initial Conditions (Cartesian Frame)

Agent	X-Location, DU	Y-Location, DU	Heading, rad
Defender	-5.00	0.00	$\pi/2$
Pursuer	5.00	0.00	$\pi/2$
Evader	0.00	10.0	$\pi/2$

Table 8. Initial Agent States (Relative Polar)

State	Variable	Value
Defender-pursuer range, DU	$R_{DP}(t_0)$	10.0000
Pursuer-evader range, DU	$R_{PE}(t_0)$	11.1803
Defender closing heading angle, rad	$\sigma_D(t_0)$	1.5708
Pursuer closing heading angle, rad	$\sigma_P(t_0)$	-0.4636
Pursuer escaping heading angle, rad	$\phi_P(t_0)$	1.5708
Evader escaping heading angle, rad	$\phi_E(t_0)$	-0.4636

Direct Method Setup.

To make a fair comparison between each of the direct methods, the dynamics and number of discrete time points are held constant between methods. Moreover, the convergence criteria, used to determine if a minimum has been found, is also held constant. Aside from the actual algorithmic implementation of each direct method, the guess size and corresponding discretization are varied to meet each method's

requirements.

Concerning the initial guess used for the four direct methods, each method is provided their required states and or control to begin the gradient based search for the minimum. Prior to running the optimization, a single shoot of a max turn rate towards the defender is computed. This single shoot is used as an initial guess for each of the methods. This provides a feasible initial guess for all methods and the information from this initial shooting of the dynamics is discretized and provided to each algorithm just as Table 10 describes.

In the case of the SSM, the discretization of time and control is defined to be evenly spaced into 50 points. By implementing the Runge-Kutta Method for forward propagation of the equations of motion, the fixed-time step solver provides trajectories of the states at every point. The initial guess for the optimal control is a max positive heading rate command. The total size of the initial guess is 50.

For the MSM, time is discretized evenly from t_0 to t_f with a total of N points, just as defined for the SSM. Similar to the SSM, the Runge-Kutta Method propagates states forward through time. The number of segments used for the MSM is 5; resulting in 24 equality constraints (See Table 10). At each of the continuity constraints, the initial guess for the states is the value of the state at the initial condition. The guess for the optimal control, just like the SSM, is a max positive heading rate command. The total size of the guess is 74.

The ECM implements the dynamics as an equality constraint, and as a result, requires a much larger guess than the SSM and MSM. Time is discretized evenly from t_0 to t_f with a total of 50 points. Since the initial state is provided as presented in Table 8, the size of the guess for the states is 294. Adding the size for the control makes the total guess size 344. The dynamics are upheld using a lower order method: first-order Euler approximation. To make the initial guess a fair comparison, the state

trajectories are guessed to be the initial conditions at every point and the optimal control is guessed to be a max positive heading rate command at every point.

For the case of the PSM, time is broken into multiple fixed segments, and for each segment, the LGR points set the discretization of time so that differentiation matrices may be implemented. Just as implemented for the ECM, the number of points for the state trajectories and control are the same. Using the multiple segments, the size of the Differentiation Matrices are selected to be of relatively low order. The use of differentiation matrixes is more accurate than the first-order Euler methods used by the ECM, but the accuracy of the dynamics is greater. The total size of the guess, for the PSM is the same as the ECM: 344. To make the initial guess a fair comparison to the other methods, the state trajectories are guessed to be the initial conditions at every point and the optimal control is guessed to be a max positive heading rate command at every point. To conclude the setup of each of the four direct methods, Table 10 describes the objective cost, initial guess, and type of discretization.

Table 9. Method Size

Method	Initial Guess	No. Ukn.	Eq. Const.	NLP Output
SSM	`u[k], k = 1..50`	50	0	$u_k^*,\ k = 1 \dots 50$
MSM	`u[k], k = 1..50` `x[j], j = 2..5`	$50 + 6(5-1) = 74$	$6(5-1) = 24$	$u_k^*,\ k = 1 \dots N$ $x_j^*,\ j = 2 \dots M$
ECM	`u[k], k = 1..50` `x[k], k = 2..50`	$50 + 6(50-1) = 344$	$6(50-1) = 294$	$u_k^*,\ k = 1 \dots 50$ $x_k^*,\ k = 2 \dots 50$
PSM	`u[k], k = 1..50` `x[k], k = 2..50`	$50 + 6(50-1) = 344$	$6(50-1) = 294$	$u_k^*,\ k = 1 \dots 50$ $x_k^*,\ k = 2 \dots 50$

Table 10. Direct Method Setup

Method	Objective Cost	Initial Guess	Guess Size	Discretization
SSM	$R_{DP}(t_f) - R_{PE}(t_f)$	$u_k = \omega_{max},\ k = 1 \dots 50$	50	Evenly Spaced 1 Shooting
MSM	$R_{DP}(t_f) - R_{PE}(t_f)$	$u_k = \omega_{max},\ k = 1 \dots 50$ $\mathbf{x}_j = \mathbf{x}_0,\ j = 2 \dots 5$	74	Evenly Spaced 5 Shootings
ECM	$R_{DP}(t_f) - R_{PE}(t_f)$	$u_k = \omega_{max},\ k = 1 \dots 50$ $\mathbf{x}_k = \mathbf{x}_0,\ k = 2 \dots 50$	344	Evenly Spaced Collocation Points
PSM	$R_{DP}(t_f) - R_{PE}(t_f)$	$u_k = \omega_{max},\ k = 1 \dots 50$ $\mathbf{x}_k = \mathbf{x}_0,\ k = 2 \dots 50$	344	LGR Collocation 5 Segments

Simulation Results.

A summary of the four direct-method simulations can be seen in Table 11. Presented in the table are metrics for each of the direct methods. The metrics are computation time, number of iterations, number of functional evaluations, function evaluation, and feasibility of the solution. The computation time represents the total time it takes from feeding the NLP the initial guess to the time the optimal control and state trajectories are produced. The number of iterations is the number of times the NLP updates the guess being optimized. Function evaluations are the number of times the objective cost is calculated until the convergence criteria of the NLP occurred. The 'Fval' column represents the value of the objective cost. The feasibility represents two-norm of the vector containing all the equality constraints upon convergence. In the MSM the feasibility represents the total error in the continuity constraints for each shooting interval. In the case of the ECM and PSM, the feasibility represents the accuracy by which the model of the dynamics is upheld. For the sake of comparison, the PSM uses LGR collocation points and a differentiation matrix which is much more accurate than using first-order Euler approximation. Although the feasibility of the ECM is better than the PSM, the method of implementing the dynamics performed by the PSM is more accurate than the ECM.

The total computation time for each direct method is presented in the third column of Table 11. From this column, the fastest direct method is observed to be the ECM, while the slowest is the SSM. The relatively slow convergence times produced by the shooting methods are a reminder that forward propagation of the dynamics obtained using an ODE solver is not computationally efficient. Moreover, the MSM efficiently computes the shootings in parallel, and the addition of the continuity constraints does not out-weigh the cost of breaking the problem into multiple segments. The collocation methods employed by the ECM and PSM are an efficient means of transcribing the dynamic problem into a static one. Although the PSM is slower than the ECM, this is attributed to the number of collocation points which are held constant across all methods. Since the LGR selected points give rise to the efficient computational methods previously described, the number of points required by the PSM to obtain a solution with the same accuracy as the other methods is less. In the effort to make a fare computational comparison, the number of collocation points is kept constant. Further, the implementation of fixed meshing makes it challenging to have enough points where necessary. Since the segmentation was fixed, the PSM is forced to have smooth state trajectories, where the other methods were free to have sharp changes. This is observed around 8 TU in Figure 31b, where the evader heading for the PSM is smoother than the other methods. As a result, the PSM would have faster convergence if fewer points and adaptive meshing were implemented.

The number of iterations and function evaluations conducted by the even collocation method were much larger than the other direct methods. Since the method converted the dynamics into nonlinear constraints, a large number of iterations and evaluations were required to satisfy the feasibility requirement. Even though more function evaluations were required, the effort to compute the equality constraints was far less expensive than using an ODE solver.

The final objective costs produced by all four methods are very similar. From Table 11 the range of the pursuer to the evader upon the capture of the pursuer by the defender is approximately 2.7 DU. The lower performance of the ECM and PSM are attributed to the lack of adaptive meshing for both the ECM and PSM.

Table 11. Direct Method Performance

Method	NLP	Comp. Time	Iter	F. Evals	Fval	Feasibility
SSM	FMINCON()	14.1 sec	32	1632	-2.76	0
MSM	FMINCON()	5.4 sec	27	2214	-2.76	$1.788\mathtt{E}-9$
ECM	FMINCON()	1.2 sec	31	10881	-2.75	$1.019\mathtt{E}-9$
PSM	FMINCON()	8.2 sec	21	6930	-2.71	$3.590\mathtt{E}-8$

In Figure 31a the engagement computed by each of the direct methods is shown. From this figure, it is observed that each of the four methods computes a similar solution for the optimal evasion engagement. Moreover, the states of the optimization are visualized in Figure 31. In Figure 31b the heading angles for each of the agents are presented. From the figure, it can be observed that around 7.5-8.5 seconds, the evader's heading rate makes a drastic change, while the pursuer and defender have smooth curves described by the PN equations. The line-of-sight ranges shown in Figure 31c show that a race to zero between the two line-of-sight rates occurs. If the line-of-sight range R_{PE} reaches zero prior to R_{DP} then the evader is captured; but, if instead R_{DP} goes to zero faster than R_{PE} then the evader successfully escapes the pursuer. In the engagement, the evader successfully escapes the pursuer by maneuvering, in such a way, as to aid the defender. In Figure 31d the optimal control determined by each of the direct methods is presented. Due to the nature of the control limits the optimal control shows the classical bang-bang behavior. In all four cases, the transition from a positive max turn rate to a negative max turn rate occurs around 8 seconds.

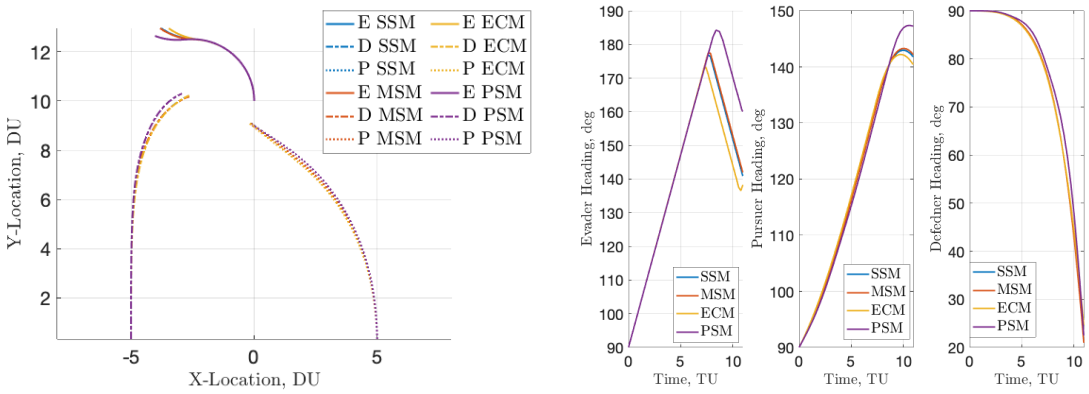

(a) Engagement Comparison

(b) Agent Heading Comparison

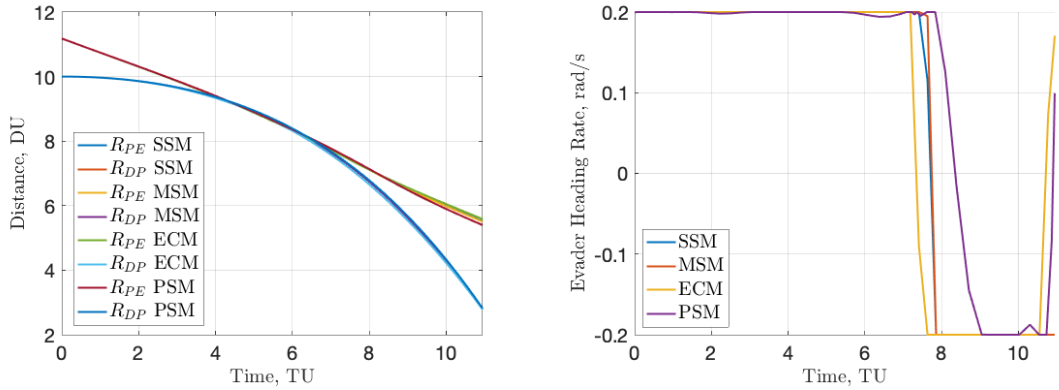

(c) Line-of-sight Comparison

(d) Optimal Control Comparison

Figure 31. The simulation results of the HVAA defense scenario when solved with each of the four direct methods of optimal control

4.5 Concluding Remarks

In this chapter, the kinetic defense of a HVAA was presented. Using differential game theory the optimal strategies for a defender and pursuer were first solved when the evader was non-maneuvering; first in 2-D in Section 4.1, next in 3-D in Section 4.2. Next, in Section 4.3 the evader was allowed to maneuver and aid in his own defense by leveraging the defender's motion, thus maximizing his separation from the pursuer/defender at final time. Finally, in Section 4.4 a comparison was conducted between different ways of finding the optimal control for the maneuvering

evader directly; four methods were considered: Single Shooting Method, Multiple Shootings Method, Even Collocation Method, and Pseudospectral Method.

In Sections 4.1 and 4.2, the use of Apollonius Circle allowed for the differential game to be transformed from a problem of minimax to one of pure minimization. Using optimal control theory the minimization problems were solved, providing the optimal defender and pursuer strategies. The examples in Section 4.1 Section 4.2 demonstrated that, for any agent, any variation from the differential game solution yielded poorer performance for that player.

In Sections 4.3 and 4.4 the kinetic defense of a maneuvering evader was considered. In the HVAA defense scenario, both the pursuer and defender are assumed to use a Proportional Navigation guidance law and the evader's control strategy is solved using optimal control theory. The resulting maneuver made by the evader was to head toward his defender in an effort to assist the defender's capture of the pursuer. In Section 4.4, attention was given to the direct method used to solve the optimal control problem. The four methods implemented were the Single Shooting Method, Multiple Shootings Method, Even Collocation Method, and Pseudospectral Method. Considering the three-player engagement, the four methods found similar solutions for the optimal control and the corresponding state trajectories; but, the size of each method varied. Using a fixed mesh, the four methods were implemented in Matlab. The results highlight the importance of adaptive meshing techniques and the advantages of using direct transcription rather than ODE solvers.

V. Directed Energy Defense of a HVAA

> Problems worthy of attack prove their worth
> by fighting back.
>
> — Paul Erdös

In defensive counter air (DCA) operations, aircraft defense can be provided by two means, kinetic or directed energy. Kinetic defense aims at providing defense through physical capture or damage by proximity. Directed energy defense provides damage by bombarding a target with electrons over time – this is achieved by leveraging the electromagnetic spectrum. Directed energy defense is unique in that defense is provided over a prolonged period of time rather than at a specific time instant, as shown previously with kinetic defense.

This chapter considers the defender to be an aircraft equipped with a directed energy weapon. Using this weapon, the defender aims to "expose the pursuer" for as long as possible. The exposure time which neutralizes an asset depends upon many factors outside the scope of this dissertation. Rather than focus on the physical aspects which dictate the amount of exposure time required to neutralize an asset, time guarantees for exposure time are presented. In this dissertation, as will be shown in this chapter, one can compute the maximum possible exposure time based upon the initial vehicle locations, speeds, and headings. The calculated exposure time can be used to provide insight into requirements for the physical systems involved and provide insight into the flight paths for a successful defense of a HVAA from a single incoming threat.

5.1 Maximum Exposure of a Non-Maneuvering Pursuer in 2-D

This section considers a two-agent scenario containing a defender and a non-maneuvering pursuer. The defender is maneuverable and is slower than the course-holding pursuer. In this scenario, the defender is endowed with a specified circular WEZ within which the defender strives to contain the pursuer for as long as possible. The heading of the defender which maximizes the exposure time, i.e. the pursuer remains inside the radius of the circular WEZ of the defender is solved using the calculus of variations. The exposure time is computed based upon the angle by which the pursuer is initially within the WEZ of the defender as well as the relative speed ratio of the defender with respect to the pursuer. Presented, along with an example, are the zero-time of exposure heading, maximum time of exposure heading, and proof that exposure is persistent under optimal control.

Optimal Control Problem.

Described in Section 3.4, an optimal control problem is developed between the pursuer and the defender concerning the defense of a non-maneuvering HVAA. From the problem definition, the motion of the agents are defined as a set of ordinary differential equations as shown in eq. (3.58). Also, the objective cost is defined in eq. (3.61). This is equivalent to maximizing exposure time where t_f is now exposure time. Define the speed ratio between the defender and the pursuer as: $\alpha = v_D/v_P$. In the scenario, the pursuer is faster than the defender and therefore: $0 < \alpha < 1$. Using the speed ratio parameter, the non-dimensional dynamics in eq. (3.58) are re-written as

$$\begin{aligned} \dot{x}_D &= \alpha \cos\psi_D, \qquad \dot{x}_P = \cos\psi_P, \\ \dot{y}_D &= \alpha \sin\psi_D, \qquad \dot{y}_P = \sin\psi_P. \end{aligned} \tag{5.1}$$

Since the objective cost is Mayer, the Hamiltonian is the inner product of the

dynamics in eq. (5.1) with the costates and is

$$\mathscr{H} = p_{x_D}\alpha\cos\psi_D + p_{y_D}\alpha\sin\psi_D + p_{x_P}\cos\psi_P + p_{y_P}\sin\psi_P, \tag{5.2}$$

where the costates are $\mathbf{p}^T = [p_{x_D},\ p_{y_D},\ p_{x_P},\ p_{y_P}]$.

Necessary Conditions for Optimality:.

Using the Hamiltonian in eq. (5.2), the necessary conditions for optimality are obtained by taking the partial derivatives as described in eqs. (3.10) to (3.12). Using the first-order necessary conditions for optimality one may be able to formulate and draw conclusions about the optimal control. Since the objective cost is Mayer, the optimal Hamiltonian at final time is zero, $\mathscr{H}^*(t_f) = 0$. Where the superscript, $*$, represents optimally. Evaluating the necessary condition described in eq. (3.12) the following is obtained:

$$\begin{aligned} 0 =& \frac{\partial}{\partial\psi_D}(p^*_{x_P}\cos\psi_P + p^*_{y_P}\sin\psi_P + p^*_{x_D}\alpha\cos\psi_D + p^*_{y_D}\alpha\sin\psi_D) \\ =& -\alpha p^*_{x_D}(t)\sin\psi^*_D(t) + \alpha p^*_{y_D}(t)\cos\psi^*_D(t) \\ =& -p^*_{x_D}(t)\sin\psi^*_D(t) + p^*_{y_D}(t)\cos\psi^*_D(t). \end{aligned} \tag{5.3}$$

Bringing the two terms in eq. (5.3) to either side of the equation, squaring, and using the trigonometric identity $\cos^2\psi^*_D = 1 - \sin^2\psi^*_D$, one may obtain the following:

$$p^{*2}_{x_D}(t)\sin^2\psi^*_D(t) = p^{*2}_{y_D}(t)(1 - \sin^2\psi^*_D). \tag{5.4}$$

Through algebraic manipulation of eq. (5.4) the following is obtained:

$$\sin^2\psi^*_D(t) = \frac{p^{*2}_{y_D}(t)}{p^{*2}_{x_D}(t) + p^{*2}_{y_D}(t)}. \tag{5.5}$$

Evaluating the necessary condition in eq. (3.11), four equations, one for each costate, are

$$\dot{p}^*_{x_D} = \dot{p}^*_{x_P} = \dot{p}^*_{y_D} = \dot{p}^*_{y_P} = 0 \tag{5.6}$$

From the necessary conditions in eq. (5.6) it may be inferred that the optimal costate trajectories are constant, i.e.: $\mathbf{p}^*(t) = \mathbf{p}^*$ because the defender is holonomic. Moreover, since the costates are constant, the optimal heading of the defender is constant under optimal play. This result may be derived from eq. (5.5). Therefore, the resulting optimal trajectory of the defender is a straight-line trajectory at an angle:

$$\psi^*_D(t) = \psi^*_D = \sin^{-1}\left(\frac{p^*_{y_D}}{\sqrt{p^{*2}_{x_D} + p^{*2}_{y_D}}}\right). \tag{5.7}$$

Transversality Conditions.

Next, consider the transversality conditions which are used to formulate the relationship between the states and costates at final time. In eq. (5.7), the optimal defender heading depends solely upon the costates, which are constant. Leveraging the transversality conditions as described by eq. (3.14), the optimal defender heading can be obtained as a function of the final states and problem parameters. From eq. (3.61), the terminal penalty in the objective cost is constant, $\frac{\partial \Phi}{\partial \mathbf{x}} = 0$. The terminal manifold is defined in eq. (3.60) and therefore the terminal manifold is

$$m(\mathbf{x}^*(t_f), t_f) = (x^*_D(t_f) - x^*_P(t_f))^2 + (y^*_D(t_f) - y^*_P(t_f))^2 - R^2_D. \tag{5.8}$$

Substitution of eq. (5.8) into the transversality conditions from eq. (3.14), the following is obtained:

$$-\mathbf{p}^*(t_f)^T = \delta \begin{bmatrix} \frac{\partial m}{\partial x_P} & \frac{\partial m}{\partial y_P} & \frac{\partial m}{\partial x_D} & \frac{\partial m}{\partial y_D} \end{bmatrix}. \tag{5.9}$$

Recall, that the slack variable from the transversality conditions is represented here by δ. Expanding eq. (5.9), the costates are:

$$\begin{aligned} p^*_{x_P} &= \frac{\partial m}{\partial x_P} = 2\delta(x_D - x_P), \qquad p^*_{y_P} = \frac{\partial m}{\partial y_P} = 2\delta(y_D - y_P), \\ p^*_{x_D} &= \frac{\partial m}{\partial x_D} = 2\delta(x_P - x_D), \qquad p^*_{y_D} = \frac{\partial m}{\partial y_D} = 2\delta(y_P - y_D). \end{aligned} \tag{5.10}$$

Taking the square root of eq. (5.5) and substituting the costates from eq. (5.10) the following is obtained:

$$\sin\psi^*_D(t_f) = \frac{\pm 2\delta(y_{P_f} - y_{D_f})}{\sqrt{4d^2(x_{P_f} - x_{D_f})^2 + 4d^2(y_{P_f} - y_{D_f})^2}}. \tag{5.11}$$

Simplifying eq. (5.11), a relationship between the states of the defender and pursuer at the final time, t_f, is

$$\sin\psi^*_D(t_f) = \frac{\pm(y_{P_f} - y_{D_f})}{R_D}. \tag{5.12}$$

From eq. (5.12), the angle from the defender to the pursuer at final time is found to be the same as the optimal heading. An illustration of the optimal engagement is shown in Figure 32. As a result of eq. (5.12), the line segment $\overline{QS}$ is collinear with $\overline{DQ}$.

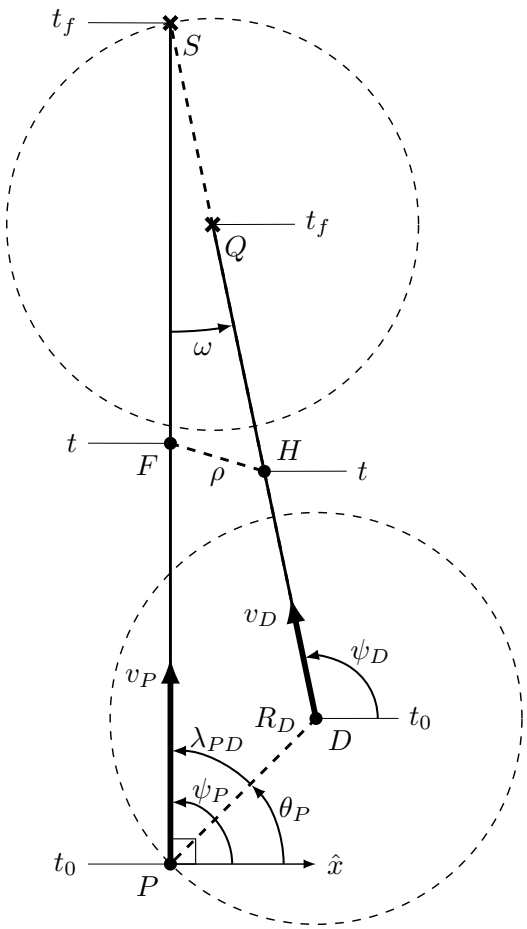

Figure 32. Optimal Two-Agent Engagement Geometry

Solution to the Optimal Control Problem.

Knowing the course of the pursuer, the optimal heading of the defender which maximizes the exposure time may be analytically obtained. Without loss of generality, the defender-pursuer scenario is rotated about the pursuer such that the pursuer velocity is aligned with the vertical axis as shown in Figure 32.

The necessary conditions of optimality in eqs. (3.10) to (3.12) have shown that optimal heading in eq. (5.7) is constant. The transversality conditions in eq. (3.14) have shown that the angle from the defender to the pursuer at final time is the same as the optimal heading eq. (5.12). Using the law of cosines, the optimal heading of

the defender may be obtained.

Theorem 4. *The optimal heading of the defender which maximizes exposure time is:* $\psi_D^* = \cos^{-1}\left(\frac{(\alpha^2-1)\sin\lambda_{PD}}{\alpha^2+2\alpha\cos\lambda_{PD}+1}\right)$*; where* $\alpha \in (0,1)$ *is the speed ratio of the defender to the pursuer and* $\lambda_{PD} \in [-\pi, \pi]$ *is the bearing from the pursuer to the defender.*

Proof. Using the law of cosines for the triangle, $\triangle DSP$:

$$\overline{DS}^2 = \overline{PS}^2 + R_D^2 - 2R_D\overline{PS}\cos\lambda_{PD}. \tag{5.13}$$

Using the speed ratio, the distance traversed by the pursuer is the same as α multiplied by the distance traversed by the defender,

$$\overline{DS} = \alpha\overline{PS} + R_D. \tag{5.14}$$

Substituting eq. (5.14) into eq. (5.13),

$$(\alpha\overline{PS} + R_D)^2 = \overline{PS}^2 + R_D^2 - 2R_D\overline{PS}\cos\lambda_{PD}. \tag{5.15}$$

Expanding eq. (5.15),

$$\alpha^2\overline{PS}^2 + R_D^2 + 2\alpha R_D\overline{PS} = \overline{PS}^2 + R_D^2 - 2R_D\overline{PS}\cos\lambda_{PD}. \tag{5.16}$$

Canceling R_D^2 terms on either side of the equals sign in eq. (5.16),

$$\alpha^2\overline{PS}^2 + 2\alpha R_D\overline{PS} = \overline{PS}^2 - 2R_D\overline{PS}\cos\lambda_{PD}. \tag{5.17}$$

Dividing both sides of eq. (5.17) by $\overline{PS}$ (this assumes that $\overline{PS} \neq 0$; but if $\overline{PS} = 0$

then capture would have occurred),

$$\alpha^2\overline{PS} + 2\alpha R_D = \overline{PS} - 2R_D \cos\lambda_{PD}. \tag{5.18}$$

Solving eq. (5.18) for $\overline{PS}$ a formulation for the time of exposure is obtained as a function of the exposure radius, $R_D \geq 0$, speed ratio $\alpha \in (0,1)$ and initial pursuer-defender angle, $\lambda_{PD} \in [-\pi, \pi]$,

$$\overline{PS} = \frac{2R_D(\alpha + \cos\lambda_{PD})}{1-\alpha^2}. \tag{5.19}$$

Since the cosine of an angle is the adjacent distance over the hypotenuse, the following is obtained:

$$\cos(\pi - \psi_D) = \frac{R_D \sin\lambda_{PD}}{\alpha\overline{PS} + R_D}. \tag{5.20}$$

Substitution of eq. (5.19) into eq. (5.20),

$$-\cos\psi_D = \frac{R_D \sin\lambda_{PD}}{\alpha\frac{2R_D(\alpha+\cos\lambda_{PD})}{1-\alpha^2} + R_D}. \tag{5.21}$$

Through algebraic manipulation of eq. (5.21) the optimal defender heading is

$$\psi_D^* = \cos^{-1}\left(\frac{(\alpha^2-1)\sin\lambda_{PD}}{\alpha^2 + 2\alpha\cos\lambda_{PD} + 1}\right). \tag{5.22}$$

■

Special Case: $\lambda_{PD} = 0$**.**

When the line-of-sight angle, λ_{PD}, is zero the speed ratio does not come into play and the optimal heading of the defender is $\psi_D = \pi/2$ as expected. This result can be obtained from setting $\lambda_{PD} = 0$ in eq. (5.22).

Invariance of Exposure.

Suppose the defender is within a range, R_D, of the pursuer at a time t_0. Under optimal play, the pursuer remains within the WEZ until the termination set is reached. Figure 32 described the geometry for the optimal two-agent scenario. The instantaneous range between P and D, ρ, is less than R_D in the open interval, (t_0, t_f) as proved in Theorem 5. Recall, t_0 is the instant in time when the pursuer is inside the defender's WEZ and t_f is the instant in time when the pursuer leaves the defender's WEZ.

Theorem 5. *$\rho < R_D \ \forall \ t \in (t_0, t_f)$, where ρ is the defender-pursuer range at any time from the open interval starting at t_0 and ending at t_f.*

Proof. Utilizing the Law of Cosines to analyze $\triangle DSP$,

$$\overline{DP}^2 = \overline{PS}^2 + (\overline{DQ} + \overline{QS})^2 - 2\overline{PS}(\overline{DQ} + \overline{QS})\cos\omega. \tag{5.23}$$

Recognize that $\overline{DP} = R_D$, $\overline{QS} = R_D$, and $\overline{PS} = \alpha\overline{DQ}$. Substitution into eq. (5.23),

$$R_D^2 = \overline{PS}^2 + (\alpha\overline{PS} + R_D)^2 - 2\overline{PS}(\alpha\overline{PS} + R_D)\cos\omega. \tag{5.24}$$

Expanding and solving eq. (5.24) for $\cos\omega$,

$$\cos\omega = \frac{\overline{PS}(1+\alpha^2) + 2\alpha R_D}{2(\alpha\overline{PS} + R_D)}. \tag{5.25}$$

Now consider a future time, $t \in (t_0, t_f)$. Using the Law of Cosines for $\triangle FHS$,

$$\rho^2 = \overline{FS}^2 + \overline{HS}^2 - 2\overline{FS}\ \overline{HS}cos\omega. \tag{5.26}$$

Recognize that $\overline{HQ} = \alpha\overline{FS}$ and $\overline{HS} = \overline{HQ} + R_D$. Substituting these into eq. (5.26),

$$\rho^2 = \overline{FS}^2 + (\alpha\overline{FS} + R_D)^2 - 2\overline{FS}(\alpha\overline{FS} + R_D)cos\omega. \tag{5.27}$$

Substituting eq. (5.25) into eq. (5.27):

$$\begin{aligned}\rho^2 =&\overline{FS}^2 + (\alpha\overline{FS} + R_D)^2 \\ &- 2\overline{FS}(\alpha\overline{FS} + R_D)\frac{\overline{PS}(1+\alpha^2) + 2\alpha R_D}{2(\alpha\overline{PS} + R_D)}.\end{aligned} \tag{5.28}$$

Algebraically manipulating eq. (5.28) the following is obtained:

$$\rho^2 = R_D^2 + \frac{\overline{FS}R_D}{(\alpha\overline{PS} + R_D)}\left(\overline{FS} - \overline{PS}\right)\left(1 - \alpha^2\right). \tag{5.29}$$

Notice in eq. (5.29),

$$\rho^2 = R_D^2 + \underbrace{\frac{\overline{FS}R_D}{(\alpha\overline{PS} + R_D)}}_{\text{Positive}}\ \underbrace{\left(\overline{FS} - \overline{PS}\right)}_{\text{Negative}}\underbrace{\left(1 - \alpha^2\right)}_{\text{Positive}}; \tag{5.30}$$

therefore, for values of $t \in (t_0, t_f)$, $\rho < R_D$.

■

Exposure Limaçon.

The function which describes the pursuer distance while being exposed is provided by eq. (5.19). The pursuer distance while being exposed is a function of the bearing from the pursuer to the defender (λ_{PD}), the radius of exposure (R_D), and speed ratio between the defender and the pursuer (α). Using the range $\overline{PS}$, the polar equation

for exposure time is

$$t_f = \frac{2R_D(\alpha + \cos\lambda_{PD})}{v_P(1-\alpha^2)} = \frac{2R_D(v_D + v_P\cos\lambda_{PD})}{v_P^2 - v_D^2}. \tag{5.31}$$

Plotting the time of exposure as a function of the angle from the pursuer to the defender (λ_{PD}) produces a limaçon whose cusp is located at the pursuer location. By setting $t_f = 0$, the angle λ_{PD} which result in Zero Exposure Time (ZET). From eq. (5.31), values of λ_{PD} which result in non-positive values of t_f represent angles for which exposure of the pursuer by the defender is not possible. Thus, setting $t_f \leq 0$ in eq. (5.31), the following is obtained:

$$\frac{2R_D}{v_P(1-\alpha^2)}(\alpha + \cos\lambda_{PD}^0) \leq 0. \tag{5.32}$$

where λ_{PD}^0 represents angles where exposure of the pursuer by the defender are not possible. From eq. (5.32), the regions where the defender is unable to expose the pursuer occurs when the angle λ_{PD} lies in the following range:

$$\lambda_{PD}^0 \in [\cos^{-1}(-\alpha), \pi] \cup [-\pi, -\cos^{-1}(-\alpha)]. \tag{5.33}$$

Assuming the defender implements the optimal heading which maximizes exposure time of the faster pursuer, eq. (5.31) can be algebraically manipulated to provide the defender-pursuer headings which guarantee a desired exposure time as follows:

$$\lambda_{PD}(t) = \cos^{-1}\left(\frac{(v_P^2 - v_D^2)t - 2R_D v_D}{2R_D v_P}\right). \tag{5.34}$$

It should be noted that the guarantees for exposure time are bounded by the following closed interval:

$$t \in \left[0,\ \frac{2R_D}{v_P - v_D}\right]. \tag{5.35}$$

Example.

Consider the scenario with radius of exposure, $R_D = 1.0$; speed ratio, $\alpha = 0.8$; pursuer's constant heading, $\psi_P = \pi/2$ rad; and pursuer-defender line-of-sight angle, $\lambda_{PD} = 7/18\pi$ rad. Also, consider the velocity of the pursuer to have speed $v_P = 1$ DU/TU. Using eq. (5.22), the optimal defender heading, ψ_D^* is computed and is $\psi_D^* \approx 1.726$ rad. Using the calculated optimal defender heading, the max-time exposure of the faster non-maneuvering pursuer can be seen in Figure 33. In the figure, the defender is represented by the black line, the WEZ is represented by the dashed line, and the faster pursuer is represented by the red line. Not pictured is the evader – it is assumed that the course taken by the pursuer is a straight-line intercept of the HVAA (evader).

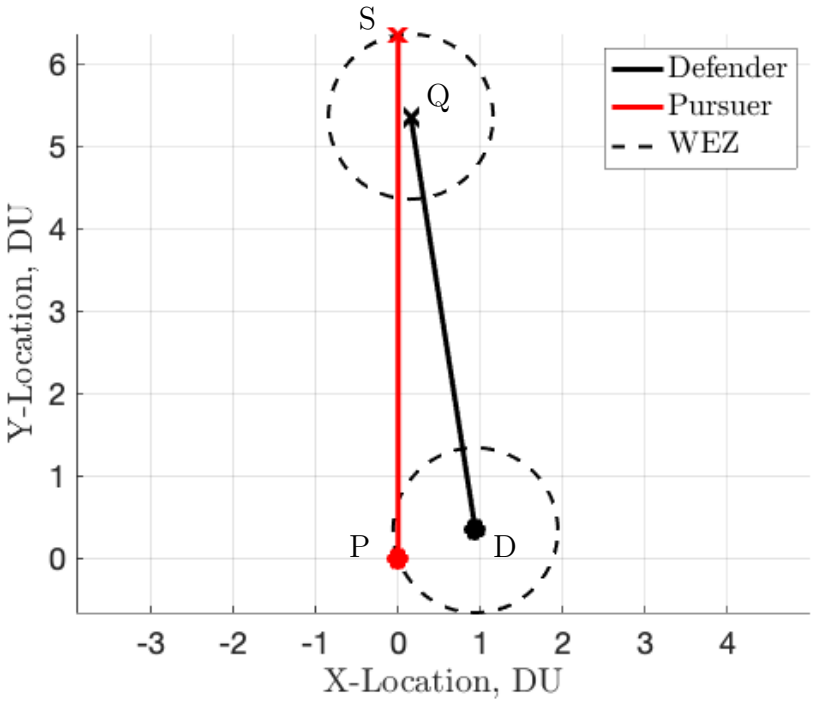

Figure 33. The max-time exposure of a faster non-maneuvering pursuer by a slower defender endowed with a circular WEZ

For the scenario described in Figure 33, consider the defender-pursuer range

throughout the engagement. In Theorem 5 the defender-pursuer range remains less than the range of the WEZ under optimal play until the pursuer escapes. In Figure 34, the defender range is represented by the dashed black line and, the instantaneous defender-pursuer range is represented by the solid black line. As expected, the defender-pursuer range remains less than the defender range for the entire engagement, as required.

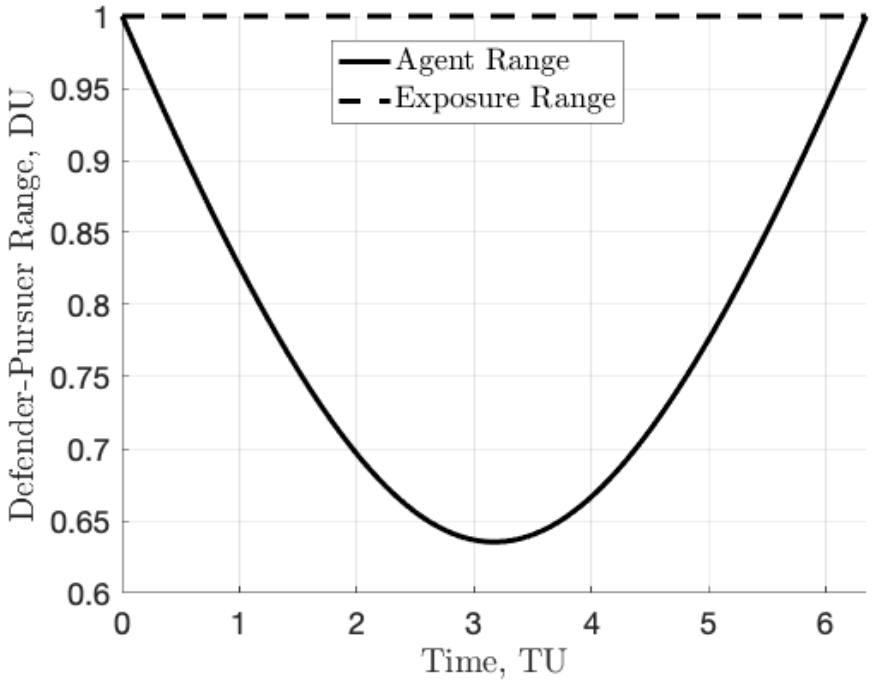

Figure 34. The instantaneous agent range is less than the exposure range for the entire engagement which lasts 6.345 time-units.

Next, consider arbitrary defender-pursuer aspect angles: $\lambda_{PD} \in [-\pi, \pi]$. In the event that the defender selects the optimal heading described by eq. (5.22), the exposure time can be computed using eq. (5.31). In Figure 35 the maximum exposure time is found for arbitrary aspect angles, λ_{PD}. From the figure, the blue line represents all cases where the defender is able to expose the pursuer for a non-zero amount of time. The green line represents the computed exposure time from eq. (5.31). While the negative values signify that the defender is unable to defender the pursuer for any

amount of time. The green dot designates the angle λ_{PD}^{0} for which there is zero exposure time. Finally, the black dot is the computed maximum exposure time, which occurs when $\lambda_{PD} = 0$.

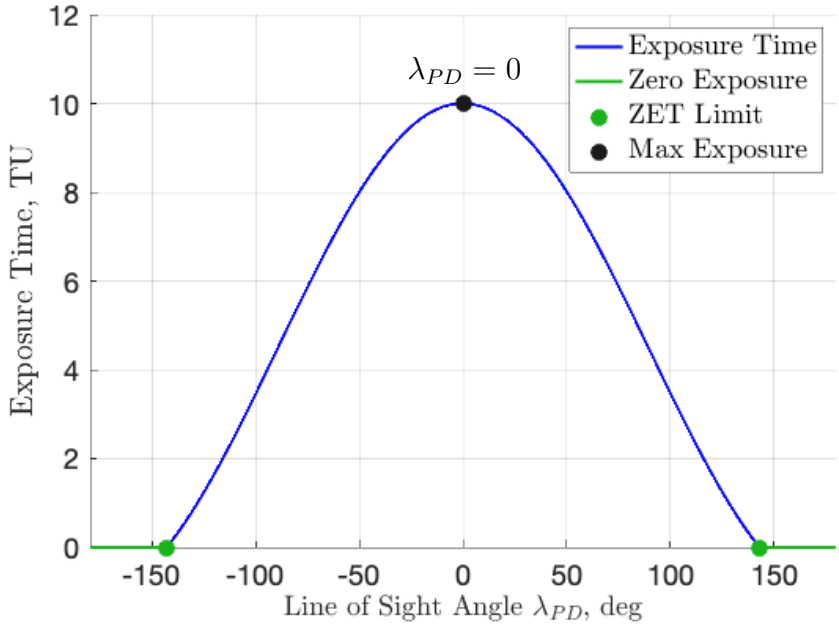

Figure 35. Time of exposure of the non-maneuvering pursuer by the defender as a function of the line-of-sight angle λ_{PD} when $\alpha = 0.8$ and $R_D = 1.0$

A plot which describes the exposure time for arbitrary defender-pursuer headings was shown in Figure 35. However, how this relates to an actual engagement scenario may be unclear. Plotting the exposure time in a polar sense for each aspect angle, λ_{PD}, the limaçon which describes the exposure time for each aspect angle, λ_{PD}, can be seen in Figure 36. In the figure, the gray shaded region represents the region where exposure of the pursuer by the defender for all possible defender-pursuer line-of-sight angles (λ_{PD}). The green region represents the pursuer headings for which the defender is unable to expose the faster pursuer. Considering, the scenario in this example, the red line represents the course taken by the pursuer, the black line represents the defender under optimal play, and the dashed black circles represent the defender's WEZ at the beginning and end of the engagement.

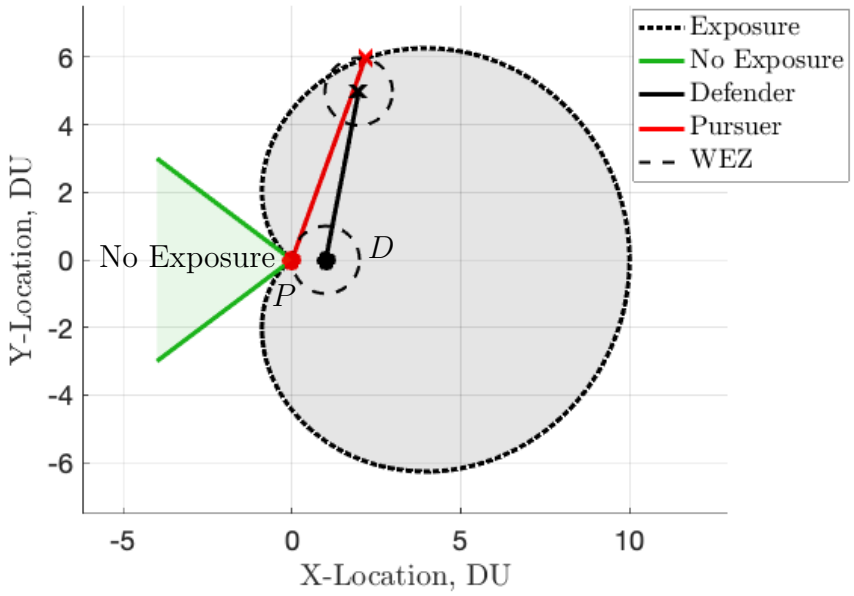

Figure 36. The exposure limaçon describes the range by which exposure is guaranteed as a function of the line-of-sight angle, λ_{PD}, for a given defender-pursuer speed ratio, α, and exposure radius, R_D.

5.2 Directed Energy Defense of a Non-Maneuvering HVAA in 2-D

In this section, directed energy is considered as a means of defending a slow non-maneuverable HVAA (evader) against an incoming threat (pursuer). In the engagement, the faster pursuer aims at intercepting the non-maneuvering evader in minimum time. To aid the evader, a teamed defender equipped with a directed energy weapon is considered. Rather than focus on the technology or the more critical aspects of the directed energy device, it is assumed that the efficacy of the defensive device is increased by maximizing the cumulative exposure time that the pursuer is in a WEZ of fixed range about the defender; and by this assumption, the objective of the defender is to maximally expose the pursuer prior to the capture of the evader.

Optimal Control Problem.

Consider a three-agent engagement scenario comprised of a fast pursuer (P) which is engaged on a slow non-maneuvering evader (E). To aid in the defense of the evader, a defender (D) is considered which aims at keeping the pursuer in its WEZ for as long as possible. A circular WEZ with radius R_D is considered. This section considers the question: How should the defender act so as to keep the pursuer in the circular WEZ for as long as possible? It is assumed that the pursuer's strategy is one of min-time capture of the evader and as a result, its strategy is unaffected by the presence of the defender.

Described in Section 3.4, two optimal control problems are developed: one for the pursuer and one for the defender. The pursuer aims to capture the evader in minimum time and the defender aims to maximize the cumulative time that the pursuer remains inside its WEZ. The three-agent scenario equations of motion are described in eq. (3.62). The objective cost of the pursuer is defined in eq. (3.66) and the objective cost of the defender is defined in eq. (3.68). The speed ratio between the pursuer and evader is defined as $\mu = v_E/v_P$. Similarly, the speed ratio between the pursuer and the defender is defined as $\alpha = v_D/v_P$. Since the pursuer is faster than both the defender and the evader the domain of the speed ratios is μ, $\alpha \in (0, 1)$. Without loss of generality, consider the non-dimensionalization of time so that the pursuer's speed is unity. Utilizing the speed ratio parameters, the equations of motion in eq. (3.62) may be simplified as

$$\begin{aligned} \dot{x}_P &= \cos\psi_P, \quad \dot{x}_E = \mu\cos\psi_E, \quad \dot{x}_D = \alpha\cos\psi_D, \\ \dot{y}_P &= \sin\psi_P, \quad \dot{y}_E = \mu\sin\psi_E, \quad \dot{y}_D = \alpha\sin\psi_D. \end{aligned} \tag{5.36}$$

Two optimization problems are formulated and solved, and their interaction is investigated in this section. The costate vectors $\mathbf{p}_A^T = [p_{x_P,A}\ p_{y_P,A}\ p_{x_E,A}\ p_{y_E,A}]$ and

$\mathbf{p}_B^T = [p_{x_P,B}\ p_{y_P,B}\ p_{x_D,B}\ p_{y_D,B}]$ are introduced in order to formulate the Hamiltonians for solving the two optimization problems (A and B) as defined by the minimization of the objective costs in eqs. (3.66) and (3.68). Using the calculus of variations, the Hamiltonian for the minimization described in eqs. (3.64) and (3.66) is the following:

$$\mathscr{H}_A = p_{x_P} \cos\psi_P + p_{y_P} \sin\psi_P + p_{x_E}\mu \cos\psi_E + p_{y_E}\mu \sin\psi_E. \tag{5.37}$$

The Hamiltonian for the minimization described in eqs. (3.65) and (3.68) is

$$\mathscr{H}_B = p_{x_P} \cos\psi_P + p_{y_P} \sin\psi_P + p_{x_D}\alpha \cos\psi_D + p_{y_D}\alpha \sin\psi_D. \tag{5.38}$$

The procedure for solving the optimal strategies of the pursuer and the defender is to first formulate and solve for the min-time capture of the evader by the pursuer – to solve the optimization problem as described in eqs. (3.64), (3.66), (3.67) and (5.37). Then, using the solution to the optimization problem A, the optimal strategy for the defender is then posed and solved as described by eqs. (3.65), (3.68), (3.69) and (5.38).

Using the first-order optimality conditions, conclusions about the optimal behavior of the defender and the pursuer can be drawn. Using the Hamiltonians in eqs. (5.37) and (5.38), the necessary conditions for optimality are found using the partial derivatives in eqs. (3.10) to (3.12). Moreover, at final time for each of the optimization problems, the optimal Hamiltonian is zero, $\mathscr{H}_A(t_{\text{go}}) = \mathscr{H}_B(t_{\text{exp}}) = 0$. Recall, the superscript, $*$, represents optimality. Also, the control, $\mathbf{u}(t)$, for the pursuer or defender (depending upon the problem being solved) are defined as $\mathbf{u}(t) = \{\psi_P(t)\}$ for problem A and $\mathbf{u}(t) = \{\psi_D(t)\}$ for problem B.

Optimal Control Problem, A - Pursuer Strategy.

Lemma 1. *The optimal strategy for the pursuer is a straight-line constant-heading strategy.*

Proof. Evaluating eq. (3.11) using the Hamiltonian, $\mathscr{H}_A$ from eq. (5.37) the costate dynamics are as follows:

$$\dot{p}^*_{x_P,A} = \dot{p}^*_{y_P,A} = \dot{p}^*_{x_E,A} = \dot{p}^*_{y_E,A} = 0. \tag{5.39}$$

where the "A" subscript notation identifies the corresponding Hamiltonian. Further, evaluating the partial of $\mathscr{H}_A$ with respect to the pursuer's control ψ_P in eq. (3.12),

$$0 = -p^*_{x_P,A} \sin\psi^*_P + p^*_{y_P,A} \cos\psi^*_P. \tag{5.40}$$

rearranging and squaring each side of eq. (5.40), the following is obtained:

$$p^{*2}_{x_P,A} \sin^2\psi^*_P = p^{*2}_{y_P,A} \cos^2\psi^*_P = p^{*2}_{y_P,A}(1 - \sin^2\psi^*_P). \tag{5.41}$$

solving for ψ^*_P,

$$\psi^*_P = \sin^{-1}\left(\frac{p^*_{y_P,A}}{\sqrt{p^{*2}_{x_P,A} + p^{*2}_{y_P,A}}}\right). \tag{5.42}$$

Since the costates are constant, the pursuer's heading is constant under optimal play. ■

By Lemma 1, the pursuer's heading is constant under optimal play; thus, the use of Apollonius Circle is a useful tool for solving for the min-time interception of the evader by the pursuer as was demonstrated in Section 4.1.

Lemma 2. *The optimal heading for the pursuer which captures the non-maneuvering evader in minimum time is* $\psi^*_P = \sin^{-1}(\mu\sin(\psi_E - \theta_E)) + \theta_E$ *where* μ *is the speed*

ratio between the evader and the pursuer, ψ_E is the heading of the evader, and θ_E is the angle from the pursuer to the evader relative to the x-axis in the Cartesian fixed frame.

Proof. From necessary conditions for optimality, the optimal strategy for the pursuer is a straight-line trajectory. Moreover, the evader is non-maneuvering, and therefore, the geometry of Apollonius provides the optimal strategy for the pursuer to capture the slower non-maneuvering evader in minimum time [9].

In Figure 37, the Apollonius Circle is shown in magenta, where the origin is located at O. The distance $d = \overline{PE}$, the speed ratio $\mu = \frac{v_E}{v_P}$, the position of P and E are used to construct the Apollonius Circle which defines the locus of min-time interceptions possible by the pursuer because the evader is non-maneuvering. Along the vector $\vec{PE}$ the geometry defined by Apollonius: $\overline{OE} = \frac{\mu^2 d}{1-\mu^2}$ and $R_{apol} = \overline{OI} = \frac{\mu d}{1-\mu^2}$.

Evaluating the distance normal to $\overline{PO}$ which locates point I from E and P, the following can be obtained:

$$\overline{EI}\sin(\psi_E - \theta_E) = \overline{PI}\sin(\psi_P^* - \theta_E). \tag{5.43}$$

Recall, the speed ratio μ defines the relationship between $\overline{EI}$ and $\overline{PI}$ to be: $\overline{EI} = \mu\overline{PI}$. Substitution into eq. (5.43), the following is obtained:

$$\mu\overline{PI}\sin(\psi_E - \theta_E) = \overline{PI}\sin(\psi_P^* - \theta_E). \tag{5.44}$$

Solving for ψ_P^*,

$$\psi_P^* = \sin^{-1}(\mu\sin(\psi_E - \theta_E)) + \theta_E. \tag{5.45}$$

■

Lemma 3. *Using the geometry provided by Apollonius Circle, the time-to-go is*

$$t_{\text{go}} = \frac{d}{v_P}\left(\sigma_1 + \sqrt{\sigma_1^2 + \sigma_2}\right), \tag{5.46}$$

where $\sigma_1 = \mu\cos(\psi_E - \theta_E)/(1-\mu^2)$, $\sigma_2 = 1/(1-\mu^2)$, *and* d *is the distance between* P *and* E.

Proof. Because the velocity of the pursuer has been normalized to 1, the time-to-go in seconds is the same as the length $\overline{PI}$. This means, the length $\overline{PI}$ provides the time-to-go, t_{go}. Consider $\triangle IEO$ in Figure 37; by the law of cosines,

$$\overline{OI}^2 = \overline{EO}^2 + \overline{EI}^2 - 2\overline{EO}\;\overline{EI}\cos(\psi_E - \theta_E). \tag{5.47}$$

Define the distance between the pursuer and evader as d and the evader-pursuer ratio is $v_E/v_P = \mu$, where $\mu < 1$. From the Apollonius Circle, $\overline{EO} = \mu^2 d/(1-\mu^2)$, $\overline{OI} = \mu d/(1-\mu^2)$, and $\overline{EI} = \mu\overline{PI}$. Substitution into eq. (5.47), the following is obtained:

$$\left(\frac{\mu d}{1-\mu^2}\right)^2 = \left(\frac{\mu^2 d}{1-\mu^2}\right)^2 + \left(\mu\overline{PI}\right)^2 - 2\left(\frac{\mu^2 d}{1-\mu^2}\right)\left(\mu\overline{PI}\right)\cos(\psi_E - \theta_E). \tag{5.48}$$

Bringing all the terms to the right hand side and simplifying eq. (5.48),

$$0 = \overline{PI}^2 - \frac{2\mu d}{1-\mu^2}\cos(\psi_E - \theta_E)\overline{PI} - \frac{d^2}{1-\mu^2}. \tag{5.49}$$

Using the quadratic equation, $\overline{PI}$ may be solved in terms of the evader-pursuer speed

ratio and the pursuer-evader distance using eq. (5.49). Letting

$$\begin{aligned} a &= 1 \\ b &= -\frac{2\mu d\cos(\psi_E - \theta_E)}{1-\mu^2} \\ c &= -\frac{d^2}{1-\mu^2}, \end{aligned}$$

the solution for $\overline{PI}$ is obtained to be $\overline{PI} = \frac{-b\pm\sqrt{b^2-4ac}}{2a}$. Substitution of a, b, and c, into the quadratic formula the distance $\overline{PI}$ can be solved. The positive case is where the pursuer moves forward and captures the evader, while the negative case is where the pursuer moves backward and intersects the Apollonius Circle at a point of no interest. The quadratic equation for the solution of $\overline{PI}$ is the following:

$$\overline{PI} = \frac{\mu d\cos(\psi_E - \theta_E)}{(1-\mu^2)} + d\sqrt{\left(\frac{\mu\cos(\psi_E - \theta_E)}{(1-\mu^2)}\right)^2 + \frac{1}{1-\mu^2}}. \tag{5.50}$$

Dividing eq. (5.50) by the pursuer's speed, v_P, the time-to-go is obtained.

$$t_{\text{go}} = \frac{d}{v_P}\left(\sigma_1 + \sqrt{\sigma_1^2 + \sigma_2}\right),$$

where $\sigma_1 = \mu\cos(\psi_E - \theta_E)/(1-\mu^2)$, $\sigma_2 = 1/(1-\mu^2)$, and d is the distance between P and E. ■

Optimal Control Problem, B - Defender Strategy.

Lemma 4. *The optimal strategy for the defender is a straight-line constant-heading strategy.*

Proof. Evaluating eq. (3.11) using the Hamiltonian, $\mathscr{H}_B$ from eq. (5.38) the costate

dynamics are as follows:

$$\dot{p}^*_{x_P,B} = \dot{p}^*_{y_P,B} = \dot{p}^*_{x_D,B} = \dot{p}^*_{y_D,B} = 0 \tag{5.51}$$

where the "B" subscript notation identifies the corresponding Hamiltonian. Thus, from eqs. (5.39) and (5.51) the costates for each individual optimization problem are constant under optimal play.

Taking the partial in eq. (3.12) using the Hamiltonian in eq. (5.38) with respect to the control of the defender ψ_D, the following is obtained:

$$0 = -p^*_{x_D,B}\alpha \sin\psi^*_D + p^*_{y_D,B}\alpha\cos\psi^*_D. \tag{5.52}$$

Therefore, as derived in Lemma 1, the optimal heading of the defender as a function of the costates from $\mathscr{H}_B$ is in agreement with eq. (5.7) in Section 5.1 and is

$$\psi^*_D = \sin^{-1}\left(\frac{p^*_{y_D,B}}{\sqrt{p^{*2}_{x_D,B} + p^{*2}_{y_D,B}}}\right). \tag{5.53}$$

Since the optimal costates are constant, the heading of the pursuer is constant under optimal play. ■

Evaluating eq. (3.12) using the Hamiltonian, $\mathscr{H}_A$ from eq. (5.37) the optimal control is found to depend solely upon the costates and the parameter μ. Similarly, evaluating eq. (3.12) using the Hamiltonian, $\mathscr{H}_B$ from eq. (5.38) the optimal control is found to depend solely upon the costates and the parameter α. Since the optimal costates are constant, it may be inferred that the optimal control for the defender and the pursuer is also constant; hence, all optimal strategies are straight-line trajectories. Because all optimal strategies for the pursuer and defender are straight-line trajectories, the optimal heading for the pursuer is described using the geometry of

Apollonius, and the optimal strategy for the defender is that of the maximum-time exposure from Section 5.1.

Three scenarios of interest are examined: When $t_{\text{go}} \geq t_{\text{exp}}$, when $t_{\text{go}} < t_{\text{exp}}$, and when $t_{\text{exp}} = 0$.

Time-to-go greater than or equal to exposure time.

The engagement when the time-to-go (t_{go}) is greater than or equal to the maximum possible exposure time (t_{exp}) is shown in Figure 37.

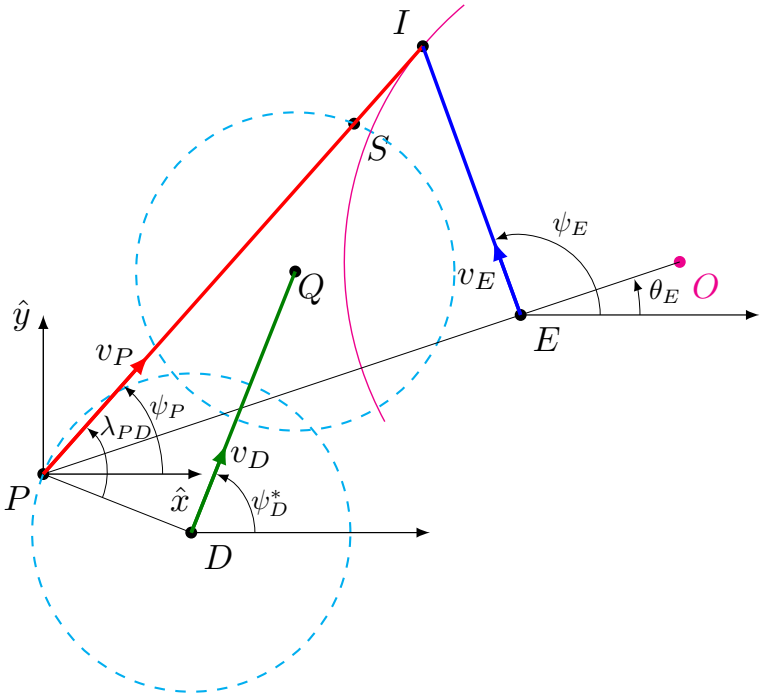

Figure 37. The directed energy defense scenario wherein the maximum possible exposure time is less than the time-to-go.

From Figure 37, the interception point made by the pursuer and evader occurs after the pursuer escapes the WEZ of the defender; this means that the heading taken by the defender is one which maximizes the time that the pursuer is inside the WEZ.

Lemma 5. *Suppose that scenario terminates in P exiting the WEZ prior to capturing*

E, then the optimal heading of the defender is

$$\psi_D^* = \cos^{-1}\left(\frac{(\alpha^2-1)\sin\lambda_{PD}}{\alpha^2+2\alpha\cos\lambda_{PD}+1}\right), \tag{5.54}$$

where α is the speed ratio between the defender and the pursuer and λ_{PD} is the line-of-sight angle (positive counter clockwise) from the pursuer to the defender.

Proof. See Theorem 4 from Section 5.1. ■

Exposure time greater than time-to-go.

Consider the case when the time-to-go is less than the maximum possible exposure time; this case is illustrated in Figure 38. Since the defender's optimal strategy provides the maximum possible exposure of the pursuer, the question which needs to be answered is, "What heading bounds provide an exposure time of at least time-to-go?" Specifically, what headings ψ_{D_1} and ψ_{D_2} provide exactly t_{go} exposure time?

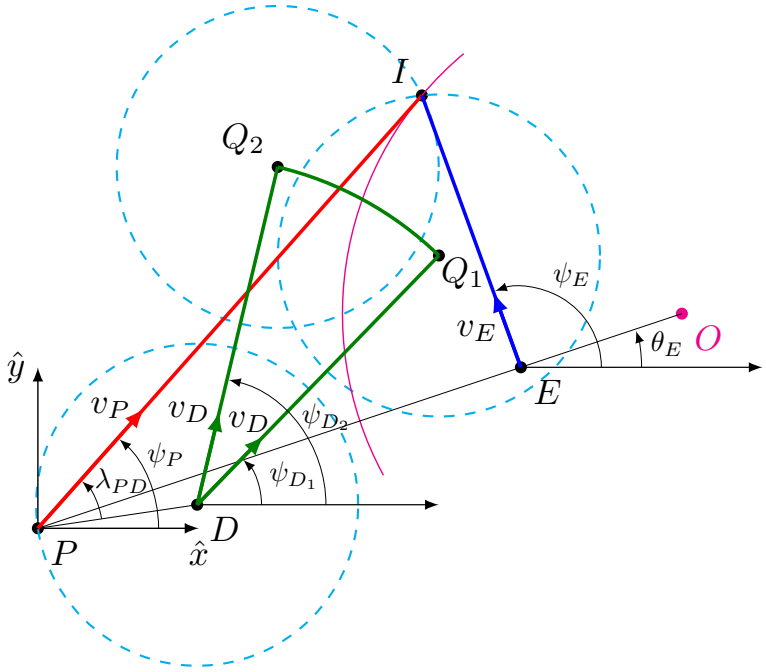

Figure 38. The directed energy defense scenario wherein the maximum possible exposure time is greater than the time-to-go. In this case, suboptimal headings may be used to provide an exposure time equal to the time-to-go.

In order to solve for the defender headings which provide exactly t_{go} exposure time, when the maximum possible exposure provided by the optimal heading from eq. (5.54) is implemented, one begins with locating the interception point with respect to the defender's initial location. Where necessary, the subscript $[D]$ is used to represent a point measured from the defender's initial position, D. For example, the point I with respect to D is $I_{[D]} = (x_{I[D]}, y_{I[D]})$; more explicitly,

$$x_{I[D]} = x_I - x_D, \quad y_{I[D]} = y_I - y_D. \tag{5.55}$$

The location of the defender at time-to-go with respect to D is $Q_{[D]} = (x_{Q[D]}, y_{Q[D]})$. Furthermore, the range between the defender and the pursuer at the time-to-go is R_D, and therefore,

$$R_D^2 = \left(x_{I[D]} - x_{Q[D]}\right)^2 + \left(y_{I[D]} - y_{Q[D]}\right)^2. \tag{5.56}$$

Recognizing that the speed ratio between the defender and the pursuer is α, the distance traversed by the pursuer is $\overline{PI}$ and the distance traversed by the defender is $\alpha\overline{PI}$. Therefore the location of the defender at the time-to-go is

$$Q_{[D]} = \alpha\overline{PI}\cos\psi_D\hat{x} + \alpha\overline{PI}\sin\psi_D\hat{y}. \tag{5.57}$$

In the pursuer Cartesian fixed frame located at P, the location of the defender at the time-to-go is

$$Q = \alpha\overline{PI}\cos\psi_D\hat{x} + \alpha\overline{PI}\sin\psi_D\hat{y} + x_D\hat{x} + y_D\hat{y}. \tag{5.58}$$

Substitution of eq. (5.57) into eq. (5.56), the following is obtained:

$$R_D^2 = \left(x_{I[D]} - \alpha\overline{PI}\cos\psi_D\right)^2 + \left(y_{I[D]} - \alpha\overline{PI}\sin\psi_D\right)^2. \tag{5.59}$$

Expanding eq. (5.59), collecting terms in ψ_D, and moving all terms to the right hand side the following is obtained:

$$0 = -R_D^2 + x_{I[D]}^2 + y_{I[D]}^2 + \alpha^2\overline{PI}^2 - 2\alpha\overline{PI}x_{I[D]}\cos\psi_D - 2\alpha\overline{PI}y_{I[D]}\sin\psi_D. \quad (5.60)$$

Notice that eq. (5.60) has the form $A\cos\psi_D + B\sin\psi_D + C = 0$, where

$$A = -2\alpha\overline{PI}x_{I[D]},\ B = -2\alpha\overline{PI}y_{I[D]},\ C = -R_D + x_{I[D]}^2 + y_{I[D]}^2 + \alpha^2\overline{PI}^2. \quad (5.61)$$

Using the trigonometric half-angle formula, $\sin\psi_D$ and $\cos\psi_D$ may be re-written as a function of $\tan\psi_D$. The identity is repeated here for the reader's convenience.

$$\cos\psi_D = \frac{1-\tan^2(\psi_D/2)}{1+\tan^2(\psi_D/2)}, \quad \sin\psi_D = \frac{2\tan(\psi_D/2)}{1+\tan^2(\psi_D/2)}$$

Let $\tau = \tan(\psi_D/2)$, then eq. (5.60) may be re-written in terms of τ.

$$\begin{aligned} 0 &= A\frac{1-\tau^2}{1+\tau^2} + B\frac{2\tau}{1+\tau^2} + C \\ &= A(1-\tau^2) + 2B\tau + C(1+\tau^2) \\ &= (C-A)\tau^2 + 2B\tau + (A+C). \end{aligned} \quad (5.62)$$

Leveraging the quadratic formula, the value of τ is

$$\begin{aligned} \tau &= \frac{-2B \pm \sqrt{4B^2 - 4(C-A)(A+C)}}{2(C-A)} \\ &= \frac{-B \pm \sqrt{B^2 - C^2 + A^2}}{C-A}. \end{aligned} \quad (5.63)$$

Therefore, because of the quadratic expression, two solutions for ψ_D exist.

$$\begin{aligned}\psi_{D_1} &= 2\tan^{-1}\left(\frac{-B+\sqrt{B^2-C^2+A^2}}{C-A}\right),\\ \psi_{D_2} &= 2\tan^{-1}\left(\frac{-B-\sqrt{B^2-C^2+A^2}}{C-A}\right).\end{aligned} \tag{5.64}$$

Axiom 1. *When the exposure time is greater than the time-to-go, all headings in the closed interval,*

$$\psi_D \in [\psi_{D_1}, \psi_{D_2}], \tag{5.65}$$

provide a final time of time-to-go.

Axiom 2. *The maximum exposure time* (t_{exp}) *as a function of the line-of-sight angle,* λ_{PD}*, the speed of the pursuer,* v_P*, the speed of the defender,* v_D*,and radius of the WEZ,* R_D *is*

$$t_{\text{exp}} = \frac{2R_D(v_D + v_P\cos\lambda_{PD})}{v_P^2 - v_D^2}. \tag{5.66}$$

Axiom 3. *The line-of-sight angle,* λ_{PD}*, takes on angles from* $[-\pi, \pi]$*. The exposure time* (t_{exp}) *is as described in eq.* (5.66)*. For all possible values of* λ_{PD}*, the maximum possible exposure time occurs when* $\lambda_{PD} = 0$*;*

$$\bar{t}_{\text{exp}} = \max_{\lambda_{PD}} \frac{2R_D(v_D + v_P\cos\lambda_{PD})}{v_P^2 - v_D^2} = \frac{2R_D}{v_P - v_D}. \tag{5.67}$$

Axiom 4. *Setting eq.* (5.66) *equal to zero, the line-of-sight angles by which exposure is not possible are in the interval*

$$\lambda_{PD} \in [-\pi, -\cos^{-1}(-\alpha)] \cup [\cos^{-1}(-\alpha), \pi]. \tag{5.68}$$

Axiom 5. *The final time is limited when the evader is captured by the pursuer before the pursuer escapes the defender's WEZ; this occurs when* $\bar{t}_{\text{exp}} > t_{\text{go}}$*. In the event*

that $2R_D/(v_P - v_D) > t_{\text{go}}$ *the line-of-sight angle where* $t_{\text{go}} = t_{\text{exp}}$ *occurs at the angle* $\lambda_{PD,\text{go}}$ *and is as follows:*

$$\lambda_{PD,go}(t) = \cos^{-1}\left(\frac{(v_P^2 - v_D^2)t_{\text{go}} - 2R_D v_D}{2R_D v_P}\right) \tag{5.69}$$

Notice, $\lambda_{PD,\text{go}}$ in eq. (5.69) is found by substituting t_{go} for the exposure time, t_{exp} in eq. (5.66) and then solving for $\lambda_{PD,\text{go}}$.

Solution to the Optimal Control Problem.

From the defender's perspective, the optimal control problem ends when either the pursuer captures the evader or when the pursuer escapes the WEZ of the defender, $\mathscr{C} = \mathscr{C}_A \cup \mathscr{C}_B$. In cases where the line-of-sight angle λ_{PD} is as described in eq. (5.68), the defender terminates immediately, as it is unable to keep the pursuer in the WEZ for any amount of time. From the pursuer's perspective, the optimal control problem ends when it captures the evader, $\mathscr{C}_B$.

Exposure Time.

Theorem 6. *Given the optimal control problem specified by eqs.* (3.65), (3.68) *and* (5.36) *and the line-of-sight angle,* $\lambda_{PD} \in [-\pi, \pi]$*, the optimal final time,* t_f^**, is*

$$t_f^* = \begin{cases} t_{\text{go}} \text{ from } eq.\ (5.46) & \lambda_{PD} \in \Lambda_{\text{go}} \\ t_{\text{exp}} \text{ from } eq.\ (5.66) & \lambda_{PD} \in \Lambda_* \\ 0 & \lambda_{PD} \in \Lambda_0 \end{cases} \tag{5.70}$$

where

$$\Lambda_0 = \left\{ \lambda_{PD} \middle| -\pi \leq \lambda_{PD} \leq -\cos^{-1}(-\alpha) \text{ or } \cos^{-1}(-\alpha) \leq \lambda_{PD} \leq \pi \right\}$$
$$\Lambda_{\text{go}} = \left\{ \lambda_{PD} \middle| \lambda_{PD} \leq \left| \cos^{-1}\left(\frac{(v_P^2 - v_D^2)t_{\text{go}} - 2R_D v_D}{2R_D v_P} \right) \right| \right\}$$
$$\Lambda_* = \left\{ \lambda_{PD} \middle| \lambda_{PD} \in \Lambda_0' \cap \Lambda_{\text{go}}' \right\}.$$

Proof. Three scenarios are possible:

1. P captures E before escaping D's WEZ.

   In the first case, $\lambda_{PD} \in \Lambda_{\text{go}}$ implies that P captures E before escaping D's WEZ. Therefore, from Lemma 3 $t_{\text{go}} < t_{\text{exp}}$. Therefore, $t_f^* = t_{\text{go}}$ by Axiom 5.

2. P captures E after escaping D's WEZ.

   In the second case, $\lambda_{PD} \in \Lambda_*$ implies that P captures E after escaping or lies on the border of D's WEZ. Therefore, from Axiom 2, $t_f^* = t_{\text{exp}}$ from eq. (5.66).

3. D is incapable of exposing P for any amount of time. $\lambda_{PD} \in \Lambda_0$ implies that D is unable to expose P for any amount of time and therefore $t_f^* = 0$ by Axiom 4.

■

Corollary 2. *In the event that* $\bar{t}_{\text{exp}} < t_{\text{go}}$, Λ_{go} *is empty.*

Proof. $\bar{t}_{\text{exp}}$ is the maximum possible time that the pursuer is contained in the WEZ of the defender by Axiom 3. If $\lambda_{PD} \in \Lambda_{\text{go}}$ then by Axiom 2,

$$t_{\text{exp}} = \frac{2R_D(v_D + v_P \cos\lambda_{PD})}{v_P^2 - v_D^2},$$

and by the definition of Λ_{go},

$$t_{\text{exp}} \geq \frac{2R_D}{v_P^2 - v_D^2}\left(v_D + v_P\left(\frac{(v_P^2 - v_D^2)t_{\text{go}} - 2R_D v_D}{2R_D v_P}\right)\right). \tag{5.71}$$

Expanding eq. (5.71),

$$t_{\text{exp}} \geq \frac{2R_D v_D}{v_P^2 - v_D^2} + \frac{2R_D v_P}{v_P^2 - v_D^2}\frac{(v_P^2 - v_D^2)t_{\text{go}}}{2R_D v_P} - \frac{2R_D v_P v_D}{(v_P^2 - v_D^2)v_P}. \tag{5.72}$$

Therefore, $t_{\text{exp}} \geq t_{\text{go}}$. By contradiction, in order for λ_{PD} to be an element of Λ_{go}, t_{exp} must be greater than t_{go}; but, by the assertion, $\bar{t}_{\text{exp}} < t_{\text{go}}$. ■

Defender Strategy.

Theorem 7. *The defender's strategy depends upon the initial locations of the agents as well the problem parameters: α, μ, λ_{PD}, and ψ_E. In the event that the defender in unable to expose the pursuer for any amount of time, e.g. $t_{\text{exp}} = 0$ no matter the heading that ψ_D should take, the defender's strategy is of no consequence. However, for exposure times greater than zero, the defender's choice of heading is*

$$\psi_D^* = \begin{cases} \{\psi_D | \psi_D \in [\psi_{D_1}, \psi_{D_2}]\} & \lambda_{PD} \in \Lambda_{\text{go}} \\ \cos^{-1}\left(\dfrac{(\alpha^2 - 1)\sin\lambda_{PD}}{\alpha^2 + 2\alpha\cos\lambda_{PD} + 1}\right) & \lambda_{PD} \in \Lambda_* \\ \text{undefined} & \lambda_{PD} \in \Lambda_0. \end{cases} \tag{5.73}$$

Proof. Three scenarios are possible

1. P captures E before escaping D's WEZ

   In the first case, $\lambda_{PD} \in \Lambda_{\text{go}}$ implies that P captures E before escaping D's WEZ. Therefore by Axiom 1, $\psi_D^* = \{\psi_D | \psi_D \in [\psi_{D_1}, \psi_{D_2}]\}$.

2. P captures E after escaping D's WEZ

In the second case, $\lambda_{PD} \in \Lambda_*$ implies that P captures E after escaping D's WEZ. Therefore from Lemma 5, $\psi_D^* = \cos^{-1}\left(\frac{(\alpha^2-1)\sin\lambda_{PD}}{\alpha^2+2\alpha\cos\lambda_{PD}+1}\right)$.

3. D is incapable of exposing P for any amount of time.

   $\psi_{DP} \in \Lambda_0$ implies that D is unable to expose P for any amount of time by Axiom 4.

■

Examples.

Consider the directed energy defense scenario with the WEZ radius of 2 distance units (DU), the speed ratio between the evader and the pursuer is $\mu = 0.5$, the speed ratio between the defender and the pursuer is $\alpha = 0.6$, and the speed of the pursuer is $v_P = 1$ DU/TU. The evader takes a heading of 110 deg. To highlight the defender strategy in eq. (5.73), two cases are considered: $\lambda_{PD} = -70$deg and $\lambda_{PD} = -40$deg. Common to the examples, the pursuer is located at the origin, $P = (0, 0)$, and the evader is located at $E = (6, 2)$.

The first step in both examples is to construct the Apollonius Circle and determine the heading of the pursuer as well as the time-to-go. Using eq. (5.45), the optimal pursuer strategy which intercepts the evader in minimum time is found to be 48.4 deg. from East. Using eq. (5.46) the time-to-go is found to be 7.189 TU. The maximum possible exposure time, independent of the bearing of the defender from the pursuer is found using eq. (5.67); $\bar{t}_{\text{exp}} = 10.000$ TU. Also, the sets $\Lambda_0, \Lambda_{\text{exp}}, \Lambda_{\text{go}},$ and Λ_* are found to be:

$$\Lambda_0 = [-180, -126.870]\text{deg} \cup [126.870, 180]\text{deg},$$

$$\Lambda_{\text{go}} = [-56.620, 56.6120]\text{deg},$$

$$\Lambda_* = (-126.870, -56.620]\text{deg} \cup [56.620, 126.870)\text{deg}.$$

Example 1: λ_{PD} = -70 deg.

The first example highlights the case where the exposure time is less than the time-to-go. For this example, consider the defender to be 70 deg starboard from the pursuer's heading and 2 DU from the pursuer – at the onset, the pursuer is inside the defender's WEZ. This example is shown in Figure 39.

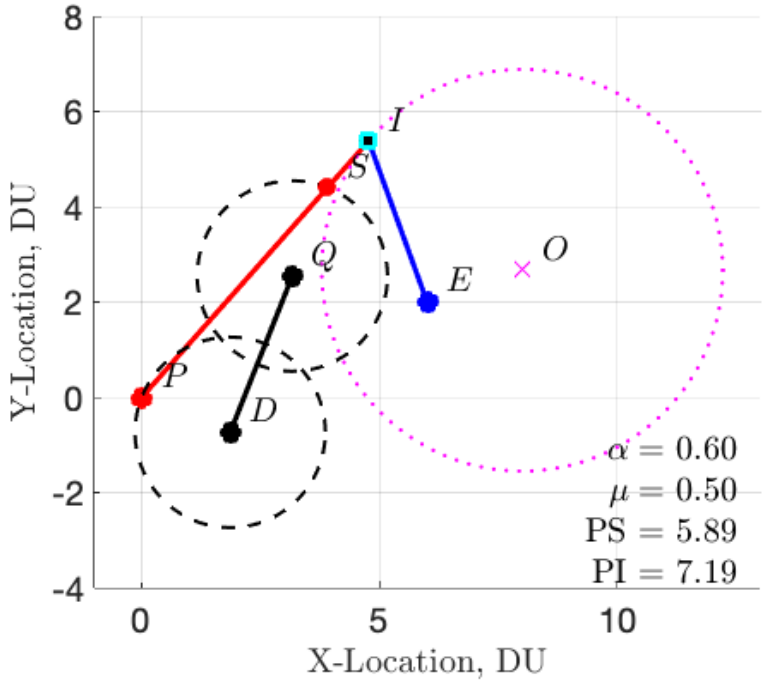

Figure 39. The directed energy defense scenario where the bearing from the pursuer to the defender is 70 deg starboard. The speed ratio between the evader to the pursuer is $\mu = 0.50$ and the speed ratio between the defender and the pursuer is $\alpha = 0.60$.

In Figure 39, the solid red line represents the pursuer's course, the solid black line represents the defender's course, and the solid blue line represents the evader's course. The points P, E, and D represent the initial location of the pursuer, evader, and defender respectively. The points S represent the location of the pursuer when it escapes the defender's WEZ, who is located at the point Q. The point I represents the capture location of the evader by the pursuer which is dictated by the Apollonius Circle centered at the point O.

In this example, the angle $\lambda_{PD} = -70$ deg $\in \Lambda_*$ and the exposure time and optimal heading are found using eqs. (5.70) and (5.73) respectively. $t_{\text{exp}} = 5.888$ TU and $\psi_D^* = 68.281$ deg from East.

From this scenario, the defender heads toward the pursuer in order to maximize the time that the pursuer stays inside the WEZ. If the defender were to deviate from this optimal heading (ψ_D^*), the time that the pursuer is exposed would be less than the calculated 5.888 TU. Since the pursuer does not capture the evader before the defender loses contact with the pursuer, the defender has a unique optimal heading that maximizes the time that the pursuer is inside the WEZ.

Example 2: λ_{PD} = -40 deg.

The second example highlights the case where the exposure time is less than the time-to-go. For this example, consider the defender to be 40 deg starboard from the pursuer's heading and 2 DU from the pursuer. This example is shown in Figure 40.

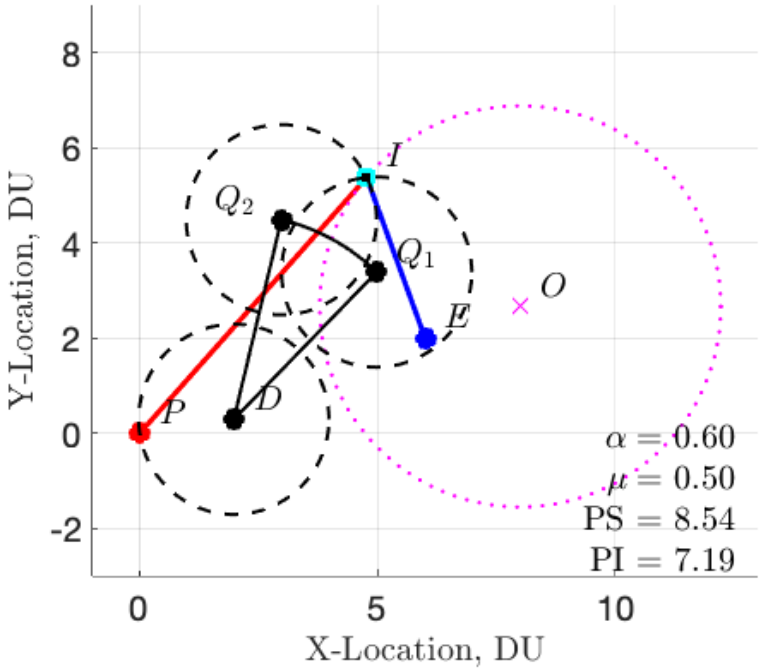

Figure 40. The directed energy defense scenario where the bearing from the pursuer to the defender is 40 deg starboard. The speed ratio between the evader to the pursuer is $\mu = 0.50$ and the speed ratio between the defender and the pursuer is $\alpha = 0.60$.

In Figure 40, the solid red line represents the pursuer's course, the solid black line represents the defender's course, and the solid blue line represents the evader's course. The points P, E, and D represent the initial location of the pursuer, evader, and defender respectively. The point I represents the capture location of the evader by the pursuer which is dictated by the Apollonius Circle centered at the point O. Since the pursuer is inside the defender's WEZ for the entire engagement, there exists an interval of headings which the defender can take which ensure that the pursuer is contained in the WEZ for the entirety of the engagement until the pursuer captures the evader. The limiting headings are shown by the arc between Q_2 and Q_1.

In this example, the angle $\lambda_{PD} = -40$ deg $\in \Lambda_{\text{go}}$ and the exposure time and optimal heading are found using eqs. (5.70) and (5.73) respectively. $t_{\text{exp}} = t_{\text{go}} = 7.189$ TU and using eq. (5.64) the limiting headings $\psi_{D_1} = 45.869$ deg and $\psi_{D_2} = 76.584$ deg

from East. This means, that if the defender takes any heading between 45.869 and 76.584 deg, the pursuer will stay inside the WEZ for the entirety of the engagement.

Next, consider every possible line-of-sight angle from the pursuer to the defender, $\lambda_{PD} \in [-180, 180]$ deg. Assuming that the defender implements the strategy described in eq. (5.73) and the pursuer captures the evader in minimum time using the optimal heading in eq. (5.45), the exposure time as a function of the line-of-sight angle λ_{PD} is shown in Figure 41.

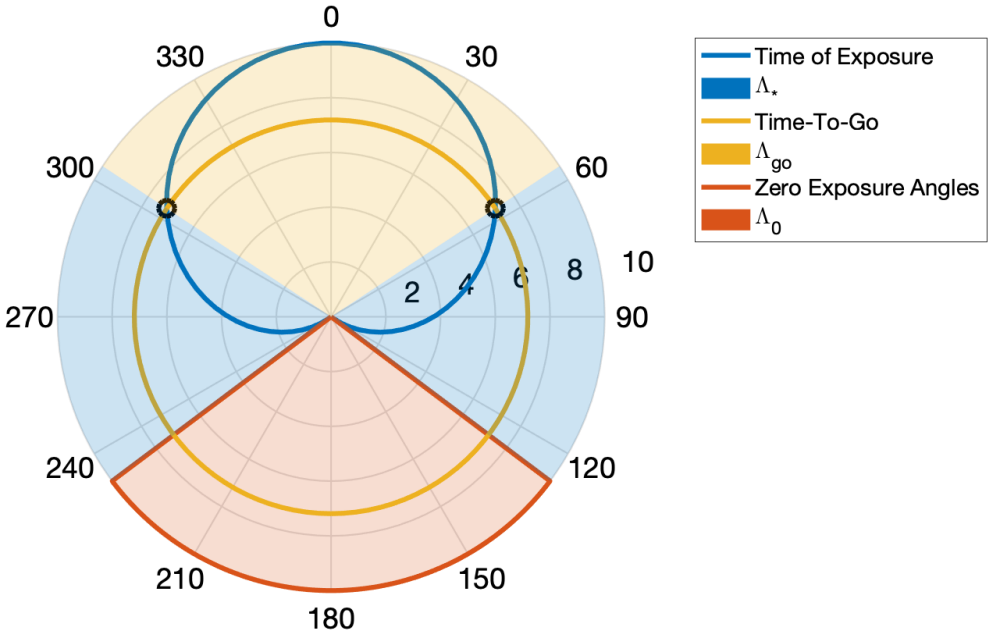

Figure 41. The exposure time as a function of the line-of-sight angle λ_{PD} is depicted in this polar plot when $E = (6, 2)$, $\alpha = 0.6$, and $\mu = 0.50$. This polar plot is a graphical representation of eq. (5.70)

In Figure 41 the blue limacǫn describes the time that the pursuer could remain inside the WEZ of the defender if the evader were not captured by the pursuer. The yellow circle represents the time-to-go – the evader is captured by the pursuer. The red lines describe the line-of-sight headings by which the pursuer is unable to be contained inside the WEZ of the defender regardless of the defender's strategy. The black circles represent the angle and time at which the pursuer is inside the defender's

WEZ for exactly the same time as the time-to-go.

In Figure 42 the strategy of the defender as a function of the line-of-sight angle λ_{PD} is presented.

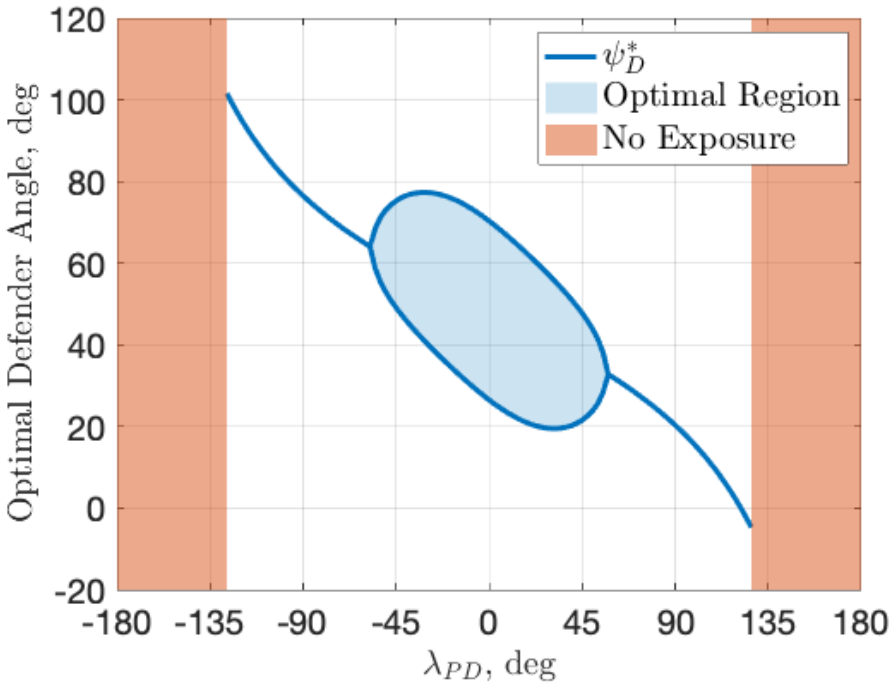

Figure 42. The defender's heading (ψ_D) as a function of the line-of-sight angle λ_{PD} as described in eq. (5.73). The case presented is that of the examples where $E = (6, 2)$, $\alpha = 0.6$, and $\mu = 0.50$.

The red regions in Figure 42 represent line-of-sight angles where the defender is unable to contain the pursuer for any amount of time. The blue line represents the optimal strategy of the defender. The shaded blue region represents the cases where the time-to-go limits the amount of time that the pursuer is contained in the defender's WEZ.

One interesting observation about the shaded blue region in Figure 42 is that the shaded region is widest at $\lambda_{PD} = 0$. This is because the maximum possible exposure time $\bar{t}_{\text{exp}}$ occurs at $\lambda_{PD} = 0$ and because the pursuer captures the evader before it can escape the WEZ of the defender. Also, due to the fact that the amount of time

that the defender can keep the pursuer inside the WEZ decreases as it deviates from the optimal heading ψ_D^*, the amount of deviation when $\lambda_{PD} = 0$ is a maximum; thus, the blue shaded region is the widest when $\lambda_{PD} = 0$.

As expected, the shaded region collapses to a unique heading at the angle $\lambda_{PD,\text{go}}$ $= \pm 56.620$ deg as described in eq. (5.69). This means that for headings $\lambda_{PD} \in \Lambda_*$ the defender's strategy is unique and is ψ_D^* as described in eq. (5.54).

5.3 Maximum Exposure of a Non-Maneuvering Pursuer in 3-D

In Section 5.1 the max-time exposure of a non-maneuvering pursuer was posed and solved. Next, in Section 5.2, the evader was introduced; as a result, special consideration was given to scenarios where the evader was captured before or after escaping the defender's WEZ. In this section, the results of Section 5.1 are extended to 3-D Cartesian space.

It is now well understood that when the pursuer and defender are holonomic (have simple motion) and the evader does not maneuver that the optimal trajectories for the pursuer and defender are straight-line trajectories. For this reason, one may omit the evader when considering the HVAA defense scenario if the pursuer's optimal strategy is a straight-line trajectory. This greatly reduces the number of free variables and directs attention to the defender's optimal strategy which maximally exposes a non-maneuvering, but faster, pursuer.

Optimal Control Problem in 3-D.

A governing assumption in this scenario is that the pursuer is faster than the defender, $v_D < v_P$. Without loss of generality, the speed ratio between the defender and the pursuer is defined as: $\alpha = v_D/v_P$, resulting in $0 < \alpha < 1$. Using normalization, the nonlinear dynamics, $\dot{\mathbf{x}}(t) = f(\mathbf{x}(t), \mathbf{u}(t), t)$, can be represented as function of the

speed ratio, α, rather than their individual speeds as follows:

$$\begin{aligned} \dot{x}_D &= \alpha \cos\gamma_D \cos\psi_D, \quad & \dot{x}_P &= \cos\gamma_P \cos\psi_P, \\ \dot{y}_D &= \alpha \cos\gamma_D \sin\psi_D, \quad & \dot{y}_P &= \cos\gamma_P \sin\psi_P, \\ \dot{z}_D &= \alpha \sin\gamma_D, & \dot{z}_P &= \sin\gamma_P. \end{aligned} \tag{5.74}$$

In this scenario, the Hamiltonian is defined as the inner product of the costates and the dynamics, $\mathscr{H} = \langle \mathbf{p}, f(\mathbf{x}, \mathbf{u}, t) \rangle$. The Hamiltonian can be written more explicitly as follows:

$$\begin{aligned} \mathscr{H} =& p_{x_D} \alpha \cos\gamma_D \cos\psi_D + p_{y_D} \alpha \cos\gamma_D \sin\psi_D + p_{z_D} \alpha \sin\gamma_D \\ &+ p_{x_P} \cos\gamma_P \cos\psi_P + p_{y_P} \cos\gamma_P \sin\psi_P + p_{z_P} \sin\gamma_P, \end{aligned} \tag{5.75}$$

where the costates are $\mathbf{p}^T = [p_{x_D},\ p_{y_D},\ p_{z_D},\ p_{x_P},\ p_{y_P},\ p_{z_P}]$.

Necessary Conditions for Optimality:.

Utilizing the Hamiltonian in eq. (5.75), the necessary conditions for optimality are formulated by taking the partial derivatives in eqs. (3.10) to (3.12). Recall, the superscript, $*$, represents optimally. Evaluating the necessary condition described in eq. (3.12), the following is obtained:

$$\begin{bmatrix} 0 \\ 0 \end{bmatrix} = \begin{bmatrix} -p^*_{x_D} \alpha \cos\gamma^*_D \sin\psi^*_D + p^*_{y_D} \alpha \cos\gamma^*_D \cos\psi^*_D \\ -p^*_{x_D} \alpha \sin\gamma^*_D \cos\psi^*_D - p^*_{y_D} \alpha \sin\gamma^*_D \sin\psi^*_D + p^*_{z_D} \alpha \cos\gamma^*_D \end{bmatrix}. \tag{5.76}$$

Algebraic manipulation of the first term in eq. (5.76) provides a relationship between the optimal heading of the defender and the costates for the defender:

$$0 = -p^*_{x_D} \alpha \cos\gamma^*_D \sin\psi^*_D + p^*_{y_D} \alpha \cos\gamma^*_D \cos\psi^*_D. \tag{5.77}$$

Through algebraic manipulation eq. (5.77) can be simplified to be the following:

$$\cos^2 \psi_D^* = \frac{p_{x_D}^{*2}}{p_{x_D}^{*2} + p_{y_D}^{*2}}. \tag{5.78}$$

Using the trigonometric identity $\sin^2(x) + \cos^2(x) = 1 \ \forall x \in \mathbb{R}$, eq. (5.78) can be written as follows:

$$\sin^2 \psi_D^* = \frac{p_{y_D}^{*2}}{p_{x_D}^{*2} + p_{y_D}^{*2}}. \tag{5.79}$$

The derivation for reaching eqs. (5.78) and (5.79) from eq. (5.77) can be found in Appendix A.1. The following equation:

$$\begin{aligned} 0 &= -p_{x_D}^* \alpha \cos\gamma_D^* \sin\psi_D^* + p_{y_D}^* \alpha \cos\gamma_D^* \cos\psi_D^* \\ &= \cos\gamma_D^* \left(-p_{x_D}^* \sin\psi_D^* + p_{y_D}^* \cos\psi_D^*\right), \end{aligned}$$

implies that either $\cos\gamma_D^* = 0$, or, more generally $\left(-p_{x_D}^* \sin\psi_D^* + p_{y_D}^* \cos\psi_D^*\right) = 0$. The general case can be written as

$$0 = \begin{bmatrix} p_{y_D}^* \\ -p_{x_D}^* \end{bmatrix} \cdot \begin{bmatrix} \sin\psi_D^* \\ \cos\psi_D^* \end{bmatrix},$$

which implies that the two vectors are perpendicular. Therefore, the optimal defender heading angle obeys the following:

$$\cos\psi_D^* = \pm\frac{p_{x_D}}{\sqrt{p_{x_D}^2 + p_{y_D}^2}}, \qquad \sin\psi_D^* = \pm\frac{p_{y_D}}{\sqrt{p_{x_D}^2 + p_{y_D}^2}}, \tag{5.80}$$

wherein the signs of the two expressions are coupled. vSimilarly, through algebraic manipulation of the second term from eq. (5.76), the optimal flight path angle of the defender is found as a function of the optimal costates of the defender. The second

term from eq. (5.76) is repeated here for convenience.

$$0 = -p^*_{x_D}\alpha \sin\gamma^*_D \cos\psi^*_D - p^*_{y_D}\alpha \sin\gamma^*_D \sin\psi^*_D + p^*_{z_D}\alpha \cos\gamma^*_D \tag{5.81}$$

Equation (5.81) can be algebraically manipulated to obtain the following:

$$\cos^2\gamma^*_D = \frac{(p^*_{x_D}\cos\psi^*_D + p^*_{y_D}\sin\psi^*_D)^2}{p^{*2}_{z_D} + (p^*_{x_D}\cos\psi^*_D + p^*_{y_D}\sin\psi^*_D)^2}. \tag{5.82}$$

Further expansion and substitution of eqs. (5.78) and (5.79) into eq. (5.82), the optimal flight path angle as a function of the optimal costates is obtained as follows:

$$\cos^2\gamma^*_D = \frac{p^{*2}_{x_D} + p^{*2}_{y_D}}{p^{*2}_{x_D} + p^{*2}_{y_D} + p^{*2}_{z_D}}. \tag{5.83}$$

The algebraic derivation which starts with eq. (5.81) and results in eq. (5.83) can be found in Appendix A.2. Further evaluation of the necessary conditions for optimality shows that the optimal heading and flight path angle by the defender is constant for the entire engagement. Evaluating the necessary condition in eq. (3.11) one finds the dynamics of the costates by evaluating the following partials:

$$\dot{p}^*_{x_D} = \dot{p}^*_{y_D} = \dot{p}^*_{z_D} = \dot{p}^*_{x_P} = \dot{p}^*_{y_Y} = \dot{p}^*_{z_P} = 0 \tag{5.84}$$

Since the states are not explicit in the Hamiltonian in eq. (5.75), the optimal costates are constant, i.e. $\mathbf{p}^*(t) = \mathbf{p}^*$ because the defender is holonomic. Since the optimal costates are constant, the optimal control is constant. Therefore the resulting optimal trajectory of the defender is a straight-line trajectory. The optimal heading

and flight path angle of the defender as a function of the costates are as follows:

$$\psi_D^*(t) = \psi_D^* = \cos^{-1}\left(\sqrt{\frac{p_{x_D}^{*2}}{p_{x_D}^{*2} + p_{y_D}^{*2}}}\right), \tag{5.85}$$

$$\gamma_D^*(t) = \gamma_D^* = \cos^{-1}\left(\sqrt{\frac{p_{x_D}^{*2} + p_{y_D}^{*2}}{p_{x_D}^{*2} + p_{y_D}^{*2} + p_{z_D}^{*2}}}\right). \tag{5.86}$$

Transversality Conditions.

Next, consider the transversality conditions from eq. (3.14) which are used to formulate the relationship between the states and costates at final time. Recalling eq. (3.14) from Section 5.1 the terminal manifold is different in the 3-D case. The terminal manifold as defined in eq. (3.74) states that the range of the pursuer and the defender is larger than the defender's WEZ at final time. Therefore the terminal manifold m is

$$\begin{aligned} m(\mathbf{x}^*(t_f), t_f) =& (x_D^*(t_f) - x_P^*(t_f))^2 + (y_D^*(t_f) - y_P^*(t_f))^2 \\ &+ (z_D^*(t_f) - z_P^*(t_f))^2 - R_D^2. \end{aligned} \tag{5.87}$$

Substitution of eq. (5.87) into the transversality condition eq. (3.14) and introducing the slack variable δ, the following is obtained:

$$-\mathbf{p}^*(t_f) = \delta \begin{bmatrix} \frac{\partial m}{\partial x_D} & \frac{\partial m}{\partial y_D} & \frac{\partial m}{\partial z_D} & \frac{\partial m}{\partial x_P} & \frac{\partial m}{\partial y_P} & \frac{\partial m}{\partial z_P}. \end{bmatrix}^T \tag{5.88}$$

Taking the partial derivatives, the costates at final time are

$$\begin{aligned} p_{x_D}^* &= \tfrac{\partial m}{\partial x_D} = 2\delta(x_{P_f} - x_{D_f}), \quad p_{x_P}^* = \tfrac{\partial m}{\partial x_P} = 2\delta(x_{D_f} - x_{P_f}), \\ p_{y_D}^* &= \tfrac{\partial m}{\partial y_D} = 2\delta(y_{P_f} - y_{D_f}), \quad p_{y_P}^* = \tfrac{\partial m}{\partial y_P} = 2\delta(y_{D_f} - y_{P_f}), \\ p_{z_D}^* &= \tfrac{\partial m}{\partial z_D} = 2\delta(z_{P_f} - z_{D_f}), \quad p_{z_P}^* = \tfrac{\partial m}{\partial z_P} = 2\delta(z_{D_f} - z_{P_f}). \end{aligned} \tag{5.89}$$

Substitution of the costates from eq. (5.89) into the optimal control from eqs. (5.85) and (5.86), the optimal heading and flight path angle of the defender can be formulated as a function of the final defender and pursuer state as follows:

$$\cos\psi_D^* = \pm\sqrt{\frac{\left(2\delta(x_{P_f}-x_{D_f})\right)^2}{\left(2\delta(x_{P_f}-x_{D_f})\right)^2+\left(2\delta(y_{P_f}-y_{D_f})\right)^2}}, \tag{5.90}$$

$$\sin\psi_D^* = \pm\sqrt{\frac{\left(2\delta\left(y_{P_f}-y_{D_f}\right)\right)^2}{\left(2\delta\left(x_{P_f}-x_{D_f}\right)\right)^2+\left(2\delta\left(y_{P_f}-y_{D_f}\right)\right)^2}}, \tag{5.91}$$

$$\cos\gamma_D^* = \pm\sqrt{\frac{\left(2\delta(x_{P_f}-x_{D_f})\right)^2+\left(2\delta(y_{P_f}-y_{D_f})\right)^2}{\left(2\delta(x_{P_f}-x_{D_f})\right)^2+\left(2\delta(y_{P_f}-y_{D_f})\right)^2+\left(2\delta(z_{P_f}-z_{D_f})\right)^2}}. \tag{5.92}$$

Simplifying eqs. (5.90) to (5.92), one is able to eliminate the slack variable and find the resulting optimal heading and flight path angle at final time as a function of the final defender and pursuer states:

$$\cos\psi_D^* = \pm\frac{(x_{P_f}-x_{D_f})}{\sqrt{(x_{P_f}-x_{D_f})^2+(y_{P_f}-y_{D_f})^2}}, \tag{5.93}$$

$$\sin\psi_D^* = \pm\frac{(y_{P_f}-y_{D_f})}{\sqrt{(x_{P_f}-x_{D_f})^2+(y_{P_f}-y_{D_f})^2}}, \tag{5.94}$$

$$\cos\gamma_D^* = \pm\frac{\sqrt{(x_{P_f}-x_{D_f})^2+(y_{P_f}-y_{D_f})^2}}{R_D}. \tag{5.95}$$

From eqs. (5.93) to (5.95) the angle from the defender to the pursuer at final time is either the same as the optimal heading or anti-parallel. The latter case is clearly suboptimal since the defender would be aimed directly away from the pursuer at final time. Thus, the sign ambiguity in eqs. (5.93) to (5.95) may be eliminated. An illustration of the optimal engagement is shown in Figure 43.

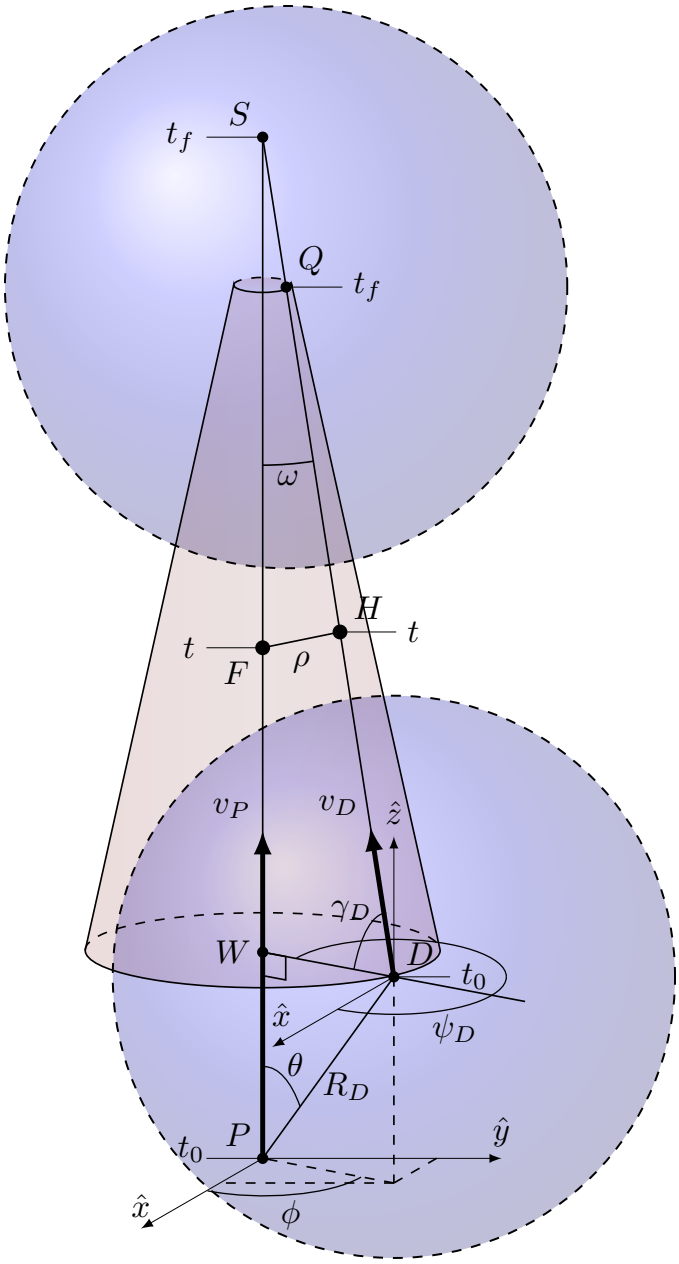

Figure 43. The max-time exposure of a faster pursuer by a slower defender in 3-D Cartesian space.

Solution to the Optimal Control Problem.

The optimal heading and flight path angle of the defender which maximizes the exposure time of a non-maneuverable pursuer may be analytically obtained, provided the pursuer's heading, flight path angle, and speed are given. Without loss of general-

ity, the defender-pursuer scenario is rotated about the pursuer such that the pursuer velocity is aligned with the vertical axis as shown in Figure 43.

Optimal Defender Heading.

Because the headings of both agents are constant, the plane formed by the points P, D, and S is invariant – it remains perpendicular to the (x, y)-plane. From eq. (5.93), the optimal defender heading is aimed directly towards the (x, y) projection of the pursuer. Thus the optimal heading of the defender which maximizes exposure time is:

$$\psi_D^* = \phi + \pi, \tag{5.96}$$

where ϕ is the (constant) azimuth of the defender with respect to the pursuer.

Optimal Defender Flight Path Angle.

A drawing of the two-agent max-time exposure scenario is shown in Figure 43. Consider $\triangle DSP$; using the law of cosines the following equation describes the relationship between the range between the defender to pursuer at final time ($\overline{DS}$), the path by which the pursuer is exposed ($\overline{PS}$), the WEZ (R_D), and the pursuer-defender angle (θ) when contact is first made,

$$\overline{DS}^2 = \overline{PS}^2 + R_D^2 - 2R_D\overline{PS}\cos(\theta). \tag{5.97}$$

Using the speed ratio between the defender and the pursuer the distance traversed by the defender over the engagement is proportional to the distance traversed by the pursuer: $\overline{DQ} = \alpha\overline{PS}$, and therefore:

$$\overline{DS} = \alpha\overline{PS} + R_D. \tag{5.98}$$

Substitution of eq. (5.98) into eq. (5.97), the following is obtained:

$$\left(\alpha\overline{PS} + R_D\right)^2 = \overline{PS}^2 + R_D^2 - 2R_D\overline{PS}\cos\theta. \tag{5.99}$$

Through algebraic manipulation, eq. (5.99) may be solved for $\overline{PS}$. The derivation is shown in Appendix A.3. The resulting solution for $\overline{PS}$ is

$$\overline{PS} = \frac{2R_D(\alpha + \cos\theta)}{1 - \alpha^2}. \tag{5.100}$$

Next, the optimal path angle is solved using triangle $\triangle DWS$. Recognizing that the Cosine of an angle in a right triangle is equal to the adjacent leg over the hypotenuse:

$$\cos\gamma_D^* = \frac{R_D\sin\theta}{\overline{DS}}. \tag{5.101}$$

Substitution of eqs. (5.98) and (5.100) into eq. (5.101), the optimal flight path is derived and shown in Appendix A.4. The resulting optimal flight path angle is as follows:

$$\gamma_D^* = \cos^{-1}\left(\frac{(1-\alpha^2)\sin\theta}{\alpha^2 + 2\alpha\cos\theta + 1}\right). \tag{5.102}$$

Special Case: $\theta \equiv 0$**.**

When the angle from the pursuer to the defender, $\theta \equiv 0$, the defender is directly in front of the path of travel of the pursuer. Substitution of $\theta \equiv 0$ in eq. (5.102), the optimal flight path angle,$\gamma_D^* = \pi/2$, as expected.

Exposure Invariance.

It is important to show that once the pursuer is inside the defender's WEZ of radius R_D) that the pursuer remains within the WEZ until the termination set is

reached. Figure 43 shows the geometry for the optimal two-agent scenario. To prove that the pursuer stays within the defender's WEZ, define the two-norm range between the defender and pursuer:

$$\rho(t) = \sqrt{(x_D(t) - x_P(t))^2 + (y_D(t) - y_P(t))^2 + (z_D(t) - z_P(t))^2} \quad \forall\, t \in (t_0, t_f).$$

Utilizing the Law of Cosines to analyze $\triangle DSP$, the following relationship is obtained:

$$\overline{DP}^2 = \overline{PS}^2 + (\overline{DQ} + \overline{QS})^2 - 2\overline{PS}(\overline{DQ} + \overline{QS}) \cos\omega. \tag{5.103}$$

Notice that eq. (5.103) is identical to eq. (5.23). Therefore, by Theorem 5, it follows that exposure is invariant in 3-D.

Exposure Manifold.

The function which describes the pursuer distance while being exposed is found in eq. (5.100). The pursuer distance while being exposed is a function of the pursuer-defender angle, θ, the radius of exposure, R_D, and the speed ratio, α. Using $\overline{PS}$ in eq. (5.100), the exposure time is found by dividing $\overline{PS}$ by the pursuer's speed. The polar equation for exposure time is therefore,

$$t_f = \frac{2R_D(\alpha + \cos\theta)}{v_P(1 - \alpha^2)} = \frac{2R_D(v_D + v_P\cos\theta)}{v_P^2 - v_D^2}. \tag{5.104}$$

Plotting the time of exposure as a function of the pursuer-defender angle, θ, produces a limaçon whose cusp is located at the pursuer location. Note that the boundary for zero-time of exposure solutions exist when $t_f = 0$. From eq. (5.104), values of θ which result in non-positive values of t_f represent angles for which the exposure time is zero. Thus, setting the length $t_f \leq 0$ in eq. (5.104), one obtains the

conditions for zero time of exposure:

$$\frac{2R_D(v_D + v_P\cos\theta)}{v_P^2 - v_D^2} \leq 0. \tag{5.105}$$

From eq. (5.105), the regions wherein the defender is unable to expose the pursuer occur when the angle θ lies in the following range:

$$\theta_{\text{ZET}} \in \left[-\pi,\ -\cos^{-1}(-\alpha)\right] \cup \left[\cos^{-1}(-\alpha), \pi\right]. \tag{5.106}$$

Assuming the defender implements the optimal heading which maximizes exposure time of the faster pursuer, eq. (5.100) can be algebraically manipulated to provide the defender-pursuer angles which guarantee a desired exposure time. The following is the equation which describes the pursuer-defender angle, θ, which guarantees the desired exposure time, t_{exp}:

$$\theta(t_{\text{exp}}) = \cos^{-1}\left(\frac{(v_P^2 - v_D^2)t_{\text{exp}} - 2R_D v_D}{2R_D v_P}\right). \tag{5.107}$$

It should be noted that the guarantees for exposure time are bounded by

$$t_{\text{exp}} \in \left[0,\ \frac{2R_D}{v_P - v_D}\right]. \tag{5.108}$$

Example.

An illustration of the maximum exposure of a slower pursuer in 3-D is presented in this section. In this example, the defender is endowed with an WEZ of $R_D = 2$. The defender is half as fast as the pursuer and as a result, the speed ratio is $\alpha = 0.5$. Consider the pursuer vehicle to be moving with a flight path angle of $\pi/2$ rad, a heading of 0 rad, and a speed of 1 DU/TU. Define the azimuth to be $\pi/3$ rad and the

pursuer-defender angle, θ, to be $\pi/6$ rad. From eq. (5.102), the optimal flight path angle is calculated to be ≈ 1.393 rad. The heading is selected to point toward the pursuer, and therefore is $4\pi/3$ rad. Using the optimal flight path angle and heading, Figure 44 shows the maximum exposure time scenario in 3-D.

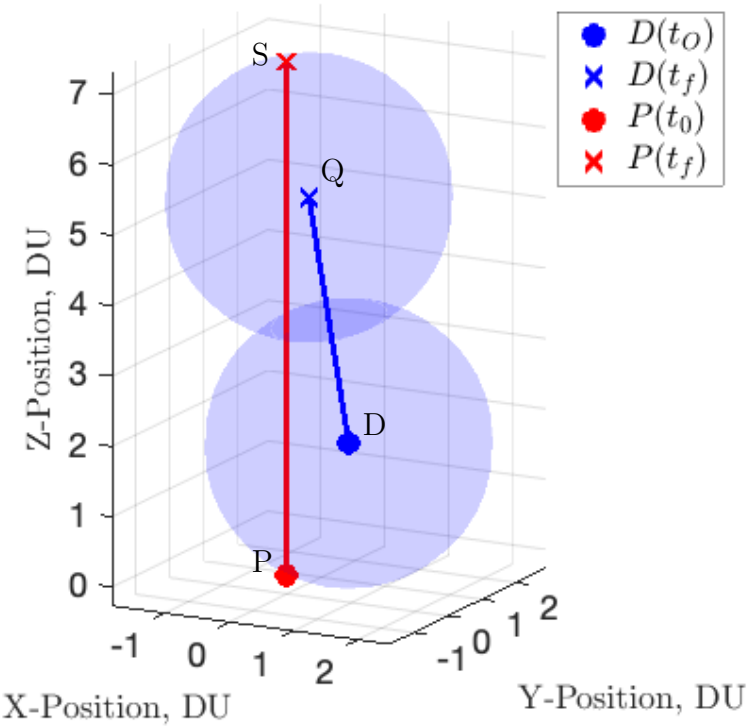

Figure 44. The maximum-time exposure of a faster pursuer by a slower defender in 3-D Cartesian Space

In Figure 44, the defender's path is represented by the blue line, the WEZ is represented by the shaded blue sphere, and the faster pursuer's path is represented by the red line. The initial locations are the filled-in circles and the final time locations of both agents are represented by crosses.

In order to ensure exposure of the pursuer by the defender, the instantaneous range between the two-agents would need to be less than or equal to the WEZ, R_D. In Figure 45 the instantaneous range between the defender and the pursuer is found to be contained in the defender's WEZ for the entire engagement.

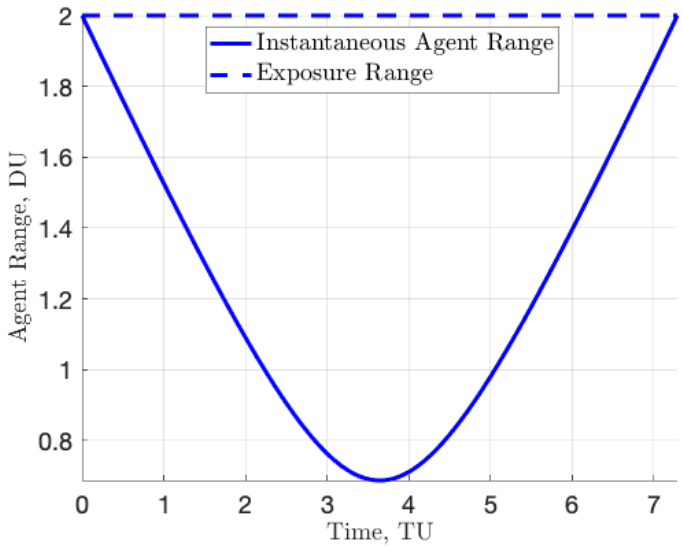

Figure 45. The instantaneous range is inside the exposure region for the entirety of the scenario.

For various angles, θ, the possible exposure time, when the defender implements the optimal strategy, is presented in Figure 46. The figure is shown in both polar and Cartesian form for the sake of presenting the angular and time information easier. Note that exposure time is independent of azimuth since ϕ does not appear in eq. (5.104) and therefore only plots for various elevation angles are presented.

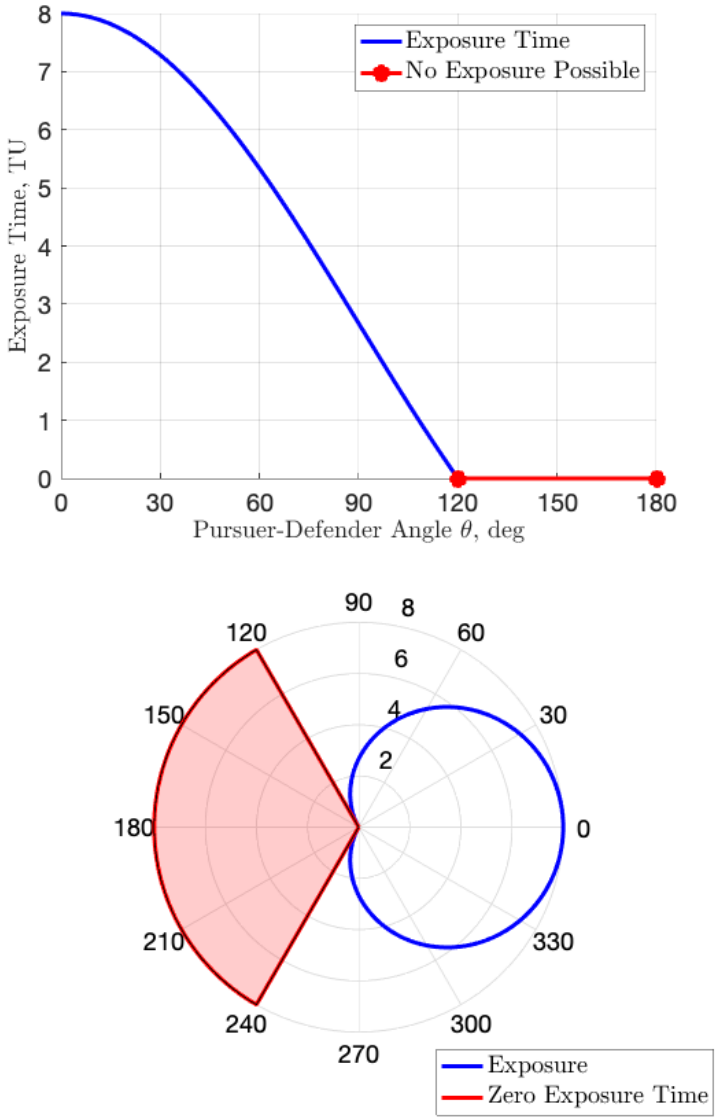

Figure 46. The relationship of the exposure time as a function of the relative elevation angle, θ, shown in both Cartesian and Polar plots

In Figure 46, the red lines represent zero-time of exposure while blue lines represent positive non-zero time of exposure. By plotting the exposure time for all possible angles, θ, the maximum exposure occurs when the pursuer and defender move co-linear with one another ($\theta = 0$) as expected. From Figure 46, one may observe the zero-exposure time angles as well as the exposure time limaçon. For the example, the zero-exposure time angle is found by computing eq. (5.106). In the example, the zero

time of exposure occurs between $\theta_{\text{ZET}} \in [-\pi, -2\pi/3] \cup [2\pi/3, \pi]$ rad.

5.4 Concluding Remarks

In this section, a defender endowed with a circular WEZ aims at maximally exposing a faster non-maneuvering pursuer. Using the calculus of variations/optimal control theory, the heading for the defender which keeps the pursuer inside the defender's WEZ for as long as possible is posed and solved. It is found that for a non-maneuvering pursuer, the optimal heading for the defender is constant under optimal play. Further, the optimal heading is only dependent upon the line-of-sight angle from the pursuer to the defender at initial time, the radius of the WEZ, and the speed ratio of the defender to the pursuer. Also proven, in this section, is the fact that exposure is invariant under optimal play, e.g. the defender-pursuer range is less than the radius of the WEZ for the entire engagement. Finally, the exposure time as a function of he initial line-of-sight angle from the pursuer to the defender is investigated. An example illustrates the exposure time as a function of the defender-pursuer line-of-sight angle; the limaçon describing the exposure time of the pursuer is shown.

In conclusion, the directed energy defense of a non-maneuvering evader against an incoming threat has been presented. Making use of the calculus of variations two optimization problems are posed and solved in tandem; first, the min-time capture of a non-maneuverable evader and then the max-time exposure of the pursuer by a defender with a circular engagement zone. From the costates, the optimal trajectories of the pursuer and the defender were shown to be straight-line trajectories. Leveraging the optimal defender strategy from Section 5.1 the optimal defender strategy and exposure time is found in closed-form.

In order to demonstrate the various intricacies surrounding the target defense

scenario, two examples are presented. The first example demonstrates the defender's optimal strategy when the pursuer captures the evader after escaping the defender's WEZ and the second demonstrates the defender's optimal strategy when the pursuer captures the evader before it can escape the defender's WEZ. Also presented are conditions for which the line-of-sight angle limits the time of exposure – the exposure time is zero, independent of the defender's chosen strategy or limited by the time-to-go.

In conclusion, using a spherical WEZ centered at the defender and commanding the instantaneous heading and flight path angle of the defender, the time by which the pursuer remains inside the WEZ has been maximized. Using the calculus of variations and optimal control theory the optimal instantaneous heading and flight path angle of the defender required to maximize the exposure of a faster non-maneuvering pursuer has been posed and solved. First, the optimal heading and flight path angle of the defender is shown to be constant. Next, the exposure time is shown to be independent of initial azimuth angle and dependent upon the relative elevation angle, WEZ, and speed ratio. Using the relations for exposure time, the regions where exposure is not possible are described. Finally, an example that highlights the maximum exposure of a non-maneuvering faster pursuer by a slower defender is presented. The figures presented in the example illustrate the optimal defender strategies which keep a pursuer inside a spherical WEZ as it relates to the HVAA defense problem of a non-maneuvering evader in 3-D.

VI. Conclusions

> When pursuing a PhD, routinely ask yourself,"Is this necessary [to graduate]?" If not, then ignore it; if so, then get to work.
> — David B. Doman

6.1 Summary of Remarks

In this dissertation, an investigation into the optimal means of defending a high value airborne asset was undertaken. First, in Chapter I, the HVAA defense scenario was motivated and described. In Chapter II a general survey of pursuit-evasion differential games involving multiple pursuers and evaders was conducted. As part of the survey, an in-depth survey of pursuit-evasion differential games as they relate to HVAA defense was performed. Special attention to work related to the kinetic and directed energy defense was highlighted along with the research gaps that this dissertation addressed. Chapter III provides a cursory overview of both differential game theory and optimal control theory. Also described in Chapter III are the various mathematical models and techniques which are leveraged to pose and solve the vagarious HVAA defense scenarios. Additionally, various kinetic and directed energy defense scenarios in the scope of the research were defined – the equations of motion as well as the metrics for optimization are presented for each scenario discussed in this dissertation.

The research contributions of Chapter IV focus on the kinetic defense of a HVAA against an incoming threat. Concerning kinetic defense, three different scenarios were posed and solved. Two scenarios involved the optimal pursuer-defender strategies when the HVAA was non-maneuvering: one in 2-D and another in 3-D. Leveraging Apollonius Circle geometry, the differential game between the pursuer and defender

was reformulated into a single-agent minimization problem. The results of the solved differential games showed that any deviation from the derived optimal strategies resulted in better performance for the adversary. The third scenario investigated a maneuvering HVAA in the 2-D Cartesian plane and assumed the PN control law for the defender and the pursuer. The tactical conclusion, in brief, was that a maneuvering HVAA should generally turn toward the defender in order to aid in the HVAA's own defense. Lastly, a comparative study for finding the optimal control for a turn-rate limited HVAA was conducted. The following four direct methods were investigated: Single Shooting Method, Multiple Shootings Method, Even Collocation Method, and Pseudospectral Method. In the investigation, special attention was given to the computational time, number of algorithmic iterations, number of cost-functional evaluations, ultimate functional evaluation, and the feasibility of solutions. The Even Collocation Method outperformed the convergence times of the other direct methods. One reason the Even Collocation Method outperformed the other methods was that an ODE solver was not used; rather, the dynamics were upheld using equality constraints. Although the Pseudospectral Method also makes use of the equality constraints to uphold the dynamics, it requires adaptive meshing in order to handle bang-bang phenomenon; as a result, the Even Collocation Method outperformed the Pseudospectral Method. Although the dynamics from the first-order Euler approximation used in the Even Collocation Method were not as accurate as the Gaussian quadrature methods used in the Pseudospectral Method, the solution was of acceptable fidelity and was provided much faster. The Even Collocation Method is, therefore, more appropriate for real-world applications.

Next, in Chapter V the HVAA defense scenario was posed and solved for a defender which uses directed energy as a defense mechanism. Because energy weapons deal damage over time rather than at a single time instant, the objective for the defender

was to keep the pursuer inside its WEZ for as long as possible. This amounted to solving for the maximum-time exposure defense. Using the calculus of variations, the flight vector for the defender which maximally exposes the superior pursuer was posed and solved in both 2-D and 3-D Cartesian space. Using the optimal flight vector for the defender, guarantees for exposure time were presented as well as the initial conditions for which the defender is unable to expose the pursuer for any amount of time. The exposure invariance was also proven, showing that the optimal defender strategy provided continuous exposure for the entire engagement. Numerical simulations were presented which confirm the analysis throughout the chapter. Also presented was the directed energy defense of a HVAA wherein a pursuer captures the HVAA in minimum time while the defender aims to maximally expose the pursuer. In the analysis of the three-agent scenario, two cases were shown to exist: the HVAA being captured before the defender loses contact with the pursuer and the HVAA begin captured after the defender loses contact with the pursuer. In the former, there exists a region of headings that the defender could take which provide an exposure time equal to that of the time-to-go (time until the HVAA is captured). Finally, the strategies of the defender, based upon the initial engagement geometry, were illustrated with examples.

6.2 Research Questions Answered

In section 1.3, the research tasks and scope of work were defined. The Hypothesis of this work was that *The successful defense of a High Value Airborne Asset may be solved utilizing differential game theory as well as optimal control theory.* Below are the original research questions and answers for each of them.

Research Question 1: *How may meaningful mathematical models be generated for HVAA defense scenarios?*

Using the kinematic models described in eqs. (3.1) to (3.4), aircraft models which neglect aircraft mass, wind disturbances, a spherical earth, and many other physical phenomenon are formed. Each of the models and their governing assumptions are discussed in section 3.2. Using these low-fidelity kinematic models, attention is driven as to the navigation and tactics of aircraft. As a result of using these low-fidelity models, the state spaces are thus reduced. The models allow for aerial engagements to be posed and solved analytically; as a result, conclusions about the actions taken by the pursuer, evader, and defender may be drawn for the purpose of HVAA defense.

Research Question 2: *How may HVAA defense scenarios be posed and solved as either optimization problems or differential games?*

In order for one to pose HVAA defense scenarios as either an optimal control problem or a differential game, one begins with the objective of each of the players/agents. Using the vehicle states, their control inputs, and time, the goals/aims of each of the agents is represented as either a function or functional. Using an objective cost or value function, as described in eqs. (3.5) and (3.30), subject to equations of motion, as described in eqs. (3.6) and (3.28), and boundary conditions or path constraints, as described in eq. (3.8) eq. (3.7) respectively, an optimization problem is formed.

Once the optimal control problem or differential game is posed. The question becomes, *How does one solve an optimal control problem or differential game?* Two approaches for solving optimal control problems include the *indirect method* and the *direct method* as described in Section 3.3. However, for solving differential games, the indirect approach is most common. In this research, differential games, where the solution is a minimax, are transformed into optimal control problems, where the solution is found from pure minimization or maximization. This transformation is made possible by leveraging the geometry of Apollonius.

The optimal control problem or differential game which develops as a result of

the individual HVAA defense scenarios are setup in Section 3.4. For each scenario, the objective cost or value function is defined (depending upon if the scenario is an optimal control problem or differential game). The solutions for these scenarios are contained within Chapters IV and V. In Sections 4.1 and 4.2, the differential games are transformed into optimal control problems – the defender's optimal strategy is formed from the geometry of Apollonius and the pursuer's strategy is obtained through minimization of the terminal pursuer-evader range at final time. In Sections 4.3 and 4.4 the optimal control for the HVAA to out-maneuver its pursuer and aid its defender is solved using the direct method. In Sections 5.1 to 5.3 the indirect method is leveraged to solve for the optimal strategies of the pursuer and defender.

Research Question 3: *How may HVAA defense differential games be transformed into optimal control problems which may be solved either analytically or numerically?*

Using Apollonius Circle, the optimal strategy for a faster pursuer to capture a slower non-maneuvering evader is found. In Section 3.3, the construction of Apollonius Circle is described. In Sections 4.1 and 4.2 the differential game which develops between the pursuer and the defender is transformed from a differential game to an optimal control problem. This transformation is performed as follows: The optimal strategies for the pursuer and defender are shown to be straight-line trajectories by evaluating the necessary conditions for optimality as described by eqs. (3.33) to (3.36). In general, for agents with simple motion, as described by eqs. (3.2) and (3.4), the partial of the Hamiltonian with respect to the costates is zero. This means, that the costates for each of the agents are constant throughout the trajectory. Also, using the partial of the Hamiltonian with respect to the control for each of the agents, the optimal control for both each player is found to depend solely upon the costates (which are known to be constant). This means that optimal trajectories for each of

the players are straight-line trajectories. Under this assumption, (optimal trajectories are straight-line trajectories trajectories) Apollonius Circle geometry describes the locus of possible interceptions of a faster agent against a slower one. This means, that if the pursuer's strategy is known by the defender and the defender is faster than the pursuer, then its course is known and dictated by Apollonius Circle geometry and the interception point is dictated based upon the course of the pursuer. All that is left is to find the course of the pursuer which minimizes the range of the interception point to the evader at the time that that interception is made. This range is determined to be the objective cost to be minimized subject to the pursuer's chosen course. The result is a transformation of a differential game involving two players to a minimization of one player's strategy – the solution of which determines the saddle point strategy and the solution to the differential game.

Research Question 4: *In the event that a HVAA can't maneuver, what are the optimal strategies of both the defender and the pursuer in the three-agent problem?*

In the event that a HAVAA can't maneuver, the optimal strategies for the pursuer are dictated upon the mechanism by which the defender uses. In Chapter IV the defense mechanism is kinetic – the defender aims to capture the pursuer. In Chapter V the defense mechanism is energy-based – the defender aims to expose the pursuer continuously for as long as possible.

In the event that the defense mechanism is kinetic, the optimal strategy for the pursuer and defender are coupled. In 2-D, the saddle point strategy for the defender and the pursuer is found in defined by the location of the intersection point in Theorem 2. Consequently, the optimal headings for the defender and pursuer are described in eqs. (4.32) and (4.33), respectively. In 3-D, the intersection point for the defender and pursuer is found through the minimization described by eq. (4.67), the resulting intersection point is defined by eq. (4.56). Once the intersection point is known,

amount of distance the pursuer traverses is given by eq. (4.59). As a result, the optimal strategy for the pursuer is described by eqs. (4.60) and (4.61) and the optimal strategy for the defender is described by eqs. (4.65) and (4.66).

In the event that the defense mechanism is energy-based, the optimal strategy for the pursuer is assumed to be of min-time capture of the evader as dictated by Apollonius Circle; this choice of heading is found in eq. (5.45). The optimal strategy of the defender is one of maximum exposure of the faster pursuer; the optimal strategy is found in eq. (5.22) when considering 2-D engagements and in eqs. (5.96) and (5.102) when considering 3-D engagements.

Research Question 5: *How should the HVAA aid in its own defense if it is able to maneuver?*

In the event that a fast pursuer engages a slower maneuverable HVAA which is teamed with a defender which is similar (in capability) to the pursuer, the HVAA should maneuver so as to minimize the defender-pursuer separation rate and maximize the pursuer-evader separation rate as defined in eq. (3.45). Using optimal control theory, the optimal evader strategy is found to depend upon the costate which corresponds to the evader's heading. The optimal control is presented in eq. (4.94). At first, this optimal control problem appears to be tractable in closed form; however, when the costates which correspond to the evader's heading are zero, the problem becomes singular and therefore direct methods are necessary to find the optimal control which maximizes the objective cost in eq. (3.45). Using an NLP, the optimal strategy for the evader is to turn toward its defender in order to "drag" the pursuer toward the defender. To separate itself from the pursuer (when captured by the defender), the evader turns away from the defender and the pursuer at a time dictated by the NLP. An example of this behavior is shown in Figure 29.

Research Question 6: *What unique aspects occur when the defender is a missile*

or directed energy weapon, and what are the critical parameters for the defender to be successful?

The unique aspects which occur when the defender is a missile are investigated in Chapter IV. When the defender is modeled as a missile, the defense mechanism is kinetic in nature – damage to the pursuer is dealt through capture. It is the aim of the defender-evader team to have the defender capture the pursuer as far from the evader at the time of capture. In this work, cases where the defender is successful are only considered; therefore, the pursuer strives to be intercepted as close to the evader as possible. These problems are solved using Apollonius Circle geometry when the evader is non-maneuvering (Sections 4.1 and 4.2) and an NLP when the evader is turn-rate limited (Sections 4.3 and 4.4).

The critical parameters for the defender to be successful include the vehicle speeds, initial state, and the control limits (if applicable) of each agent. The vehicle speeds dictate the speed ratios which are used to simplify the equations of motion for each of the posed scenarios. The initial conditions must be in the escape set – defense is successful. The control limits for the turn-rate of the evader dictate how the evader can maneuver to escape the pursuer and aid the defender in its own defense.

The unique aspects which occur when the defender is a directed energy weapon are investigated in Chapter V. When the defender is modeled as a directed energy weapon, the defender strives to keep the incoming threat inside its weapon engagement zone for as long as possible – damage to the pursuer is dealt over time. It is the aim of the pursuer to capture the evader in minimum time and for the defender to contain the pursuer inside its WEZ for as long as possible. The optimal strategies for the defender are solved using the indirect method of optimal control theory (Sections 5.1 to 5.3).

The critical parameters for the defender to be successful include the relative vehicle

speeds, initial state of the agents, and WEZ radius of the defender. The relative vehicle speeds dictate the amount of time that the pursuer is contained inside the WEZ of the defender as well as the optimal defender heading. The initial state of the agents are used to determine if exposure of the pursuer is even possible and if so, for how long the pursuer could be exposed. The WEZ radius is critical, as it appears in the equation for the optimal heading that the defender should take to keep the pursuer inside its WEZ for as long as possible.

Research Question 7: *What numeric methods are suitable for aerospace hardware systems which require fixed time steps and minimal computational effort?*

In general, it is important to reduce the computational effort to compute a solution. For this reason, closed form solutions are desired in the aerospace community. Closed form solutions may be computed quickly and efficiently when compared to running a nonlinear program solver. When closed form solutions aren't possible, numeric solutions which require few evaluations are desired, this could be a table look up, or a selection between multiple candidate solutions. Less desired are solutions which require the use of an NLP solver. Modern techniques for solving NLPs in conjunction with more capable hardware have made it possible to solve NLPs in real time onboard aerospace platforms. Least desired of all possible approaches are algorithms which require brute force search over an entire state space. These generally require large amounts of memory and the computational effort, in some cases, can cause a problem to be unsolvable.

In Section 4.1, eight candidate solutions for the optimal defense are found in closed form when solving the roots of the polynomial in eq. (4.10). These candidates are then evaluated, one at a time, to find the optimal interception point and consequently, the optimal saddle-point strategies for the defender and the pursuer.

In Section 4.2, a Quasi-Newton gradient search is performed to solve the optimiza-

tion problem defined in eq. (4.67). This search provides an approximate location of the interception point and consequently, approximate optimal saddle-point strategies for the defender and the pursuer.

In Sections 4.3 and 4.4 NLPs are used to pose the kinetic defense of a maneuvering HVAA in 2-D where the pursuer and defender are assumed to be guided by the proportional navigation guidance law and the HVAA maneuvers to escape capture of the pursuer while assisting the defender in capturing the pursuer. In Section 4.4, four direct methods for solving the optimal control problem are compared. The four methods compared were the Single Shooting Method, Multiple Shootings Method, Even Collocation Method, and Pseudospectral Method. Assuming a fixed mesh, the Even Collocation Method outperformed the convergence time of the other direct methods. Since the dynamics are approximated using low-order methods, and the use of ODE solvers is no longer required, the solution converges very fast. However, the use of ODE solvers to forward propagate the dynamics makes shooting methods more accurate. In a real-world scenario, where the evader is a piloted aircraft, fast solutions of low fidelity are more valuable than late solutions of high-fidelity. For this reason, the Even Collocation Method outperforms the other direct methods and is more appropriate for real-time applications.

In Chapter V the optimal strategies for the defender are obtained in closed-form using the indirect method of optimal control theory. The optimal defender strategies are straight-line trajectories and therefore implementation in aerospace systems is feasible.

6.3 Publications and Presentations

Papers and presentation which have been produced as a result of this body of work are listed in Appendix C.

6.4 Contributions

This research improves beyond visual range analysis for the defense of HVAAs through mathematical analysis and simulation. Specifically, the contributions address the expectations in Section 1.5 and are the following:

1. Numeric and analytic solutions to HVAA defense optimal control problems and differential games

2. Optimal strategies for providing successful defense of a HVAA using either a kinetic or directed energy defense weapon

3. A comparative study of direct methods for finding optimal strategies for HVAA defense, focusing on methods suitable for hardware implementation

4. Provide tools for mission analysis concerning HVAA defense, remote sensing, and pursuit-evasion.

A summary of the optimal HVAA defense scenarios, as defined in Table 1, are provided in Table 12 below. The optimal strategies are found either numerically or analytically. Where analytic solutions are available, the referenced equation or theorem is provided. The definitions for each of the optimal defense scenarios is found in Section 3.4.

Table 12. HVAA Defense Strategies

Scenario	Optimal Strategy Summary
1	Using ECM, as described in Section 3.3, the HVAA should steer toward its defender in order to assist the closure of the defender-pursuer range; Figure 29 illustrates this behavior.
2	The optimal headings for the defender and pursuer are provided by eqs. (4.32) and (4.33), respectively.
3	The optimal strategy for the pursuer is provided by eqs. (4.60) and (4.61) and the optimal strategy for the defender is provided by eqs. (4.65) and (4.66). The optimal interception point which defines these strategies is found using gradient based search.
4	The optimal defender heading which maximally exposes a non-maneuvering pursuer is provided by eq. (5.22). Using this strategy, the time of exposure is provided by eq. (5.31).
5	The optimal pursuer heading which captures a non-maneuvering evader in minimum time is provided by eq. (5.45). The optimal defender heading which maximally exposes the pursuer is provided by eq. (5.54). If the time-to-go is less than the maximum possible exposure time, the headings which the defender should take are in the interval provided by eq. (5.65).
6	The optimal defender's heading and flight path angle which maximally exposes a non-maneuvering pursuer are provided by eqs. (5.96) and (5.102), respectively.

6.5 Future Research

There are a myriad of avenues one can take which extend the work of this dissertation. The following are a list of some of the more obvious extensions or research which is out of the scope of this dissertation and can be considered as future work.

The investigations performed in this work were restricted to games of degree – it was always assumed that the defender was able to provide successful defense for the evader. Future extensions to this work include considerations of game of kind, especially in 3-D.

Another extension is the consideration of a HVAA which is restricted to "race-tracks", "circles", or a series of "linear flight paths". How may the defender or pursuer be influenced if the evader is maneuvering from a prescribed flight-path?

Obvious extensions for the directed energy defense scenario are to consider scenarios where the defender does not make initial contact with the pursuer. Questions arise as to the multi-phase optimal control problem for the acquisition of the pursuer and maximum exposure prior to the pursuer's capture of the evader. The defense of a maneuvering HVAA was considered for kinetic defense in Chapter IV, future work should consider the cooperation of a maneuvering HVAA which is teamed with a defender, equipped with a directed energy weapon.

The directed energy defense scenarios which were posed and solved in this dissertation assumed a circular or spherical WEZ. The directed energy weapon was considered to be effective, independent of angle, and have a fixed effective range. This makes solving the optimal control problems convenient to solve, but is not realistic. Rather than considering a circle or spherical WEZ, a pie-shaped or cone-shaped WEZ would allow for angular limits on the WEZ. More generally, a numeric model for WEZ range and effectiveness would be desired; but, such models would require the use of numeric techniques for analysis of optimal strategies for the HVAA, the defender, and the pursuer.

One interesting idea is to consider flight-testing the proposed algorithms on real hardware to investigate the efficacy of the analytic solutions in the "real world". As is common in engineering, the models used in this dissertation have a set of assumptions which abstract them from the real world. This abstraction allows engineers to draw conclusions; but, the accuracy of the underlying models is reduced. One idea is to try and "fly" the proposed algorithms to ascertain if the analytic solutions (based upon an abstracted reality) actually work in the real world on hardware.

Other future research includes other Air Force operations which relate to defensive counter air missions. Some examples include mutual support, fighter combat air patrol, and intelligence, surveillance, and reconnaissance. It may be possible to use the

mathematical tools from this dissertation to pose and solve other kinds of engagements which may be of use for mission analysis (sea, land, air, and space).

6.6 Summary

This dissertation has shown the optimal strategies for a defender to protect a high value airborne asset by either kinetic or directed energy means. Using the calculus of variations, optimal control theory, and the geometry of Apollonius, the optimal strategies were found either analytically or numerically. The impacts of this work have made a significant contribution to the war-gaming analysis within Air Force Research Laboratory, Aerospace Systems Directorate. Using the optimal strategies for the defender, more complex and realistic air combat analysis can be performed as it relates to the mission of the Untied States Air Force. Moreover, this research provides some foundation for 3-D engagements as they relate to space applications in support of the United States Space Force.

Appendix A. Select Derivations

In this appendix, select derivations which are too wordy to be included in the body of the dissertation are provided herein.

A.1 Optimal Heading as a Function of Optimal Costates

This derivation starts with eq. (5.77) and derives eqs. (5.78) and (5.79) through algebraic manipulation.

$$
\begin{aligned}
0 &= -p^*_{x_D}\alpha\cos\gamma^*_D\sin\psi^*_D + p^*_{y_D}\alpha\cos\gamma^*_D\cos\psi^*_D \\
0 &= -p^*_{x_D}\sin\psi^*_D + p^*_{y_D}\cos\psi^*_D \\
p^*_{x_D}\sin\psi^*_D &= p^*_{y_D}\cos\psi^*_D \\
p^{*2}_{x_D}\sin^2\psi^*_D &= p^{*2}_{y_D}\cos^2\psi^*_D \\
p^{*2}_{x_D}(1-\cos^2\psi^*_D) &= +p^{*2}_{y_D}\cos^2\psi^*_D \\
p^{*2}_{x_D} - p^{*2}_{x_D}\cos^2\psi^*_D &= p^{*2}_{y_D}\cos^2\psi^*_D \\
p^{*2}_{x_D} &= (p^{*2}_{x_D} + p^{*2}_{y_D})\cos^2\psi^*_D \\
\cos^2\psi^*_D &= \frac{p^{*2}_{x_D}}{p^{*2}_{x_D} + p^{*2}_{y_D}}
\end{aligned}
$$

$$
1-\sin^2\psi^*_D = \frac{p^{*2}_{x_D}}{p^{*2}_{x_D} + p^{*2}_{y_D}} \Rightarrow \sin^2\psi^*_D = \frac{p^{*2}_{y_D}}{p^{*2}_{x_D} + p^{*2}_{y_D}}
$$

A.2 Optimal Flight Path Angle as a Function of Optimal Costates

This derivation starts with eq. (5.81) and derives eq. (5.83) through algebraic manipulation.

$$
\begin{aligned}
0 &= -p^*_{x_D}\alpha \sin\gamma^*_D \cos\psi^*_D - p^*_{y_D}\alpha \sin\gamma^*_D \sin\psi^*_D + p^*_{z_D}\alpha\cos\gamma^*_D \\
0 &= -p^*_{x_D}\sin\gamma^*_D \cos\psi^*_D + p^*_{y_D}\sin\gamma^*_D \sin\psi^*_D + p^*_{z_D}\cos\gamma^*_D \\
0 &= -\sin\gamma^*_D(p^*_{x_D}\cos\psi^*_D + p^*_{y_D}\sin\psi^*_D) + p^*_{z_D}\cos\gamma^*_D \\
\sin\gamma^*_D(p^*_{x_D}\cos\psi^*_D + p^*_{y_D}\sin\psi^*_D) &= p^*_{z_D}\cos\gamma^*_D \\
\sin^2\gamma^*_D(p^*_{x_D}\cos\psi^*_D + p^*_{y_D}\sin\psi^*_D)^2 &= p^{*2}_{z_D}\cos^2\gamma^*_D \\
(1-\cos^2\gamma^*_D)(p^*_{x_D}\cos\psi^*_D + p^*_{y_D}\sin\psi^*_D)^2 &= p^{*2}_{z_D}\cos^2\gamma^*_D \\
(p^*_{x_D}\cos\psi^*_D + p^*_{y_D}\sin\psi^*_D)^2 - \cos^2\gamma^*_D(p^*_{x_D}\cos\psi^*_D + p^*_{y_D}\sin\psi^*_D)^2 &= p^{*2}_{z_D}\cos^2\gamma^*_D \\
(p^*_{x_D}\cos\psi^*_D + p^*_{y_D}\sin\psi^*_D)^2 &= \cos^2\gamma^*_D(p^*_{x_D}\cos\psi^*_D + p^*_{y_D}\sin\psi^*_D)^2 + p^{*2}_{z_D}\cos^2\gamma^*_D \\
(p^*_{x_D}\cos\psi^*_D + p^*_{y_D}\sin\psi^*_D)^2 &= \cos^2\gamma^*_D((p^*_{x_D}\cos\psi^*_D + p^*_{y_D}\sin\psi^*_D)^2 + p^{*2}_{z_D})
\end{aligned}
$$

Therefore:

$$\cos^2\gamma^*_D = \frac{(p^*_{x_D}\cos\psi^*_D + p^*_{y_D}\sin\psi^*_D)^2}{p^{*2}_{z_D} + (p^*_{x_D}\cos\psi^*_D + p^*_{y_D}\sin\psi^*_D)^2}$$

Expanding further and substitution of eqs. (5.78) and (5.79) for $\cos^2\psi^*_D$ and $\sin^2\psi^*_D$:

$$\cos^2\gamma_D^* = \frac{(p_{x_D}^*\cos\psi_D^* + p_{y_D}^*\sin\psi_D^*)^2}{p_{z_D}^{*2} + (p_{x_D}^*\cos\psi_D^* + p_{y_D}^*\sin\psi_D^*)^2}$$
$$= \frac{p_{x_D}^{*2}\cos^2\psi_D^* + p_{y_D}^{*2}\sin^2\psi_D^* + 2p_{x_D}^*p_{y_D}^*\cos\psi_D^*\sin\psi_D^*}{p_{z_D}^{*2} + p_{x_D}^{*2}\cos^2\psi_D^* + p_{y_D}^{*2}\sin^2\psi_D^* + 2p_{x_D}^*p_{y_D}^*\cos\psi_D^*\sin\psi_D^*}$$
$$= \frac{p_{x_D}^{*2}\left(\frac{p_{x_D}^{*2}}{p_{x_D}^{*2}+p_{y_D}^{*2}}\right) + p_{y_D}^{*2}\left(\frac{p_{y_D}^{*2}}{p_{x_D}^{*2}+p_{y_D}^{*2}}\right) + 2p_{x_D}^*p_{y_D}^*\left(\frac{p_{x_D}^{*2}}{p_{x_D}^{*2}+p_{y_D}^{*2}}\right)^{1/2}\left(\frac{p_{y_D}^{*2}}{p_{x_D}^{*2}+p_{y_D}^{*2}}\right)^{1/2}}{p_{z_D}^{*2} + p_{x_D}^{*2}\left(\frac{p_{x_D}^{*2}}{p_{x_D}^{*2}+p_{y_D}^{*2}}\right) + p_{y_D}^{*2}\left(\frac{p_{y_D}^{*2}}{p_{x_D}^{*2}+p_{y_D}^{*2}}\right) + 2p_{x_D}^*p_{y_D}^*\left(\frac{p_{x_D}^{*2}}{p_{x_D}^{*2}+p_{y_D}^{*2}}\right)^{1/2}\left(\frac{p_{y_D}^{*2}}{p_{x_D}^{*2}+p_{y_D}^{*2}}\right)^{1/2}}$$

As an aside:

$$2p_{x_D}^*p_{y_D}^*\left(\frac{p_{x_D}^{*2}}{p_{x_D}^{*2}+p_{y_D}^{*2}}\right)^{1/2}\left(\frac{p_{y_D}^{*2}}{p_{x_D}^{*2}+p_{y_D}^{*2}}\right)^{1/2} = 2\frac{p_{x_D}^{*2}p_{y_D}^{*2}}{p_{x_D}^{*2}+p_{x_D}^{*2}}$$

Therefore $\cos^2\gamma_D$ may be written as:

$$\cos^2\gamma_D^* = \frac{p_{x_D}^{*2}\left(\frac{p_{x_D}^{*2}}{p_{x_D}^{*2}+p_{y_D}^{*2}}\right) + p_{y_D}^{*2}\left(\frac{p_{y_D}^{*2}}{p_{x_D}^{*2}+p_{y_D}^{*2}}\right) + 2\frac{p_{x_D}^{*2}p_{y_D}^{*2}}{p_{x_D}^{*2}+p_{x_D}^{*2}}}{p_{z_D}^{*2} + p_{x_D}^{*2}\left(\frac{p_{x_D}^{*2}}{p_{x_D}^{*2}+p_{y_D}^{*2}}\right) + p_{y_D}^{*2}\left(\frac{p_{y_D}^{*2}}{p_{x_D}^{*2}+p_{y_D}^{*2}}\right) + 2\frac{p_{x_D}^{*2}p_{y_D}^{*2}}{p_{x_D}^{*2}+p_{x_D}^{*2}}}$$
$$= \frac{p_{x_D}^{*2}p_{x_D}^{*2} + p_{y_D}^{*2}p_{y_D}^{*2} + 2p_{x_D}^{*2}p_{y_D}^{*2}}{p_{z_D}^{*2} + p_{x_D}^{*2}p_{x_D}^{*2} + p_{y_D}^{*2}p_{y_D}^{*2} + 2p_{x_D}^{*2}p_{y_D}^{*2}}$$

Also as an aside:

$$\frac{(p_{x_D}^{*2} + p_{y_D}^{*2})(p_{x_D}^{*2} + p_{y_D}^{*2})}{p_{x_D}^{*2} + p_{y_D}^{*2}} = \frac{p_{x_D}^{*2}p_{x_D}^{*2} + p_{y_D}^{*2}p_{y_D}^{*2} + 2\lambda_{x_D}^{*2}p_{y_D}^{*2}}{p_{x_D}^{*2} + p_{y_D}^{*2}}$$

$$\frac{(p_{x_D}^{*2} + p_{y_D}^{*2})(p_{x_D}^{*2} + p_{y_D}^{*2})}{p_{x_D}^{*2} + p_{y_D}^{*2}} - \frac{2p_{x_D}^{*2}p_{y_D}^{*2}}{p_{x_D}^{*2} + p_{y_D}^{*2}} = \frac{p_{x_D}^{*2}p_{x_D}^{*2} + p_{y_D}^{*2}p_{y_D}^{*2}}{p_{x_D}^{*2} + p_{y_D}^{*2}}$$

Therefore $\cos^2\gamma_D$ may be written as:

$$\begin{aligned}
\cos^2\gamma_D^* &= \frac{\frac{(p_{x_D}^{*2}+p_{y_D}^{*2})(p_{x_D}^{*2}+p_{y_D}^{*2})}{p_{x_D}^{*2}+p_{y_D}^{*2}}}{p_{z_D}^{*2} + \frac{(p_{x_D}^{*2}+p_{y_D}^{*2})(p_{x_D}^{*2}+p_{y_D}^{*2})}{p_{x_D}^{*2}+p_{y_D}^{*2}}} \\
&= \frac{\frac{(p_{x_D}^{*2}+p_{y_D}^{*2})(p_{x_D}^{*2}+p_{y_D}^{*2})}{p_{x_D}^{*2}+p_{y_D}^{*2}}}{p_{z_D}^{*2}\frac{p_{x_D}^{*2}+p_{y_D}^{*2}}{p_{x_D}^{*2}+p_{y_D}^{*2}} + \frac{(p_{x_D}^{*2}+p_{y_D}^{*2})(p_{x_D}^{*2}+p_{y_D}^{*2})}{p_{x_D}^{*2}+p_{y_D}^{*2}}} \\
&= \frac{(p_{x_D}^{*2}+p_{y_D}^{*2})(p_{x_D}^{*2}+p_{y_D}^{*2})}{p_{z_D}^{*2}(p_{x_D}^{*2}+p_{y_D}^{*2}) + (p_{x_D}^{*2}+p_{y_D}^{*2})(p_{x_D}^{*2}+p_{y_D}^{*2})} \\
&= \frac{p_{x_D}^{*2}+p_{y_D}^{*2}}{p_{x_D}^{*2}+p_{y_D}^{*2}+p_{z_D}^{*2}}
\end{aligned}$$

Therefore:

$$\cos^2\gamma_D^* = \frac{p_{x_D}^{*2}+p_{y_D}^{*2}}{p_{x_D}^{*2}+p_{y_D}^{*2}+p_{z_D}^{*2}}$$

A.3 Optimal Path of Target Exposure, $\overline{PS}$

The derivation of the target exposure length starts with eq. (5.99) and derives eq. (5.100) through algebraic manipulation.

$$\left(\alpha\overline{PS} + R_D\right)^2 = \overline{PS}^2 + R_D^2 - 2R_D\overline{PS}\cos\theta$$

Expanding all terms in the equation the following is obtained:

$$\alpha^2\overline{PS}^2 + R_D^2 + 2R_D\alpha\overline{PS} = \overline{PS}^2 + R_D^2 - 2R_D\overline{PS}\cos\theta$$

Removing R_D^2 from both sides:

$$\alpha^2\overline{PS}^2 + 2R_D\alpha\overline{PS} = \overline{PS}^2 - 2R_D\overline{PS}\cos\theta$$

Divide both sides of the equation by $\overline{PS}$:

$$\begin{aligned}
\alpha^2\overline{PS} + 2R_D\alpha &= \overline{PS} - 2R_D\cos\theta \\
\alpha^2\overline{PS} &= \overline{PS} - 2R_D\cos\theta - 2R_D\alpha \\
\alpha^2\overline{PS} - \overline{PS} &= -2R_D\cos\theta - 2R_D\alpha \\
(\alpha^2 - 1)\overline{PS} &= -2R_D(\cos\theta + \alpha) \\
(1 - \alpha^2)\overline{PS} &= 2R_D(\alpha + \cos\theta)
\end{aligned}$$

Therefore:

$$\overline{PS} = \frac{2R_D(\alpha + \cos\theta)}{1 - \alpha^2}$$

A.4 Optimal Flight Path Angle

Substitution of eqs. (5.98) and (5.100) into eq. (5.101) the optimal flight path angle in eq. (5.102) is derived. Starting with eq. (5.101):

$$\cos\gamma_D^* = \frac{R_D \sin\theta}{\overline{DS}}$$

Substitution of eq. (5.98) for $\overline{DS}$ the following is obtained

$$\cos\gamma_D^* = \frac{R_D \sin\theta}{\alpha\overline{PS} + R_D}$$

Further, substitution of eq. (5.100) for $\overline{PS}$, the following is obtained:

$$\begin{aligned}
\cos\gamma_D^* &= \frac{R_D \sin\theta}{\alpha(\frac{2R_D(\alpha+\cos\theta)}{1-\alpha^2}) + R_D} \\
&= \frac{R_D \sin\theta}{\frac{2R_D\alpha(\alpha+\cos\theta)}{1-\alpha^2} + R_D} \\
&= \frac{R_D \sin\theta}{\frac{2R_D\alpha(\alpha+\cos\theta)}{1-\alpha^2} + R_D\frac{1-\alpha^2}{1-\alpha^2}} \\
&= \frac{(1-\alpha^2)R_D \sin\theta}{2R_D\alpha(\alpha+\cos\theta) + R_D(1-\alpha^2)} \\
&= \frac{(1-\alpha^2)\sin\theta}{2\alpha(\alpha+\cos\theta) + (1-\alpha^2)} \\
&= \frac{(1-\alpha^2)\sin\theta}{2\alpha^2 + 2\alpha\cos\theta + 1 - \alpha^2} \\
&= \frac{(1-\alpha^2)\sin\theta}{\alpha^2 + 2\alpha\cos\theta + 1}
\end{aligned}$$

Therefore

$$\gamma_D^* = \cos^{-1}\left(\frac{(1-\alpha^2)\sin\theta}{\alpha^2 + 2\alpha\cos\theta + 1}\right)$$

Appendix B. On Pontryagin's Optimal Control Canonical Example

Appendix B contains an in-depth analysis of Pontryagin's optimal control canonical example when the target set is not a simpleton – circular and rectangular target sets are considered. This work contains the same analysis that was important in describing how a popular optimal control problem may be approached using differential game theory. The result of the work is worth inclusion in this dissertation, but publication was not made possible until after the dissertation.

On Pontryagin's Optimal Control Canonical Example

Isaac E. Weintraub and Meir Pachter

Abstract

In this paper, Pontryagin's canonical optimal control example, which entails a double integrator plant, is revisited. However, rather than controlling the state to the origin, we require the end state to reach a terminal set that contains the origin in its interior. Indeed, in industry, it is required to control to a prescribed tolerance rather than reach a desired end state; achieving tight tolerances is expensive, and from a theoretical point of view, constraining the end state to a terminal manifold of co-dimension n-1 renders the optimal control problem well-posed. Thus, the correct solution of the optimal control problem is obtained. Two target sets are considered: a smooth circular target and a square target with corners. Closed-loop state-feedback control laws are developed which drive the double integrator plant from an arbitrary initial state to the target set in minimum time. This is accomplished using Isaacs' method for the solution of differential games, which entails Dynamic Programming (DP), working backward from the Usable Part of the target set, as opposed to obtaining the optimal trajectories using the necessary conditions provided by Pontryagin's Maximum Principle (PMP). Special attention is given to the critical Usable Part of the target set in the process of obtaining the global solution of the optimal control problem at hand. In this paper, Isaacs' method for the solution of differential games is applied to the solution of optimal control problems and the juxtaposition of the PMP and DP is undertaken.

I. Introduction

In this paper, the Pontryagin Maximum Principle (PMP) and Dynamic Programming (DP) methods for the solution of optimal control problems are juxtaposed. Isaacs' method for the solution of differential games is applied to the solution of optimal control problems and the canonical example from [1, pp. 23-27] concerning the application of the PMP to the synthesis of optimal controls is revisited. The objective in [1] is to show that the necessary conditions for optimality embodied in the PMP yield a closed set of conditions such that the optimal control time-history can be obtained. The application of the PMP assumes the existence of an optimal control time-history and requires a Two-Point Boundary-Value Problem (TBVP) be solved, but with the provision that hard control constraints are allowed – it is a necessary condition for optimality akin to the situation in the calculus of variations. The objective of this work is to use the canonical example from reference [1] to demonstrate the application of differential game theory / Isaacs' method [2] to optimal control problems and obtain their global solution. Isaacs' method is based on the constructive method of DP which provides sufficient conditions for optimality. It entails solving the Hamilton-Jacobi-Bellman-Isaacs (HJBI) Partial Differential Equation (PDE) using the method of characteristics. The hyperbolic HJBI PDE is solved using the method of characteristics with the boundary conditions exclusively specified on the Usable Part (UP) of the terminal manifold / target set which is of co-dimension 1 and where the pursuer / controller can enforce termination. The optimal state feedback control law is synthesized as opposed to obtaining an optimal control time history. The global solution is thus obtained and, in addition, the part of the state space where optimal trajectories exist is characterized. In this paper, rather than using the PMP, Isaacs' method for the solution of Differential Games is adapted to the solution of (much simpler) optimal control problems. The importance of the UP of the terminal manifold, where the boundary conditions are specified, is emphasized. Furthermore, we

I. Weintraub is with the Aerospace Systems Directorate, Air Force Research Laboratory, Wright-Patterson AFB, OH 45433. isaac.weintraub.1@us.af.mil

M. Pachter is with the Department of Electrical and Computer Engineering, Air Force Institute of Technology, Wright-Patterson AFB, OH 45433. meir.pachter@afit.edu

Approved for public release; distribution unlimited. (88ABW-2019-6099)

derive time-optimal state feedback control laws which extend Pontryagin's canonical example concerning the regulation to a terminal state to that of a target manifold of co-dimension 1. This is very much in-line with engineering practice where tolerances are specified - "zero tolerance" is expensive. And from a mathematical point of view, this renders the optimal control problem well-posed.

In this paper Isaacs' method [2] is employed rather than using PMP to synthesize time-optimal controls for reaching a desired terminal manifold. Emphasizing the advantages of using Isaacs' method rather than PMP, we focus on the iconic example from [1] which entails the dynamics of a double integrator. Time-optimal state feedback control laws are derived which globally cover the whole state space rather than constructing an optimal trajectory which leads from a specified state to a terminal state / the origin. Furthermore, instead of a specific terminal state / point target, in this paper, a terminal manifold is considered. This is in tune with the engineering practice of using a finite tolerance and also renders the optimal control problem well-posed. We submit, that this is the mathematically correct way to deal with controlling to a point target in optimal control and differential games.

We consider the problem of reaching a specified target manifold, $\mathscr{C}$, of co-dimension 1 rather than a terminal state from an arbitrary initial state in the state space in minimum time. Physical systems commonly cope with some allowable tolerance such as position or velocity error. Thus, it is the objective of this paper to investigate time-optimal control which drive a double-integrator plant which models a point mass traveling on a straight line and needs to be brought to rest at the origin in minimum time, allowing for a small error in terminal position and velocity.

Indeed, when using Isaacs' method, it becomes clear that the proper termination of optimal control problems (and differential games) in $\mathbb{R}^n$ calls for the specification of terminal manifolds whose dimension is $n-1$. And in the context of pursuit-evasion differential games, the proper treatment of "point capture" requires the consideration of a terminal manifold which is a sphere of radius $0 < \epsilon << 1$ centered at the origin and point capture means letting $\epsilon \to 0$. This is required from a mathematical point of view and makes sense from and engineering point of view.

The paper is organized as follows. In Section II, the physical control problem is posed using non-dimensional variables. In Section III, a circular terminal manifold centered at the origin with radius l is considered. The control to a non smooth target manifold with corners, a square, is investigated in Section IV. Lastly, in Section V we draw conclusions.

II. Control Problem

Consider a point-mass with mass, m, which is controlled on a straight line using a bounded force, F. The maximum applicable force is $F_{\max}$. According to Newton's Second Law,

$$F(t) = ma(t), \qquad -F_{max} \leq F(t) \leq F_{max}.$$

Hence, the dynamics are

$$\begin{aligned} \dot{x}(t) &= v(t), \qquad x(0) = x_0 \\ \dot{v}(t) &= \frac{1}{m}F(t), \quad v(0) = v_0, \quad 0 \leq t \leq t_f, \end{aligned}$$

where x is the position on the line of the point mass, and v is its velocity. The initial position of the point-mass is x_0 and its initial velocity is v_0. The goal is to drive in minimum time, t_f, the position and the velocity to a bounded region described as

$$-L \leq x(t_f) \leq L, \quad -V \leq v(t_f) \leq V.$$

It is convenient to use non-dimensional variables. The non-dimensionalization is performed as follows:

$$\begin{aligned} &x \to x/L, \quad x_0 \to x_0/L, \quad v \to v/V, \quad v_0 \to v_0/V, \\ &t \to t\frac{V}{L}, \quad t_f \to t_f\frac{V}{L}, \quad u \triangleq \frac{F}{F_{max}}; \end{aligned}$$

where L is a characteristic length and V is a characteristic velocity. As is best practice in physics, also the time variable is rendered dimensionless. The dynamics in non-dimensional form are

$$\begin{aligned}
&\frac{dx}{dt} = v(t), \qquad x(0) = x_0 \\
&\frac{dv}{dt} = \alpha u(t), \qquad v(0) = v_0, \quad 0 \le t \le t_f \\
&-1 \le u(t) \le 1,
\end{aligned}$$

where the non-dimensional parameter

$$\alpha \triangleq \frac{LF_{max}}{mV^2}.$$

III. Circular Target Set

The physical state variables: $x_1(t) \triangleq x(t)$, $x_2(t) \triangleq v(t)$ ans the non-dimensional dynamics are

$$\begin{aligned}
&\frac{dx_1}{dt} = x_2(t),\ x_1(0) = x_{10} \\
&\frac{dx_2}{dt} = \alpha u(t),\ x_2(0) = x_{20} \\
&0 \le t \le t_f,\ -1 \le u(t) \le 1.
\end{aligned} \tag{1}$$

Consider the terminal manifold $l^2 = x^2(t_f) + \beta^2 v^2(t_f)$. The parameter l is non-dimensional – it is the tolerance parameter and β is a non-dimensional weight parameter which trades off the importance of the terminal position error and the terminal velocity error. The optimal control problem is parameterized by $\alpha > 0$, $l > 0$, and $\beta > 0$. For the sake of demonstration, the weight parameter β is assumed to have the value $\beta = 1$ so we confine our attention to the terminal manifold / target set, $\mathscr{C}$, described by a circle with radius l about the origin of the state space (x_1, x_2) and the physical parameter $\alpha = 1$.

The terminal manifold of co-dimension 1 (as required) is the circle:

$$l^2 = x_1^2(t_f) + x_2^2(t_f).$$

The terminal manifold of co-dimension 1 is parameterized by $0 \le \theta \le 2\pi$ and therefore

$$\begin{aligned}
&x_1(t_f) = l\cos\theta \\
&x_2(t_f) = l\sin\theta, \quad 0 \le \theta \le 2\pi.
\end{aligned} \tag{2}$$

The terminal manifold is parameterized by $0 \le \theta \le 2\pi$: $\mathscr{C} = \{(x_1, x_2) | x_1 = l\cos\theta, x_2 = l\sin\theta\}$. The outward pointing unit normal to the terminal manifold at $(l\cos\theta, l\sin\theta)$ is $\vec{n} = \left(\begin{smallmatrix}\cos\theta \\ \sin\theta\end{smallmatrix}\right)$. The circular target set and the associated normals are shown in Figure 1.

A. Isaacs' Method

The Usable Part (UP) of the terminal manifold is where its penetration can be enforced by the controller. The Usable Part, Boundary of the Usable Part (BUP) and the Non-Usable Part (NUP) are

$$\begin{aligned}
\text{UP} &\triangleq \{\mathbf{x} | \min_u \langle \vec{n}, \mathbf{f}(\mathbf{x}, u)\rangle < 0\} \\
\text{BUP} &\triangleq \{\mathbf{x} | \min_u \langle \vec{n}, \mathbf{f}(\mathbf{x}, u)\rangle = 0\} \\
\text{NUP} &\triangleq \{\mathbf{x} | \min_u \langle \vec{n}, \mathbf{f}(\mathbf{x}, u)\rangle > 0\}.
\end{aligned} \tag{3}$$

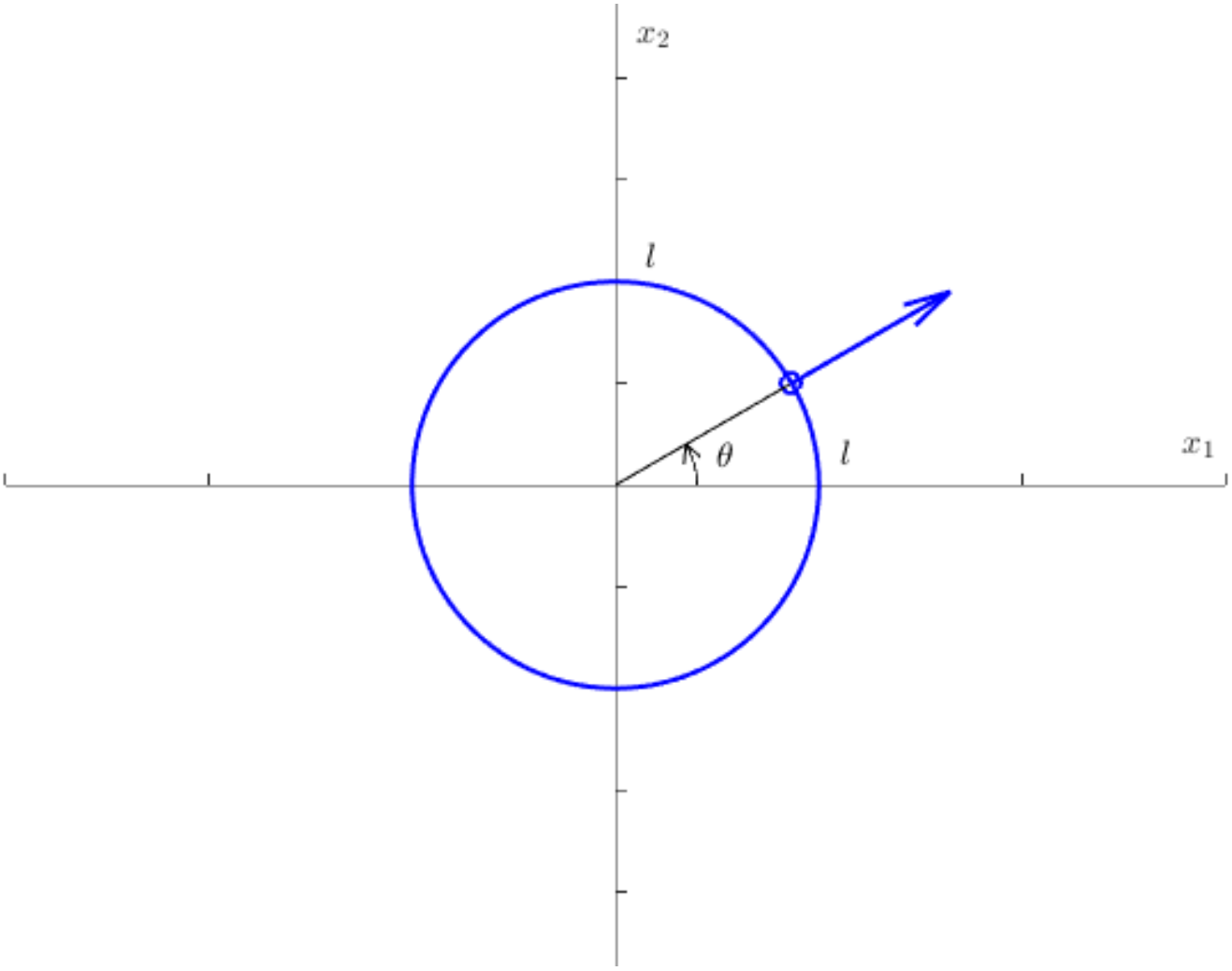

Fig. 1: Circular target set with outward pointing normal

For the circular terminal manifold and double-integrator system the UP, NUP and BUP – see (3) – are as follows

$$\begin{aligned} \text{UP} &= \{ \left(\begin{smallmatrix} l\cos\theta \\ l\sin\theta \end{smallmatrix}\right) \,|\, \min_{-1\le u\le 1} \langle \left(\begin{smallmatrix} \cos\theta \\ \sin\theta \end{smallmatrix}\right), \left(\begin{smallmatrix} x_2 \\ \alpha u \end{smallmatrix}\right) \rangle < 0 \} \\ \text{BUP} &= \{ \left(\begin{smallmatrix} l\cos\theta \\ l\sin\theta \end{smallmatrix}\right) \,|\, \min_{-1\le u\le 1} \langle \left(\begin{smallmatrix} \cos\theta \\ \sin\theta \end{smallmatrix}\right), \left(\begin{smallmatrix} x_2 \\ \alpha u \end{smallmatrix}\right) \rangle = 0 \} \\ \text{NUP} &= \{ \left(\begin{smallmatrix} l\cos\theta \\ l\sin\theta \end{smallmatrix}\right) \,|\, \min_{-1\le u\le 1} \langle \left(\begin{smallmatrix} \cos\theta \\ \sin\theta \end{smallmatrix}\right), \left(\begin{smallmatrix} x_2 \\ \alpha u \end{smallmatrix}\right) \rangle > 0 \} \end{aligned} \tag{4}$$

Having assumed, $\beta = 1$, the UP will depend on the problem parameters, α and l. The UP is therefore

$$\text{UP} = \{ \left(\begin{smallmatrix} l\cos\theta \\ l\sin\theta \end{smallmatrix}\right) \,|\, \min_{-1\le u\le 1} (x_2\cos\theta + \alpha u \sin\theta) < 0 \}$$

.

Therefore

$$\text{UP} = \{ \left(\begin{smallmatrix} l\cos\theta \\ l\sin\theta \end{smallmatrix}\right) \,|\, \min_{-1\le u\le 1} ((l\cos\theta + \alpha u)\sin\theta) < 0 \}$$

.

Therefore $\theta = 0, \theta = \pi$ are not in the UP.

1) Consider the θ range $0 < \theta < \pi$

$$\text{UP}_a = \begin{cases} \{ \left(\begin{smallmatrix} l\cos\theta \\ l\sin\theta \end{smallmatrix}\right) \,|\, \cos^{-1}\frac{\alpha}{l} < \theta < \pi \} & \text{if } \frac{\alpha}{l} < 1 \\ \{ \left(\begin{smallmatrix} l\cos\theta \\ l\sin\theta \end{smallmatrix}\right) \,|\, 0 < \theta < \pi \} & \text{if } \frac{\alpha}{l} \ge 1 \end{cases}$$

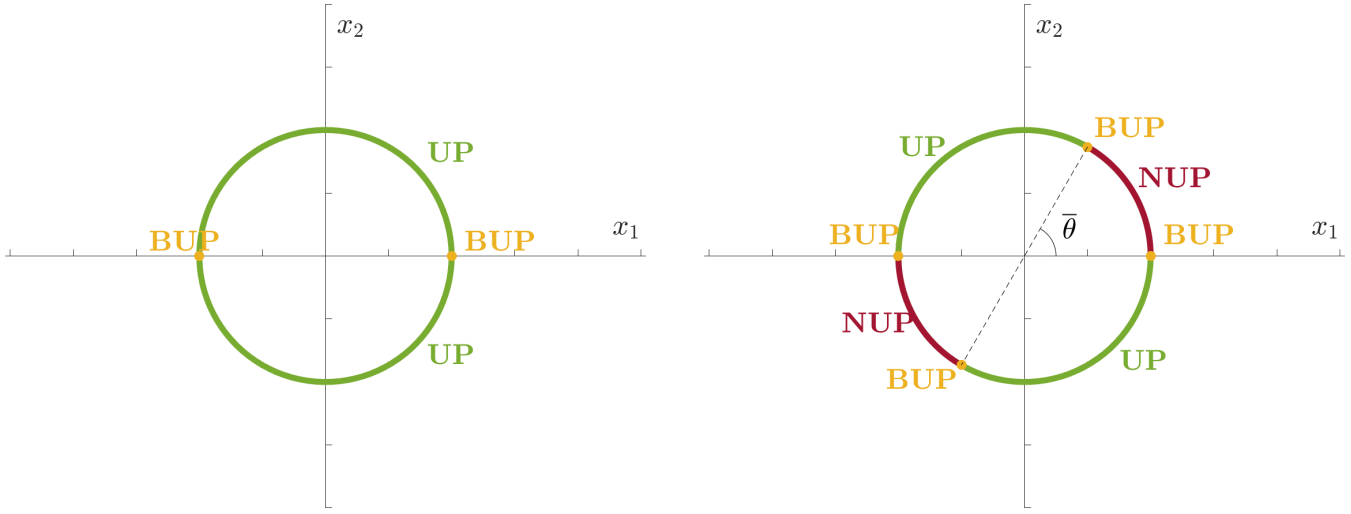

(a) The circular terminal manifold when $0 < \frac{l}{\alpha} \leq 1$

(b) The circular terminal manifold when $\frac{l}{\alpha} > 1$

Fig. 2: The UP, BUP, and NUP of the circular terminal manifold varies depending upon the problem parameters l and α. The NUP presents itself when $\frac{l}{\alpha} > 1$

2) Consider the θ range $\pi < \theta < 2\pi$

$$\text{UP}_b = \begin{cases} \{ \left(\begin{smallmatrix} l\cos\theta \\ l\sin\theta \end{smallmatrix}\right) | \pi + \cos^{-1}\frac{\alpha}{l} < \theta < 2\pi \} & \text{if } \frac{\alpha}{l} < 1 \\ \{ \left(\begin{smallmatrix} l\cos\theta \\ l\sin\theta \end{smallmatrix}\right) | \pi < \theta < 2\pi \} & \text{if } \frac{\alpha}{l} \geq 1 \end{cases}$$

The $\text{UP} = \text{UP}_a \cup \text{UP}_b$. Hence

$$\text{UP} = \begin{cases} \{ \left(\begin{smallmatrix} l\cos\theta \\ l\sin\theta \end{smallmatrix}\right) | 0 < \theta < \pi, \pi < \theta < 2\pi \} & \text{if } \frac{l}{\alpha} \leq 1 \\ \{ \left(\begin{smallmatrix} l\cos\theta \\ l\sin\theta \end{smallmatrix}\right) | \cos^{-1}\frac{\alpha}{l} < \theta < \pi, \pi + \cos^{-1}\frac{\alpha}{l} < \theta < 2\pi \} & \text{if } \frac{l}{\alpha} > 1 \end{cases} \tag{5}$$

When $\frac{l}{\alpha} > 1$, let $\overline{\theta} \triangleq \cos^{-1}(\frac{\alpha}{l})$. The UP, BUP, and NUP of the circular terminal manifold varies depending upon the problem parameters l and α as described in (5). In Figure 2, the BUP, UP, and NUP for the circular terminal manifold is shown.

For the rest of this paper, the problem parameter is assumed to be $\alpha = 1$, so the terminal manifold varies upon l.

The Hamiltonian,

$$\mathscr{H} = 1 + \lambda_1(t)x_2(t) + \lambda_2(t)\alpha u(t). \tag{6}$$

With the understanding that the co-states, λ_1 and λ_2, are the partial derivatives of the Value function with respect to the states, DP yields the condition for optimality, $\min_u \mathscr{H}$, such that $u(t)^* = -\text{sign}(\lambda_2(t))$. Therefore the optimal Hamiltonian is

$$\mathscr{H}^* = 1 + \lambda_1(t)x_2(t) - \alpha|\lambda_2(t)|$$

$\mathscr{H}^*(t) \equiv 0$, so

$$\mathscr{H}^*|_{t=t_f} = 0 \tag{7}$$

The method of characteristics employed to solve the HJBI PDE yields the Euler-Lagrage equations

$$\begin{aligned} \dot{x}_1(t) &= x_2(t), & x_1(t=0) &= x_{10} \\ \dot{x}_2(t) &= -\alpha\text{sign}(\lambda_2(t)), & x_2(t=0) &= x_{20} \\ \dot{\lambda}_1(t) &= 0, & \lambda_1(t=t_f) &= a\cos\theta \\ \dot{\lambda}_2(t) &= -\lambda_1(t), & \lambda_2(t=t_f) &= a\sin\theta, \quad a > 0 \end{aligned}$$

The terminal costates are also established courtesy of DP. We consider trajectories which emanate from the UP in (10), in retrograde time $\tau > 0$, and therefore we have the retrograde dynamics,

$$\begin{aligned}
\mathring{x}_1(\tau) &= -x_2(\tau), & x_1(\tau=0) &= l\cos\theta \\
\mathring{x}_2(\tau) &= \alpha \text{sign}(\lambda_2(\tau)), & x_2(\tau=0) &= l\sin\theta \\
\mathring{\lambda}_1(\tau) &= 0, & \lambda_1(\tau=0) &= a\cos\theta \\
\mathring{\lambda}_2(\tau) &= \lambda_1(\tau), & \lambda_2(\tau=0) &= a\sin\theta,\ \tau \ \ \geq 0;\ \theta \in \text{UP}
\end{aligned} \tag{8}$$

The optimal Hamiltonian is zero, also at final time, and when evaluated at retrograde time, $\tau = 0$ where the co-states are specified,

$$\mathscr{H}^*|_{\tau=0} = 0$$

so evaluating (6) at final time, the coefficient a is found to be:

$$a = \frac{1}{\alpha|\sin\theta| - l\sin\theta\cos\theta}, \quad \forall\ \theta \in \text{UP} \tag{9}$$

From the structure of the UP we deduce that a is positive, as required. Two cases need to be considered: when $0 < \frac{l}{\alpha} \leq 1$ and when $\frac{l}{\alpha} > 1$. As will be demonstrated later the UP, BUP, and NUP as defined in (4) differs in both cases.

Assuming, $0 < \frac{l}{\alpha} \leq 1$, the Usable Part (UP) and the Boundary of the Usable Part (BUP) are

$$\begin{aligned}
\text{UP} &= \{\left(\begin{smallmatrix} l\cos\theta \\ l\sin\theta \end{smallmatrix}\right) \mid 0 < \theta < \pi, \pi < \theta < 2\pi\} \\
\text{BUP} &= \{\left(\begin{smallmatrix} l\cos\theta \\ l\sin\theta \end{smallmatrix}\right) \mid \theta = 0, \theta = \pi\}.
\end{aligned}$$

Recall, $\overline{\theta} \triangleq \cos^{-1}(\frac{\alpha}{l})$; assuming, $\frac{l}{\alpha} > 1$, the UP, BUP, and NUP are

$$\begin{aligned}
\text{UP} &= \{\left(\begin{smallmatrix} l\cos\theta \\ l\sin\theta \end{smallmatrix}\right) \mid \overline{\theta} < \theta < \pi, \overline{\theta} + \pi < \theta < 2\pi\} \\
\text{BUP} &= \{\left(\begin{smallmatrix} l\cos\theta \\ l\sin\theta \end{smallmatrix}\right) \mid \theta = 0, \theta = \overline{\theta}, \theta = \pi, \theta = \pi + \overline{\theta}\} \\
\text{NUP} &= \{\left(\begin{smallmatrix} l\cos\theta \\ l\sin\theta \end{smallmatrix}\right) \mid 0 < \theta < \overline{\theta}, \pi < \theta < \pi + \overline{\theta}\}.
\end{aligned}$$

Therefore the UP, BUP, and the NUP of the circular terminal manifold / target set are

$$\text{UP} = \begin{cases} \{\left(\begin{smallmatrix} l\cos\theta \\ l\sin\theta \end{smallmatrix}\right) \mid 0 < \theta < \pi, \pi < \theta < 2\pi\} & \text{if } 0 < \frac{l}{\alpha} \leq 1 \\ \{\left(\begin{smallmatrix} l\cos\theta \\ l\sin\theta \end{smallmatrix}\right) \mid \overline{\theta} < \theta < \pi, \overline{\theta} + \pi < \theta < 2\pi\} & \text{if } \frac{l}{\alpha} > 1 \end{cases} \tag{10}$$

$$\text{BUP} = \begin{cases} \{\left(\begin{smallmatrix} l\cos\theta \\ l\sin\theta \end{smallmatrix}\right) \mid \theta = 0, \theta = \pi\}. & \text{if } 0 < \frac{l}{\alpha} \leq 1 \\ \{\left(\begin{smallmatrix} l\cos\theta \\ l\sin\theta \end{smallmatrix}\right) \mid \theta = 0, \theta = \overline{\theta}, \theta = \pi, \theta = \pi + \overline{\theta}\} & \text{if } \frac{l}{\alpha} > 1 \end{cases} \tag{11}$$

$$\text{NUP} = \begin{cases} \varnothing & \text{if } \frac{l}{\alpha} \leq 1 \\ \{\left(\begin{smallmatrix} l\cos\theta \\ l\sin\theta \end{smallmatrix}\right) \mid 0 < \theta < \overline{\theta}, \pi < \theta < \pi + \overline{\theta}\}. & \text{if } \frac{l}{\alpha} > 1 \end{cases} \tag{12}$$

Using the evaluation of the coefficient a according to (9) the retrograde equations in (8) are:

$$\begin{aligned}
\mathring{x}_1(\tau) &= -x_2(\tau), & x_1|_{\tau=0} &= l\cos\theta \\
\mathring{x}_2(\tau) &= \alpha \text{sign}(\lambda_2(\tau)), & x_2|_{\tau=0} &= l\sin\theta \\
\lambda_1 &= \tfrac{\cos\theta}{\alpha|\sin\theta| - l\sin\theta\cos\theta} & & \\
\mathring{\lambda}_2(\tau) &= \lambda_1(\tau), & \lambda_2|_{\tau=0} &= \tfrac{\sin\theta}{\alpha|\sin\theta| - l\sin\theta\cos\theta} \\
\tau &\geq 0, & \theta &\in (0,\pi) \cup (\pi, 2\pi)
\end{aligned} \tag{13}$$

Therefore:

$$\lambda_2(\tau) = \tfrac{\sin\theta + \tau\cos\theta}{\alpha|\sin\theta| - l\sin\theta\cos\theta},\ \tau \geq 0,\ \theta \in (0,\pi) \cup (\pi, 2\pi)$$

We first consider the case where the problem parameters satisfy $0 < \frac{l}{\alpha} \leq 1$. The following abbreviations are used as necessary: $c_\theta \equiv \cos\theta$, $s_\theta \equiv \sin\theta$, $t_\theta \equiv \tan\theta$. The UP of the circular terminal manifold $\{(x_1, x_2)|x_1^2 + x_2^2 = l^2\}$ is partitioned into four quadrants as follows:

1) Trajectories "emanating" in retrograde fashion from points on the UP of the terminal manifold which correspond to the parameter $0 < \theta < \pi/2$. For this case, $\lambda_2(\tau) > 0 \quad \forall\, \tau \geq 0$, so the optimal control $u^*(t) = -1$.

$$\mathring{x}_2 = 1,\ \tau \geq 0$$

Therefore

$$x_2(\tau) = l\sin\theta + \tau$$
$$x_1(\tau) = l\cos\theta - l\tau\sin\theta - \frac{1}{2}\tau^2,\ \tau \geq 0$$

Solving for the curve:

$$x_1 = -\tfrac{1}{2}x_2^2 + l\cos\theta + \tfrac{1}{2}l^2\sin^2\theta,$$
$$x_2 > l\sin\theta, \quad \theta \in (0, \pi/2)$$

2) Trajectories "emanating" from points on the terminal manifold which correspond to $\pi/2 \leq \theta < \pi$. In this case $\lambda_2(\tau)$ changes sign from positive to negative at $\tau = -\tan\theta(> 0)$. For this case:

$$\mathring{x}_2 = \begin{cases} 1, & \text{if } 0 \leq \tau < -t_\theta \\ -1, & \text{if } -t_\theta < \tau \end{cases}$$

Therefore

$$x_2(\tau) = \begin{cases} ls_\theta + \tau, & \text{if } 0 \leq \tau < -t_\theta \\ ls_\theta - 2t_\theta - \tau, & \text{if } -t_\theta < \tau \end{cases}$$

Therefore

$$x_1(\tau) = \begin{cases} l(c_\theta - \tau s_\theta) - \frac{1}{2}\tau^2, & \text{if } 0 \leq \tau < -t_\theta \\ l(c_\theta - \tau s_\theta) + t_\theta^2 + \frac{1}{2}\tau^2 + 2\tau t_\theta, & \text{if } -t_\theta < \tau \end{cases}$$

Therefore when $\theta \in (\pi, \frac{\pi}{2})$,

$$x_1(x_2) = \begin{cases} lc_\theta - \frac{1}{2}x_2^2 + \frac{1}{2}l^2 s_\theta^2, & \text{if } ls_\theta \leq x_2 < ls_\theta - t_\theta \\ lc_\theta + \frac{1}{2}x_2^2 + 2l\frac{s_\theta^2}{c_\theta} - \frac{1}{2}l^2 s_\theta^2 - t_\theta^2, & \text{if } ls_\theta - t_\theta > x_2 \end{cases}$$

3) Trajectories "emanating" from points on the terminal manifold which correspond to $\pi < \theta < 3\pi/2$. In this case $\lambda_2(\tau)$ is negative for all $\tau \geq 0$.

$$\mathring{x}_2 = -1,\ \tau \geq 0$$

Therefore

$$x_2(\tau) = l\sin\theta - \tau,\ \tau \geq 0$$

Therefore

$$x_1(\tau) = l\cos\theta - \tau l\sin\theta + \tfrac{1}{2}\tau^2, \tau \geq 0$$

Therefore

$$x_1(x_2) = \tfrac{1}{2}x_2^2 + l\cos\theta - \tfrac{1}{2}l^2\sin^2\theta,\ \theta \in (\pi, \tfrac{3\pi}{2})$$

4) Trajectories "emanating" from points on the terminal manifold which correspond to $3\pi/2 \leq \theta < 2\pi$. For this case $\lambda_2(\tau)$ changes sign from negative to positive at $\tau = -\tan\theta(> 0)$.

$$\mathring{x}_2 = \begin{cases} -1, & \text{if } 0 \leq \tau < -t_\theta \\ 1, & \text{if } -t_\theta < \tau \end{cases}$$

Therefore

$$x_2(\tau) = \begin{cases} ls_\theta - \tau, & \text{if } 0 \le \tau < -t_\theta \\ ls_\theta + 2t_\theta + \tau, & \text{if } -t_\theta < \tau \end{cases}$$

Therefore

$$x_1(\tau) = \begin{cases} l(c_\theta - \tau s_\theta) + \frac{1}{2}\tau^2, & \text{if } 0 \le \tau < -t_\theta \\ lc_\theta - t_\theta^2 - \frac{1}{2}\tau^2 - (ls_\theta + 2t_\theta)\tau, & \text{if } -t_\theta < \tau \end{cases}$$

Therefore, when $\theta \in (\frac{3\pi}{2}, 2\pi)$:

$$x_1(x_2) = \begin{cases} lc_\theta + \frac{1}{2}x_2^2 - \frac{1}{2}l^2 s_\theta^2, & \text{if } ls_\theta \ge x_2 > ls_\theta + t_\theta \\ lc_\theta - \frac{1}{2}x_2^2 + 2l\frac{s_\theta^2}{c_\theta} + t_\theta^2 + \frac{1}{2}l^2 s_\theta^2, & \text{if } ls_\theta + t_\theta > x_2 \end{cases}$$

The optimal trajectories are parabolae of the form $x_1(x_2) = \pm x_2^2 + c$.
When $\theta \in (0, \frac{\pi}{2}) \cup (\pi, \frac{3\pi}{2})$ no switching occurs.
When $\theta \in (\frac{\pi}{2}, \pi)$, $\tau_s = -\tan\theta$. We calculate $x_1(\tau_s) = \frac{l}{\cos\theta} - \frac{1}{2}\tan^2\theta$ and $x_2(\tau_s) = l\sin\theta - \tan\theta$.
When $\theta \in (\frac{3\pi}{2}, 2\pi)$, $\tau_s = -\tan\theta$. We calculate $x_1(\tau_s) = \frac{l}{\cos\theta} + \frac{1}{2}\tan^2\theta$ and $x_2(\tau_s) = l\sin\theta + \tan\theta$.
Two switching lines exist. In parametric form they are

$$\begin{aligned} x_1(\theta) &= \frac{l}{\cos\theta} - \frac{1}{2}\tan^2\theta \\ x_2(\theta) &= l\sin\theta - \tan\theta,\ \theta \in (\tfrac{\pi}{2}, \pi) \end{aligned} \tag{14}$$

and

$$\begin{aligned} x_1(\theta) &= \frac{l}{\cos\theta} + \frac{1}{2}\tan^2\theta \\ x_2(\theta) &= l\sin\theta + \tan\theta,\ \theta \in (\tfrac{3\pi}{2}, 2\pi) \end{aligned} \tag{15}$$

The switching line (14) is anchored to the circular terminal manifold on the BUP point $(-l, 0)$ where $\theta = \pi$ and the switching line (15) is attached to the circular terminal manifold at the BUP point $(l, 0)$ where $\theta = 0$.

Consider the $x_1(\theta)$ equation in (14). We obtain

$$\cos\theta = \frac{l \pm \sqrt{l^2 + 1 - 2x_1}}{2x_1 - 1}$$

Therefore:

$$\sin\theta = \frac{\sqrt{4x_1^2 - 2x_1 - 2l^2 \mp 2l\sqrt{l^2 - 2x_1 + 1}}}{2x_1 - 1}$$

Similarly the x_1 equation in (15) yields:

$$\cos\theta = \frac{l \pm \sqrt{l^2 + 2x_1 - 1}}{2x_1 - 1}$$

Therefore:

$$\sin\theta = \frac{\sqrt{4x_1^2 - 6x_1 + 2 - 2l^2 \mp 2l\sqrt{l^2 + 2x_1 - 1}}}{2x_1 - 1}$$

Hence, the equation of the switching line from (14) is:

$$x_2 = \left(l - \frac{2x_1 - 1}{l \pm \sqrt{l^2 - 2x_1 + 1}}\right) \frac{\sqrt{4x_1^2 - 2x_1 - 2l^2 \mp 2l\sqrt{l^2 - 2x_1 + 1}}}{2x_1 - 1}$$

and the equation for the switching line from (15) is:

$$x_2 = \left(l + \frac{2x_1 - 1}{l \pm \sqrt{l^2 + 2x_1 - 1}} \right) \frac{\sqrt{4x_1^2 - 6x_1 + 2 - 2l^2 \mp 2l\sqrt{l^2 + 2x_1 - 1}}}{2x_1 - 1}$$

The overall picture of the optimal flow field when the tolerance parameter, $0 < l \leq 1$ is shown in Figure 3 or when the tolerance parameter $l > 1$ is shown in Figure 4. The parts of the terminal manifold which correspond to the UP, BUP, and NUP are clearly indicated.

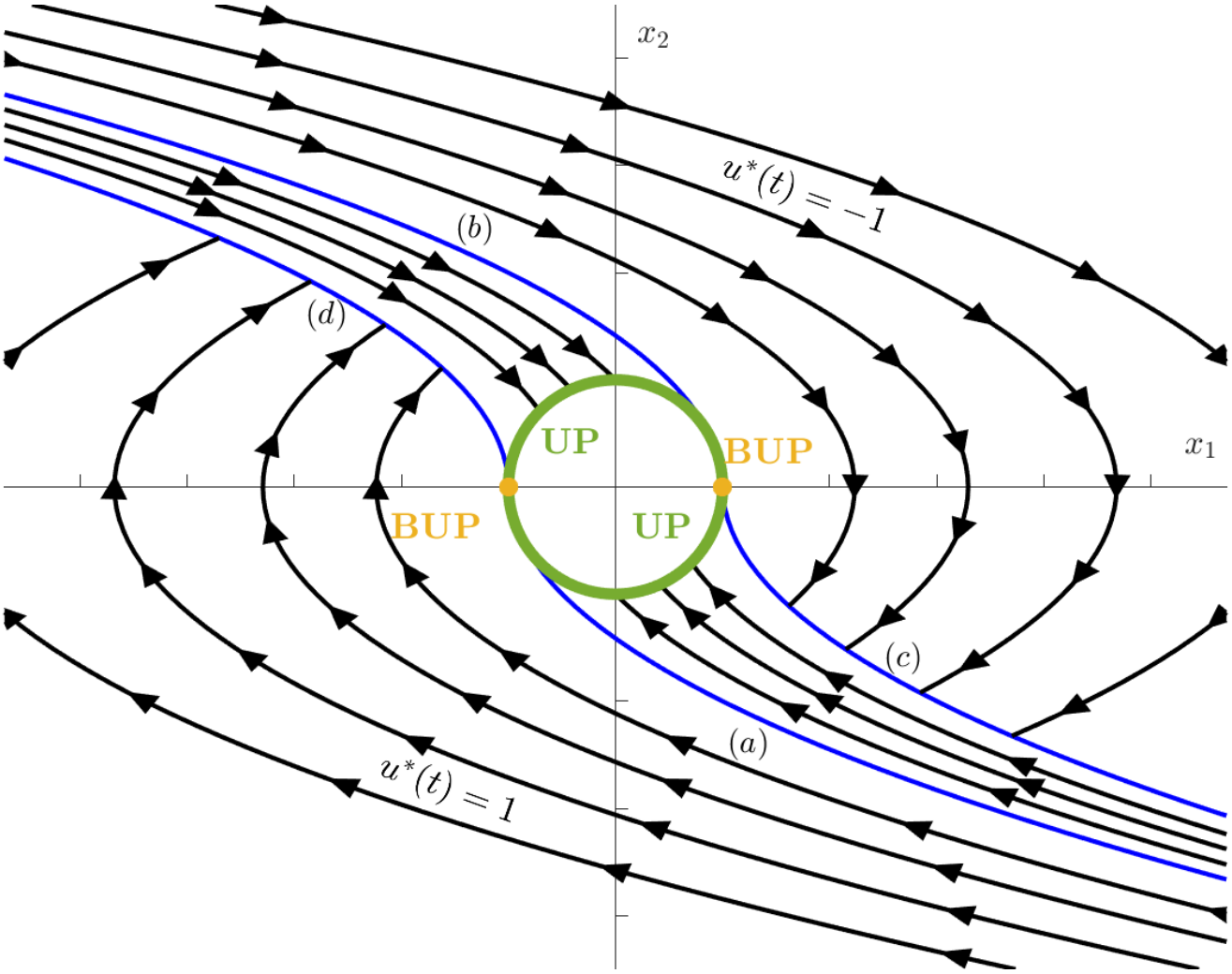

Fig. 3: The circular terminal manifold and family of trajectories in the state space when the parameters $\alpha = 1$ and $l = 1$. The curves (a) and (b) are where the value function is not continuous. The switching lines, curves (c) and (d), determine when the optimal control switches from -1 to 1 or from 1 to -1 respectively.

In Figures 3 and 4, curves (c) and (d) are switching lines (SL) which are momentarily crossed by the optimal trajectories, incurring an infinitesimal loss of optimality. The SL terminate at the BUP and therefore are not optimal trajectories themselves. Curves (a) and (b) are those where the value function / time-to-go is not continuous. The value function increases / jumps from above the curve (a) to below curve (a). The value function decreases/ jumps from above curve (b) to below curve (b). It is, however, continuously differentiable away from the curves (a) and (b). In Figure 5 the canonical optimal flow field where the target set is the origin is shown. The action in Figures 3 and 4 is lost in the case of a point target because the curves (a) and (c) coalesce into one curve and so do curves (b), (d) and the optimal

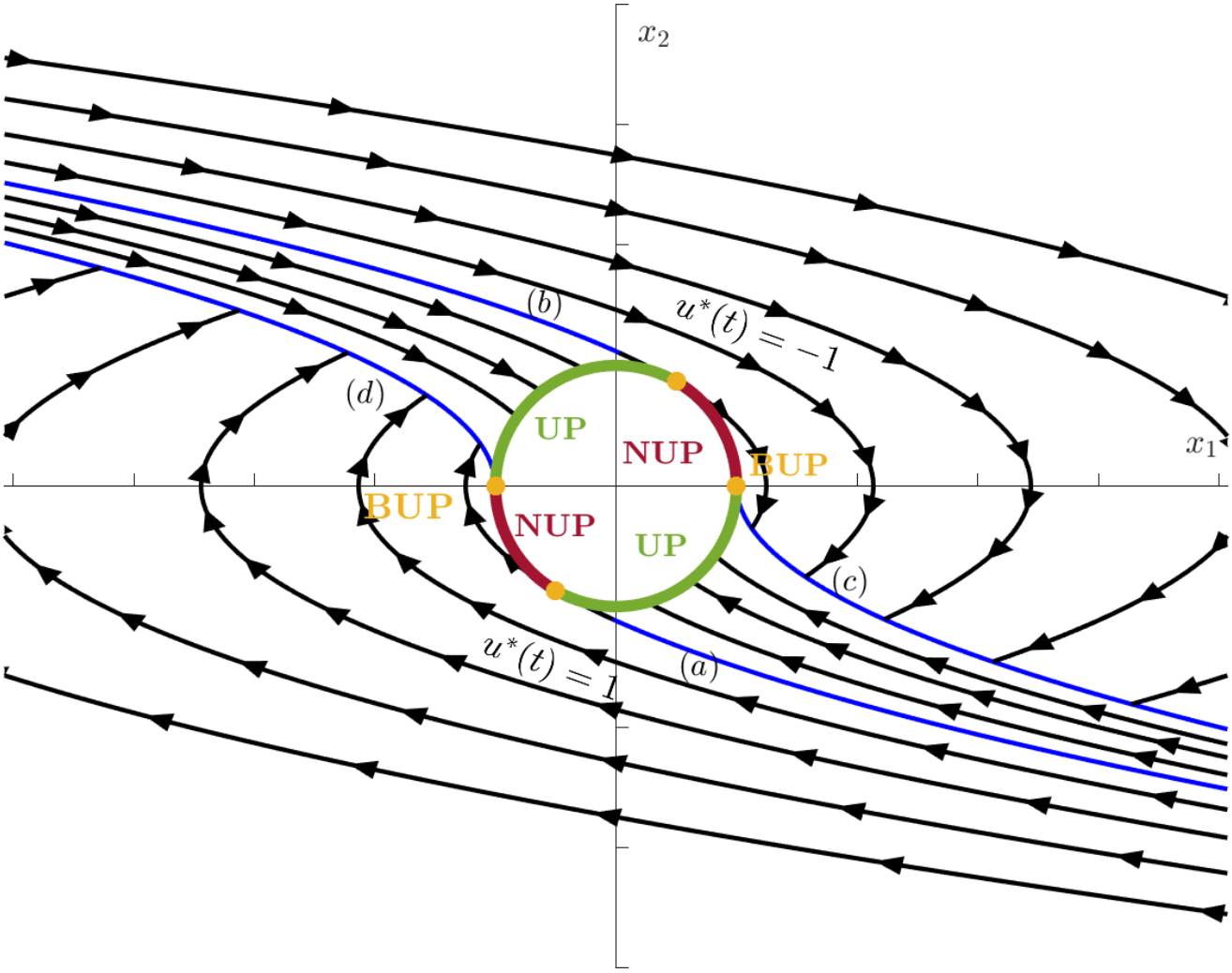

Fig. 4: The circular terminal manifold and family of trajectories in the state space when the parameters $\alpha = 1$ and $l = 2$. The curves (a) and (b) are where the value function is not continuous. The switching lines, curves (c) and (d), determine when the optimal control switches from -1 to 1 or from 1 to -1 respectively.

flow field in between. And these two consolidated curves, contrary to popular belief, are not optimal trajectories. This demonstrates the need to eschew "point targets" and rephrase the control problem so that it is mathematically well posed, and is engineering relevant. We see that Figure 5 is quite different from the optimal flow fields shown in Figures 3 and 4.

It is also interesting to present the isocost surfaces. The isocost "surfaces" are curves in the (x_1, x_2) state space / plane. The $\tau = 0$ isocost surface / curve is the UP of the target set.

$$\text{UP} = \left\{ \begin{pmatrix} l\cos\theta \\ l\sin\theta \end{pmatrix} \,\middle|\, 0 < \theta < \pi, \pi < \theta < 2\pi \right\} \tag{16}$$

A τ-isocost surface, S_τ, $\tau > 0$, is parameterized by θ, $0 < \theta < \pi$, $\pi < \theta < 2\pi$,

$$S_\tau = \left\{ \begin{pmatrix} x_1(\theta;\tau) \\ x_2(\theta;\tau) \end{pmatrix} \,\middle|\, 0 < \theta < \pi, \pi < \theta < 2\pi \right\} \tag{17}$$

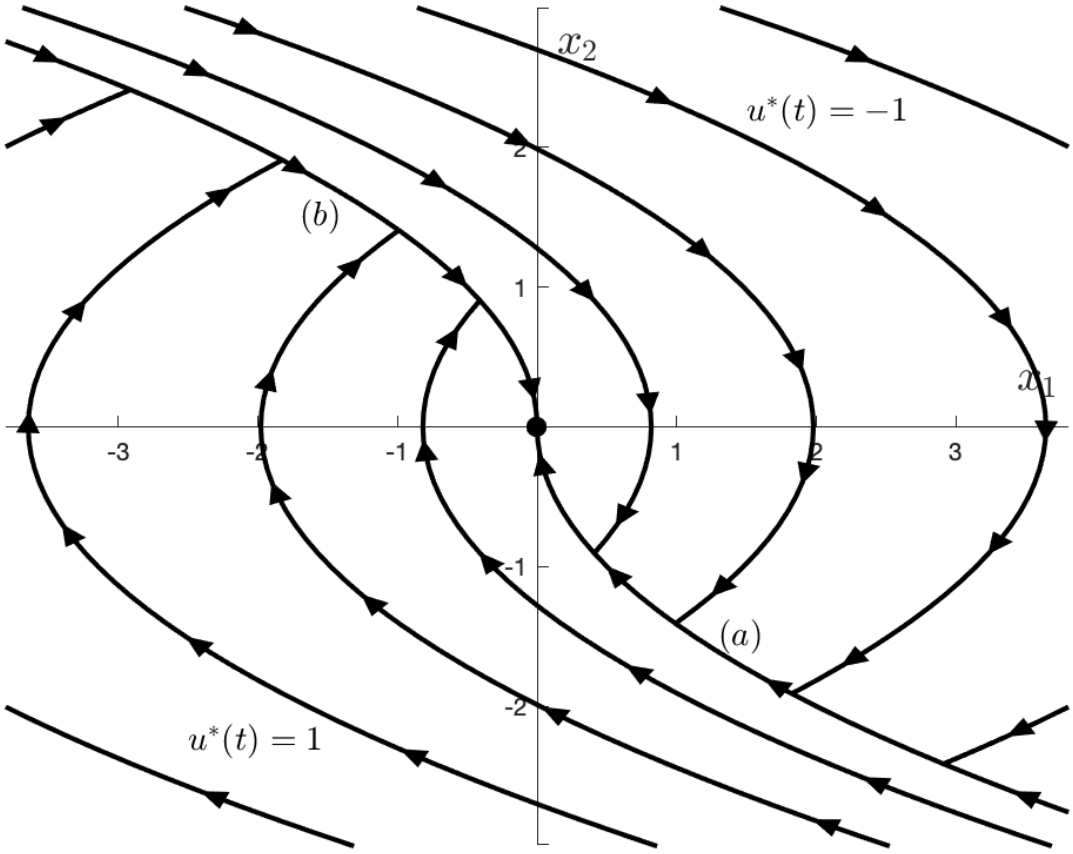

Fig. 5: The "classical" rendition of the optimal flow field. Note that lines (a) and (b) here represent optimal trajectories, but in-fact, line (a) is the consolidated curve (d) from Figures 3 and 4 and a part of the optimal flow field trajectories from Figures 3 and 4. Similarly, line (b) here is the consolidated curve (c) and part of the optimal flow field from Figures 3 and 4.

The parameter range $\{\theta|\ 0 < \theta < \pi, \pi < \theta < 2\pi\}$ is partitioned as follows:

$$\begin{aligned}
&\{\theta \mid 0 < \theta < \pi, \pi < \theta < 2\pi\} = \\
&\quad \{\theta \mid 0 < \theta \leq \tfrac{\pi}{2}\} \\
&\quad \cup \{\tfrac{\pi}{2} < \theta < \pi, \tan\theta < -\tau\} \\
&\quad \cup \{\theta | \tfrac{\pi}{2} < \theta < \pi, \tan\theta \geq -\tau\} \\
&\quad \cup \{\theta | \pi < \theta \leq \tfrac{3\pi}{2}\} \\
&\quad \cup \{\theta | \tfrac{3\pi}{2} < \theta < 2\pi, \tan\theta < -\tau\} \\
&\quad \cup \{\theta | \tfrac{3\pi}{2} < 2\pi, \tan\theta \geq -\tau\}
\end{aligned}$$

Let

$$\overline{\phi} \triangleq \arctan(\tau), \tau > 0,$$

then,

$$\begin{aligned}
&\{\theta|0<\theta<\pi,\pi<\theta<2\pi\}=\\
&\quad\{\theta|0<\theta\leq\tfrac{\pi}{2}\}\\
&\quad\cup\{\theta|\tfrac{\pi}{2}<\theta<\pi-\overline{\phi}\}\\
&\quad\cup\{\theta|\pi-\overline{\phi}\leq\theta<\pi\}\cup\{\theta|\pi<\theta\leq\tfrac{3\pi}{2}\}\\
&\quad\cup\{\theta|\tfrac{3\pi}{2}<\theta<2\pi-\overline{\phi}\}\\
&\quad\cup\{\theta|2\pi-\overline{\phi}\leq\theta<2\pi\}.
\end{aligned}$$

The S_τ isocost surface contained within the two switching lines, $\tau>0$, is:

$$x_1(\theta|\tau)=\begin{cases}
l(\cos\theta-\tau\sin\theta)-\frac{1}{2}\tau^2 & 0<\theta\leq\frac{\pi}{2}\\
l(\cos\theta-\tau\sin\theta)-\frac{1}{2}\tau^2 & \frac{\pi}{2}<\theta<\pi-\overline{\phi}\\
l(\cos\theta-\tau\sin\theta)+\frac{1}{2}\tau^2+\tan^2\theta+2\tau\tan\theta & \pi-\overline{\phi}\leq\theta<\pi\\
l(\cos\theta-\tau\sin\theta)+\frac{1}{2}\tau^2 & \pi<\theta\leq\frac{3\pi}{2}\\
l(\cos\theta-\tau\sin\theta)+\frac{1}{2}\tau^2 & \frac{3\pi}{2}<\theta<2\pi-\overline{\phi}\\
l(\cos\theta-\tau\sin\theta)-\frac{1}{2}\tau^2-\tan^2\theta-2\tau\tan\theta & 2\pi-\overline{\phi}\leq\theta<2\pi
\end{cases}$$

$$x_2(\theta|\tau)=\begin{cases}
l\sin\theta+\tau & 0<\theta\leq\frac{\pi}{2}\\
l\sin\theta+\tau & \frac{\pi}{2}<\theta<\pi-\overline{\phi}\\
l\sin\theta-2\tan\theta-\tau & \pi-\overline{\phi}\leq\theta<\pi\\
l\sin\theta-\tau & \pi<\theta\leq\frac{3\pi}{2}\\
l\sin\theta-\tau & \frac{3\pi}{2}<\theta<2\pi-\overline{\phi}\\
l\sin\theta+2\tan\theta+\tau & 2\pi-\overline{\phi}\leq\theta<2\pi
\end{cases}\tag{18}$$

The τ-isocost curves are continuous. A figure showing the isocost curves for $\tau=1,2,\cdots,8$ are shown in Figure 6. In order to obtain the isocost surfaces which lie outside the switching lines (yellow lines) in Figure 6 the retrograde equations are propagated backward in time ($\tau>0$) from the switching lines in the state space (x_1,x_2). The total sum of the propagation from the switching line and the retrograde time corresponding to a point on the switching line is equal to the total retrograde time as pictured in Figure 6.

IV. Square Target Set

Recall, the tolerance specification from Section II repeated here for convenience.

$$-L\leq x(t_f)\leq L,\ -V\leq v(t_f)\leq V$$

and also let L be the characteristic length. Using the non-dimensional variables as defined in Section II, the terminal manifold is the square

$$-1\leq x(t_f)\leq 1,\ -1\leq v(t_f)\leq 1.$$

The square, non-smooth, terminal manifold $ABCD$ and the associated normals is shown in Figure 7.

A square target set is used to show how to solve optimal control problems using Isaacs' method when the terminal manifold has corners and is not smooth. This is not apparent when considering a point target rather than a proper terminal manifold of co-dimension 1.

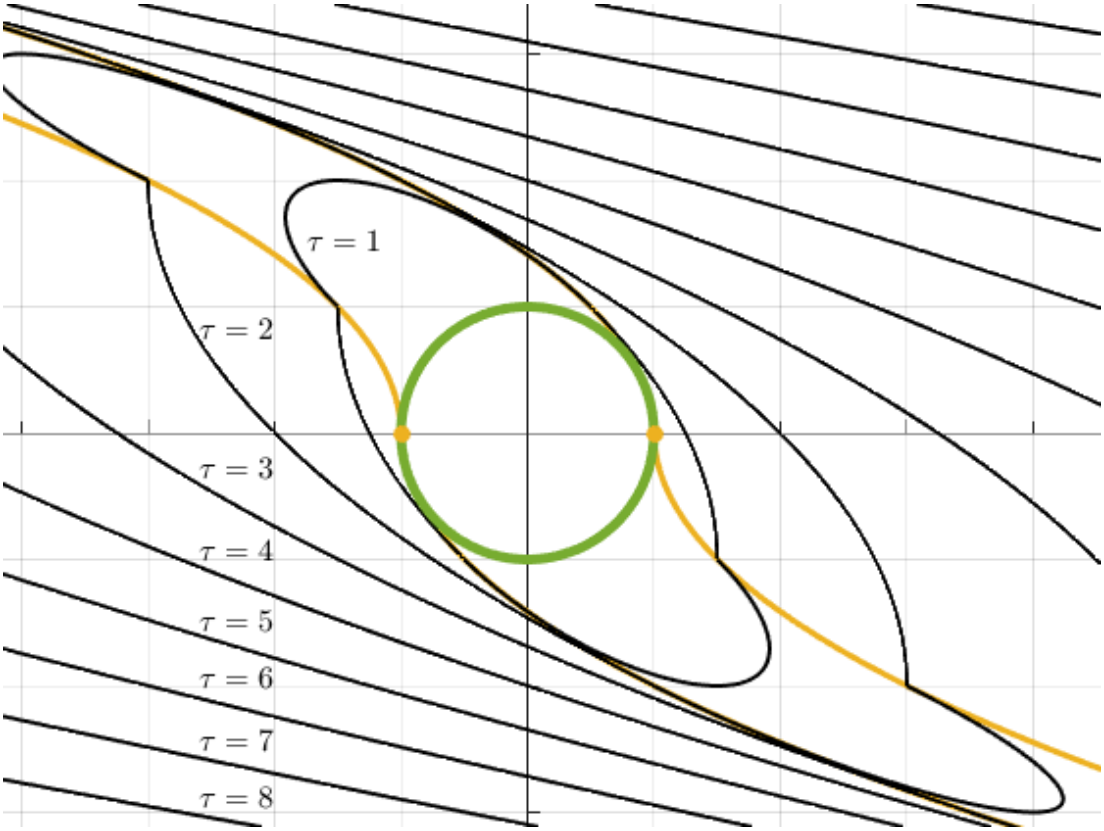

Fig. 6: The Isocost surfaces for $\tau = \{1, 2, \ldots, 8\}$ in the state space, (x_1, x_2)

TABLE I: Usable Part of the Square Terminal Manifold

Segment	$\vec{n}$	$\langle \vec{n} \cdot \mathbf{f} \rangle$	Usable Part (UP)
$\overline{AB}$	$\binom{-1}{0}$	$-x_2$	$\{(x_1, x_2) \vert x_1 = -1, x_2 \in (0, 1]\} \subset$ UP
$\overline{BC}$	$\binom{0}{-1}$	$-u$	$u = 1 \Rightarrow \overline{BC} \subset$ UP
$\overline{CD}$	$\binom{1}{0}$	x_2	$\{(x_1, x_2) \vert x_1 = 1, x_2 \in [-1, 0)\} \subset$ UP
$\overline{AD}$	$\binom{0}{1}$	u	$u = -1 \Rightarrow \overline{AB} \subset$ UP

A. Usable Part

In the best tradition of dynamic programs, we again "start" from the end. We start with identifying the UP of the terminal manifold by analyzing each of its four sides which make up the square $ABCD$, $\overline{AB}$, $\overline{BC}$, $\overline{CD}$, and $\overline{AD}$. For each side, the inner-product used to determine the UP, the BUP, and the nonusable part (NUP) are presented in Table I.

Note that the vertices $\{B, D\} \notin$ UP, so no optimal trajectories terminate at points B and D. Also, at the square's vertices / corners A and C, multiple optimal trajectories terminate because at A and C, the normals to the terminal manifold are not unique, but form a cone whose vertex angle is $\pi/2$. And these normals are the terminal costates, each of which will give rise to an optimal trajectory. Such a family of optimal of optimal trajectories will contribute to forming the optimal flow field which must cover the

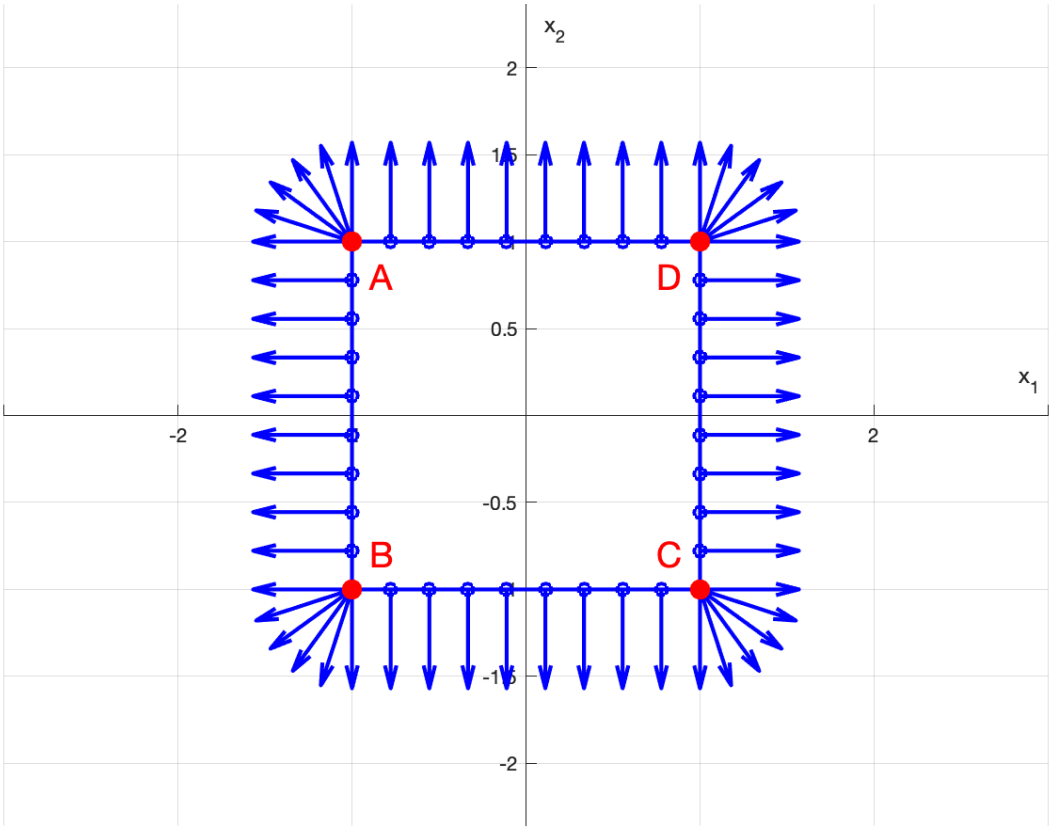

Fig. 7: The square target set $ABCD$ with outward pointing normals shown in the state space (x_1, x_2).

entire state space. The terminal state is

$$x_1(t_f) = \begin{cases} -1 & \text{on } \overline{AB} \\ s_1, -1 < s_1 \leq 1 & \text{on } \overline{BC} \\ 1 & \text{on } \overline{CD} \\ s_2, -1 \leq s_2 < 1 & \text{on } \overline{AD} \end{cases} \tag{19}$$

$$x_2(t_f) = \begin{cases} s_3, 0 < s_1 \leq 1 & \text{on } \overline{AB} \\ -1 & \text{on } \overline{BC} \\ s_4, -1 \leq s_4 < 0 & \text{on } \overline{CD} \\ 1 & \text{on } \overline{AD} \end{cases} \tag{20}$$

The terminal co-states are aligned with the outward pointing normals

$$\lambda_1(t_f) = \begin{cases} -a_1 & \text{on } \overline{AB} \\ 0 & \text{on } \overline{BC} \\ a_2 & \text{on } \overline{CD} \\ 0 & \text{on } \overline{AD} \\ a_5 \cos\theta_1 & \text{at } A, \text{ where } \frac{\pi}{2} < \theta_1 < \pi \\ a_5 \cos\theta_2 & \text{at } C, \text{ where } \frac{3\pi}{2} < \theta_2 < 2\pi \end{cases} \tag{21}$$

$$a_1 > 0,\ a_2 > 0,\ a_5 > 0$$

$$\lambda_2(t_f) = \begin{cases} 0 & \text{on } \overline{AB} \\ -a_3 & \text{on } \overline{BC} \\ 0, & \text{on } \overline{CD} \\ a_4 & \text{on } \overline{AD} \\ a_6 \sin\theta_1 & \text{at } A, \text{ where } \frac{\pi}{2} < \theta_1 < \pi \\ a_6 \sin\theta_2 & \text{at } C, \text{ where } \frac{3\pi}{2} < \theta_2 < 2\pi \end{cases} \tag{22}$$
$$a_3 > 0,\ a_4 > 0,\ a_6 > 0$$

Therefore a family of optimal trajectories will terminate at points A and C.

Recall the Hamiltonian, $\mathscr{H} = 1 + \lambda_1 x_2 + \lambda_2 u$, and since $u^* = -\text{sign}(\lambda_2)$, the optimal Hamiltonian, $\mathscr{H}^* = 1 + \lambda_1 x_2 - \text{sign}(\lambda_2)\lambda_2$. The optimal Hamiltonian is zero, including at the final time, just as described in Section III. The coefficient a is determined by evaluating the Hamiltonian at the final time, t_f where the co-states are known. This is accomplished by substitution of the values from (19) to (22) into (6). The resulting values for a_1 through a_6 are

$$\begin{aligned} a_1 &= \frac{1}{s_3}, \quad 0 < s_3 \leq 1 \\ a_2 &= -\frac{1}{s_4}, \quad -1 \leq s_4 < 0 \\ a_3 &= 1 \\ a_4 &= 1 \\ a_5 &= \frac{1}{\sin\theta_1 - \cos\theta_1}, \quad \tfrac{\pi}{2} \leq \theta_1 \leq \pi \\ a_6 &= \frac{1}{\cos\theta_2 - \sin\theta_2}, \quad \tfrac{3\pi}{2} \leq \theta_2 \leq 2\pi \end{aligned} \tag{23}$$

Note that $a_5 > 0$ and $a_6 > 0$ over the domain of θ_1 and θ_2 as required. Moreover, substitution of the a parameters from (23) into the co-state equations Eqs. (21) and (22) provides the final co-states.

$$\lambda_1(t_f) = \begin{cases} -\frac{1}{s_3},\ 0 < s_3 \leq 1 & \text{on } \overline{AB} \\ 0 & \text{on } \overline{BC} \\ -\frac{1}{s_4},\ -1 \leq s_4 < 0 & \text{on } \overline{CD} \\ 0 & \text{on } \overline{AD} \\ \frac{\cos\theta_1}{\sin\theta_1 - \cos\theta_1},\ \frac{\pi}{2} \leq \theta_1 \leq \pi & \text{at } A \\ \frac{\cos\theta_2}{\cos\theta_2 - \sin\theta_2},\ \frac{3\pi}{2} \leq \theta_2 \leq 2\pi & \text{at } C \end{cases} \tag{24}$$

$$\lambda_2(t_f) = \begin{cases} 0 & \text{on } \overline{AB} \\ -1 & \text{on } \overline{BC} \\ 0, & \text{on } \overline{CD} \\ 1 & \text{on } \overline{AD} \\ \frac{\sin\theta_1}{\sin\theta_1 - \cos\theta_1},\ \frac{\pi}{2} \leq \theta_1 \leq \pi & \text{at } A \\ \frac{\sin\theta_2}{\cos\theta_2 - \sin\theta_2},\ \frac{3\pi}{2} \leq \theta_2 \leq 2\pi & \text{at } C \end{cases} \tag{25}$$

The Euler-Lagrage / characteristic equations are

$$\begin{aligned} \dot{x}_1(t) &= x_2(t), & x_1(t=0) &= x_{10} \\ \dot{x}_2(t) &= -\text{sign}(\lambda_2(t)), & x_2(t=0) &= x_{20} \\ \dot{\lambda}_1(t) &= 0, & \lambda_1(t=t_f) &= \text{Eq. (24)} \\ \dot{\lambda}_2(t) &= -\lambda_1(t), & \lambda_2(t=t_f) &= \text{Eq. (25)} \end{aligned}$$

In retrograde time, τ, we consider trajectories which emanate from the UP, and therefore we have

$$\begin{aligned}
&\mathring{x}_1(\tau) = x_2(\tau), && x_1(\tau=0) = \text{Eq. (19)}\\
&\mathring{x}_2(\tau) = -\text{sign}(\lambda_2(\tau)), && x_2(\tau=0) = \text{Eq. (20)}\\
&\mathring{\lambda}_1(\tau) = 0, && \lambda_1(\tau=0) = \text{Eq. (24)}\\
&\mathring{\lambda}_2(\tau) = -\lambda_1(\tau), && \lambda_2(\tau=0) = \text{Eq. (25)}\\
&\quad \tau \geq 0
\end{aligned} \tag{26}$$

Because the dynamics for λ_1 are zero, $\lambda_1(\tau) = \lambda_1(\tau=0), \tau \geq 0$. Using this information, we calculate, in retrograde, $\lambda_2(\tau),\ \tau \geq 0$. Integrating $\mathring{\lambda}_2(\tau)$

$$\begin{aligned}
\lambda_2(\tau) = &\begin{cases}
-\frac{1}{s_3}\tau,\ 0 < s_3 \leq 1 & \text{on } \overline{AB}\\
-1 & \text{on } \overline{BC}\\
-\frac{1}{s_4}\tau,\ -1 \leq s_4 < 0 & \text{on } \overline{CD}\\
1 & \text{on } \overline{AD}\\
\frac{\tau\cos\theta_1+\sin\theta_1}{\sin\theta_1-\cos\theta_1},\ \frac{\pi}{2} \leq \theta_1 \leq \pi & \text{at } A\\
\frac{\tau\cos\theta_2+\sin\theta_2}{\cos\theta_2-\sin\theta_2},\ \frac{3\pi}{2} \leq \theta_2 \leq 2\pi & \text{at } C
\end{cases}\\
&\tau \geq 0
\end{aligned}$$

Next, we calculate the optimal trajectories in retrograde fashion.

$$x_2(\tau) = \begin{cases}
s_3 - \tau,\ 0 < s_3 \leq 1 & \text{on } \overline{AB}\\
-1 - \tau & \text{on } \overline{BC}\\
s_4 + \tau,\ -1 \leq s_4 < 0 & \text{on } \overline{CD}\\
1 + \tau & \text{on } \overline{AD}\\
1 + \tau,\ 0 \leq \tau \leq -\tan\theta_1 & \text{at } A\\
1 - 2\tan\theta_1 - \tau,\ -\tan\theta_1 \leq \tau & \text{at } A\\
-1 - \tau,\ 0 \leq \tau \leq -\tan\theta_2 & \text{at } C\\
-1 + 2\tan\theta_2 + \tau,\ -\tan\theta_2 \leq \tau & \text{at } C
\end{cases} \tag{27}$$

$$x_1(\tau) = \begin{cases}
-1 - s_3\tau + \frac{\tau^2}{2},\ 0 < s_3 \leq 1 & \text{on } \overline{AB}\\
s_1 + \tau + \frac{\tau^2}{2},\ -1 < s_1 \leq 1 & \text{on } \overline{BC}\\
1 - s_4\tau - \frac{\tau^2}{2},\ -1 \leq s_4 < 0 & \text{on } \overline{CD}\\
s_2 - \tau - \frac{\tau^2}{2},\ -1 \leq s_2 < 1 & \text{on } \overline{AD}\\
-1 - \tau - \frac{\tau^2}{2},\ 0 \leq \tau \leq -\tan\theta_1 & \text{at } A\\
-1 - \tau & \\
\quad + 2\tau\tan\theta_1 & , -\tan\theta_1 \leq \tau \quad \text{at } A\\
\quad + \dfrac{\tau^2}{2} + \tan^2\theta_1 & \\
1 + \tau + \frac{\tau^2}{2},\ 0 \leq \tau \leq -\tan\theta_2 & \text{at } C\\
1 + \tau - 2\tau\tan\theta_2 & \\
\quad -\dfrac{\tau^2}{2} - \tan^2\theta_2, & -\tan\theta_2 \leq \tau \quad \text{at } C
\end{cases} \tag{28}$$

$$\frac{\pi}{2} \leq \theta_1 \leq \pi, \frac{3\pi}{2} \leq \theta_2 \leq 2\pi$$

The optimal trajectories with x_1 as a function of x_2, are

$$x_1(x_2) = \begin{cases} \frac{x_2^2 - s_3^2 - 2}{2}, & x_2 \le s_3, \mathbf{x}_f \in \overline{AB} \\ \frac{x_2^2 - 1 + 2s_1}{2}, & x_2 \le -1, \mathbf{x}_f \in \overline{BC} \\ \frac{s_4^2 - x_2^2 + 2}{2}, & x_2 \ge s_4, \mathbf{x}_f \in \overline{CD} \\ \frac{1 - x_2^2 + 2s_2}{2}, & x_2 \ge 1, \mathbf{x}_f \in \overline{AD} \\ \\ \frac{-x_2^2 - 1}{2}, & 1 \le x_2 \le 1 - \tan\theta_1, \\ & \mathbf{x}_f \in A \\ \frac{x_2^2 - 3}{2} & \\ + 2\tan\theta_1, & x_2 \le 1 - \tan\theta_1, \\ - \tan^2\theta_1 & \mathbf{x}_f \in A \\ \frac{x_2^2 + 1}{2}, & \tan\theta_2 - 1 \le x_2 \le -1, \\ & \mathbf{x}_f \in C \\ \frac{-x_2^2 + 3}{2} & \\ - 2\tan\theta_2, & \tan\theta_2 - 1 \le x_2, \\ + \tan^2\theta_2 & \mathbf{x}_f \in C \end{cases} \tag{29}$$

$$-1 < s_1 \le 1, \quad -1 \le s_2 < 1$$
$$0 < s_3 \le 1, \quad -1 \le s_4 < 0$$
$$\tfrac{\pi}{2} \le \theta_1 \le \pi, \tfrac{3\pi}{2} \le \theta_2 \le 2\pi$$

Notice that the sign of λ_2 changes at the time instant $\tau_s = -\tan\theta_1$ for trajectories emanating from point A, and $\tau_s = -\tan\theta_2$ for trajectories emanating from point C. The trajectories specified in (29) provide the optimal trajectories for x_1 and x_2, provided a single parameter: s_1, s_2, s_3, s_4, θ_1, or θ_2. These trajectories potentially fill the two-dimensional state space: (x_1, x_2).

Two switching curves exist:

1) The switching curve pertaining to the family of optimal trajectories which terminate at vertex, A of the terminal manifold (an which are parameterized by $\pi/2 \le \theta_1 \le \pi$ is:

$$x_1 = -\frac{1}{2}x_2^2 - \frac{1}{2}, \quad x_2 \ge 1 \tag{30}$$

2) The switching curve pertaining to the family of optimal trajectories which terminate at the vertex C of the terminal manifold (an which are parameterized by $3\pi/2 \le \theta_2 \le 2\pi$) is:

$$x_1 = \frac{1}{2}x_2^2 + \frac{1}{2}, \quad x_2 \le -1 \tag{31}$$

No switching occurs on the four families of optimal trajectories which terminate on the four sides of the terminal manifold. The optimal flow field for reaching the square target manifold is shown in Figure 8.

In Figure 8 the blue lines with blue arrow heads represent switching lines. The switching line which is anchored at point A is described by (30); while the switching line which is anchored at point C is described by (31). The switching lines (a) and (b) are, themselves, optimal trajectories for reaching the UP since they are anchored at point A and C respectively. The switching lines (a) and (b) are when the optimal control used for reaching the UP of the terminal manifold switches from 1 to -1 and from -1 to 1, respectively.

The corners B and D are not in the UP and therefore trajectories which pass thought these points continue and terminate at points A and C respectively. These are "touch-and-go" trajectories. The touch-and-go trajectory which passes though point B has the equation: $x_1 = x_2^2/2 - 3/2$ and the touch-and-go trajectory which passes through point D has equation $x_1 = -x_2^2/2 + 3/2$. All of this is missed when the target set is a point, as in Pontryagin's canonical example.

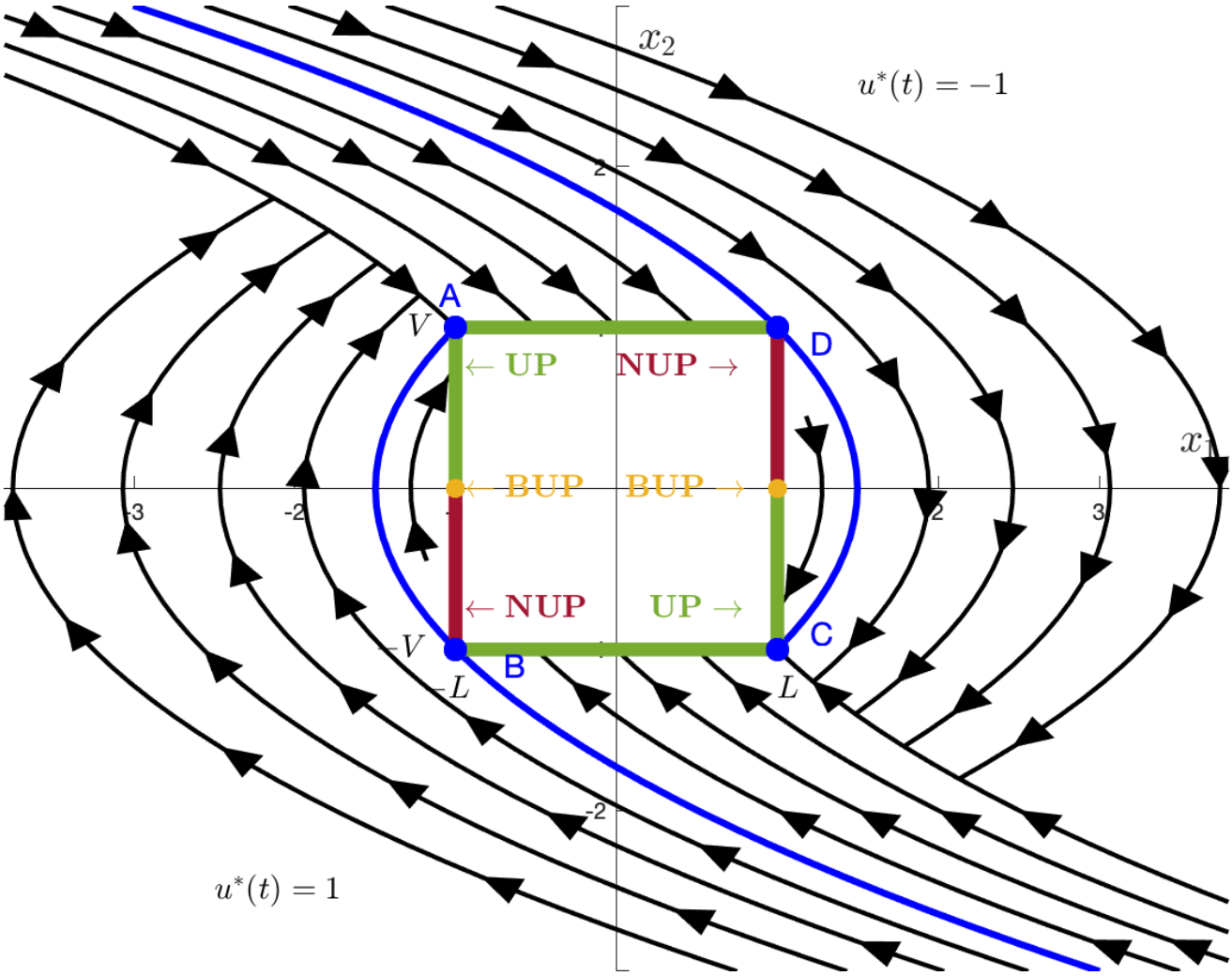

Fig. 8: The optimal flow-field and two switching curves, (a) and (b), for the square target manifold.

V. Conclusion

In this paper, the PMP and DP methods for solution of optimal control problems are juxtaposed. We advocate solving optimal control problems by leveraging Isaacs' constructive method for the solution of differential games. Isaacs' method is based on the method of DP as opposed to the PMP which is rooted in the calculus of variations and provides necessary conditions for optimality, which however can afford the construction of an optimal trajectory. We also emphasize the importance of formulating mathematically well-posed optimal control problems, that is, the need to move away from "point capture" and instead consider terminal manifolds of co-dimension 1; point capture is then the limiting case where the terminal manifold is shrunk to a singleton and the terminal manifold is a point target. This is also aligned with engineering practice where finite tolerances are specified.

Two examples are used to highlight the solution of min-time optimal control problem for reaching both a smooth and non-smooth terminal manifold, rather than a point target. This not only renders the mathematical optimal control problem well-posed, but from an engineering point of view, is more realistic, in that it represents an acceptable terminal tolerance / error. The first case is a circular terminal manifold, the second is a square terminal manifold with corners. The former highlights how to pose and solve optimal control problems when the terminal manifold is smooth, while the latter highlights the solution process when the terminal manifold has corners. While Isaacs' method naturally requires the terminal manifold being of co-dimension 1, it becomes apparent the classical PMP based approach hides critical aspects of

the optimal control problem when a point target is considered; this is highlighted in this paper. While PMP is a necessary condition of optimality, which however allows the construction of candidate optimal trajectories, Isaacs' method directly yields the optimal flow field and also the region of controllability.

REFERENCES

[1] L. S. Pontryagin, V. G. Boltyanskii, R. V. Gamkrelidze, and E. F. Mishchenko. *The Mathematical Theory of Optimal Processes*. Interscience Publishers John Wiley & Sons, Inc., New York–London, 1962.

[2] Rufus Isaacs. *Differential Games*. John Wiley and Sons, 1965.

Appendix C. Publications and Presentations

Papers and presentations which have been produced as a result of this body of work are presented in this Appendix.

Journal Papers

1. I. Weintraub, E. Garcia, M. Pachter, "An Optimal Guidance Strategy for the Defense of a Non-Maneuverable Evader in 3-D," in IET Control Theory and Applications, Volume 14, Issue 11, 23, July 2020, pp. 1531 – 1538. doi: 10.1049/iet-cta.2019.0541

2. I. Weintraub, A. Von Moll, E. Garcia, M. Pachter, "Maximum Observation of a Target by a Slower Observer in 3-Dimensions," in Journal of Guidance, Control, and Dynamics, Volume 44, Issue 3, 21, December, 2020, pp. 646-643. doi: 10.2514/1.G005619

Conference Papers

1. I. Weintraub, E. Garcia, D. Casbeer, M. Pachter, "An Optimal Aircraft Defense Strategy for the Active Target Defense Scenario," in AIAA Guidance, Navigation, and Control Conference, Grapevine, TX, 9-13 January, 2017, pp. 1-10, doi: 10.2514/6.2017-1917

2. I. Weintraub, E. Garcia, M. Pachter, "An Optimal-Stochastic Aircraft Defense Strategy for the Active Target Defense Scenario," in 2018 AIAA Guidance, Navigation, and Control Conference, Kissimmee, FL, 8-12 January, 2018, pp. 1-17, doi: 10.2514/6.2018-1336

3. I. Weintraub, E. Garcia, M. Pachter, "A Kinematic Rejoin Method for Active Defense of Non-Maneuverable Aircraft," in 2018 American Control Conference, Milwaukee, WI, 27-29 June, 2018, pp.6533-6538. doi: 10.23919/ACC.2018.8431129

4. G. Clem, J. Willhelm, D. Casbeer, I. E. Weintraub, D. Grymin, "An Intercept and Following Strategy for a Multi-rotor Platform using a Modified Proportional Navigation," in AIAA Scitech 2019 Forum, San Diego, CA, 7-11 January, 2019, pp. 1-10, doi: 10.2514/6.2019-0683

5. I. Weintraub, R. Cobb, W. Baker, M. Pachter, "Direct Methods Comparison for the Active Target Defense Scenario," in AIAA SciTech 2020 Forum, Orlando, FL, 6-10 January, 2020, doi: 10.251/6.2020-0612

6. I. Weintraub, A. Von Moll, E. Garcia, D. Casbeer, Z. Demers, M. Pachter, "Maximum Observation of a Faster Non-Maneuvering Target by a Slower Observer," in 2020 American Control Conference, Denver, CO, 1-3 July, 2020, pp. 100-105, doi: 10.23919/ACC45564.2020.9147340

7. I. Weintraub, M. Pachter, E. Garcia, "An Introduction to Pursuit-evasion Differential Games," in 2020 American Control Conference, Denver, CO, 1-3 July, 2020, doi: 10.23919/ACC45564.2020.9147205

8. I. Weintraub, M. Pachter, E. Garcia, "Optimal Evasion in an Active Target Defense Scenario," in AIAA Intelligent Systems Conference, Virtual Event, 11-15 & 19-21 January, 2021, doi: 10.2514/6.2021-1881

9. I. Weintraub, A. Von Moll, D. Casbeer, E. Garcia, M. Pachter, "Engagement Zone Defense of a Non-Maneuvering Evader," Under Review 2021 5th IEEE Conference on Control Theory and Applications, San Diego, California, 8-11 August, 2021.

Presentations

1. I. Weintraub, "Direct Methods Comparison for the Active Target Defense Scenario," Air Force Institute of Technology, presented at Controls and Optimization Brown Bag (COBB), 2018.

2. I. Weintraub, "Optimal Defense of High Value Aerial Assets," presented to Aerospace Vehicle Technology Assessment & Simulation (AVTAS) Branch, Air Force Research Laboratory, 2019.

3. I. Weintraub, "Optimal Defense of High Value Aerial Assets," presented to Control Science Center of Excellence, Air Force Research Laboratory, 2019.

4. I. Weintraub, "Optimal Defense of High Value Airborne Assets - Prospectus Defense," presented at the Aerospace Vehicles Technology Assessment and Simulations Branch Tactics Talk, 2020.

5. I. Weintraub, "Optimal Defense of High Value Airborne Assets - Prospectus Defense," presented to Electrical Engineering Department, Air Force Institute of Technology, 2020.

6. I. Weintraub, "Optimal Defense of High Value Airborne Assets - Dissertation Defense," presented to Electrical Engineering Department, Air Force Institute of Technology, 2021.

Bibliography

1. Joint Chiefs of Staff, "Joint Publication 3-01: Countering Air and Missile Threats," Joint Chiefs of Staff, Tech. Rep. JP3-01, 2017.

2. J. C. of Staff, "Joint Publication 3-13.1: Electronic Warfare," Joint Chiefs of Staff, Tech. Rep. JP 3-13.1, 2012.

3. Office of the Chief Scientist, "Autonomous Horizons: System Autonomy in the Air Force - A Path to the Future, Volume 1: Human-Autonomy Teaming," United States Air Force, Tech. Rep., 2015.

4. Enterprise Capability Collaboration Team, "Air Superiority 2030 Flight Plan," United States Air Force, Tech. Rep. May, 2016.

5. J. A. Winnefeld Jr. and F. Kendall, "Unmanned Systems Integrated Roadmap," Department of Defense, Tech. Rep., 2013.

6. D. L. James and M. A. Welsh III, "United States Air Force RPA Vector: Vision and Enabling Concepts 2013 - 2038," Headquarters, United States Air Force, Tech. Rep., 2014.

7. Deputy Chief of Staff for ISR (A2), "Small Unmanned Aircraft Systems (SUAS) Flight Plan: 2016 - 2036," United States Air Force, Tech. Rep., 2016.

8. Office of the Under Secretary of Defense for Acquisition Technology Logistics, "The Role of Autonomy in DoD Systems," Defense Science Board, Washington, DC, Tech. Rep. July, 2012.

9. R. Isaacs, *Differential Games*. John Wiley and Sons, 1965.

10. D. E. Kirk, *Optimal Control Theory*. Mineola, NY: Dover Publications, Inc, 1998.

11. A. E. Bryson and Y.-C. Ho, *Applied Optimal Control: Optimization, Estimation and Control*. Waltham, MA: Blaisdell Pub. Co., 1975.

12. I. M. Gelfand and S. V. Fomin, *Calculus of Variations*. New York, NY: Dover Publications, Inc, 2000.

13. H. Bock and K. Plitt, "A Multiple Shooting Algorithm for Direct Solution of Optimal Control Problems," *IFAC Proceedings Volumes*, vol. 17, no. 2, pp. 1603–1608, 1984.

14. M. Kiehl, "Parallel multiple shooting for the solution of initial value problems," *Parallel Computing*, vol. 20, no. 3, pp. 275–295, 1994.

15. C. L. Darby, D. Garg, and A. V. Rao, "Costate Estimation using Multiple-Interval Pseudospectral Methods," in *Guidance, Navigation and Control Conference*. Portland, OR: AIAA, 2011, p. 24.

16. J. Nocedal and S. J. W. Springer, *Numerical Optimization*. Springer-Verlag New York, Inc., 1999.

17. J. T. Betts, *Practical Methods for Optimal Control and Estimation Using Nonlinear Programming*. Philadelphia, PA: Society for Industrial and Applied Mathematics, 2010.

18. M. Kelly, "An Introduction to Trajectory Optimization: How to Do Your Own Direct Collocation," *SIAM Review*, vol. 59, no. 4, pp. 849–904, 2017.

19. A. V. Rao, "A Survey of Numerical Methods for Optimal Control," *Advances in the Astronautical Sciences*, vol. 135, no. 1, pp. 497–528, 2009.

20. R. Isaacs, "Games of Pursuit," RAND Corporation, Santa Monica, CA, Tech. Rep., 1951.

21. ——, "Differential Games I: Introduction," RAND Corporation, Santa Monica, CA, Tech. Rep., 1954.

22. ——, "Differential Games II: The Definition and Formulation," RAND Corporation, Santa Monica, CA, Tech. Rep., 1954.

23. ——, "Differential Games III: The Basic Principles of the Solution Process," RAND Corporation, Santa Monica, CA, Tech. Rep., 1954.

24. ——, "Differential Games IV: Mainly Examples," RAND Corporation, Santa Monica, CA, Tech. Rep., 1955.

25. M. H. Breitner, "The Genesis of Differential Games in Light of Isaacs' Contributions," *Journal of Optimization Theory and Applications*, vol. 124, no. 3, pp. 523–559, 2005.

26. R. Bellman, *Dynamic Programming*. Princeton, NJ: Princeton University Press, 1957.

27. A. Lew, "Richard Bellman's Contributions to Computer Science," *Journal of Mathematical Analysis and Applications*, vol. 119, no. 1-2, pp. 90–96, 1986.

28. P. Bernhard, "Isaacs , Breakwell , and their sons," no. 1927, Chateau Vaalsbroek, Maastricht, NL, 1998, pp. 1–16.

29. Y. C. Ho, A. E. Bryson, and S. Baron, "Differential Games and Optimal Pursuit-Evasion Strategies," *IEEE Transactions on Automatic Control*, vol. 10, no. 4, pp. 385–389, 1965.

30. S. Baron, "Differential Games and Manual Control," National Aeronautics and Space Administration, Washington, DC, Tech. Rep., 1966.

31. N. Satimov, "Problems of Pursuit and Evasion in Differential Games," Ph.D. dissertation, Tashkent State University, 1981.

32. C. Marchal, "Analytical Study of a Case of the Homicidal Chauffeur Game Problem," in *Optimization Techniques IFIP Technical Conference*, G. Marchuk, Ed. Springer, Berlin, Heidelberg, 1975, pp. 472–481.

33. V. S. Patsko and V. L. Turova, "Homicidal Chauffeur Game: History and Modern Studies," in *Advances in Dynamic Games. Annals of the International Society of Dynamic Games*, M. Breton and K. Szajowski, Eds. Ekaterinburg, Russia: Birkhäuser Boston, 2009, pp. 3–43.

34. M. Falcone, "Numerical Methods for Differential Games Based on Partial Differential Equations," *International Game Theory Review*, vol. 8, no. 2, pp. 231–272, 2006.

35. Anthony W. Merz, "The Homicidal Chauffeur - A Differential Game," Guidance and Control Laboratory, Wright-Patterson AFB, OH, Tech. Rep., 1971.

36. J. V. Breakwell and A. W. Merz, "Toward a Complete Solution of the Homicidal Chauffeur Game," in *Proceedings of the first international conference on the theory and applications of differential games*, Amherst, MA, 1969, pp. III 1 – III 5.

37. L. I. Meier, "A New Technique for Solving Pursuit-Evasion Differential Games," *IEEE Transactions on Automatic Control*, vol. AC-14, no. 4, pp. 352–359, 1969.

38. W. M. Getz and M. Pachter, "Two-Target Pursuit-Evasion Differential Games in the Plane," *Journal of Optimization Theory and Applications*, vol. 34, no. 3, pp. 383–403, 1981.

39. ——, "Capturability in a two-target game of two cars," *Journal of Guidance and Control*, vol. 4, no. 1, pp. 15–21, 1981.

40. I. Greenfeld, "A differential game of surveillance evasion of two identical cars," *Journal of Optimization Theory and Applications*, vol. 52, no. 1, pp. 53–79, 1987.

41. J. Lewin and J. V. Breakwell, "The Surveillance-Evasion Game of Degree," *Journal of Optimization Theory and Applications*, vol. 16, no. 3-4, pp. 339–353, 1975.

42. R. Bera, V. R. Makkapati, and M. Kothari, "A Comprehensive Differential Game Theoretic Solution to a Game of Two Cars," *Journal of Optimization Theory and Applications*, vol. 174, no. 3, pp. 818–836, 2017.

43. J. F. Fisac and S. S. Sastry, "The Pursuit-Evasion-Defense Differential Game in Dynamic Constrained Environments," in *Proceedings of the IEEE Conference on Decision and Control*. Osaka, Japan: IEEE, 2015, pp. 4549–4556.

44. D. W. Oyler, P. T. Kabamba, and A. R. Girard, "Pursuit–Evasion Games in the Presence of Obstacles," *Automatica*, vol. 65, pp. 1–11, 2016.

45. Z. E. Fuchs and P. P. Khargonekar, "Generalized engage or retreat differential game with escort regions," *IEEE Transactions on Automatic Control*, vol. 62, no. 2, pp. 668–681, 2017.

46. S. Sundaram, K. Kalyanam, and D. W. Casbeer, "Pursuit on a graph under partial information from sensors," in *Proceedings of the American Control Conference*, 2017, pp. 4279–4284.

47. K. Kalyanam, D. W. Casbeer, and M. Pachter, "Pursuit on a graph using partial information," *Proceedings of the American Control Conference*, vol. 2015-July, pp. 4269–4275, 2015.

48. E. Roxin and C. P. Tsokos, "On the Definition of a Stochastic Differential Game," *Mathematical Systems Theory*, vol. 4, no. 1, pp. 60–64, 1969.

49. F. L. Chernousko and A. A. Melikyan, "Some Differential Games with Incomplete Information," in *Optimization Techniques IFIP Technical Conference*, vol. 27. Novosibirsk: Springer, Berlin, Heidelberg, 1974, pp. 445–450.

50. Y. Yavin, "A Pursuit-Evasion Differential Game with Noisy Measurements of the Evader's Bearing from the Pursuer," *Journal of Optimization Th*, vol. 51, no. 1, pp. 161–177, 1986.

51. C. Giovannangeli, M. Heymann, and E. Rivlin, "Pursuit-Evasion Games in Presence of Obstacles in Unknown Environments : Towards an Optimal Pursuit Strategy," in *Cutting Edge Robotics*. IntechOpen, 2010, ch. 4, pp. 47–81.

52. G. Hexner, "A Differential Game of Incomplete Information," *Journal of Optimization Theory and Applications*, vol. 28, no. 2, pp. 213–231, 1979.

53. M. Pachter and Y. Yavin, "A Stochasic Homicidal Chauffeur Pursuit-Evasion Differential Game," *Journal of Optimization Theory and Applications*, vol. 34, no. 3, pp. 405–424, 1981.

54. S. Battistini and T. Shima, "Differential Games Missile Guidance with Bearings-Only Measurements," *IEEE Transactions on Aerospace and Electronic Systems*, vol. 50, no. 4, pp. 2906–2915, 2014.

55. O. Basimanebotlhe and X. Xue, "Stochastic Optimal Control to a Nonlinear Differential Game," *Advances in Difference Equations*, vol. 266, no. 1, 2014.

56. W. Lin, Z. Qu, and M. A. Simaan, "Nash strategies for pursuit-evasion differential games involving limited observations," *IEEE Transactions on Aerospace and Electronic Systems*, vol. 51, no. 2, pp. 1347–1356, 2015.

57. K. Kalyanam, D. W. Casbeer, and M. Pachter, "Pursuit of a Moving Target with Bounded Speed on a Directed Acyclic Graph Under Partial Information," *IMA Journal of Mathematical Control and Information*, pp. 1–16, 2016.

58. J. Shinar and S. Gutman, "Recent advances in optimal pursuit and evasion," in *Conference on Decision and Control including the 17th Symposium on Adaptive Processes*, vol. 17. San Diego, CA: IEEE, 1978, pp. 960–965.

59. J. Shinar, "Solution Techniques for Realistic Pursuit Evasion Games," Technion - Isreal Institute of Technology, Haifa, Israel, Tech. Rep., 1980.

60. M. Pachter and T. Milch, "The 'Homicidal Chauffeur' Model in Naval Pursuit-Evasion," in *Guidance, Navigation and Control Conference*. AIAA, 1987.

61. N. Greenwood, "A Differential Game in Three Dimensions: The Aerial Dogfight Scenario," *Dynamics and Control*, vol. 2, no. 2, pp. 161–200, 1992.

62. H. Ehtamo and T. Raivio, "On Applied Nonlinear and Bilevel Programming for Pursuit-Evasion Games," *Journal of Optimization Theory and Applications*, vol. 108, no. 1, pp. 65–96, 2001.

63. F. Imado and T. Kuroda, "A Method to Solve Missile-Aircraft Pursuit -Evasion Differential Games," in *16th Triennial World Congress*. Prague, Czech Republic: IFAC, 2005, pp. 176–181.

64. J. Shinar, V. Y. Glizer, and V. Turetsky, "A Pursuit-Evasion Game with Hybrid Pursuer Dynamics," in *Proceedings of the European Control Conference*. Kos, Greece: IEEE, 2007, pp. 1306–1313.

65. ——, "A Pursuit-Evasion Game with Hybrid Evader Dynamics," in *Proceedings of the European Control Conference*. Budapest, Hungary: IEEE, 2009, pp. 121–126.

66. A. W. Merz, "To Pursue or to Evade - That is the Question," *Guidance*, vol. 8, no. 2, pp. 161–166, 1984.

67. M. Pachter, E. Garcia, and D. W. Casbeer, "Active Target Defense Differential Game," in *Fifty-second Annual Allerton Conference*, Allerton House, UIUC, Illinois, USA, 2014, pp. 46–53.

68. E. Garcia, D. W. Casbeer, and M. Pachter, "Active Target Defense Differential Game with a Fast Defender," in *American Control Conference*, vol. Jul 1-3. Chicago, IL: American Automatic Control Council, 2015, pp. 3752–3757.

69. G. Leitmann, "A simple differential game," *Journal of Optimization Theory and Applications*, vol. 2, no. 4, pp. 220–225, 1968.

70. A. J. Calise and X.-M. Yu, "An Analysis of a Four State Model for Pursuit-Evasion Games," in *Conference on Decision and Control*. Ft. Lauderdale, FL: IEEE, 1985, pp. 1119–1121.

71. M. Quincampoix, "Differential Games," in *Computational Complexity: Theory, Techniques, and Applications*, R. A. Meyers, Ed. Springer New York, 2012, vol. 69, pp. 854–861.

72. P. Hagedorn and J. V. Breakwell, "A Differential Game with Two Pursuers and One Evader," *Journal of Optimization Theory and Applications*, vol. 18, no. 1, pp. 15–29, 1976.

73. A. G. Pashkov and S. D. Terekhov, "A differential game of approach with two pursuers and one evader," *Journal of Optimization Theory and Applications*, vol. 55, no. 2, pp. 303–311, 1987.

74. A. Y. Levchenkov and A. G. Pashkov, "Differential game of optimal approach of two inertial pursuers to a noninertial evader," *Journal of Optimization Theory and Applications*, vol. 65, no. 3, pp. 501–518, 1990.

75. S. A. Ganebny, S. S. Kumkov, S. Le Ménec, and V. S. Patsko, "Numerical Study of Two-on-One Pursuit-Evasion Game," in *Proceedings of the 18th World Congress*. Milano, Italy: International Federation of Automatic Control, 2011, pp. 9326–9333.

76. K. Kalyanam, S. Darbha, P. P. Khargonekar, M. Pachter, and P. R. Chandler, "Optimal Cooperative Pursuit on a Manhattan Grid," *AIAA Guidance, Navigation, and Control (GNC) Conference*, pp. 1–10, 2013.

77. E. Garcia, Z. E. Fuchs, and D. Milutinovic, "A Geometric Approach for the Cooperative Two-Pursuer One-Evader Differential Game," *IFAC-PapersOnLine*, vol. 50, no. 1, pp. 15 774–15 779, 2017.

78. S. Y. Hayoun and T. Shima, "A Two-on-One Linear Pursuit–Evasion Game with Bounded Controls," *Journal of Optimization Theory and Applications*, vol. 174, no. 3, pp. 837–857, 2017.

79. H. Huang, W. Zhang, J. Ding, D. M. Stipanović, and C. J. Tomlin, "Guaranteed Decentralized Pursuit-Evasion in the Plane with Multiple Pursuers," in *Proceedings of the IEEE Conference on Decision and Control*. Orlando, FL: IEEE, 2011, pp. 4835–4840.

80. E. Bakolas and P. Tsiotras, "Optimal Pursuit of Moving Targets Using Dynamic Voronoi Diagrams," in *IEEE Conference on Decision and Control*. Atlanta, GA: IEEE, 2010, pp. 7431–7436.

81. P. Borowko and W. Rzymowski, "Avoidance of Many Pursuers in the Simple Motion Case," *Journal of Mathematical Analysis and Applications*, vol. 111, no. 2, pp. 535–546, 1985.

82. W. Chodun and L. D. Berkovitz, "Differential Games of Evasion with Many Pursuers," *Journal of Mathematical Analysis and Applications*, vol. 142, no. 2, pp. 370–389, 1989.

83. G. I. Ibragimov, M. Salimi, and M. Amini, "Evasion from Many Pursuers in Simple Motion Differential Game with Integral Constraints," *European Journal of Operational Research*, vol. 218, no. 2, pp. 505–511, 2012.

84. I. A. Alias, R. Noorsuria, R. Ramli, G. Ibragimov, and A. Narzullaev, "Simple Motion Pursuit Differential Game of Many Pursuers and One Evader on Convex Compact Set," *International Journal of Pure and Applied Mathematics*, vol. 102, no. 4, pp. 733–745, 2015.

85. M. Kothari, J. G. Manathara, and I. Postlethwaite, "Cooperative Multiple Pursuers against a Single Evader," *Journal of Intelligent and Robotic Systems: Theory and Applications*, vol. 86, no. 3-4, pp. 551–567, 2017.

86. M. D. Awheda and H. M. Schwartz, "Decentralized Learning in Pursuit-Evasion Differential Games with Multi-Pursuer and Single-Superior Evader," in *Systems Conference (SysCon), 2016 Annual IEEE*. Orlando, FL: IEEE, 2016, p. 8.

87. A. A. Al-Talabi, "Multi-Player Pursuit-Evasion Differential Game with Equal Speed," in *International Automatic Control Conference*. Pingtung, Taiwan: IEEE, 2017, pp. 1–6.

88. A. Von Moll, D. Casbeer, E. Garcia, D. Milutinović, and M. Pachter, "The Multi-pursuer Single-Evader Game," *Journal of Intelligent & Robotic Systems*, 2019.

89. A. Von Moll, D. W. Casbeer, E. Garcia, and D. Milutinovic, "Pursuit-evasion of an Evader by Multiple Pursuers," in *International Conference on Unmanned Aircraft Systems, (ICUAS)*. Dallas, TX: IEEE, 2018, pp. 133–142.

90. M. Pachter, A. Von Moll, E. Garcia, D. W. Casbeer, and D. Milutinovic, "Singular Trajectories in the Two Pursuer One Evader Differential Game," in *International Conference on Unmanned Aircraft Systems (ICUAS)*. Atlanta, GA: IEEE, 2019, pp. 1153–1160.

91. Z. E. Fuchs, P. P. Khargonekar, and J. Evers, "Cooperative defense within a single-pursuer, two-evader pursuit evasion differential game," *Proceedings of the IEEE Conference on Decision and Control*, pp. 3091–3097, 2010.

92. Z. E. Fuch and P. P. Khargonekar, "Encouraging attacker retreat through defender cooperation," in *IEEE Conference on Decision and Control*. Orlando, FL: IEEE, 2011, pp. 235–242.

93. W. Scott and N. E. Leonard, "Pursuit, Herding and Evasion: A Three-Agent Model of Caribou Predation," in *American Control Conference*. Washington, DC: IEEE, 2013, pp. 2978–2983.

94. J. V. Breakwell and P. Hagedorn, "Point Capture of Two Evaders in Succession," *Journal of Optimization Theory and Applications*, vol. 27, no. 1, pp. 89–97, 1979.

95. M. Pachter and Y. Yavin, "One Pursuer and Two Evaders on the Line: A Stochasic Pursuit-Evasion Diffferential Game," *Journal of Optimization Theory and Applications*, vol. 39, no. 4, pp. 513–539, 1983.

96. T. G. Abramyants, E. P. Maslov, and V. P. Yakhno, "Evasion from Detection in Three-Dimensional Space," *Journal of Computer and Systems Sciences International*, vol. 46, no. 5, pp. 675–680, 2007.

97. S. Liu and Z. Zhou, "Evasion as a team against a faster pursuer," in *American Control Conference (ACC)*. Washington, DC: IEEE, 2013, pp. 5368–5373.

98. D. Wang and Z. Peng, "Pursuit-evasion games of multi-players with a single faster player," in *Chinese Control Conference, CCC*, vol. July 27-29, Chengdu, China, 2016, pp. 2583–2588.

99. I. N. Katz, H. Mukai, H. Schättler, M. Zhang, and M. Xu, "Solution of a differential game formulation of military air operations by the method of characteristics," *Journal of Optimization Theory and Applications*, vol. 125, no. 1, pp. 113–135, 2005.

100. I. Rusnak, "The Lady, The Bandits and the Body Guards - A Two Team Dynamic Game," *International Federation of Automatic Control*, vol. 38, no. 1, pp. 441–446, 2005.

101. M. D. Awheda and H. M. Schwartz, "A Decentralized Fuzzy Learning Algorithm for Pursuit-Evasion Differential Games with Superior Evaders," *Journal of Intelligent and Robotic Systems: Theory and Applications*, vol. 83, no. 1, pp. 35–53, 2016.

102. I. E. Weintraub, E. Garcia, D. W. Casbeer, and M. Pachter, "An Optimal Aircraft Defense Strategy for the Active Target Defense Scenario," in *AIAA Guidance, Navigation, and Control Conference*. Grapevine, TX: American Institute of Aeronautics and Astronautics, 2017, p. 10.

103. I. E. Weintraub, E. Garcia, and M. Pachter, "An Optimal-Stochastic Aircraft Defense Strategy for the Active Target Defense Scenario," in *AIAA Guidance, Navigation, and Control Conference*. Kissimmee, FL: AIAA, 2018, p. 17.

104. P. Cardaliaguett, "A Differential Game with Two Players and One Target," *SIAM Journal on Control and Optimization*, vol. 34, no. 4, pp. 1441–1460, 1996.

105. R. L. Boyell, "Defending a Moving Target Against Missile or Torpedo Attack," *IEEE Transactions on Aerospace and Electronic Systems*, vol. AES-12, no. 4, pp. 522–526, 1976.

106. ——, "Counterweapon Aiming for Defense of a Moving Target," *IEEE Transactions on Aerospace and Electronic Systems*, vol. AES-16, no. 3, pp. 402–408, 1979.

107. T. Yamasaki and S. N. Balakrishnan, "Triangle Intercept Guidance for Aerial Defense," in *Guidance, Navigation, and Control Conference*. Toronto, Ontario, Canada: AIAA, 2010, p. 22.

108. T. Yamasaki, S. N. Balakrishnan, and H. Takano, "Modified Command to Line-of-Sight Intercept Guidance for Aircraft Defense," *Journal of Guidance, Control, and Dynamics*, vol. 36, no. 3, pp. 901–905, 2013.

109. S. Rubinsky and S. Gutman, "Three Body Guaranteed Pursuit and Evasion," in *AIAA Guidance, Navigation, and Control Conference*. Minneapolis, MN: AIAA, 2012, p. 24.

110. ——, "Three-Player Pursuit and Evasion Conflict," *Journal of Guidance, Control, and Dynamics*, vol. 37, no. 1, pp. 98–110, 2014.

111. I. Rusnak, H. Weiss, and G. Hexner, "Guidance Laws in Target–Missile–Defender Scenario with an Aggressive Defender," in *18th World Congress*. Milano, Italy: International Federation of Automatic Control, 2011, pp. 9349–9354.

112. A. Ratnoo and T. Shima, "Line-of-Sight Interceptor Guidance for Defending an Aircraft," *Journal of Guidance, Control, and Dynamics*, vol. 34, no. 2, pp. 522–532, 2011.

113. ——, "Guidance Strategies Against Defended Aerial Targets," *Journal of Guidance, Control, and Dynamics*, vol. 35, no. 4, pp. 1059–1068, 2012.

114. T. Shima, "Optimal Cooperative Pursuit and Evasion Strategies Against a Homing Missile," *Journal of Guidance, Control, and Dynamics*, vol. 34, no. 2, pp. 414–425, 2011.

115. V. Shaferman and T. Shima, "Cooperative Multiple Model Adaptive Guidance for an Aircraft Defending Missile," *Journal of Guidance, Control, and Dynamics*, vol. 33, no. 6, p. 25, 2010.

116. M. G. Earl and R. D'andrea, "A decomposition approach to multi-vehicle cooperative control," *Robotics and Autonomous Systems*, vol. 55, pp. 276–291, 2007.

117. Q. Sun, Z. Chen, N. Qi, and H. Lin, "Pursuit and evasion conflict for three players based on differential game theory," in *Control And Decision Conference (CCDC), 2017 29th Chinese*. Chongqing, China: IEEE, 2017, pp. 4527–4531.

118. E. Garcia, D. W. Casbeer, and M. Pachter, "Cooperative Aircraft Defense from an Attacking Missile," *Journal of Guidance, Control, and Dynamics*, vol. 38, no. 8, pp. 1510–1520, 2015.

119. D. W. Casbeer, E. Garcia, and M. Pachter, "The Target Differential Game with Two Defenders," in *International Conference on Unmanned Aircraft Systems (ICUAS)*, Arlington, VA, 2016, pp. 202–210.

120. ——, "The Target Differential Game with Two Defenders," *Journal of Intelligent and Robotic Systems: Theory and Applications*, vol. 89, no. 1-2, pp. 87–106, 2018.

121. E. Garcia, D. W. Casbeer, and M. Pachter, "Active Target Defense using First Order Missile Models," *Automatica*, vol. 78, pp. 139–143, 2017.

122. E. Garcia, D. W. Casbeer, Z. E. Fuchs, and M. Pachter, "Cooperative Missile Guidance for Active Defense of Air Vehicles," *IEEE Transactions on Aerospace and Electronic Systems*, pp. 1–14, 2017.

123. E. Garcia, D. W. Casbeer, and M. Pachter, "Optimal Target Capture Strategies in the Target-Attacker-Defender Differential Game," in *2018 Annual American Control Conference (ACC)*. Milwaukee, Wisconson: IEEE, 2018, pp. 68–73.

124. Z. S. Wowczuk, E. D. Pertl, M. A. Clarke, J. E. Smith, S. Bjorge, and R. McNutt, "Complete Command, Control, Communications, Intelligence, Surveillance, and Reconnaissance System for C-130 Aircraft," *Journal of Aerospace Computing, Information, and Communication*, vol. 7, no. 6, pp. 179–187, 2010.

125. D. J. Henry, "ISR Systems: Past, Present, and Future," in *Airborne Intelligence, Surveillance, Reconnaissance (ISR) Systems and Applications XIII*, vol. 9828. Baltimore, MD: SPIE, 2016, p. 982802.

126. B. M. Kent and R. A. Ehret, "Rethinking Intelligence, Surveillance, and Reconnaissance in a Wireless Connected World," in *IEEE Antennas and Propagation Society, AP-S International Symposium (Digest)*. Chicago, IL: IEEE, 2012, p. 2.

127. M. Wilkins and T. Marchelli, "An Optimal Approach to Unmanned Maritime Surveillance Analysis," in *12th AIAA/ISSMO Multidisciplinary Analysis and*

Optimization Conference. Victoria, British Columbia, Canada: American Institute of Aeronautics and Astronautics (AIAA), 2012, pp. 1–7.

128. R. He, A. Bachrach, and N. Roy, "Efficient Planning Under Uncertainty for a Target-Tracking Micro-Aerial Vehicle," in *Proceedings - IEEE International Conference on Robotics and Automation*. Anchorage, AK: IEEE, 2010, pp. 1–8.

129. R. A. Livermore, "Optimal UAV Path Planning for Tracking a Moving Ground Vehicle With a Gimbaled Camera." M.S. Thesis. Air Force Institute of Technology, 2014, pp. 1–106.

130. M. Wohlsen, "The Ex-Googlers Building Drones that Anybody can Pilot With a Phone," https://www.wired.com/2015/01/skydio-drones/, 2015.

131. T. A. Wettergren and C. M. Traweek, "The Search Benefits of Autonomous Mobility in Distributed Sensor Networks," *International Journal of Distributed Sensor Networks*, vol. 2012, no. 2, p. 11, 2012.

132. B. Liu, O. Dousse, P. Nain, and D. Towsley, "Dynamic Coverage of Mobile Sensor Networks," *IEEE Transactions on Parallel and Distributed Systems*, vol. 24, no. 2, pp. 301–311, 2013.

133. J. M. Dobbie, "Solution of Some Surveillance-Evasion Problems by Methods of Differential Games," in *Proceedings of the 4th International Conference on Operational Research, MIT*. New York, New York: John Wiley and Sons, 1966, pp. 170–184.

134. J. G. Taylor, "Application of Differential Games to Problems of Naval Warware: Surveillance-Evasion - Part 1," United States Naval Postgraduate School, Monterey, CA, Tech. Rep., 1970.

135. J. Lewin and G. J. Olsder, "Conic Surveillance Evasion," *Journal of Optimization Theory and Applications*, vol. 27, no. 1, pp. 107–125, 1979.

136. Z. E. Fuchs and J. Metcalf, "Equilibrium Radar-Target Interactions in an ATR Scenario: A Differential Game," in *2018 IEEE Radar Conference, RadarConf 2018*. Oklahoma City, OK: IEEE, 2018, pp. 1228–1233.

137. V. Patsko, S. Kumkov, and V. Turova, "Pursuit-Evasion Games," in *Handbook of Dynamic Game Theory*, Z. G. Basar T., Ed. Springer, Cham, 2018, pp. 1–87.

138. R. J. Garnett and A. Flenner, "Optimal Control for Improved UAV Communication," in *AIAA Scitech Forum*. San Diego, CA: American Institute of Aeronautics and Astronautics (AIAA), 2019, pp. 1–14.

139. J. V. Breakwell, "Pursuit of a Faster Evader," in *The Theory and Application of Differential Games*, J. D. Grote, Ed. Springer, Dordrecht, 1975, pp. 243–256.

140. E. Garcia, D. Tran, D. Casbeer, D. Milutinovic, and M. Pachter, "Beyond Visual Range," in *AIAA Scitech Forum*. Virtual Event: AIAA, 2021.

141. E. Garcia, D. W. Casbeer, K. Pham, and M. Pachter, "Cooperative Aircraft Defense from an Attacking Missile using Proportional Navigation," in *AIAA Guidance, Navigation and Control Conference*. Kissimmee, FL: AIAA, 2015, pp. 1–10.

142. N. Hanlon, E. Garcia, D. W. Casbeer, and M. Pachter, "AFSIM Implementation and Simulation of the Active Target Defense Differential Game," in *AIAA Guidance, Navigation, and Control Conference*, no. January 8-12. Kissimmee, FL: AIAA, 2018, p. 12.

143. M. Pachter, A. Von Moll, E. Garcia, D. W. Casbeer, and D. Milutinović, "Two-on-One Pursuit," *Journal of Guidance, Control, and Dynamics*, vol. 42, no. 7, pp. 1638–1644, 2019.

144. E. Garcia, D. W. Casbeer, and M. Pachter, "Design and Analysis of State-Feedback Optimal Strategies for the Differential Game of Active Defense," *IEEE Transactions on Automatic Control*, vol. 64, no. 2, pp. 553–568, 2019.

145. J. T. Betts, "Survey of Numerical Methods for Trajectory Optimization," *Journal of Guidance, Control, and Dynamics*, vol. 21, no. 2, pp. 193–207, 1998.

146. D. E. Kirk, *Optimal Control Theory: An Introduction*, ser. Dover Books on Electrical Engineering Series. Dover Publications, 2004.

147. G. Elnagar, M. A. Kazemi, and M. Razzaghi, "The Pseudospectral Legendre Method for Discretizing Optimal Control Problems," *IEEE Transactions on Automatic Control*, vol. 40, no. 10, pp. 1793 – 1796, 1995.

148. F. Fahroo and I. M. Ross, "Advances in Pseudospectral Methods for Optimal Control," in *Guidance, Navigation and Control Conference*, no. August. Honolulu, Hawaii: American Institute of Aeronautics and Astronautics, 2008, p. 23.

149. C. L. Darby, D. Garg, and A. V. Rao, "Costate Estimation using Multiple-Interval Pseudospectral Methods," in *Guidance, Navigation, and Control Conference*, Portland, 2011, p. 24.

150. L. C. Young, "Orthogonal collocation revisited," *Computer Methods in Applied Mechanics and Engineering*, vol. 345, pp. 1033–1076, 2019.

151. L. S. Pontryagin, V. G. Boltyanskii, R. V. Gamkrelidze, and E. F. Mishchenko, *The Mathematical Theory of Optimal Processes*. New York–London: Interscience Publishers John Wiley & Sons, Inc., 1962.

152. J. C. Butcher, "Runge–Kutta Methods," in *Numerical Methods for Ordinary Differential Equations*. Wiley-Blackwell, 2008, ch. 3, pp. 137–316.

153. F. Fahroo and I. M. Ross, "Costate Estimation by a Legendre Pseudospectral Method," in *Guidance, Navigation, and Control Conference*, Monterey, CA, 1998, pp. 643–653.

154. ——, "Pseudospectral Methods for Infinite-Horizon Nonlinear Optimal Control Problems," in *Guidance, Navigation and Control Conference*. San Francisco, CA: AIAA, 2005.

155. C. L. Darby and A. V. Rao, "A State Approximation-Based Mesh Refinement Algorithm for Solving Optimal Control Problems Using Pseudospectral Methods," in *AIAA Guidance, Navigation and Control Conference*, no. August. Chicago, IL: AIAA, 2009, pp. 1–26.

156. M. A. Patterson and A. V. Rao, "GPOPS-II: A MATLAB Software for Solving Multiple-Phase Optimal Control Problems Using hp-Adaptive Gaussian Quadrature Collocation Methods and Sparse Nonlinear Programming," *ACM Transactions on Mathematical Software (TOMS)*, vol. 41, no. 1, p. 37, 2014.

157. A. E. Bryson and Y.-C. Ho, *Applied Optimial Control*. New York, NY: Taylor and Francis Group, 1975.

158. H. W. Kuhn and A. W. Tucker, "Nonlinear Programming," in *Proceedings of the Second Berkeley Symposium on Mathematics Statatistics and Probability*, Berkeley, CA, 1951, pp. 481–492.

159. I. E. Weintraub, E. Garcia, and M. Pachter, "A Kinematic Rejoin Method for Active Defense of Non-Maneuverable Aircraft," in *Proceedings of the American Control Conference*, vol. 2018-June, 2018, pp. 6533–6538.

160. M. V. Ramana and M. Kothari, "Pursuit-Evasion Games of High Speed Evader," *Journal of Intelligent & Robotic Systems*, vol. 85, pp. 293–306, 2017.

161. R. H. Venkatesan and N. K. Sinha, "A New Guidance Law for the Defense Missile of Nonmaneuverable Aircraft," *IEEE Transactions on Control Systems Technology*, vol. 23, no. 6, pp. 2424–2431, 2015.

Vita

Isaac Weintraub was born and raised in Toledo, Ohio. After graduating in 2005 from the Toledo Technology Academy, where he specialized in industrial automatic control and manufacturing, Isaac attended Rose-Hulman Institute of Technology. He graduated magna cum laude in 2009 with a bachelor's of science in mechanical engineering, minoring in electrical engineering, and receiving a certificate in robotics.

In 2009, Isaac was accepted to the University of Texas at Arlington. Working under Frank Lewis, Isaac specialized in control theory, consensus, and robotics. In 2011 he graduated magna cum laude with a masters of science in electrical engineering.

Upon completion of his masters, Isaac was employed by General Dynamics Information Technology Corporation at Wright-Patterson Air Force Base, OH. At General Dynamics, Isaac worked at Air Force Research Laboratory (AFRL) developing flapping-wing micro-air vehicles capable of controllable flight.

In 2015, Isaac accepted a position at Air Force Research Laboratories, working in the Aerospace Vehicle Technology Assessment and Simulation Branch of the Aerospace Systems Directorate. Presently, he is a Ph.D. candidate studying optimal control and differential game theory in the Department of Electrical and Computer Engineering at the Air Force Institute of Technology (AFIT).

REPORT DOCUMENTATION PAGE

Form Approved
OMB No. 0704–0188

1. REPORT DATE *(DD–MM–YYYY)*	2. REPORT TYPE	3. DATES COVERED *(From — To)*
8 MAR 2021	Doctoral Dissertation	Aug 2013 – Mar 2021

4. TITLE AND SUBTITLE

Optimal Defense of High Value Airborne Assets

5a. CONTRACT NUMBER
N/A

5b. GRANT NUMBER
N/A

5c. PROGRAM ELEMENT NUMBER
N/A

6. AUTHOR(S)

Isaac E. Weintraub, CIV, USAF

5d. PROJECT NUMBER
N/A

5e. TASK NUMBER
N/A

5f. WORK UNIT NUMBER
N/A

7. PERFORMING ORGANIZATION NAME(S) AND ADDRESS(ES)

Air Force Institute of Technology
Graduate School of Engineering and Management (AFIT/EN)
2950 Hobson Way
WPAFB OH 45433-7765

8. PERFORMING ORGANIZATION REPORT NUMBER

AFIT-ENG-DS-21-M-091

9. SPONSORING / MONITORING AGENCY NAME(S) AND ADDRESS(ES)

Intentionally Left Blank

10. SPONSOR/MONITOR'S ACRONYM(S)
N/A

11. SPONSOR/MONITOR'S REPORT NUMBER(S)
N/A

12. DISTRIBUTION / AVAILABILITY STATEMENT

DISTRIBUTION STATEMENT A. APPROVED FOR PUBLIC RELEASE: DISTRIBUTION UNLIMITED. (AFRL-2021-05291)

13. SUPPLEMENTARY NOTES

14. ABSTRACT

Optimal control theory and differential game theory is applied to the study of the defense of high value airborne assets, particularly in the case of a single threat such as an adversarial aircraft or missile. Rather than utilizing onboard defenses of the high value airborne asset, defense is proposed using a teamed unmanned combat air vehicle. The unmanned combat air vehicle provides defense by one of two ways: kinetic or directed energy. When defense if kinetic in nature, the defender launches a missile which strives to reach the threat before the threat reaches the high value airborne asset – damage to the pursuer is dealt though capture. When defense is provided though directed energy, the defender strives to keep the incoming threat inside its weapon engagement zone for as long as possible – damage to the pursuer is dealt over time. Optimal strategies for unmanned combat air vehicle, high value airborne asset and the pursuing threat are investigated though a series of engagements which are posed as either optimal control problems or differential games.

15. SUBJECT TERMS

Optimal Control Theory, Differential Game Theory

16. SECURITY CLASSIFICATION OF:			17. LIMITATION OF ABSTRACT	18. NUMBER OF PAGES	19a. NAME OF RESPONSIBLE PERSON
a. REPORT	b. ABSTRACT	c. THIS PAGE			Dr. Meir M. Pachter (ENG)
U	U	U	UU	244	19b. TELEPHONE NUMBER *(include area code)* (937) 255-3636 x7247 Meir.Pachter@afit.edu